The Pennsylvania State University

The Graduate School

Intercollege Graduate Degree Program in Plant Biology

INTEGRATING ROOT AND LEAF PHENOTYPES TO ENHANCE NITROGEN USE EFFICIENCY IN MAIZE (*Zea Mays* L.)

A Dissertation in

Plant Biology

by

Jennifer T. Yang

Submitted in Partial Fulfillment
of the Requirements
for the Degree of

Doctor of Philosophy

December 2017

The dissertation of Jennifer T. Yang was reviewed and approved* by the following:

Jonathan Lynch
Distinguished Professor of Plant Nutrition
Dissertation Advisor
Chair of Committee

Kathleen Brown
Professor of Plant Stress Biology

Gabriele Monshausen
Associate Professor of Biology

Timothy Ryan
Associate Professor of Anthropology

Teh-hui Kao
Distinguished Professor of Biochemistry and Molecular Biology
Chair of the Intercollege Graduate Degree Program in Plant Biology

*Signatures are on file in the Graduate School

ABSTRACT

Developing crop varieties with greater resource use efficiency and tolerance to abiotic and biotic stress is a key strategy for mitigating effects of climate change and resource depletion, while ensuring food security for a rapidly growing human population. Nitrogen is the mineral element required in greatest abundance by plants, and its availability is a primary determinant of plant growth and crop yield. Yet, nitrogen fertilizer is one of the most costly agricultural inputs, and inaccessible in sufficient quantities to low-input farmers. Conversely, excess application of fertilizer to maximize yields in intensive commercial operations has resulted in environmental damage and economic losses; an estimated 50% of applied nitrogen is not captured by crops, and contaminates ground water, creates hypoxic zones, or volatilizes as harmful greenhouse gases.

Maize (*Zea mays* L.) is a dominant crop, with approximately 1 billion tons produced globally for food, fuel, and industrial uses per year. Breeding maize varieties with enhanced nitrogen use efficiency (NUE, defined as grain yield per unit soil nitrogen) – both in capturing nitrogen in soil ("uptake efficiency", NUpE) and converting acquired nitrogen into grain yield ("utilization efficiency", NUtE) – would have substantial environmental and economic benefits. Selection under increased planting densities has indirectly contributed to modest gains in NUE in modern maize varieties, along with agronomic advances. However, trait-based approaches could lead to targeted improvement in NUE for both high-input farms and nitrogen-deficient soils.

In maize, a shoot-borne, nodal root system is responsible for the majority of nitrogen uptake, and consists of successive nodes ("whorls") of axial roots with multiple orders of lateral branching. These root nodes develop acropetally as leaves emerge, and increase in diameter and number to support exponential shoot growth. My research had three primary objectives: (1) to evaluate the extent of genotypic variation in anatomical phenotypes across root nodes and develop optimal phenotyping strategies under different nitrogen conditions, (2) to identify nodal root traits or trait combinations associated with improved NUpE, and (3) to determine whether variation in root and leaf anatomy are strongly linked, and explore combinations of root and shoot phenotypes which could optimize NUE in maize.

TABLE OF CONTENTS

LIST OF FIGURES

LIST OF TABLES

ACKNOWLEDGEMENTS

I am grateful to my committee members, Jonathan Lynch, Kathy Brown, Gaby Monshausen, and Tim Ryan, for their invaluable support and feedback throughout my research and writing. As an advisor, Jonathan provided me with many opportunities to grow as a scientist and as a person, through international collaborations, remote field work, and by recruiting a talented and diverse lab group, which has been a privilege to work with. I am grateful to Kathy for her excellent feedback, professional advice, and encouragement, without which it would have been impossible to finish my chapters. I thank Gaby for sharing her scientific expertise, enthusiasm, and dedication, all of which I admire. I thank Tim for being an encouraging mentor, an imaging expert, and for bringing fresh and useful perspectives to my research.

For inspiration and comradery, I thank all of the lab group members, past and present. A shout-out to Hannah Schneider for noticing that first dust storm, and for many "fun" field seasons. Thanks to Molly Hanlon for being a role model in both the dissemination of science and baked goods. Many thanks to Tania Galindo-Castañeda, Anica Massas, Reham Abdalla, Harini Rangarajan, and others who welcomed me into the lab and inspired me with their grace, humor, and resilience. While I can't list every lab member, know that you are in my thoughts and also in many embarrassing photos taken through the years, which will bring fond memories – thank you.

For excellent technical support and undefeatable can-do attitudes, I thank Bob Snyder, Michael Williams, Johan Prinsloo, and Scott DiLoreto. A big thank you to Ben Hall for his innovative spirit and unwavering support. I am grateful to the dedicated undergraduates who made important contributions to this research, including Dannielle Gibson, Ainiz Fauzi, Cleoniki Kesidis, Pufan Wang, Jonathan Wu, Ryan Burnett, Garrett Morrison, and Katie Ayers. For funding and support, I thank Penn State's Huck Institutes Plant Biology Graduate Program, the College of Agriculture's Plant Science department, the USDA, the Howard G. Buffett Foundation, Edmund Optics, NVIDIA, and many other wonderful collaborators and facilities.

For moral support, I thank my first year Plant Biology cohort members – Lihua, Yue, Ningxiao, Tina, Bastian, Tim, and Nikki. I am grateful to my first year mentor, Claire, for her friendship and support. I appreciate the wonderful folks at Penn State's Community Garden, and the Bellefonte Children's Garden, both of which refreshed my mind and gave me the opportunity to grow many exciting plants other than corn.

I thank my scientific mentors who have inspired and encouraged me: Emily Buchholtz, Kristina Jones, Alden Griffith, Martina Königer, Jocelyne Dolce, Kaye Peterman, and others at

Wellesley College. I thank Tom Sharkey, Sean Weise, Ziru Li, and others at Michigan State, as well as the National Science Foundation for funding summer undergraduate research programs. I also thank the many dedicated teachers and mentors through my time in NH, MA, PA and beyond, who have shaped me and offered their wisdom and support along the way.

To all of my friends and family who kept me grounded through the years, and inspire me on a daily basis – a huge, heartfelt thank you! Some quick shout-outs: Karen, thanks for always "getting it" and being a wonderful friend. Grace, thanks for always reaching out with wise words. Mia, thanks for being a fellow plant nerd. Cynthia, thanks for your encouragement (and pies!). Alex, thanks for fun Catan nights and long chats. Jane, Becca, Rachel, Nicole – thank you for being there through highs and lows for many years. To Kirsty, thank you for your compassion, strength, and frequent encouragement to lead a balanced and mindful life. I thank Bella (though she would prefer treats to words) for being full of love, waggles, and enthusiasm for adventures.

Last but not least, I thank my sister, Melissa, and my parents, Steve and Kuochu Yang, for being with me every step of the way, encouraging me to pursue a love of reading, writing, and wondering, and continuing to inspire me with their integrity, courage, and perseverance toward a brighter tomorrow.

Chapter 1

General Introduction

The post-Green Revolution challenge

Maize, rice, and wheat are the most widely cultivated crops, and provide over 40 percent of food calories for the human population (FAO, 2016). Since the Green Revolution, cereal productivity has increased with the transition from traditional to intensive cultivation methods; reliance on on-farm inputs and local cultivars has been supplanted by the use of purchased chemical fertilizers, pesticides, mechanization, increased irrigation, and high density monocropping with commercial, high-yielding cultivars (FAO, 2016). This concerted approach substantially boosted global food production and reduced malnourishment and poverty in developing regions. However, in recent years, costs of agricultural intensification have begun to diminish returns; a re-invention of the food system is needed to address unprecedented acceleration of anthropogenic climate change, environmental degradation, and population growth. Therefore, the challenge of the post-Green Revolution era is to maintain or increase food production and nutrition with less land, water, and chemical inputs, while reducing greenhouse gas emissions and other ecological disruptors.

The cultivation of maize exemplifies this conundrum. At peak growth in July, the United States Midwest Corn Belt has the highest gross primary productivity of all terrestrial ecosystems on the planet, as well as the highest fertilization rates (Guanter et al., 2014; Dhital and Raun, 2016). Maize yields and fertilizer usage have risen together over the past half century, with fertilizer as the most expensive single input for maize production in the United States (USDA, 2016). Over half of applied nitrogen is not captured by plants, with an estimated 24% to 37% recovered in grain (Dhital and Raun, 2016). Globally, 17% of applied nitrogen in crop production is lost through leaching, 15% is lost as gaseous emissions such as nitrous oxide, and 9% is lost through erosion, surface runoff, or remains in soil (Liu et al., 2016). In addition to direct economic losses, these processes result in environmental damage and contribute to climate change. For example, fertilizer runoff from the Midwest Corn Belt contributed to the largest hypoxic “dead zone” ever recorded in the Gulf of Mexico this August (NOAA, 2017).

The United States accounts for about 35% of global maize production; however, the majority is used for animal feed (46%), fuel ethanol (29%), and exports (15%), with only 0.2% consumed as seed, and the remainder processed into food additives and industrial products (USDA, 2016). By contrast, maize in developing regions is essential for nourishment, yet yields are fractional, due to poor soil quality, lack of fertilizer and other agronomic disadvantages in smallholder farms (Vitousek, 2009). Rapid population growth and climate change will disproportionately impact these regions; for example, maize yields in Africa are projected to decrease by 20% due to climate change, and maize imports to meet demand in developing nations could triple by 2050 (FAO, 2016).

Breeding for nitrogen use efficiency

One sustainable strategy for addressing both excessive and deficient nitrogen is through breeding maize varieties with greater nitrogen use efficiency (NUE), defined as the grain yield per unit of available soil nitrogen (Moll et al., 1982). Enhanced NUE varieties could produce greater yield for a given level of applied nitrogen (nitrogen "responsiveness"), or maintain yields in reduced or nitrogen-deficient conditions (yield "stability"); these objectives would require testing under appropriate nitrogen conditions. Both approaches could involve enhancing the acquisition of soil nitrogen by roots, termed nitrogen uptake efficiency (NUpE), and/or improving the conversion of the acquired nitrogen into grain, primarily through assimilation and remobilization of nitrogen in the shoot, termed nitrogen utilization efficiency (NUtE) (Moll et al., 1982).

Evaluating NUE is straightforward; if soil nitrogen is uniform across an experimental condition, dry grain weight is sufficient for comparing NUE among maize genotypes. The NUpE and NUtE components can be derived from measuring total shoot nitrogen at silking and at physiological maturity, and grain nitrogen content at maturity (Moll et al., 1982). Variation for both NUtE and NUpE has been demonstrated in maize germplasm (e.g. summarized in Brauer and Shelp, 2010). In recent decades, agronomic improvements combined with selection for greater yield under high planting densities has resulted in modest NUE gains in modern maize varieties, with increased post-silking nitrogen uptake as an important contributor (Tollenaar and Lee, 2002; Boomsma et al., 2009; Ciampitti and Vyn, 2012; York et al., 2015; Chen et al., 2016; Dhital and Raun, 2016; DeBruin et al., 2017). In maize, nitrogen status at kernel set about two

weeks pre-anthesis, as well as post-anthesis nitrogen uptake, are critical for grain yield (Hirel et al., 2007).

Improvement of nitrogen uptake and utilization efficiency is complicated by many interacting genetic and environmental factors. Strategies for enhancing NUE can be broad and indirect (e.g. selecting for better yield under higher planting density), targeted and trait-based (e.g. altered expression of nitrate transporters), or select for plasticity and trait combinations (for crops in general, Hirel et al., 2007; Good et al., 2007; Garnett et al., 2009; Masclaux-Daubresse et al., 2010; Foyer et al., 2011; Kant et al., 2011; Han et al., 2015; Fan et al., 2017; Li et al., 2017; Havé et al., 2017; for maize, Moll et al., 1982; Kamprath et al., 1982; Lee et al., 1992; Greef, 1994; Pan et al., 1995; Muchow and Davis, 1998; Rajcan and Tollenaar, 1999; Hirel et al., 2001; Borrell et al., 2001; Presterl et al., 2002; Worku et al., 2007; Boomsma et al., 2009; Zhang et al., 2010; Cañas et al., 2012; Liu et al., 2012; Zamboni et al., 2014; Yu et al., 2015 a, b; Li et al., 2015; Han et al., 2015; Plett et al., 2016; Li et al., 2016; Mu et al., 2016; Ning et al., 2017). Under low nitrogen, adaptive responses increase NUpE in maize; these responses could be exploited to enhance NUpE under high nitrogen (e.g. Gaudin et al., 2011 a, b; Gao et al., 2015). As such, there is substantial breeding potential for improved NUpE for high nitrogen, without tradeoffs under low nitrogen.

Nitrogen availability and acquisition

Nitrogen acquisition in plants occurs by the absorption of nitrate (NO_3^-) and ammonium (NH_4^+) ions, and in lesser quantities urea and amino acids, which are dissolved in the soil solution. Soil nitrogen is generated through the fixation of unreactive atmospheric nitrogen (N_2) into reactive, organic nitrogen, either by nitrogen-fixing soil microbes or synthetically (e.g. through the Haber-Bosch process) and applied as fertilizer. In addition, organic matter is mineralized (decomposed) into ammonium, with rates of conversion depending on temperature, moisture, and aeration. Soil microorganisms rapidly convert ammonium into nitrate through the process of nitrification. In typical, non-flooded agricultural soils, nitrate is the predominant form of plant-available nitrogen (Bacon, 1995), and is the preferred form of nitrogen taken up by maize plants.

However, soil nitrate availability is spatiotemporally dynamic; due to the negative charge of soil particles, nitrate is highly mobile and leaches with water. Particularly in sandy soils, nitrate

can move rapidly into deep soil horizons with each precipitation or irrigation event; this occurs to a lesser extent in soils with high clay content. Additionally, in wet soils, denitrification can occur; soil bacteria convert nitrate into nitrous oxide, which is lost to the atmosphere. Conversely, in dry conditions, ammonium can be volatilized and lost as ammonia (NH_3), which commonly occurs when urea fertilizers are surface-applied. Thus, nitrate acquisition by plants must be sensitive to temporal and spatial heterogeneity (Bacon, 1995).

Under optimal conditions, with high nutrient and water availability, maize can acquire sufficient nitrate entirely through transpiration-driven mass flow (Okajima and Taniyama, 1980). In this process, dissolved nitrate is brought to the surface of root apical zones as the plant transpires (Reidenbach and Horst, 1997). Transporter proteins (also called "transceptors" due to dual roles of ion transport and sensing) embedded in the root epidermis actively transport nitrate across the plasma membrane; these include various high-affinity transporters (HATs) active at low nitrate concentrations, low-affinity transporters (LATs) active at high nitrate concentrations, and dual-affinity transporters which can switch modes (Glass, 2009; Bouguyon et al., 2012; Nacry et al., 2013). Thus, transporter activity, local nitrate concentrations, and transpiration rates influence nitrate acquisition through mass flow (Reidenbach and Horst, 1997; Gorska et al., 2008).

At low concentrations, nitrate uptake can occur via diffusion, in which nitrate passively moves from higher concentrations in the bulk soil solution toward the root surface, where it is absorbed; the root surface must be in contact with the soil, and nutrients must be located within millimeters of the root to be acquired. Thus, root length density, root hair density, root diameter, and soil properties such as bulk density and moisture can strongly influence this process. Ammonium, which is positively charged and thus adheres strongly to soil particles, is also acquired primarily through diffusion, and high affinity ammonium transporters (Bacon, 1995; Nacry et al., 2013).

Nitrogen assimilation and utilization

Once acquired, nitrate is transported across the root cortex into xylem for translocation to shoots, or stored locally in root cell vacuoles (Bloom et al., 2012). Nitrate assimilation, its conversion into usable forms within the plant, is catalyzed by several enzymes, and primarily takes place in shoot tissues due to its high carbon requirement (Bloom et al., 2012). Nitrate

reductase converts nitrate to nitrite, nitrite reductase converts nitrate to ammonium, which is then used to synthesize amino acids through the glutamine synthetase and glutamine-2-oxoglutarate aminotransferase (GOGAT) cycle and other aminotransferases (reviewed in Xu et al., 2012). The amino acids are then incorporated into essential molecules such as chlorophyll, Rubisco and other proteins, DNA and RNA nucleotides, and cell wall and cell membrane components.

In maize, nitrate is accumulated in the leaves and stalk during early, vegetative growth, to be remobilized for ear and kernel development post-anthesis (Hirel et al., 2001). Remobilization accounts for about half of grain nitrogen in maize, and the remainder is acquired post-anthesis (Hirel et al., 2007), with some variation among genotypes (e.g. Rajcan and Tollenaar, 1999). In nitrogen deficient conditions, nitrogen is first remobilized from the stalk and the oldest, basal leaves, leading to earlier senescence of lower leaves. The upper leaves, and the flag leaf in particular, maintain the highest light capture and photosynthesis rates. Additionally, as a C4 plant, maize photosynthetic NUE is high, with optimal leaf anatomy and reduced Rubisco needed compared to C3 plants (Oaks, 1994).

Thus, genotypic variation in leaf development and shoot traits, and the timing of sink-source transitions (e.g. how much nitrogen a leaf can accumulate prior to becoming a net exporter, followed by leaf senescence) could be important for nitrogen utilization efficiency. Nitrogen remobilization from roots, by contrast, is minimal; therefore, NUE could potentially be improved by minimizing excess root construction costs. Delayed leaf senescence and prolonged root activity post-anthesis have been associated with greater NUE (Rajcan and Tollenaar, 1999).

Additional efforts relevant for improving NUtE in maize have included mapping genetic loci associated with carbon and nitrogen metabolism (Hirel et al., 2001; Zhang et al., 2010; Zhang et al., 2014); mapping genetic loci for leaf angle, number, width, and length (Tian et al., 2011; Wassom, 2013); understanding optimization of within-leaf nitrogen allocation among chloroplasts and proteins under nitrogen stress (Mu et al., 2016); and comparing genotypic variation in root-shoot allocation under nitrogen stress (Sen et al., 2016). Many of these studies used populations of recombinant inbred lines such as IBM (intermated B73 x Mo17) to discern the effects of genetics, environment (or nitrogen treatment), and the interaction of genes by environment (G x E).

Root system phenotypes and functions

Compared to maize shoot traits for improving NUE, root system phenotypes and rhizospheric interactions have been underexplored and are difficult to study, yet have strong potential for influencing nitrate acquisition. In the first two weeks of growth, the maize root system consists of a seed-borne primary root and a variable number of seminal roots ("embryonic root system"), followed by lateral branching and the first node of shoot-borne roots ("early post-embryonic"). These are genetically distinct from the development of later shoot-borne nodal roots ("late post-embryonic"), including axial (conducting) and lateral (absorption) roots, which emerge acropetally through development either belowground ("crown") or aboveground ("brace") (Hochholdinger et al., 2004). These nodal roots comprise the bulk of the root system, and are typically responsible for the majority of water and nutrient uptake through growth.

Root anatomy, the internal arrangement of cells and tissues within the root, can influence the construction and respiratory costs of root segments, the hydraulic conductance rate, microbial colonization, mechanical strength in terms of plant anchorage and soil penetration, and resilience to damage from pests and other stress, which can determine the longevity of the root. The maize root is composed of a cortex (outer cylinder) and stele (inner cylinder). The outermost protective root epidermis has small cells which slough off and becomes degraded as the root matures; this is often replaced in function by a suberized hypodermis (or exodermis), the outermost layer of cortical cells (Hose et al., 2001). Cortical cell layers of "files" occur radially, with cell sizes differing from the outer to inner files. The innermost file is the endodermis, a suberized barrier of small cells which regulate entry of molecules into the stele. Cortical cells can be replaced with lysigenous aerenchyma, or air spaces, which form through programmed cell death as the root ages and in response to stress (Jackson and Armstrong, 1999). Within the stele, mature roots have a ring of large metaxylem vessels (McCully, 1995), surrounded by smaller protoxylem and phloem tissue, with a central pith of parenchyma cells. Lateral roots are initiated from the pericycle, the outermost layer of the stele.

In general, thicker roots with a greater density of living cells (e.g. many, small cells), thicker cell walls, and less aerenchyma will incur greater carbon and nitrogen construction costs. A greater proportion of living tissue (e.g. less aerenchyma, less vessel area) will increase respiratory costs (Jaramillo et al., 2013). Root respiration, supporting nitrate assimilation in particular, demand the greatest proportion of carbon allocated to roots (e.g. Kramer and Boyer, 1995; Bloom et al., 2012). Thicker roots with dense tissue and a strong stele can improve root

penetration strength in compacted soils, and improve plant anchorage, which can reduce root lodging (Stamp and Kiel, 1992; Liu et al., 2012; Jin et al., 2013; Chimungu et al., 2015).

Hydraulic conductance, determined by the resistance (e.g. in cell membranes) in the path from the root surface to and through the vessels, can be limited radially and axially; a greater proportion of aerenchyma can reduce hydraulic conductance rates (Fan et al., 2007), whereas a larger proportion of vessel area, and larger metaxylem vessel diameters in particular, can substantially increase hydraulic conductance (Richards and Passioura, 1989; Li and Shao, 2003; Kirkham, 2005). Finally, greater living cortical area could potentially increase beneficial mycorrhizal colonization, or lead to greater pathogen susceptibility (Tania Galindo-Castañeda, personal communication).

Previous studies of maize genotypes have found variation in anatomical traits such as the root diameter, cortex to stele area ratio, number of cortical and stele cell files, cell diameters, number and diameter of vessels, and percent of aerenchyma in the cortex (e.g. Stamp and Kiel 1992; Burton et al., 2014; Gao et al., 2015; York et al., 2015). Root system strategies proposed to improve nitrogen acquisition have included anatomical traits. For example, Lynch (2013) proposed a "steep, cheap, and deep" hypothesis, which suggests anatomical traits that reduce metabolic costs could allocate more carbon to rapid root elongation, increase depth distribution, and "chase" leaching nitrate and water. Elements of this hypothesis have been tested in maize inbred lines; for example, Chimungu et al. (2014 a, b) found that fewer cortical cell files and larger cortical cells reduced root segment respiration, resulting in deeper rooting and improved drought tolerance. Similarly, Saengwilai et al. (2014) found that increased cortical aerenchyma reduced metabolic costs of roots, increased rooting depth, and improved nitrogen stress tolerance. By contrast, Schmidt and Gaudin (2016) proposed a strategy for irrigated systems, hypothesizing that traits should maximize hydraulic conductance, beneficial microbial interactions, and have strong plasticity (or responsiveness) to local water and nutrient availability.

However, these broad physiological mechanisms – such as metabolic efficiency, hydraulic conductance, and growth rate – are important beyond the root system, and may have integrated shoot responses. Root and shoot trait gene mapping efforts have largely occurred in isolation, yet genes which affect root system architecture and anatomy could have pleiotropic effects on shoot growth and development. For example, both root and shoot meristem development involve key genes such as WUSCHEL and SCARECROW (Laux et al., 2004; Slewinski et al., 2012). An integrated ideotype which optimizes root traits for nitrogen uptake and shoot development for nitrogen utilization efficiency must be prefaced by an understanding of

which root and shoot traits may have strong genetic linkages. Therefore, in conjunction with focal root anatomy traits, my research included a novel, parallel assessment of leaf traits, including leaf lamina and midrib anatomy, to understand these relationships.

Finally, the effect of root anatomy and other structural traits on nitrate acquisition must be considered in context of nitrogen conditions. Nitrate is a signaling molecule; genotypes have coordinated root and shoot responses to perceived levels of nitrogen, and further understanding of the effect of nitrate on maize root system phenotypes, through hormone-mediated and other signaling pathways, is needed (e.g. Forde and Lorenzo, 2001; Rellán-Álvarez et al., 2016). Nitrate transporters in the model plant Arabidopsis have been shown to facilitate auxin accumulation in lateral root primordia; high nitrate levels inhibit transporter activity and auxin transport, inhibiting lateral root development (Krouk et al., 2010). Low nitrogen stimulates increased carbon allocation to roots, but partitioning among root classes, structures, and metabolism could vary among genotypes.

There are several important considerations in evaluating root system phenotypes. To discern genotypic contrast, controlled conditions are optimal; thus, plants are often screened at early growth stages indoors, in artificial media. However, these results do not translate well into the field, due to substantial root plasticity and interactions between genotype and environment, as well as differences in root development as the plant matures (e.g. Meister et al., 2014; Kuijken et al., 2015). Therefore, my research employed multiple field and greenhouse studies for in-depth characterization of anatomical variation across maize root nodes among inbred and hybrid genotypes, as well as root architecture traits such as nodal root number, and leaf anatomy and shoot morphology. Root depth, carbon and nitrogen costs, conductance, photosynthesis, biomass partitioning, and yield under high and low nitrogen conditions were evaluated, with the goal of identifying and integrating beneficial phenotypes for enhanced NUE in maize.

Additional perspectives

The goal of improving nitrogen use efficiency in crop production in a timely, sustainable manner requires the integration of interacting genetics, environment, and management (often denoted as G x E x M), and a strategic understanding of the gains possible from each of these elements. Additional topics which deserve attention include breeding for multiple interacting stresses (e.g. drought and low nitrogen; Dathe et al., 2016), the effect of soil properties and

management on root growth (e.g. Gao et al., 2015; Thorup-Kristensen and Kirkegaard, 2016), the effect of different nitrogen forms and cycling (e.g. rates of mineralization, nitrification inhibitors, and compensatory ammonium uptake; Andrews et al., 2013; Misselbrook et al., 2014; Osterholz et al., 2017; Hachiya and Sakakibara, 2017), and polyculture methods for nutrient management (e.g. crop rotations, interplanting; Tiemann et al., 2015; Finney and Kaye, 2016; Weiner, 2017).

Beyond optimizing maize breeding strategies, agriculture-based NUE improvement can come from development of crop species to maximize nutrition, biodiversity, resource use efficiency, and stress resilience, including directing research funding toward native food crops and perennials (Glover et al., 2010; Massawe et al., 2016; Osterberg et al., 2017). Moonshot goals, such as breeding nitrogen-fixing cereals (Fox et al., 2016; Vicente and Dean, 2017; Dent and Cocking, 2017) and converting crops from C3 to C4 photosynthesis (Burnell, 2011; Covshoff and Hiberd, 2012), are also underway.

Finally, global NUE could be improved through changes in human diet, government policy, and reducing food waste (Townsend and Howarth, 2010; Seitzinger and Phillips, 2017). About three-quarters of global crop production is currently used for livestock feed (Lassaletta et al., 2016), and reducing meat consumption would substantially reduce global nitrogen input in the food system (Liu et al., 2016), and greenhouse gas emissions (Garnett, 2011). Effective policies which improve NUE could guide socioeconomic development forward to meet food demands, reduce nitrogen pollution, and sustain human growth in the long term (Zhang et al., 2015).

Objectives

The objectives of this research were:

To develop effective phenotyping procedures and characterize variation in maize root anatomy across nodes, for hybrid and inbred maize genotypes, under different nitrogen conditions (Chapter 2);

To identify nodal root phenotypes associated with improved nitrogen use efficiency among hybrid and inbred maize genotypes (Chapter 2);

To evaluate anatomical phenotypes in context of root architecture, and identify effective root trait combinations for improved nitrogen uptake efficiency (Chapter 3);

To evaluate the relationship between leaf and root anatomy traits, and identify effective combinations of root and shoot traits for improved nitrogen use efficiency (Chapter 4).

References

Andrews M, Raven JA, Lea PJ. 2013. Do plants need nitrate? the mechanisms by which nitrogen form affects plants. Annals of Applied Biology **163**, 174–199.

Bacon, P. 1995. Nitrogen Fertilization in the Environment. 1st ed. CRC Press.

Bloom AJ, Randall L, Taylor AR, Silk WK. 2012. Deposition of ammonium and nitrate in the roots of maize seedlings supplied with different nitrogen salts. Journal of Experimental Botany **63**, 1997–2006.

Boomsma CR, Santini JB, Tollenaar M, Vyn TJ. 2009. Maize morphophysiological responses to intense crowding and low nitrogen availability: An analysis and review. Agronomy Journal **101**, 1426–1452.

Borrell BA, Hammer G, van Oosterom E. 2001. Stay-green : A consequence of the balance between supply and demand for nitrogen during grain filling ? Annals of Applied Biology **138**, 91–95.

Bouguyon E, Gojon A, Nacry P. 2012. Nitrate sensing and signaling in plants. Seminars in Cell and Developmental Biology **23**, 648–654.

Brauer EK, Shelp BJ. 2010. Nitrogen use efficiency: re-consideration of the bioengineering approach. Botany **88**, 103–109.

Burnell JN. 2011. Hurdles to Engineering Greater Photosynthetic Rates in Crop Plants: C4 Rice. In: Raghavendra AS,, In: Sage RF, eds. C4 Photosynthesis and Related CO2 Concentrating Mechanisms. Springer Science+Business Media B.V., 361–378.

Burton AL, Johnson J, Foerster J, Hanlon MT, Kaeppler SM, Lynch JP, Brown KM. 2014. QTL mapping and phenotypic variation of root anatomical traits in maize (Zea mays L.). Theoretical and Applied Genetics **128**, 93–106.

Cañas RA, Quilleré, Gallais A, Hirel B. 2012. Can genetic variability for nitrogen metabolism in the developing ear of maize be exploited to improve yield? New Phytologist **194**, 440–452.

Chen K, Camberato JJ, Tuinstra MR, Kumudini S V., Tollenaar M, Vyn TJ. 2016. Genetic improvement in density and nitrogen stress tolerance traits over 38 years of commercial maize hybrid release. Field Crops Research **196**, 438–451.

Chimungu JG, Loades KW, Lynch JP. 2015. Root anatomical phenes predict root penetration ability and biomechanical properties in maize (Zea Mays). Journal of Experimental Botany **66**, 3151–3162.

Chimungu JG, Brown KM, Lynch JP. 2014. Reduced root cortical cell file number improves drought tolerance in maize. Plant Physiology **166**, 1943–1955.

Chimungu JG, Brown KM, Lynch JP. 2014. Large root cortical cell size improves drought tolerance in maize. Plant Physiology **166**, 2166–2178.

Ciampitti IA, Vyn TJ. 2012. Physiological perspectives of changes over time in maize yield dependency on nitrogen uptake and associated nitrogen efficiencies: A review. Field Crops Research **133**, 48–67.

Covshoff S, Hibberd JM. 2012. Integrating C 4 photosynthesis into C 3 crops to increase yield potential. Current Opinion in Biotechnology **23**, 209–214.

Cox TS, Crews TE, Culman SW, *et al.* 2010. Increased Food and Ecosystem Security via Perennial Grains. Science **328**, 1638–1639.

Dathe A, Postma JA, Postma-Blaauw MB, Lynch JP. 2016. Impact of axial root growth angles on nitrogen acquisition in maize depends on environmental conditions. Annals of Botany **118**, 401–14.

DeBruin JL, Schussler JR, Mo H, Cooper M. 2017. Grain Yield and Nitrogen Accumulation in Maize Hybrids Released during 1934 to 2013 in the US Midwest. Crop Science **57**, 1–16.

Dent D, Cocking E. 2017. Establishing symbiotic nitrogen fixation in cereals and other non - legume crops : The Greener Nitrogen Revolution. Agriculture & Food Security, 1–9.

Dhital S, Raun WR. 2016. Variability in optimum nitrogen rates for maize. Agronomy Journal **108**, 2165–2173.

Fan M, Bai R, Zhao X, Zhang J. 2007. Aerenchyma formed under phosphorus deficiency contributes to the reduced root hydraulic conductivity in maize roots. Journal of Integrative Plant Biology **49**, 598–604.

Fan X, Naz M, Fan X, Xuan W, Miller AJ, Xu G. 2017. Plant nitrate transporters: from gene function to application. Journal of Experimental Botany, 1–13.

FAO. 2016. *Save and grow in practice: maize, rice and wheat. A guide to sustainable cereal production.*

Finney DM, Kaye JP. 2017. Functional diversity in cover crop polycultures increases multifunctionality of an agricultural system. Journal of Applied Ecology **54**, 509–517.

Forde BG, Lorenzo H. 2001. The nutritional control of root development. Plant and Soil **232**, 51–68.

Fox AR, Soto G, Valverde C, *et al.* 2016. Major cereal crops benefit from biological nitrogen fixation when inoculated with the nitrogen-fixing bacterium Pseudomonas protegens Pf-5 X940. Environmental Microbiology **18**, 3522–3534.

Foyer CH, Noctor G, Hodges M. 2011. Respiration and nitrogen assimilation: Targeting mitochondria-associated metabolism as a means to enhance nitrogen use efficiency. Journal of Experimental Botany **62**, 1467–1482.

Gao K, Chen F, Yuan L, Zhang F, Mi G. 2015. A comprehensive analysis of root morphological changes and nitrogen allocation in maize in response to low nitrogen stress. Plant, Cell and Environment **38**, 740–750.

Gao W, Hodgkinson L, Jin K, *et al.* 2016. Deep roots and soil structure. Plant, Cell and Environment **39**, 1662–1668.

Garnett T. 2011. Where are the best opportunities for reducing greenhouse gas emissions in the food system (including the food chain)? Food Policy **36**, S23–S32.

Garnett T, Conn V, Kaiser BN. 2009. Root based approaches to improving nitrogen use efficiency in plants. Plant, Cell and Environment **32**, 1272–1283.

Gaudin ACM, McClymont SA, Raizada MN. 2011. The nitrogen adaptation strategy of the wild teosinte ancestor of modern maize, Zea mays subsp. parviglumis. Crop Science **51**, 2780–2795.

Gaudin ACM, McClymont SA, Holmes BM, Lyons E, Raizada MN. 2011. Novel temporal, fine-scale and growth variation phenotypes in roots of adult-stage maize (Zea mays L.) in response to low nitrogen stress. Plant, Cell and Environment **34**, 2122–2137.

Glass ADM. 2009. Nitrate uptake by plant roots. Botany **87**, 659–667.

Good AG, Johnson SJ, De Pauw M, Carroll RT, Savidov N, Vidmar J, Lu Z, Taylor G, Stroeher V. 2007. Engineering nitrogen use efficiency with alanine aminotransferase. Canadian Journal of Botany **85**, 252–262.

Gorska A, Zwieniecka A, Michele Holbrook N, Zwieniecki MA. 2008. Nitrate induction of root hydraulic conductivity in maize is not correlated with aquaporin expression. Planta **228**, 989–998.

Greef JM. 1994. Productivity of Maize (Zea mays L.) in Relation to Morphological and Physiological Characteristics under Varying Amounts of Nitrogen Supply. Journal of Agronomy and Crop Science **172**, 317–326.

Guanter L, Zhang Y, Jung M, *et al.* 2014. Global and time-resolved monitoring of crop photosynthesis with chlorophyll fluorescence. Proceedings of the National Academy of Sciences of the United States of America **111**, E1327-33.

Hachiya T, Sakakibara H. 2016. Interactions between nitrate and ammonium in their uptake, allocation, assimilation, and signaling in plants. Journal of Experimental Botany **68**, erw449.

Han M, Okamoto M, Beatty PH, Rothstein SJ, Good AG. 2015. The Genetics of Nitrogen Use Efficiency in Crop Plants. Annu. Rev. Genet **49**, 1–9.

Havé M, Marmagne A, Chardon F, Masclaux-Daubresse C. 2016. Nitrogen remobilisation during leaf senescence: lessons from Arabidopsis to crops. Journal of Experimental Botany **68**, erw365.

Hirel B, Bertin P, Quilleré I, *et al.* 2001. Towards a Better Understanding of the Genetic and Physiological Basis for Nitrogen Use Efficiency in Maize. Plant Physiology **125**, 1258 LP-1270.

Hirel B, Le Gouis J, Ney B, Gallais A. 2007. The challenge of improving nitrogen use efficiency in crop plants: Towards a more central role for genetic variability and quantitative genetics within integrated approaches. Journal of Experimental Botany **58**, 2369–2387.

Hochholdinger F, Woll K, Sauer M, Dembinsky D. 2004. Genetic dissection of root formation in maize (Zea mays) reveals root-type specific developmental programmes. Annals of Botany **93**, 359–68.

Hose E, Clarkson DT, Steudle E, Schreiber L, Hartung W. 2001. The exodermis: a variable apoplastic barrier. Journal of experimental botany **52**, 2245–2264.

Jackson MB, Armstrong W. 1999. Formation of Aerenchyma and the Processes of Plant Ventilation in Relation to Soil Flooding and Submergence. Plant Biology **1**, 274–287.

Jaramillo RE, Nord EA, Chimungu JG, Brown KM, Lynch JP. 2013. Root cortical burden influences drought tolerance in maize. Annals of Botany **112**, 429–437.

Jin K, Shen J, Ashton RW, Dodd IC, Parry MAJ, Whalley WR. 2013. How do roots elongate in a structured soil? Journal of Experimental Botany **64**, 4761–4777.

Kamprath EJ, Moll RH, Rodriguez N. 1982. Effects of nitrogen fertilization and recurrent selection on performance of hybrid populations of corn. Agronomy Journal **74**, 955–958.

Kant S, Bi Y, Rothstein SJ. 2011. Understanding plant response to nitrogen limitation for the improvement of crop nitrogen use efficiency. Journal of experimental botany **62**, 1499–509.

Kirkham MB. 2005. Principles of soil and plant water relations. Elsevier Academic Press.

Kramer PS, Boyer JS. 1995. Water relations of plants and soils. Academic Press, Inc.

Krouk G, Lacombe B, Bielach A, *et al.* 2010. Nitrate-regulated auxin transport by NRT1.1 defines a mechanism for nutrient sensing in plants. Developmental Cell **18**, 927–937.

Kuijken RCP, Van Eeuwijk FA, Marcelis LFM, Bouwmeester HJ. 2015. Root phenotyping: From component trait in the lab to breeding. Journal of Experimental Botany **66**, 5389–5401.

Lassaletta L, Billen G, Garnier J, Bouwman L, Velazquez E, Mueller ND, Gerber JS. 2016. Nitrogen use in the global food system: Past trends and future trajectories of agronomic performance, pollution, trade, and dietary demand. Environmental Research Letters **11**, 1–14.

Laux T, Würschum T, Breuninger H. 2004. Genetic regulation of embryonic pattern formation. The Plant Cell **16 Suppl**, S190–S202.

Lee RB, Purves J V., Ratcliffe RG, Saker LR. 1992. Nitrogen assimilation and the control of ammonium and nitrate absorption by maize roots. Journal of Experimental Botany **43**, 1385–1396.

Li F, Chung T, Pennington JG, Federico ML, Kaeppler HF, Kaeppler SM, Otegui MS, Vierstra RD. 2015. Autophagic Recycling Plays a Central Role in Maize Nitrogen Remobilization. The Plant Cell **27**, tpc.15.00158.

Li H, Hu B, Chu C. 2017. Nitrogen use efficiency in crops: lessons from Arabidopsis and rice. Journal of Experimental Botany **68**, 2477–2488.

Li P, Zhuang Z, Cai H, Cheng S, Soomro AA, Liu Z, Gu R, Mi G, Yuan L, Chen F. 2016. Use of genotype-environment interactions to elucidate the pattern of maize root plasticity to nitrogen deficiency. Journal of Integrative Plant Biology **58**, 242–253.

Li Y, Shao M. 2003. Responses of Radial and Axial Hydraulic Resistances in Maize Root to Nitrogen Availability. Journal of Plant Nutrition **26**, 821–834.

Liu J, Ma K, Ciais P, Polasky S. 2016. Reducing human nitrogen use for food production. Scientific Reports **6**, 30104.

Liu R, Zhang H, Zhao P, Zhang Z, Liang W, Tian Z, Zheng Y. 2011. Mining of Candidate Maize Genes for Nitrogen Use Efficiency by Integrating Gene Expression and QTL Data. Plant Molecular Biology Reporter **30**, 297–308.

Liu S, Song F, Liu F, Zhu X, Xu H. 2012. Effect of Planting Density on Root Lodging Resistance and Its Relationship to Nodal Root Growth Characteristics in Maize (Zea mays L.). Journal of Agricultural Science **4**, 182–189.

Lynch JP. 2013. Steep, cheap and deep: an ideotype to optimize water and N acquisition by maize root systems. Annals of Botany **112**, 347–57.

Masclaux-Daubresse C, Daniel-Vedele F, Dechorgnat J, Chardon F, Gaufichon L, Suzuki A. 2010. Nitrogen uptake, assimilation and remobilization in plants: Challenges for sustainable and productive agriculture. Annals of Botany **105**, 1141–1157.

Massawe F, Mayes S, Cheng A. 2016. Crop Diversity: An Unexploited Treasure Trove for Food Security. Trends in Plant Science **21**, 365–368.

Mccully M. 1995. How Do Real Roots Work? Plant Physiol **109**, 1–6.

Meister R, Rajani MS, Ruzicka D, Schachtman DP. 2014. Challenges of modifying root traits in crops for agriculture. Trends in Plant Science **19**, 779–788.

Misselbrook TH, Cardenas LM, Camp V, Thorman RE, Williams JR, Rollett AJ, Chambers BJ. 2014. An assessment of nitrification inhibitors to reduce nitrous oxide emissions from UK agriculture. Environmental Research Letters **115006**, 1–11.

Moll RH, Kamprath EJ, Jackson WA. 1982. Analysis and Interpretation of Factors Which Contribute to Efficiency of Nitrogen Utilization 1. Agronomy Journal **74**, 562–564.

Mu X, Chen Q, Chen F, Yuan L, Mi G. 2016. Within-Leaf Nitrogen Allocation in Adaptation to Low Nitrogen Supply in Maize during Grain-Filling Stage. Frontiers in Plant Science **7**, 1–11.

Muchow RC. 1998. Nitrogen utilization efficiency in maize and grain sorghum. Field Crops Research **56**, 209–216.

Nacry P, Bouguyon E, Gojon A. 2013. Nitrogen acquisition by roots: Physiological and developmental mechanisms ensuring plant adaptation to a fluctuating resource. Plant and Soil **370**, 1–29.

Ning P, Fritschi FB, Li C. 2017. Temporal dynamics of post-silking nitrogen fluxes and their effects on grain yield in maize under low to high nitrogen inputs. Field Crops Research **204**, 249–259.

NOAA. 2017. Cited Aug 28, 2017. http://www.noaa.gov/media-release/gulf-of-mexico-dead-zone-is-largest-ever-measured

Oaks A. 1994. Efficiency of nitrogen utlization in C3 and C4 cereals. Plant Physiol. **106**, 407 414.

Okajima H, Taniyama I. 1980. Significance of mass flow in nitrate-nitrogen supply to plant roots. Soil Science and Plant Nutrition **26**, 363–374.

Østerberg JT, Xiang W, Olsen LI, *et al.* 2017. Accelerating the Domestication of New Crops: Feasibility and Approaches. Trends in Plant Science **22**, 373–384.

Osterholz WR, Rinot O, Liebman M, Castellano MJ. 2017. Can mineralization of soil organic nitrogen meet maize nitrogen demand? Plant and Soil **415**, 73–84.

Pan WL, Camberato JJ, Moll RH, Kamprath EJ, Jackson WA. 1995. Altering source-sink relationships in prolific maize hybrids: Consequences for nitogen uptake and remobilization. Crop Science **35**, 836–845.

Plett D, Baumann U, Schreiber AW, *et al.* 2016. Maize maintains growth in response to decreased nitrate supply through a highly dynamic and developmental stage-specific transcriptional response. Plant Biotechnology Journal **14**, 342–353.

Presterl T, Groh S, Landbeck M, W.Schmidt, Geiger HH. 2002. Nitrogen uptake and utilization efficiency of European maize hybrids developed under conditions of low and high nitrogen input. Plant Breeding Reviews **121**, 480–486.

Rajcan I, Tollenaar M. 1999. Source : sink ratio and leaf senescence in maize: wII. Nitrogen metabolism during grain filling. Field Crops Research **60**, 255–265.

Reidenbach G, Horst WJ. 1997. Nitrate-uptake capacity of different root zones of Zea mays (L.) in vitro and in situ. Plant and Soil, 295–300.

Rellán-Álvarez R, Lobet G, Dinneny JR. 2016. Environmental control of root system biology. Annual Reviews Plant Biology **67**, 1–26.

Richards RA, Passioura JB. 1989. A breeding program to reduce the diameter of the major xylem vessel in the seminal roots of wheat and its effect on grain yield in rain-fed environments. Australian Journal of Agricultural Research (Australia) **v. 40**.

Sen S, Smith ME, Setter T. 2016. Effects of low nitrogen on chlorophyll content and dry matter accumulation in maiz. African Journal of Agricultural Research **11**, 1001–1007.

Saengwilai P, Nord E a, Chimungu JG, Brown KM, Lynch JP. 2014. Root cortical aerenchyma enhances nitrogen acquisition from low-nitrogen soils in maize. Plant Physiology **166**, 726–735.

Schmidt JE, Gaudin ACM. 2017. Toward an Integrated Root Ideotype for Irrigated Systems. Trends in Plant Science **22**, 433–443.

Seitzinger SP, Phillips L. 2017. Nitrogen stewardship in the Anthropocene. Science **357**, 3–5

Stamp P, Kiel C. 1992. Root Morphology of Maize and Its Relationship to Root Lodging. Journal of Agronomy and Crop Science **168**, 113–118.

Slewinski TL, Anderson AA, Zhang C, Turgeon R. 2012. Scarecrow plays a role in establishing Kranz anatomy in maize leaves. Plant and Cell Physiology **53**, 2030–2037.

Thorup-Kristensen K, Kirkegaard J. 2016. Root system-based limits to agricultural productivity and efficiency : the farming systems context. Annals of Botany **118**, 573–592.

Tian F, Bradbury PJ, Brown PJ, Hung H, Sun Q, Flint-Garcia S, Rocheford TR, McMullen MD, Holland JB, Buckler ES. 2011. Genome-wide association study of leaf architecture in the maize nested association mapping population. Nature Genetics **43**, 159–162.

Tiemann LK, Grandy AS, Atkinson EE, Marin-Spiotta E, Mcdaniel MD. 2015. Crop rotational diversity enhances belowground communities and functions in an agroecosystem. Ecology Letters **18**, 761–771.

Tollenaar M, Lee EA. 2002. Yield potential, yield stability and stress tolerance in maize. Field Crops Research **75**, 161–169.

Townsend AR, Howarth RW. 2010. Fixing the Global Nitrogen Problem. Scientific American, 64–71.

USDA. 2016. Economic Research Service. Cited Aug 28, 2017. https://www.ers.usda.gov/data-products/

Vicente EJ, Dean DR. 2017. Keeping the nitrogen-fixation dream alive. Proceedings of the National Academy of Sciences **114**, 201701560.

Vitousek P.M. et al. 2009. Nutrient imbalances in agricultural development. Science **324**, 1519–1520.

Wassom JJ. 2013. Quantitative trait loci for leaf angle, leaf width, leaf length, and plant height in a maize (Zea mays L) B73 × Mo17 population. Maydica **58**, 318–321.

Weiner J. 2017. Applying plant ecological knowledge to increase agricultural sustainability. Journal of Ecology **105**, 865–870.

Worku M, Bänziger M, Erley G, Friesen D, Diallo AO, Horst WJ. 2007. Nitrogen uptake and utilization in contrasting nitrogen efficient tropical maize hybrids. Crop Science **47**, 519–528.

Xu G, Fan X, Miller AJ. 2012. Plant nitrogen assimilation and use efficiency. Annual review of plant biology **63**, 153–82.

York LM, Galindo-Castañeda T, Schussler JR, Lynch JP. 2015. Evolution of US maize (Zea mays L.) root architectural and anatomical phenes over the past 100 years corresponds to increased tolerance of nitrogen stress. Journal of Experimental Botany **66**, 2347–2358.

Yu P, Hochholdinger F, Li C. 2015. Root-type-specific plasticity in response to localized high nitrate supply in maize (Zea mays). Annals of Botany **116**, 751–762.

Yu P, Li X, White PJ, Li C. 2015. A large and deep root system underlies high nitrogen-use efficiency in maize production. PLoS ONE **10**, 1–18.

Zamboni A, Astolfi S, Zuchi S, Pii Y, Guardini K, Tononi P, Varanini Z. 2014. Nitrate induction triggers different transcriptional changes in a high and a low nitrogen use efficiency maize inbred line. Journal of Integrative Plant Biology **56**, 1080–1094.

Zhang N, Gibon Y, Gur A, *et al.* 2010. Fine Quantitative Trait Loci Mapping of Carbon and Nitrogen Metabolism Enzyme Activities and Seedling Biomass in the Intermated Maize IBM Mapping Population. Plant physiology **154**, 1753–1765.

Zhang X, Davidson EA, Mauzerall DL, Searchinger TD, Dumas P, Shen Y. 2015. Managing nitrogen for sustainable development. Nature **528**, doi:10.1038/nature15743.

Chapter 2

Genotypic variation and nitrogen stress effects on root anatomy traits in maize (*Zea mays* L.) are node-specific

Abstract

Root phenotypes that improve nitrogen acquisition are avenues for trait-based breeding in maize. Root anatomy affects nutrient and metabolic economy, hydraulic conductance, anchorage, and soil penetration. Maize root phenotyping has centered on primary, seminal, and early nodal roots. Yet, critical nitrogen uptake occurs when the nodal root system is well developed. This study examined root anatomy across nodes in field-grown maize hybrids and inbreds under high and low nitrogen regimes. Genotypes with high nitrogen use efficiency (NUE) had larger root diameter and less cortical aerenchyma across nodes under stress than genotypes with lower NUE, and these differences appeared to be independent of plant size. Anatomical plasticity varied across genotypes; most genotypes showed decreases in root diameter under stress when averaged across nodes. Cortex, stele, total metaxylem vessel areas, and cortical cell file and metaxylem vessel numbers scaled strongly with root diameter across nodes. Metaxylem vessel size and cortical cell size were correlated within-node, and root anatomy phenotypes in the first and second nodes were not representative of subsequent nodes. The success of plant phenomics depends upon effective phenotyping strategies, and evaluating root traits across nodes allows a more accurate analysis of genotypic variation, allometry, and plasticity of maize root anatomy.

Highlight

Maize nodal root anatomy phenotypes vary significantly across nodes and nitrogen stress treatments, which affects the evaluation of genotypic variation, allometry, and adaptive trait plasticity among field-grown hybrids and inbreds.

Key words and abbreviations

Root anatomy, maize, nitrogen stress, node, phenotyping, plasticity

NUE – Nitrogen use efficiency
RIL – Recombinant inbred line

Introduction

Maize is a dominant global crop, with over 1 billion tons produced for food, fuel, and industrial uses. Nitrogen (N) fertilizer is the most expensive input, costing an estimated $56 billion for a total 113 million tons of N produced globally in 2014 (FAO 2014). However, only 33% of applied N is converted to grain yield, with the remainder lost as harmful pollution in the form of surface runoff, volatilized ammonia, nitrogen oxide emissions, or leached beyond the root zone as nitrate, contaminating waterways and creating eutrophic "dead zones" which require costly remediation (Hirel et al., 2011; Dhital and Raun, 2016). Conversely, low soil N is the primary constraint on yield in sub-Saharan Africa, where maize production primarily occurs in low-input farms, and is essential for food security (Gibbon et al., 2007).

Improving nitrogen use efficiency (NUE) in maize is a sustainable strategy for boosting yields in both large commercial operations and food-insecure regions. NUE is defined as the grain weight produced per unit of soil N, as a result of N uptake (NUpE) and utilization (NUtE) processes, including absorption, assimilation, and remobilization (Moll et al. 1982; Xu et al. 2012). Given the greater potential for agronomic and genetic improvement in NUpE, trait-based or "ideotype" breeding could improve NUE in relevant environments (Donald, 1968; Lea and Azevedo, 2006; Fischer et al., 2014).

Root system ideotypes, including anatomical, architectural, and physiological traits, have been proposed for optimizing N capture in maize (Clarke and McCaig, 1993; Lynch, 2013; Fischer et al., 2014; Schmidt and Gaudin, 2017). To evaluate genotypic variation and impact of root traits, high-throughput phenotyping methods have been developed, ranging from germination paper to artificial media to field excavation (reviewed in Meister et al., 2014). Studies have largely focused on primary, seminal, and early nodal roots in maize, which develop by the four-leaf stage, within two weeks depending on growth conditions. Typically, the shoot-borne nodal

root system is responsible for the majority of N uptake, and maize genotypes develop up to six acropetal crown root nodes belowground, with up to three additional brace root nodes emerging aboveground (Hoppe et al., 1986; Hochholdinger et al., 2004). Critical N uptake in field-grown maize occurs during the development of these later nodes, with maximum uptake occurring at the 10- to 14-leaf stage, beginning about four weeks after planting (DeBruin et al., 2017).

Several studies of root anatomical traits have evaluated and based conclusions upon phenotypes of the second root node of mature plants, due to initial screening of these genotypes occurring at earlier growth stages in the greenhouse (Burton et al., 2012; Saengwilai et al., 2014; Chimungu et al., 2014a, b). It has been shown in a limited number of genotypes, however, that both anatomical and architectural traits, including root number, diameter, branching, angle, and consequently, root depth, vary greatly across nodes, with relatively less variation within-node (Yamazaki and Kaeriyama, 1982; Girardin et al. 1987; Demotes-Mainard and Pellerin, 1992; Stamp and Kiel 1992; Jordan et al. 1993; Araki et al., 2000; Burton et al. 2013a, b; York and Lynch, 2015).

Rigorous assessment and validation of phenotyping procedures for target traits is essential to the success of plant phenomics studies. To better understand genotypic variation and N stress effects on maize nodal root anatomy, anatomical traits were evaluated across nodes in 44 hybrid and 39 inbred genotypes in the field, under various N conditions. Effects of node, N level, and genotype on nodal root anatomy are presented, as well as trait relationships and novel quantification of cell diameter across cortical files and metaxylem vessel dimensions.

Materials & Methods

Plant material

The 2016 field study, PA16, included 44 maize hybrid genotypes. The 2015 field study, PA15, included 11 recombinant inbred lines (RILs) from the intermated B73 x Mo17 (IBM) population. The 2014 field study in PA, PA14, and the 2013 field study in PA, PA13, respectively included 27 and 30 RILs from the IBM, NYH (Ny821 x H99) and OWRI (Oh43 x W64a) populations. The 2014 field study in South Africa, SA14, included 25 IBM and NYH RILs. Hybrid seed from select genotypes was provided by the Genomes to Fields (G2F) Consortium,

and curated for diversity and regional adaptation by G2F. Details are available at this link: http://www.genomes2fields.org/about/project-overview-and-scope/ and the genotypes used are listed in **Appendix A, Table S1**. IBM, NYH, and OWRI maize seeds were provided by Dr. Shawn Kaeppler at U-Wisconsin, Madison. Genotypes are listed in **Appendix A, Table S1**.

Field conditions

PA13, PA14, PA15, and PA16 field trials were conducted in 0.4 ha fields maintained with split high and low nitrogen treatments (field #87, 85, 105, 103 in 2013; 105, 85 in 2014; 103 in 2015; 105, 85 in 2016) at The Pennsylvania State University's Russell Larson Research Farm (40°42'40.915"N, 77°,57'11.120"W, central coordinate between field #105 and 85), which has Hagerstown silt loam soil (fine, mixed, semi-active, mesic Typic Hapludalf). To generate low N conditions, approximately 2.5 cm of sawdust was tilled into fields #85, 103, 105 in May 2011 and 2012, and applied to field #87 in 2012 only. The high-nitrogen sides of the fields were fertilized with 146 kg N ha^{-1} applied as urea (46-0-0) in 2013 and 2014; 157 kg N ha^{-1} in 2015; and 213 kg N ha^{-1} in 2016 while no N fertilizer was applied on the low-nitrogen sides. Fields received drip irrigation, nutrients other than N, and pest management as needed.

Seeds were planted using hand jab planters in rows with 76 cm row spacing, 91 cm alleys, 23 cm plant spacing, 4.6 m plot length with 3.7 m planted, or approximately 56,800 plants ha^{-1}. In PA13, PA14, and PA15, each genotype was planted in 3-row plots, and plants from the middle row of each 3-row plot were sampled; in PA16, single-row plots were used, and plants were sampled from the middle section of the plot. Planting dates were: May 18, 2013, May 31, 2014, June 14, 2015, and May 25, 2016, respectively. Following anthesis, root harvest began on: Aug 21, 2013, Aug 25, 2014, Sept 3, 2015, and Aug 8, 2016, respectively.

SA14 was conducted at the Ukulima Root Biology Center in Alma, Limpopo, South Africa in the Nebraska Farm pivot (24°33'0.12" S, 28°7'25.84 E, 1235 m asl), which has Clovelly loamy sand (Typic Ustipsamment). A total of 184 kg N ha^{-1} was applied to high N plots, through five applications of fertigation and granular urea. A total of 23 N ha^{-1} was applied to the low N plots at planting via fertigation. Pivot irrigation, nutrients and pesticides were applied as needed. Hand-planting was completed November 26, 2013 and root sampling began Feb 10, 2014. Planting density was approximately 80,000 plants ha^{-1} with 76 cm row spacing. Genotypes were planted in 3-row plots, and plants were sampled from the middle row of each plot.

Experimental design

All experiments were split-plot randomized block designs with different configurations. In PA13 and PA14, 30 genotypes were randomized in each of 4 replicates (blocks) of 2 nitrogen treatments (sub-plots within blocks), totaling 240 plots. In PA15, 11 genotypes were randomized in 4 blocks within 2 N treatments, totaling 88 plots. In PA16, 44 genotypes were randomized in 2 blocks with 2 nitrogen treatments, totaling 178 plots. In SA14, 25 genotypes were randomized into each of 4 high N and 4 low N blocks, totaling 208 plots. In PA13 and PA16, separate 1-acre fields were used for each block; in PA14 two 1-acre fields were sub-divided into 8 blocks; in PA15, one 1-acre field was sub-divided into 8 blocks. In SA14, blocks were randomly assigned within a center pivot and split N treatments were applied.

Plant harvest and root sampling

A representative plant from each plot was excavated using a shovel (Trachsel et al., 2011). Root crowns were separated from the shoots, soaked in water with detergent, and rinsed to remove remaining soil. Each node of roots was excised, and up to 3 representative roots from select nodes for each study (see Appendix A, Table S1) were sampled at 2 to 4 cm from the base of the stem and preserved in 75% ethanol for anatomical processing. See Appendix A, Fig. S1 for excised root crown images. Shoot biomass was separated into stem, leaves, and ears, dried at approximately 70°C, and weighed. Ears from eight plants per plot (PA16) and five plants per plot (PA15) were collected at physiological maturity, dried to approximately 15% moisture content, shelled and weighed. Dried leaves were ground, homogenized, and a 2 mg subsample was analyzed for total nitrogen content with a CHN elemental analyzer (2400 CHNS/O Series II, PerkinElmer, Waltham, MA) using the Dumas combustion method.

Image analysis

The middle portion of two representative root segments per node of each plant were ablated and imaged using laser ablation tomography (LAT). This technique employs a nanosecond pulsed UV laser (Avia 355-7000, Coherent, Santa Clara, CA) focused into a single-

line scanning beam with a HurryScan 10 galvanometer (Scanlab, Puchheim, Germany) to ablate the cross-sectional surface of a root secured to a three-axis motorized stage (ATS100-100, Aerotech Inc, Pittsburgh, PA). The root is moved into the laser beam at about 30 μm s^{-1} (rate is adjusted according to root quality), and as each surface is ablated and exposed, images lit by the laser UV light are captured using a stage-mounted (#62-009, Edmund Optics, Barrington, NJ) camera and 5X macro lens (Canon EOS Rebel T3i camera with 65mm MP-E 1-5x variable magnification, Canon USA Inc, Melville NY). Image scale was 1.173 pixels per micron. See Fig. 1 for LAT image examples.

Images were analyzed using one of two workflows. Images from all studies except PA14 were analyzed using custom macros created with the open-source ObjectJ plug-in (https://sils.fnwi.uva.nl/bcb/objectj/) in ImageJ (https://imagej.nih.gov/ij/index.html), in which cortex, stele, aerenchyma, vessel and cell outlines were manually traced, and cell files manually counted (detailed in **Appendix A, Fig. S2**). This allowed careful quantification of cell and vessel sizes. Images from PA14 were analyzed using the open-source Java program RootScan2 (code by Cleoniki Kesidis, http://plantscience.psu.edu/research/labs/roots/methods/computer/rootscan), which is based on RootScan (Burton et al., 2012) but optimized for LAT images. Cortical cell file and metaxylem vessel numbers were manually confirmed.

Trait descriptions and abbreviations are provided in **Table 1-1**. Total vessel conductance (JSM) was calculated as the sum of J_{vessel} for all vessels in a root cross-section, using Hagen-Poiseuille corrected for an ellipse (Lewis and Boose, 1995), where $J_{vessel} = (-\pi/64\nu)(a^3b^3/(a^2+b^2))(\Delta p/\Delta x)$, with ν = viscosity (MPa s^{-1}), a=major axis length (m), b=minor axis length (m), $(\Delta p/\Delta x)$ = pressure gradient.

Statistical analysis

Statistical analysis and visualizations were generated using R version 3.3.1 (R Core Team, 2016). Analysis of variance was performed using the linear mixed-effects *lmer* function in the *nlme* package, with genotype, N treatment, and node as fixed effects, and N treatment nested within block as a random effect. Effect sizes on the three-way interaction of genotype, N treatment, and node were calculated using the *etaSquared* function in the *lsr* package. Boxplots and bar plots were generated using data aggregation functions from the package *plyr* and plotting functions from the package *ggplot2*. Principle components analysis (PCA) was performed with

scaled, centered data using the *prcomp* function and visualized with *autoplot* function in the *ggfortify* package. Correlation matrices of scaled, centered data were generated with the *corrplot* package. Color coded values are Spearman's rank coefficient, and circle size scales with p-value, with blank cells when correlations are not significant at $p<0.05$. Trait arrangement and grouping (large boxes) is based on hierarchical clustering for the predetermined number of clusters. Power models were generated using the natural log of X and Y variables, with the r^2 value and p-value from simple linear regression (*lm*, Y~X) indicated on each plot. The percent of genotypes with significant plastic response across nodes was calculated using a paired Type II t-test, matched by node and replicate; the percent of genotypes with a significant plastic response within each node was calculated using a paired Type II t-test, matched by replicate. Allometric relationships were modeled using a linear regression of the natural log of anatomical traits against the natural log of shoot biomass; the significance nitrogen treatment on allometric scaling constants and intercepts in these relationships was determined using analysis of covariance.

Results

Node, genotype, and nitrogen treatment affected root anatomy

Maize root anatomy differed significantly by genotype, nitrogen treatment, and node, as well as interactions of these factors (**Table 1-2** and **Appendix A, Table S2**). All root anatomy traits (see **Table 1-1** for abbreviations) showed significant variation by genotype, and all traits except the percent of aerenchyma in the cortex (AAP) showed significant variation by root node, for three nodes of roots in field-grown maize hybrids (**Table 1-2**). In field-grown maize inbreds, all traits evaluated showed significant variation by genotype, while all except the percent of metaxylem vessel area in the stele (MXP) showed significant variation by node (**Appendix A, Table S2**). Genotype by nitrogen and genotype by node interactions were significant for many traits, while nitrogen stress, the interaction of nitrogen and node, and the three-way interaction of genotype, nitrogen, and node were less important (**Table 1-2** and **Appendix A, Table S2**).

Nodal root anatomy traits were clustered into four groups

Root anatomy traits across nodes were analyzed using principle components analysis, and clustered into four groups (**Fig 1-2**). "Root diameter related" traits included the most strongly related traits – root cross-sectional area (RXA), cortex cross-sectional area (CXA), stele cross-sectional area (SXA), total metaxylem cross-sectional area (MXA) – as well as cortical cell file number (CF) and the number of metaxylem vessels (MXN). These six traits loaded strongly negatively on the first principle component (PC1), which explained 67% of the total trait variance (**Fig 1-2**). "Proportion related traits" included cortex-to-stele area ratio (CSR), the percent of metaxylem vessel area in the stele (MXP), and the percent of aerenchyma area in the cortex (AAP). These traits loaded negatively on PC2, which explained 10% of trait variance. The median cross-sectional area of a single metaxylem vessel (MXM) and median cortical cell size (CCS) also loaded strongly negatively on PC2 (**Fig 1-2**).

Node effects exceeded genotypic and nitrogen stress effects on root anatomy

The amount of variation attributable to root node exceeded all other sources of variation for root-diameter related traits, as well as CSR, MXP, and the total estimated conductance rate of metaxylem vessels (JSM) (**Table 1-3**). Metaxylem vessel and cortical cell related traits, as well aerenchyma, showed the greatest relative amount of random (residual) variation, among maize hybrids and inbreds (**Table 1-3** and **Appendix A, Table S2**).

Node-specific trait ranges and plant variability in root anatomy

Maize crown roots develop in successive acropetal tiers, from the thinnest roots in the first node to the youngest, often thickest, fifth or sixth node, followed by brace roots (**Appendix A, Fig. S1**). Root diameter related traits increased with each younger node, with greater relative increases in total stele and metaxylem vessel areas; by contrast, median metaxylem vessel size increased and then plateaued after the first three nodes, and cortical cell size patterns varied, with modest increases in the maximum and median cell diameters balanced by decreasing hypodermis and outer file cell sizes (**Fig 1-3** and **Appendix A, Fig S3**).

Genotypic variation in nodal root anatomy

Trait variation among maize hybrids ranged from 12% for CF to 96% for AAP among maize hybrids across nodes 2, 3, and 4, and from 3% for median metaxylem vessel eccentricity (ECC) to 32% for AAP among inbreds across nodes 1, 2, and 3 (**Table 1-4** and **Appendix A, Table S3**). Stele and vessel traits (SXA, MXA, JSM, MXN, MXM) consistently showed greater genotypic variation than cortical traits (CXA, CF, CCS) among hybrids and inbreds, but also had greater within-genotype variation (**Table 1-4** and **Appendix A, Table S3**; **Appendix A, Table S4**). Genotypic variation differed modestly by nitrogen treatment and node; low N induced a slight reduction in genotypic variation, while the first node showed the least variation (**Table 1-4** and **Appendix A, Table S3**). These percentages reflect the variation in mean trait values among genotypes, but not within genotypes. Trait variation within genotypes ranged from an average of 11% for median cortical cell diameter (CDM) to 96% for total aerenchyma area (AA) across nodes among hybrids, and from 10% for CF to 64% for AAP across nodes among maize inbreds, a metric specific to the populations studied and experimental conditions (**Appendix A, Table S4**). Within-genotype trait variability was similar across nodes and nitrogen treatments for most traits (**Appendix A, Table S4**).

Genotypic differences in anatomical plasticity under low nitrogen

Anatomical plasticity in response to low N differed across genotypes; for example, hybrid genotypes 1, 11, and 27 showed no significant change in MXA under low N, when averaged across nodes (**Fig 1-4**). By contrast, genotypes 2, 23, 35, and 42 showed significant decreases in MXA under low N, while genotype 28 showed a significant positive change in MXA under low N (**Fig 1-4**). Genotypes also differed in the magnitude of trait plasticity; genotypes 2, 23, and 42 had strong plastic responses of greater than 50% decrease in MXA under low N, whereas genotypes 35 and 28 had weaker plastic responses (**Fig 1-4**).

The relative plasticity of each anatomical trait was calculated as the percentage of genotypes which had a statistically significant trait response under low N ("plastic genotypes"), and the percentage of those genotypes which had either a negative (decrease in trait value) response and/or a strong (over 50% increase or decrease in trait value) response (**Table 1-5**). Trait plasticity ranged from 0% (ECC) to 31% (RXA) of hybrid genotypes showing any significant

change under low N, across nodes, with lower percentages when calculated for traits of any single node (**Table 1-5**). The relatively low percentages of genotypes with significant trait responses reflected strong within-genotype trait variability; for example, only 11% of genotypes had a statistically significant low N response in SXA, but 43% of genotypes showed a strong (>50%) change in trait value under low N (**Table 1-5**; data not shown). Anatomical trait responses among plastic genotypes varied in magnitude, but were relatively uniform in terms of direction; under low N, most trait values decreased across nodes, with some variation depending on node (**Table 1-5**).

Anatomical differences among high and low NUE genotypes

Maize genotypes were matched according to high N yield, then sorted into high or low nitrogen use efficiency groups (HNUE, LNUE) according to low N yield. For hybrids, LNUE genotypes had an average of 32% less yield under low N compared to HNUE genotypes; for inbreds, the difference was 22% (**Fig 1-5**). Anatomical traits averaged across three nodes showed patterns in HNUE and LNUE phenotypic responses to low N; HNUE genotypes generally had greater RXA, MXA, CCS, and MXM, and less AAP, under low N, relative to LNUE genotypes (**Fig 1-5**). The magnitude of these differences was small under both high and low N, and less among inbreds with milder N stress (**Fig 1-5**). Overall, HNUE and LNUE differed the least in anatomical traits and responses in the third node; the second and fourth nodes showed similar trait patterns and responses, but the fourth node typically showed greater separation between HNUE and LNUE trait values (**Fig 1-5**; not all traits shown).

Node-specific nitrogen stress effects on root anatomy

Root diameter related traits were reduced under N stress, with greater decreases in the youngest nodes in hybrids; this progression across nodes was less evident in inbreds, which had milder N stress (**Fig. 1-6** and **Appendix A, Fig. S5** and **Table S5**). The exception was CF, which changed little under low N relative to decreases in cortical cell size (CCS, INN) in all nodes; OUT reached a stable minimum in nodes three to five and was not affected by N stress (**Fig. 1-6**).

In contrast to hybrids, MXN also was insensitive to low N; reduction in MXM drove the decrease in MXA across nodes in inbreds, similar to the CF and CCS pattern (**Appendix A, Fig. S4**).

For maize hybrids, the cortex-to-stele ratio (CSR) and percent of metaxylem vessel area in the stele (MXP) showed substantial node-specific low N stress responses, with low N-induced increase in CSR increasing in each younger node, whereas maize inbreds showed little change in CSR and MXP under low N, and by node (**Fig. 1-6** and **Appendix A, Fig. S4**). The percent of aerenchyma area (AAP) increased over two-fold in response to low N stress in the first node, the largest low N induced change in root anatomy, and increased in nodes two to four to similar levels under low N; node five had little AAP, with a slight increase under low N (Fig. 1-6 and **Appendix A, Table S4**). AAP showed less pronounced differences under milder low N in maize inbreds (**Appendix A, Fig. S4**).

Root anatomy traits in younger nodes are more strongly correlated

Root anatomy traits showed significant correlations across nodes among genotypes, but the strength of correlation differed by node. For most root anatomy traits, the second node clustered independently from nodes three and four, and was more strongly related to other traits within its node (**Fig. 1-7**). CCS and MXM correlated more strongly within node, a novel association (**Fig. 1-7**). From nodes two to four in maize hybrids, CF and MXN correlated strongly independent of node; sampling any of these nodes would generally result in similar CF and MXN phenotypes (**Fig. 1-7**).

Root anatomy traits scale with root diameter across nitrogen treatments

Evaluating across five field studies of maize hybrids and inbreds, across five root nodes, the power relationships between RXA and all anatomical traits were significant, with the exception vessel eccentricity (ECC) and median cortical cell diameter averaged across the cortex (CDM) (**Fig 1-8**). Nitrogen stress did not affect these relationships, with the exception of AAP, in which the slope of the scaling relationship increased under low N (**Fig. 1-8**). Within nodes, the scaling relationships differed depending on trait; traits strongly related to root diameter showed small, progressive changes in slope with each node. Hypodermis and outer cortical cell diameters

were less related to RXA in some nodes. Overall, scaling relationships between RXA and anatomical traits were more similar in nodes 3, 4, and 5, and the first node showed the most distinct patterns (**Appendix A, Fig S5**).

Allometric relationships of root diameter are similar across nitrogen treatments

The allometric scaling coefficients of RXA against shoot biomass (quantified only at anthesis) did not differ significantly between high and low N for nodes 2, 3, and 4; however, allometric relationships were stronger under low N, and were not statistically significant under high N in nodes 2 and 4 (**Fig. 1-9**). Shoot biomass was more strongly related to RXA in the third and fourth nodes, relative to the second node, among maize hybrids (**Fig. 1-9**).

Cortical cell size distribution is strongly dependent on file number

In the root cortex, cells align in radial files, and cell diameters vary across these files. Inner (near stele) and outer cell files have smaller diameter cells, while the hypodermis and mid-cortical region have larger cells (e.g. **Appendix A, Fig. S2**). For roots with the same CF, cell diameters by file did not differ strongly under N stress or among genotypes (**Fig. 1-10** A, B, C). In roots with the fewest CF, cell diameters varied the least across files, whereas in roots with greater total CF, there was a gradual increase in cell diameter across the outer cortical files, followed by about six files of maximum cell diameter, and a slight decrease in cell diameter in the innermost file(s) (**Fig. 1-10** A, B, C). Cortical cell diameter averaged across a root cross-section therefore confounds changes in the number of files of small, outer-layer cortical cells with changes in the maximum cell diameter. Among field-grown hybrids, maximum cortical cell diameters differed by an average of 5 μm (high N, 51 to 56 μm) and 7 μm (low N, 44 to 51 μm) between the thinnest (6 to 11 CF) and thickest (15 to 27 CF) roots across nodes (not shown).

Metaxylem vessel sizes show greater variation in younger nodes

Metaxylem vessels within a root cross-section vary in size, with vessels occasionally in the process of splitting into two or three vessels depending on sampling position. Large roots in younger nodes may have alternating larger and smaller vessels. Vessel size distribution, in terms of the relative number of very small or very large vessels, relative variability in size (coefficient of variation) among vessels in a cross-section, and maximum, minimum, median, and other percentile values of vessel size, was evaluated. Vessel size distributions varied intra-plant and within-node. Vessel size variability within a root was greatest in the first node and younger nodes from four onward; N stress reduced variability slightly in younger nodes (**Fig. 1-11A**). The relative number of both very small and very large vessels increased in younger nodes, with the exception of the first node (**Fig. 1-11B**). Minimum vessel sizes were similar across nodes, while maximum vessel size increased with node (**Fig. 1-11C**).

Genotypic variation in the minimum and maximum metaxylem vessel size, and the number and percentage of very small and very large metaxylem vessels was significant across three root nodes, but the coefficient of variation of vessel sizes did not vary significantly by genotype (**Appendix A, Table S6**). Of these traits, only minimum vessel size did not differ significantly under low N treatment; all traits varied significantly by node (**Appendix A, Table S6**).

Root and shoot development are coordinated across nodes

Nodal root emergence occurs in coordination with shoot growth, with some variation in magnitude depending on genotype and under nitrogen stress (**Appendix A, Fig S6 A, B, C**). Root diameter near the stem base typically does not change significantly until after anthesis, when some degradation may occur and cortical cell sizes shrink, particularly in older nodes (**Appendix A, Fig S6D**; data on other anatomical traits and nodes not shown).

Three-dimensional analysis of maize root anatomy

Genotypic contrast and plasticity in root anatomy traits which are not evident with cross-section image analysis may be assessed using three-dimensional reconstruction and other methods. For example, volumes and related metrics of aerenchyma, vessels, and cells can be extracted using MIPAR™ and Avizo™ software (**Appendix A, Fig S7**). Cell and vessel lengths can be quantified throughout a root segment (not shown).

Discussion

The maize nodal root system is unique among grass species

Modern maize (*Zea mays* L.) is one of the most widely-cultivated and productive crop species, the result of over 9,000 years of human selection from the wild grass teosinte (*Zea mays* ssp. *parviglumis*) (Doebley, 2004). Unlike teosinte and other tillering grasses, maize primarily invests in a single stalk, and produces one or more large ears. A leaf extends from each node, growing successively larger from base to mid-section, then smaller near the stem apex. This distinctive shoot architecture resulted from suppression of tillering through altered expression of the *teosinte branched1* gene, which encodes a transcription factor involved in apical dominance (Doebley et al., 1997).

The maize root system is similarly distinct. The embryonic (primary and seminal roots) and early post-embryonic (coleoptile node and primary laterals) root architecture is similar to other grass seedlings. However, without tillering, the genetically distinct late post-embryonic maize root system (all crown and brace roots, except the first node) is confined to a single apex, producing successive nodes (also called whorls) of shoot-borne roots (Hochholdinger 2004). The first four root nodes are closely arranged, with increasing internodal distance between subsequent root nodes (e.g. **Appendix A, Fig S1**). The first three nodes are occupied by an average of four roots per node, increasing to an average of ten roots per node in the sixth node and up to 22 brace roots per node, depending on genotype (e.g. **Appendix A, Fig S6A**).

Gaudin and colleagues (2011) found that teosinte and maize produce similar numbers of nodal roots, and both exhibit a reduction in root number in response to nitrogen stress, but by different mechanisms; teosinte reduces tiller number, while maize reduces the number of roots

elongated, particularly in younger nodes. However, nodal root diameter and other anatomical traits were not characterized in teosinte, and nitrogen adaptation strategies for these traits are still unclear. Phenotypic diversity in both root anatomy and architecture was characterized among *Zea* species (Burton et al., 2013), but not under stress conditions. York and colleagues (2015) studied 16 commercially successful hybrids across different planting densities and nitrogen levels, and found that changes in nodal root architecture and anatomy, related to cultivation practices over different eras, could contribute to increases in nitrogen use efficiency. Modern genotypes had fewer, shallower nodal roots, and a greater number of metaxylem vessels in the second root node.

This study found substantial anatomical variation across crown root nodes. In contrast to the relatively stable number of roots in the first three nodes, genotypes showed a distinct increase in root diameter and related anatomical traits, such as cortical cell file number and metaxylem vessel number, in each successive node. However, the median cross-sectional area of a metaxylem vessel plateaued after the third node (as reported by Stamp and Kiel, 1992), possibly reaching a maximum functional size, balancing greater conductance with risk of embolism; this coincides with the transition to increasing numbers of roots per node. Similarly, median cortical cell diameters were relatively consistent across nodes. The maximum diameter of mid-cortex cells increased modestly with each node, accompanied by an increase in the number of files of smaller, outer layer cortical cells.

The increase in root diameter with each node could relate to the increasing demand for water and nutrients, as exponential plant growth occurs through the season. For example, between the emergence of the fourth and fifth nodes, dry shoot biomass can increase by over 400% (e.g. **Appendix A, Fig S6**). Increased metaxylem vessel area per root and an increase in the number of roots results in an average 140% increase in total conductance capacity in the fifth node, relative to the fourth node, estimated from field-grown maize hybrids in high nitrogen (data not shown). The maize nodal root system therefore exhibits a distinct “root thickening” strategy with each new node, analogous to the secondary thickening function of taproot systems in dicotyledonous plants, which support prolific resource acquisition and plant growth via a single main stem.

Root anatomical traits influence stress adaptation

Root anatomical traits have received relatively little attention, compared to root system architecture (RSA) and morphology, in stress adaptation studies. Several recent reviews of trait-

based breeding and phenotyping focused almost exclusively on methods and gene targets relating to RSA (e.g. Cobb et al. 2013; Fiorani and Schurr, 2013; Meister et al., 2014; Paez-Garcia et al., 2015). Anatomical traits have been discussed in root ideotypes for stress tolerance. Lynch (2013) suggested traits which reduce metabolic cost per root segment, such as fewer cortical cell files and greater proportion of aerenchyma, could enable rapid, deeper rooting, beneficial under drought or low nitrogen stress, particularly in sandy soils. Similarly, increasing root cortical senescence in barley has been found to reduce respiratory and nutrient costs, and has been proposed as a trait for stress adaptation (Schneider et al., 2017). Schmidt and Gaudin (2017) suggested optimizing aerenchyma formation and endodermal barrier development could enhance tolerance of saline, waterlogged soil common in irrigated environments, and discuss tradeoffs of increasing specific root length, including restriction of hydraulic conductivity. Richards and Passioura (1989) bred wheat varieties to contrast by 10 μm in vessel diameter in seminal roots, and found that genotypes with narrower vessels showed up to 11% increased yield under drought. Strock and colleagues (2017) found that reduced secondary root growth in common bean reduced metabolic costs and increased phosphorus stress tolerance. Variation in metaxylem vessel size and number has also been assessed for drought tolerance in legumes (Purushothaman et al., 2013; Prince et al., 2017).

This study found that hybrid maize genotypes with high nitrogen use efficiency (HNUE) differed in root anatomy under low nitrogen, compared to lower yielding (LNUE) genotypes; the HNUE and LNUE groups differed significantly in yield, but not shoot biomass, under low nitrogen. Overall, HNUE genotypes had 14% larger root diameter, 22% greater total metaxylem vessel conductance, and 54% less aerenchyma formation under low nitrogen, compared to LNUE genotypes. HNUE genotypes had 9% greater median metaxylem vessel size and 6% more cortical cell files than LNUE genotypes under low nitrogen. Vessel eccentricity did not differ between HNUE and LNUE genotypes. These anatomical patterns were evident across nodes, although differences between HNUE and LNUE genotypes were most pronounced in the fourth node, compared to the second and third nodes (data not shown for all traits by node). For maize inbreds under milder nitrogen stress, root anatomy showed less contrast but similar patterns; HNUE genotypes had 9% larger root diameter, 9% larger mid-cortical cell size, 6% larger median metaxylem vessel size, and 17% less aerenchyma formation under low nitrogen compared to LNUE genotypes. These genotypes were grown in silt loam fields in PA, with moderate soil compaction.

These results contrast from previous findings which have shown some genotypes with greater aerenchyma induction performed better under nitrogen stress, as evaluated in the second root node (Saengwilai et al., 2014). However, this study has also found that aerenchyma percent in the second node was either weakly correlated or not correlated with aerenchyma in other nodes within a genotype. Similar studies found benefits of reduced cortical cell file number and larger mid-cortical cell diameter under drought, due to reduced metabolic cost per root segment, as evaluated in the second node (Chimungu et al., 2014 a, b). However, this study suggests that the relatively independent relationship between mid-cortical cell size and cortical cell file number is unique to the first and second nodes; in subsequent nodes, larger diameter roots have more cortical files as well as slightly larger mid-cortical cells. Additionally, cortical cell size was either inversely or not related across nodes within a genotype (e.g. **Fig 1-7**). The relative metabolic costs and functions of roots across nodes are still to be characterized.

This study found that HNUE genotypes maintained larger axial root diameter and greater vessel conductance, through both larger size and number of cells and vessels, and had reduced induction of aerenchyma formation under nitrogen stress. These traits could be interpreted as beneficial (i.e. directly contributing to improved NUE) or indirectly related to improved NUE (e.g. influenced by allometry or other variables; discussed in the next section). Maximizing hydraulic conductance with long-lived roots rather than greater proliferation of fine roots has been suggested as an adaptive strategy for irrigated systems, given relatively lower root construction and maintenance costs (Schmidt and Gaudin, 2017). Additionally, optimizing hydraulic conductance is a primary function of axial roots, determined by metaxylem vessel properties, whereas absorptive functions and greater specific root length tend to be central to the function of lateral roots, and exist under separate genetic control (Jordan et al., 1993; Hochholdinger et al., 2004).

Larger diameter axial roots, which often have layers of small, suberized outer cortical cells and less root porosity (both in terms of intercellular space and aerenchyma lacunae), have greater mechanical strength, and support better anchorage and lodging resistance, resilience to herbivory, longevity, and soil penetration in drying soils and hardpans (Eissenstat 1992; Eissenstat et al., 2000; Striker et al., 2007; and in maize, Stamp and Kiel, 1992; Jordan et al., 1993; Liu et al., 2012a; Chimungu et al., 2015). Developing thicker roots would not substantially increase external intra-plant root competition, which has been suggested as a key trade-off to overproduction in number of roots, due to increased probability of overlapping uptake zones of mobile nutrients and water (Postma et al., 2014).

The slower development of large diameter roots could also reduce inter-plant competition in monoculture. Studies have shown that roots in the third and younger nodes have steeper angles and greater rooting depth, depending on genotype and soil conditions (Yamazaki and Kaeriyama 1982; Hoppe et al. 1986; Araki et al., 2000; Liu et al., 2012b; York and Lynch, 2015), supporting the potential importance of larger diameter roots in penetrating deep soil for mobile resources. Larger diameter roots, with greater cortical area, may also promote beneficial mycorrhizal associations (Galindo-Castañeda et al., unpublished); Galindo-Castañeda (personal communication) has also found that effects of anatomical traits on fungal colonization vary across cortical regions in recent work. The functional utility and trade-offs of these root anatomy traits under different environmental conditions require further study.

Anatomical plasticity and allometry of root anatomy traits differ among genotypes

Plasticity and allometry often complicate the analysis of trait variation and function in plants (e.g. Weiner, 2004). For example, Wahl and colleagues (2001) found that shading had specific effects on axial root anatomy in grasses, increasing the size of stele cells and metaxylem vessels, while nutrient deprivation resulted in anatomical changes that were proportional to changes in plant size.

This study found that genotypes varied in anatomical trait plasticity in response to nitrogen stress; 31% of hybrid genotypes had a statistically significant change in root diameter under nitrogen stress, whereas there was no plasticity (0% of genotypes) and little genotypic variation in metaxylem vessel eccentricity. Of the genotypes with a significant diameter response, 91% of genotypes decreased in root diameter, and 64% had a diameter change of 50% or greater under nitrogen stress. Given strong trait variability in each node, the overall plastic response of genotypes was best classified using aggregate data across nodes.

Root diameter and cortical aerenchyma were similar for HNUE and LNUE genotypes in high nitrogen conditions, and both HNUE and LNUE genotypes decreased in root diameter under nitrogen stress. However, HNUE genotypes decreased less, resulting in significant differences in trait values under low nitrogen. These patterns were most evident in each node, but the fourth node showed the strongest contrast. The lack of anatomical plasticity displayed by HNUE genotypes could be interpreted in several ways: 1) less anatomical plasticity is beneficial under nitrogen stress, 2) larger diameter roots and reduced aerenchyma confer adaptive benefits under

nitrogen stress, or 3) the lack of plasticity, larger root diameter and reduced aerenchyma are a result of HNUE genotypes being less stressed than LNUE genotypes, and anatomical differences in each younger node reflected gaps in performance in these later growth stages (see *Chapter 3* for further discussion). Therefore, genotype screening for root anatomical traits should consider stress effects and variation in anatomical plasticity among genotypes, and the relevance of phenotyping root anatomy in younger nodes. Root anatomy traits in younger nodes are relevant for nitrogen uptake at critical growth stages, but it may be difficult to distinguish whether traits are adaptive or reflective of plant performance at later growth stages. Further study is needed on the relative benefits of stable versus plastic, stress-responsive root anatomy phenotypes.

HNUE genotypes did not have significantly greater shoot biomass at anthesis than LNUE genotypes; however, it is still relevant to consider the effect of plant size on root anatomy traits. In this study, root diameter was weakly but significantly allometric, although nitrogen conditions did not significantly change the scaling constant of root diameter (averaged across three nodes) and dry shoot biomass. In other words, allometric constraints on root anatomy were limited. Smaller, nitrogen-stressed plants had reduced root diameter in general, but several genotypes either increased in root diameter under stress, or showed varying degrees of increasing or decreasing root diameter under stress depending on root node. This suggests that root diameter and related anatomical traits could play a role in adaptive stress responses, independent of plant size.

The magnitude and direction of plastic responses in root traits such as axial and lateral root number and length under nitrogen stress has been found to vary among maize genotypes (Yu et al., 2015; Li et al., 2016). York and Lynch (2015) similarly found that genotypes showed contrasting morphological and architectural trait responses from node to node under nitrogen stress. Analyzing adaptive stress responses in terms of allometric instability and recovery could be a useful application of phenotyping root traits across multiple nodes, paired with monitoring of plant responses across growth stages, in future studies (Coleman et al., 1994; Wilhelm, 1995; Anfodillo et al., 2016). Further studies are needed to quantify the relationship of nodal root anatomy with plant size, and the effect of genotype and stress conditions on these allometric relationships.

Another important dimension is the interaction of root anatomical traits with architectural traits. Nodal root anatomy exists in a specific context; for each node, the effects of a given tissue composition or select anatomical features are multiplied by the number and length of the roots, and the placement of the root given its angle, emergence rate, and environment. Genotypes which

show an increased or stable root diameter response despite smaller plant size under nitrogen stress could alter traits such as nodal root number in order to compensate (see Chapter 3). Nitrogen stress has been shown to cause reduced nodal root number, increased root cell length, increased lateral to axial root ratio, and decreased root hair length and density; all of these changes have been interpreted as adaptive, with the exception of root hair response, which was associated with decreased plant size using a time course study (Gaudin et al., 2011; Gao et al., 2015).

Adaptive responses exist ultimately as preferential resource allocation to traits which confer an advantage (Bloom, 1985); for a given anatomical composition, there are either synergistic interactions or tradeoffs with other root traits, including root angle, number, elongation rate, branching, and exudation. Additionally, common genetic networks and hormonal signaling underlie root development and affect anatomical, morphological, and architectural root traits (Wachsman et al., 2015). For example, the *DEEPER ROOTING 1 (DRO1)* gene affects root system angle and depth through differential modulation of cell elongation at the crown root tip, in response to auxin (Uga et al., 2013). Select root trait synergisms have been explored (reviewed in York et al., 2013), and analyzing the interaction of traits in terms of modules, or modular plasticity, has been proposed (de Kroon et al., 2004). Modelling is another method for exploring resource allocation in terms of the costs and benefits, or source and sink strength, of multiple traits (e.g. Drouet and Pagès, 2007; Postma et al., 2017; Marshall-Colon et al., 2017). A stronger understanding of trait benefits and tradeoffs in plant stress adaptation will require further modes of analysis for trait interactions, plasticity, and allometric effects.

Optimizing crop root phenotyping strategies

Optimizing root phenotyping procedures and evaluating the impact of relevant traits is key to the success of trait-based breeding of crop varieties with enhanced nutrient and water use efficiency. Few studies have addressed trait variation within root systems (e.g. across nodes, positions, age, and root classes) across multiple genotypes, particularly in the field. Phenotyping of axial and lateral root traits along different positions in maize root systems has been conducted in limited genotypes in hydroponic and aeroponic systems (e.g. Gaudin et al., 2011; Gao et al., 2015). Select maize root anatomy and architecture traits have been evaluated in multiple nodes in the field, typically in one or two genotypes (Yamazaki and Kaeriyama, 1982; Hoppe et al., 1986; Girardin et al., 1987; Demotes-Mainard and Pellerin, 1992; Jordan et al., 1993; Aguirrezabal et

al., 1993; Pellerin, 1994; Liu et al., 2012b). Stamp and Kiel (1992) characterized 28 hybrid genotypes and evaluated six nodes with a focus on metaxylem vessel traits, and Mano and colleagues (2006) evaluated aerenchyma formation across root nodes and positions in multiple *Zea* species. An intensive nodal root architecture phenotyping effort among several field-grown maize genotypes found significant node effects on root number and diameter, and weaker node effects on angle and lateral root branching (York and Lynch, 2015).

This study found that root anatomy phenotyping results were strongly influenced by node in field-grown maize. Root anatomy varied within genotype, and genotypic contrast and patterns in nitrogen stress responses were better discerned from aggregating data across three root nodes. The first two nodes were distinct from younger nodes, in terms of trait relationships and stress responses, possibly reflecting developmental transitions that require further study. Phenotyping third and fourth nodes may lead to more representative characterization of nodal root anatomy among genotypes, while phenotyping across nodes is useful for more detailed studies of allometry, plasticity, and trait interactions. Functional significance of anatomical traits in the first two nodes at early growth stages has not been characterized.

The strongest anatomical variation across nodes occurred in traits closely related to root diameter, including the number of cortical cell files, the number of metaxylem vessels, and the total cortex, stele, and metaxylem vessel areas, which increased overall from the first to fifth nodes in both magnitude and range. Median metaxylem vessel and cortical cell sizes increased more modestly, and showed similar ranges in the latter three nodes. In younger nodes, stele and pith areas increased disproportionately, resulting in decreased ratios of cortex to stele area and total metaxylem vessel to stele area. The percent of cortical aerenchyma was the most variable trait, and ranged up to 50% in the first four nodes, with a sharp decrease in the fifth node. Nitrogen stress caused an overall reduction in root diameter and an increase in cortex-to-stele ratio in younger nodes. Total metaxylem vessel area progressed from no change under nitrogen stress in the first node to an average 36% decrease in the fifth node.

Among all traits evaluated, cortical cell file number had the least genotypic variation (7 to 13%). Metaxylem vessel and cortical cell diameter related traits, in addition to percent aerenchyma, had the greatest amount of residual variation, relative to genotype, nitrogen stress, and node effects, and suggests genotypic contrast in these traits may also be difficult to discern. To better interpret metaxylem vessel size and cortical cell size metrics, within-root size distributions were analyzed. The distribution and variability of vessel sizes and cortical cell diameters showed strong dependence on node and cell file, respectively. The maximum

metaxylem vessel diameters increased with node and root diameter, as did the maximum cortical cell diameter, although variation in this trait was minimal. Instead, average cortical cell diameters reflected changes in the number of small, outer layer cortical cells. Thus, aggregate metrics of an average or median vessel or cell diameter may confound differences in root diameter with genotypic contrasts in vessel or cell size, specifically, and the functional benefits of cell sizes (e.g. for metabolic cost versus structural integrity) should be studied in the context of these different cortical regions.

Further study of anatomical traits would benefit from more specific quantification methods and more robust automated or semi-automated applications. Several studies have used RootScan (Burton et al., 2012) to analyze second-node maize root cross-sections. An updated RootScan 2 application (coded by Cleo Kesidis) for more detailed anatomical quantification of cells and vessels is under development. Software such as CellSeT (Pound et al., 2012) has been modified to provide file-specific cortical cell data from maize root cross-sections (in collaboration with Michael Pound; not shown), and ImageJ plugins (e.g. as used in this study) and MIPAR™ software "recipes" (Sosa et al., 2014; recipes in collaboration with John M. Sosa) have been developed to expedite analysis of maize, rice and bean root cross section images. In addition, three-dimensional reconstruction of root anatomy allows quantification of aerenchyma volumes, cell lengths or volumes, vessel lengths, and other novel dimensions which could help elucidate genotypic differences and stress adaptations (e.g. **Appendix A, Fig S7**, and Fig 4 in Bucksch et al., 2017).

Future directions

This study evaluated basal crown root cross-sections from field-grown maize, with a focus on root diameter related traits, tissue proportions, aerenchyma area, and novel characterization of vessel and cell diameter distributions and trait relationships across nodes. However, many anatomical traits remain to be studied. Vessel and cell lengths and development, aerenchyma volume and distribution, cell wall thickness and composition, suberization, endodermal development, pith, protoxylem and phloem traits, and characteristics of the root elongation zone and root tips were not evaluated. Root elongation and cell lengths have been shown to be sensitive to nitrate availability and drought stress in maize (Fraser et al., 1990; Tian et al., 2008; Gao et al., 2015), but genotypic contrast in these responses have not been described.

Additionally, the effect of position along the root axis, as well as different root classes, were not assessed, and pose particular challenges under field conditions. Anatomical plasticity may be affected as soil conditions change over depth, and genotypic variation that manifests in the mature root segments near the stem could be altered near the root tip. Lateral roots, as opposed to axial roots characterized in this study, typically comprise over 90% of total root length and are optimized for water and nutrient absorption. Lateral root development is also under separate genetic control (Hochholdinger and Tuberosa, 2009; Benková and Bielach 2010). Lateral root proliferation, branching (particularly second-order branching), and apoplastic barrier development have been studied in the context of abiotic stress tolerance (Gaudin et al., 2011; Yu et al., 2015; Zhan et al., 2015; Tylová et al., 2017). Lateral root traits involved in mycorrhizal association, root hair morphology, transporters, branching, and responsiveness to heterogeneous resources patches all contribute to resource uptake and use efficiency, and genotypic variation in lateral root traits remains largely unexplored.

Conclusions

The maize root system develops in distinctive, successive nodes, in coordination with shoot growth. Nodal root architecture, morphology and anatomy has the potential to impact the efficiency and capacity of water and nutrient uptake. To better understand the relationship between root anatomy, resource acquisition, and plant growth, this study explored existing genotypic variation in root anatomical traits across nodes, and the plasticity of traits under nitrogen stress. Node effects were substantial, and phenotyping across nodes enabled better resolution of trait relationships, plasticity under nitrogen stress, genotypic variation, and allometric analyses. Further development of root phenotyping methods would be useful, and would enable exploration of novel root traits for improving stress tolerance and resource use efficiency.

Acknowledgements

We thank Shawn Kaeppler and the G2F consortium for providing plant materials.

For agronomic and technical support, we thank Robert Snyder, Michael Williams, Johan Prinsloo, Hannah Schneider, Tania Galindo-Castañeda, Stephanie Klein, Claire Lorts, Jonathan Wu, Pufan Wang, Ryan Burnett, Andy Evensen, Larry York, and Joseph Chimungu.

We thank Benjamin Hall at L4IS and support from the Edmund Optics Higher Education Grant for technical support and improvements to the LAT platform, and Dannielle Gibson, John Sosa, and Tim Ryan for work on three-dimensional root segmentations.

This work was supported by USDA NIFA's AFRI grant 2013-02682 to JPL, the Howard G. Buffett Foundation for research in South Africa, and the USDA National Institute of Food and Agriculture, Hatch project 4372. Any opinions, findings, conclusions, or recommendations expressed in this publication are those of the author(s) and do not necessarily reflect the view of the National Institute of Food and Agriculture (NIFA) or the United States Department of Agriculture (USDA).

References

Aguirrezabal LAN, Pellerin S, Tardieu F. 1993. Carbon nutrition, root branching and elongation: can the present state of knowledge allow a predictive approach at the whole-plant level? Environmental and Experimental Botany **33**, 121–130.

Anfodillo T, Petit G, Sterck F, Lechthaler S, Olson ME. 2016. Allometric Trajectories and 'Stress': A Quantitative Approach. Frontiers in Plant Science **7**, 1–6.

Araki H, Hirayama M, Hirasawa H, Iijima M. 2000. Which roots penetrate the deepest in rice and maize root systems? Plant Prod. Sci. **3**, 281–288.

Benková E, Bielach A. 2010. Lateral root organogenesis - from cell to organ. Current Opinion in Plant Biology **13**, 677–683.

Bloom AJ, Chapin FS, Mooney H a. 1985. Resource Limitation in Plants- An economic analogy. Ann. Rev. Ecol. Syst. **16**, 363–392.

Bucksch A, Atta-Boateng A, Azihou AF, *et al.* 2017. Morphological Plant Modeling: Unleashing Geometric and Topological Potential within the Plant Sciences. Frontiers in Plant Science **8**, 900.

Burton AL, Brown KM, Lynch JP. 2013. Phenotypic Diversity of Root Anatomical and Architectural Traits in Species. Crop Science **53**, 1042–1055.

Burton AL, Lynch JP, Brown KM. 2013. Spatial distribution and phenotypic variation in root cortical aerenchyma of maize (*Zea mays L.*). Plant and Soil **367**, 263–274.

Burton AL, Williams M, Lynch JP, Brown KM. 2012. *RootScan*: Software for high-throughput analysis of root anatomical traits. Plant and Soil **357**, 189–203.

Chimungu JG, Loades KW, Lynch JP. 2015. Root anatomical phenes predict root penetration ability and biomechanical properties in maize (*Zea mays L.*). Journal of Experimental Botany **66**, 3151–3162.

Chimungu JG, Brown KM, Lynch JP. 2014. Large root cortical cell size improves drought tolerance in maize. Plant Physiology **166**, 2166–2178.

Chimungu JG, Brown KM, Lynch JP. 2014. Reduced root cortical cell file number improves drought tolerance in maize. Plant Physiology **166**, 1943–1955.

Clarke JM, McCaig TN. 1993. Breeding for efficient root systems. In: Plant Breeding: Principles and prospects, eds. Hayward MD, Bosemark NO, Romagosa I. Dordrecht: Springer Netherlands, 485–499.

Cobb JN, DeClerck G, Greenberg A, Clark R, McCouch S. 2013. Next-generation phenotyping: Requirements and strategies for enhancing our understanding of genotype-phenotype relationships and its relevance to crop improvement. Theoretical and Applied Genetics **126**, 867–887.

Coleman JS, McConnaughay KDM, Ackerly DD. 1994. Interpreting phenotypic variation in plants. Trends in Ecology and Evolution **9**, 187–191.

De Kroon H, Huber H, Stuefer JF, Van Groenendael JM. 2005. A modular concept of phenotypic plasticity in plants. New Phytologist **166**, 73–82.

DeBruin JL, Schussler JR, Mo H, Cooper M. 2017. Grain Yield and Nitrogen Accumulation in Maize Hybrids Released during 1934 to 2013 in the US Midwest. Crop Science **57**, 1–16.

Demotes-Mainard S, Pellerin S. 1992. Effect of mutual shading on the emergence of nodal roots and the root/shoot ratio of maize. Plant and Soil **147**, 87–93.

Doebley J. 2004. The Genetics of Maize Evolution. Annual Review of Genetics **38**, 37–59.

Doebley J, Stec A, Hubbard L. 1997. The evolution of apical dominance in maize. Nature **386**, 485–488.

Donald CM. 1968. The breeding of crop ideotypes. Euphytica **17**, 385–403.

Drouet JL, Pagès L. 2003. GRAAL: A model of GRowth, Architecture and carbon ALlocation during the vegetative phase of the whole maize plant. Model description and parameterisation. Ecological Modelling **165**, 147–173.

Eissenstat DM, Wells CE, Yanai RD, Whitbeck JL. 2000. Building roots in a changing environment: Implications for root longevity. New Phytologist **147**, 33–42.

Eissenstat DM. 1992. Costs and benefits of constructing roots of small diameter. Journal of Plant Nutrition **15**, 763–782.

FAO. 2014. FAOSTAT. Cited May 18, 2017. http://www.fao.org/faostat/en/#data

Fiorani F, Schurr U. 2013. Future Scenarios for Plant Phenotyping. Annual Review of Plant Biology **64**, 267–291.

Fischer T, Byerlee D, Edmeades G. 2014. Crop yields and global food security. Australian Centre for International Agricultural Research, 1–660.

Fraser TE, Silk WK, Rost TL. 1990. Effects of Low Water Potential on Cortical Cell Length in Growing Regions of Maize Roots. Plant Physiology **93**, 648–651.

Gao K, Chen F, Yuan L, Zhang F, Mi G. 2015. A comprehensive analysis of root morphological changes and nitrogen allocation in maize in response to low nitrogen stress. Plant, Cell & Environment **38**, 740–750.

Gaudin ACM, McClymont SA, Holmes BM, Lyons E, Raizada MN. 2011. Novel temporal, fine-scale and growth variation phenotypes in roots of adult-stage maize (*Zea mays L.*) in response to low nitrogen stress. Plant, Cell & Environment **34**, 2122–2137.

Gibbon D, Dixon J, Flores D. 2007. Beyond Drought Tolerant Maize: Study of Additional Priorities in Maize. Report to Generation Challenge Program, 1–42.

Girardin P, Morel-fourrier B, Jordan M, Meyer J, Mercier J. 1987. Développement des racines adventives chez le maïs. Agronomie, EDP Sciences **7**, 353–360.

Hirel B, Tétu T, Lea PJ, Dubois F. 2011. Improving nitrogen use efficiency in crops for sustainable agriculture. Sustainability **3**, 1452–1485.

Hochholdinger F, Tuberosa R. 2009. Genetic and genomic dissection of maize root development and architecture. Current Opinion in Plant Biology **12**, 172–7.

Hochholdinger F, Woll K, Sauer M, Dembinsky D. 2004. Genetic dissection of root formation in maize (Zea mays) reveals root-type specific developmental programmes. Annals of Botany **93**, 359–368.

Hoppe DC, McCully ME, Wenzel CL. 1986. The nodal roots of Zea : their development in relation to structural features of the stem. Canadian Journal of Botany **64**, 2524–2537.

Horikoshi M, Tang Y. 2016. ggfortify: Data Visualization Tools for Statistical Analysis Results.

Jordan MO, Harada J, Bruchou C, Yamazaki K. 1993. Maize nodal root ramification: Absence of dormant primordia, root classification using histological parameters and consequences on sap conduction. Plant and Soil **153**, 125–143.

Kjemtrup S, Boyes DC, Christensen C, McCaskill AJ, Hylton M, Davis K. 2003. Growth Stage-Based Phenotypic Profiling of Plants. In: Plant Functional Genomics, ed. Grotewold E. Totowa, NJ: Humana Press, 427–441.

Lea PJ, Azevedo RA. 2006. Nitrogen use efficiency. 1. Uptake of nitrogen from the soil. Annals of Applied Biology **149**, 243–247.

Lewis AM, Boose ER. 1995. Estimating volume flow rates through xylem conduits. American Journal of Botany **82**, 1112–1116.

Li P, Zhuang Z, Cai H, Cheng S, Soomro AA, Liu Z, Gu R, Mi G, Yuan L, Chen F. 2016. Use of genotype-environment interactions to elucidate the pattern of maize root plasticity to nitrogen deficiency. Journal of Integrative Plant Biology **58**, 242–253.

Liu S, Song F, Liu F, Zhu X, Xu H. 2012. Effect of Planting Density on Root Lodging Resistance and Its Relationship to Nodal Root Growth Characteristics in Maize (*Zea mays L.).* Journal of Agricultural Science **4**, 182–189.

Liu S, Song F, Zhu X, Xu H. 2012. Dynamics of Root Growth and Distribution in Maize from the Black Soil Region of NE China. Journal of Agricultural Science **4**, 21–30.

Lynch JP. 2013. Steep, cheap and deep: an ideotype to optimize water and N acquisition by maize root systems. Annals of Botany **112**, 347–57.

Lynch JP. 2014. Root phenes that reduce the metabolic costs of soil exploration: opportunities for 21st century agriculture. Plant, Cell & Environment, 1–10.

Mano Y, Omori F, Takamizo T, Kindiger B, Bird RM, Loaisiga CH. 2006. Variation for root aerenchyma formation in flooded and non-flooded maize and teosinte seedlings. Plant and Soil **281**, 269–279.

Marshall-Colon A, Long SP, Allen DK, *et al.* 2017. Crops In Silico: Generating Virtual Crops Using an Integrative and Multi-scale Modeling Platform. Frontiers in Plant Science **8**, 1–7.

Meister R, Rajani MS, Ruzicka D, Schachtman DP. 2014. Challenges of modifying root traits in crops for agriculture. Trends in Plant Science **19**, 779–788.

Moll RH, Kamprath EJ, Jackson WA. 1982. Analysis and Interpretation of Factors Which Contribute to Efficiency of Nitrogen Utilization 1. Agronomy Journal **74**, 562–564.

Paez-Garcia A, Motes C, Scheible W-R, Chen R, Blancaflor E, Monteros M. 2015. Root Traits and Phenotyping Strategies for Plant Improvement. Plants **4**, 334–355.

Pellerin S. 1994. Number of maize nodal roots as affected by plant density and nitrogen fertilization : relationships with shoot growth. European Journal of Agronomy **3**, 101–110.

Pinheiro J, Bates D, DebRoy S, Sarkar D and R Core Team. 2016. nlme: Linear and Nonlinear Mixed Effects Models. R package version 3.1-128

Postma JA, Dathe A, Lynch JP. 2014. The Optimal Lateral Root Branching Density for Maize Depends on Nitrogen and Phosphorus Availability. Plant Physiology **166**, 590–602.

Postma JA, Kuppe C, Owen MR, Mellow N, Griffiths M, Bennett MJ, Lynch JP, Watt M. 2017. OpenSimRoot: Widening the scope and application of root architectural models. New Phytologist.

Pound MP, French AP, Wells DM, Bennett MJ, Pridmore TP. 2012. CellSeT: Novel Software to Extract and Analyze Structured Networks of Plant Cells from Confocal Images. The Plant Cell **24**, 1353–1361.

Prince SJ, Murphy M, Mutava RN, Durnell LA, Valliyodan B, Grover Shannon J, Nguyen HT. 2017. Root xylem plasticity to improve water use and yield in water-stressed soybean. Journal of Experimental Botany **68**, 2027-2036.

Purushothaman R, Zaman-Allah M, Mallikarjuna N, Pannirselvam R, Krishnamurthy L, Gowda CLL. 2013. Root Anatomical Traits and Their Possible Contribution to Drought Tolerance in Grain Legumes. Plant Production Science **16**, 1–8.

Rahaman MM, Chen D, Gillani Z, Klukas C, Chen M. 2015. Advanced phenotyping and phenotype data analysis for the study of plant growth and development. Frontiers in plant science **6**, 619.

Raun WR, Johnson GV. 1999. Improving nitrogen use efficiency for cereal production. Agronomy Journal **91**, 357–363.

Richards RA, Passioura JB. 1989. A breeding program to reduce the diameter of the major xylem vessel in the seminal roots of wheat and its effect on grain yield in rain-fed environments. Australian Journal of Agricultural Research **40**, 943-950.

Saengwilai P, Nord E a, Chimungu JG, Brown KM, Lynch JP. 2014. Root cortical aerenchyma enhances nitrogen acquisition from low-nitrogen soils in maize. Plant physiology **166**, 726–735.

Schmidt JE, Gaudin ACM. 2017. Toward an Integrated Root Ideotype for Irrigated Systems. Trends in Plant Science **22**, 433–443.

Schneider HM, Wojciechowski T, Postma JA, Brown KM, Lücke A, Zeisler V, Schreiber L, Lynch JP. 2017. Root cortical senescence decreases root respiration, nutrient content and radial water and nutrient transport in barley. Plant, Cell & Environment.

Sebastian J, Yee M-C, Goudinho Viana W, *et al.* 2016. Grasses suppress shoot-borne roots to conserve water during drought. Proceedings of the National Academy of Sciences **113**, 8861–8866.

Sosa JM, Huber DE, Welk B, Fraser HL. 2014. Development and application of MIPAR^{TM}: a novel software package for two- and three-dimensional microstructural characterization. Integrating Materials and Manufacturing Innovation **3**, 18.

Stamp P, Kiel C. 1992. Root Morphology of Maize and Its Relationship to Root Lodging. Journal of Agronomy and Crop Science **168**, 113–118.

Striker GG, Insausti P, Grimoldi AA, Vega AS. 2007. Trade-off between root porosity and mechanical strength in species with different types of aerenchyma. Plant, Cell & Environment **30**, 580–589.

Strock CF, De la Riva LM, Lynch JP. 2017. Reduction in root secondary growth as a strategy for phosphorus acquisition. Plant Physiology, in press.

Tian Q, Chen F, Liu J, Zhang F, Mi G. 2008. Inhibition of maize root growth by high nitrate supply is correlated with reduced IAA levels in roots. Journal of Plant Physiology **165**, 942–951.

Trachsel S, Kaeppler SM, Brown KM, Lynch JP. 2011. Shovelomics: High throughput phenotyping of maize (Zea mays L.) root architecture in the field. Plant and Soil **341**, 75–87.

Tylová E, Pecková E, Blascheová Z, Soukup A. 2017. Casparian bands and suberin lamellae in exodermis of lateral roots: an important trait of roots system response to abiotic stress factors. Annals of Botany, 1–15.

Uga Y, Sugimoto K, Ogawa S, *et al.* 2013. Control of root system architecture by DEEPER ROOTING 1 increases rice yield under drought conditions. Nature Genetics **45**, 1097–1102.

Wachsman G, Sparks EE, Benfey PN. 2015. Genes and networks regulating root anatomy and architecture. New Phytologist **208**, 26–38.

Wahl S, Ryser P, Edwards P. 2001. Phenotypic Plasticity of Grass Root Anatomy in Response to Light Intensity and Nutrient Supply. Annals of Botany **88**, 1071–1078.

Wei T, Simko V. 2016. corrplot: Visualization of a Correlation Matrix. R package version 0.77.

Weiner J. 2004. Allocation, plasticity and allometry in plants. Perspectives in Plant Ecology, Evolution and Systematics **6**, 207–215.

Wickham H. 2009. ggplot2: Elegant Graphics for Data Analysis. Springer-Verlag New York.

Wickham H. 2011. The Split-Apply-Combine Strategy for Data Analysis. Journal of Statistical Software, 40(1), 1-29. URL http://www.jstatsoft.org/v40/i01/.

Wilhelm WW, McMaster GS. 1995. Importance of the phyllocrhron in studying development and growth in grasses. Crop Science **35**, 1–3.

Xu G, Fan X, Miller AJ. 2012. Plant nitrogen assimilation and use efficiency. Annual Review of Plant Biology **63**, 153–82.

Yamazaki K, Kaeriyama N. 1982. The Morphological Characters and the Growing Directions of Primary Roots of Corn Plants. Japan. Jour. Crop Sci. **51**, 584–590.

York LM, Galindo-Castaneda T, Schussler JR, Lynch JP. 2015. Evolution of US maize (*Zea mays* L.) root architectural and anatomical phenes over the past 100 years corresponds to increased tolerance of nitrogen stress. Journal of Experimental Botany **66**, 2347–2358.

York LM, Lynch JP. 2015. Intensive field phenotyping of maize (Zea mays L.) root crowns identifies phenes and phene integration associated with plant growth and nitrogen acquisition. Journal of Experimental Botany **66**, 5493–5505.

York LM, Nord EA, Lynch JP. 2013. Integration of root phenes for soil resource acquisition. Frontiers in Plant Science **4**, 355.

Yu P, Hochholdinger F, Li C. 2015. Root-type-specific plasticity in response to localized high nitrate supply in maize (*Zea mays*). Annals of Botany **116**, 751–762.

Zhan A, Lynch JP. 2015. Reduced frequency of lateral root branching improves N capture from low-N soils in maize. Journal of Experimental Botany **66**, 2055–2065.

Zhu XG, Lynch JP, Lebauer DS, Millar AJ, Stitt M, Long SP. 2016. Plants in silico: Why, why now and what?-an integrative platform for plant systems biology research. Plant, Cell and Environment **39**, 1049–1057.

Figures and Tables

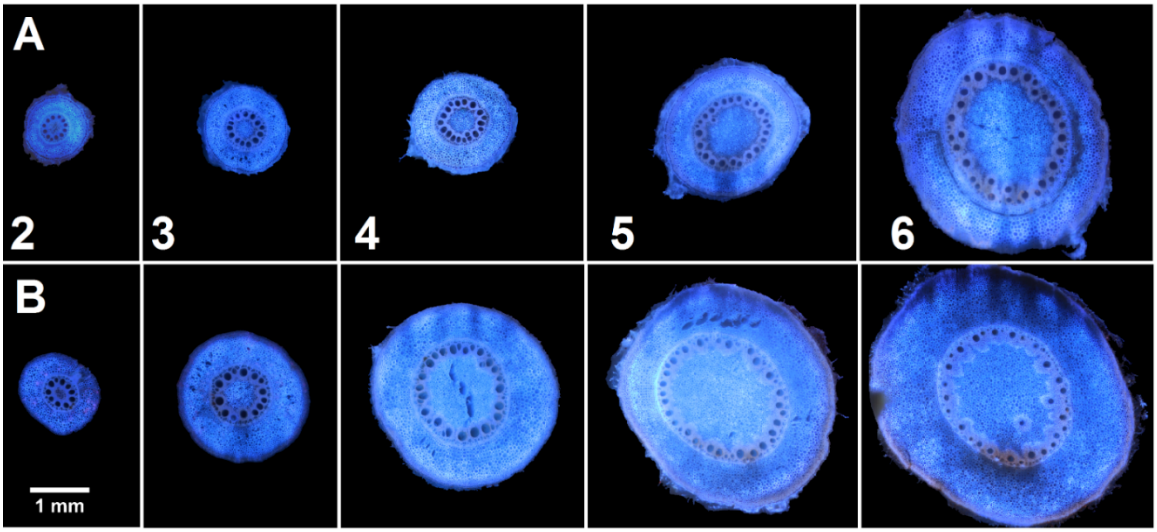

Figure 1-1. Nodal variation in maize root anatomy. Nodal root cross-section images from high nitrogen field-grown maize hybrids, sampled from older to younger nodes (left to right, numbered) from two genotypes (row A, B). Scale applies to all images.

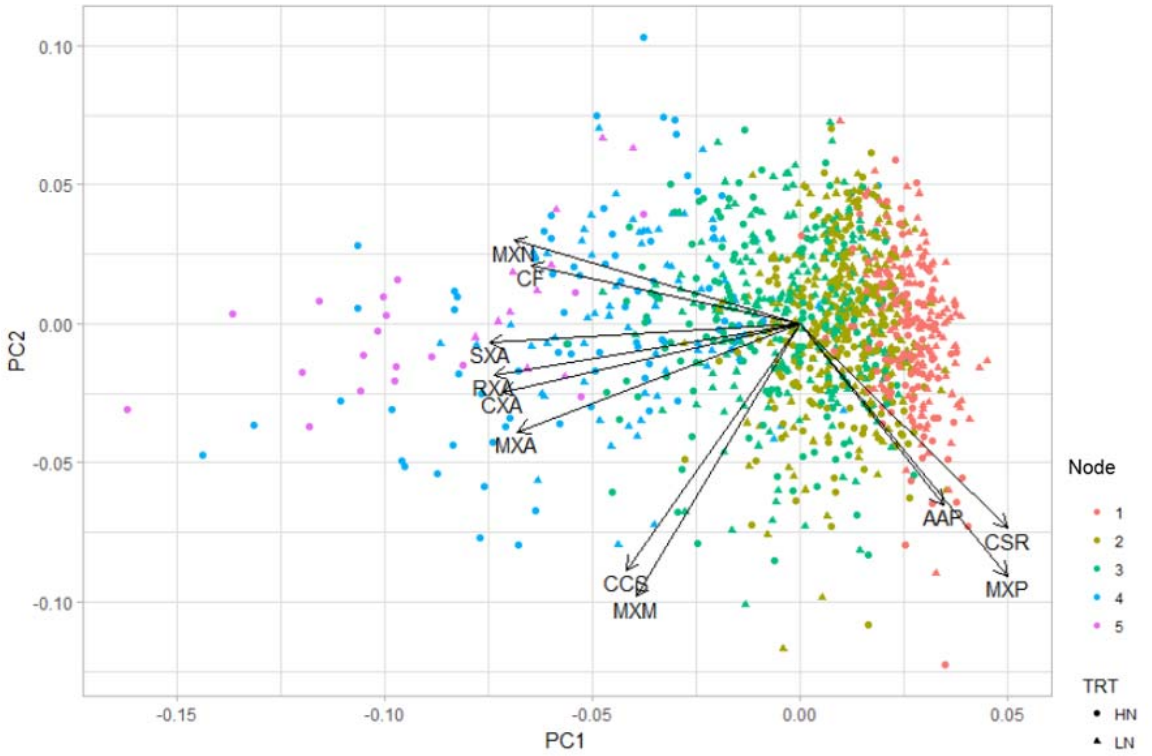

Figure 1-2. Principle components analysis of root anatomy traits. Biplot of the first two principle components (PC 1, 2) of a principle components analysis on 11 root anatomy traits. Points indicate scores of individual roots on these two components, from nodes 1 to 5 (by color) of field-grown maize inbreds and hybrids (PA14, PA15, PA16, total n=1171) in high and low nitrogen treatments (by shape). Arrows represent loadings of root anatomy traits (labeled) on these two components. See Table 1-1 for trait abbreviations. PC1 and PC2 explained 66.7% and 9.7% of total variance, respectively.

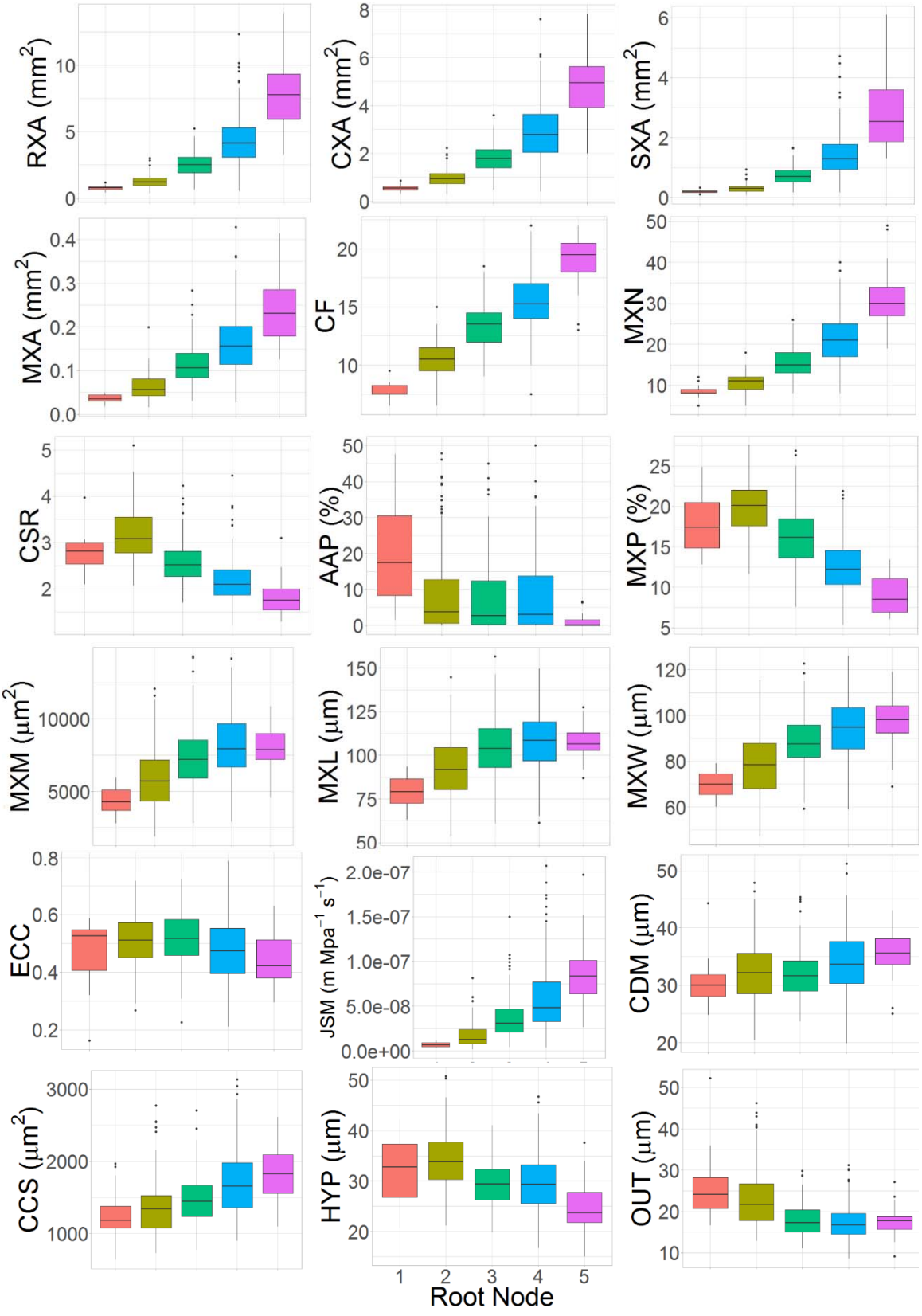
RXA (mm2)
CXA (mm2)
SXA (mm2)
MXA (mm2)
CF
MXN
CSR
AAP (%)
MXP (%)
MXM (µm2)
MXL (µm)
MXW (µm)
ECC
JSM (m Mpa-1 s-1)
CDM (µm)
CCS (µm2)
HYP (µm)
OUT (µm)
Root Node

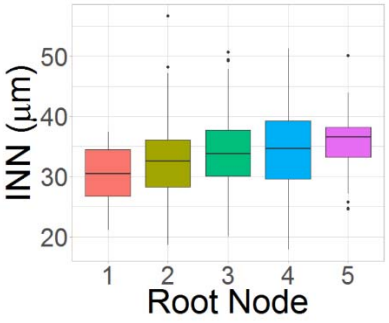

Figure 1-3. Root anatomy variation by node in field-grown maize hybrids. Boxplots of nodal root anatomy traits evaluated in nodes 1 (oldest) through 5 (left to right in each plot) from 44 field-grown maize hybrid genotypes, including high and low nitrogen treatments (PA16). Horizontal box lines indicate 25th, 50th, and 75th percentile; whiskers indicates range, excluding outliers (points). Total n = 469 per plot. See Table 1-1 for trait abbreviations and units.

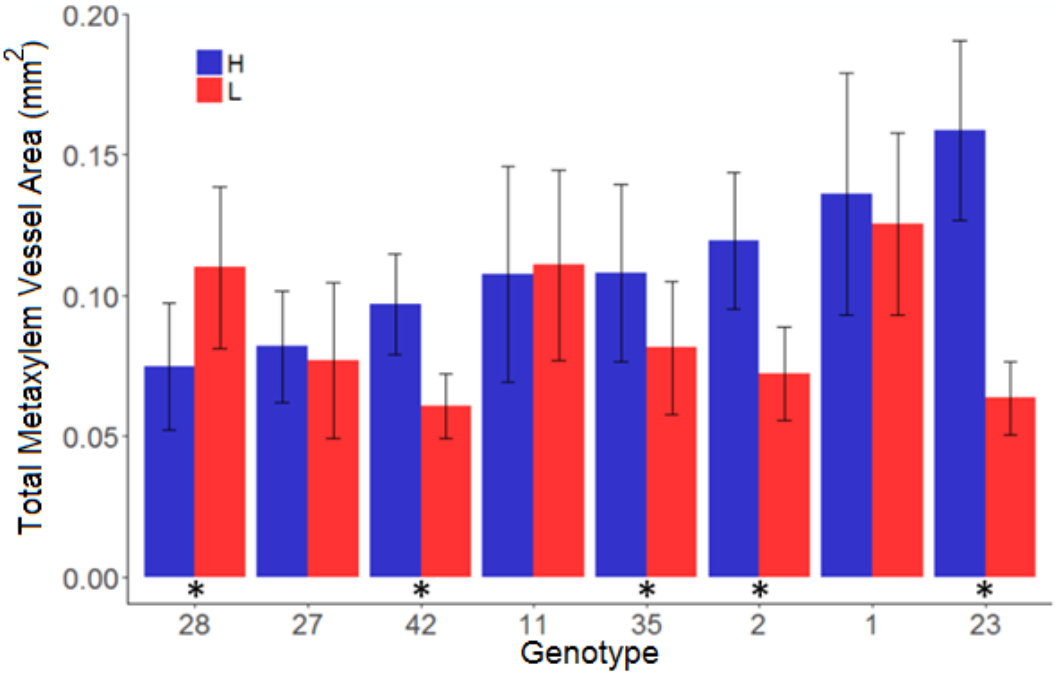

Figure 1-4. Genotypic variation in plasticity of total metaxylem vessel area (mm^2) under low nitrogen. Mean ± S.E. metaxylem vessel area (mm^2) across nodes 2, 3, and 4 under high or low nitrogen (H, blue; L, red) for select maize hybrid genotypes (see Appendix A, Table S1 for genotype codes). Asterisks represent genotypes with significant differences ($p<0.05$) between nitrogen treatments according to a pairwise comparison of trait values matched by node.

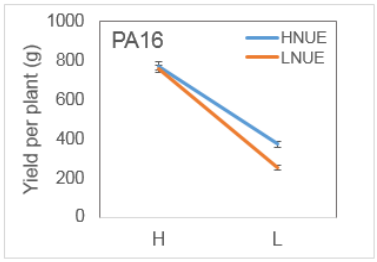

PA16

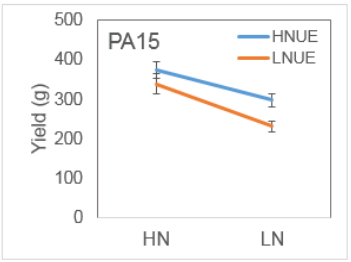

PA15

PA16:

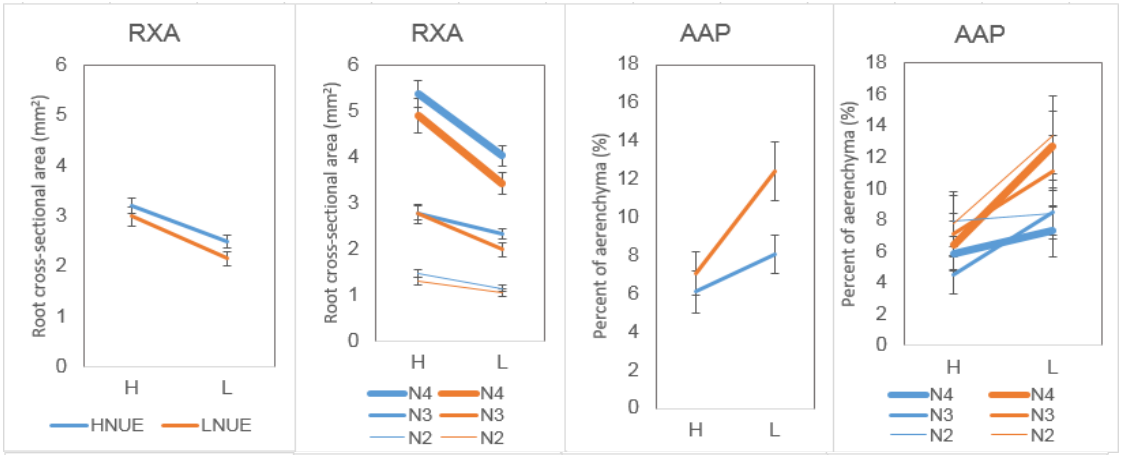

PA15:

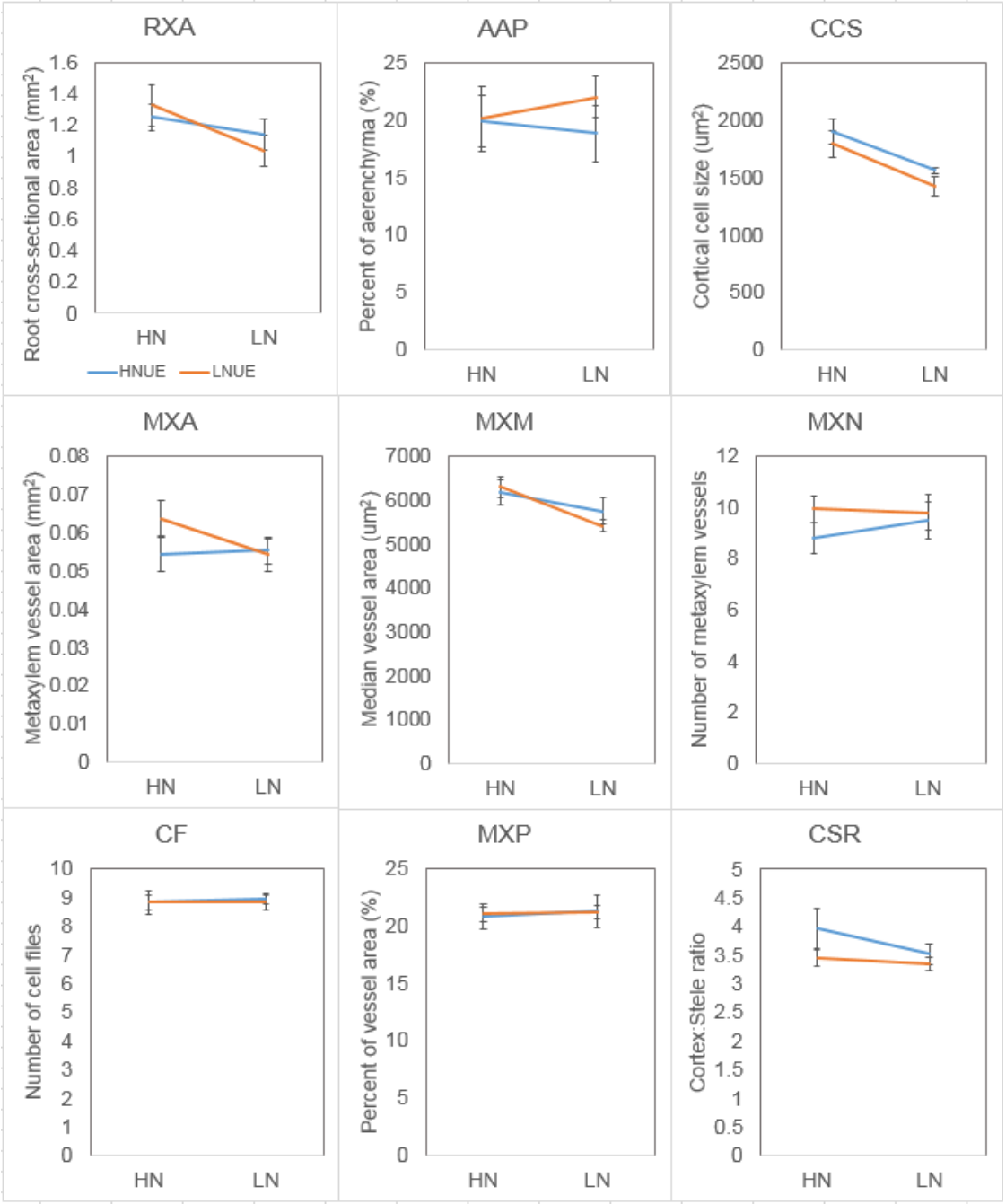

Figure 1-5. Anatomical differences among HNUE and LNUE genotypes. Genotypes were matched based on high N yield and then grouped according to high or low N use efficiency (HNUE, blue; LNUE, orange) based on low N yield. For PA16 (left), 22 hybrid genotypes were included in each group; for PA15 (right), 4 inbred genotypes were in each group. Genotypes with variable performance were excluded. Mean ± SE of yield and select anatomical traits under high and low N (H, L) conditions are plotted; traits are averaged across nodes 2, 3, and 4 for PA16, and nodes 1, 2, and 3 for PA15, unless indicated by line thickness in the legend (as N1, N2, N3, N4). See Table 1-1 for trait abbreviations and units.

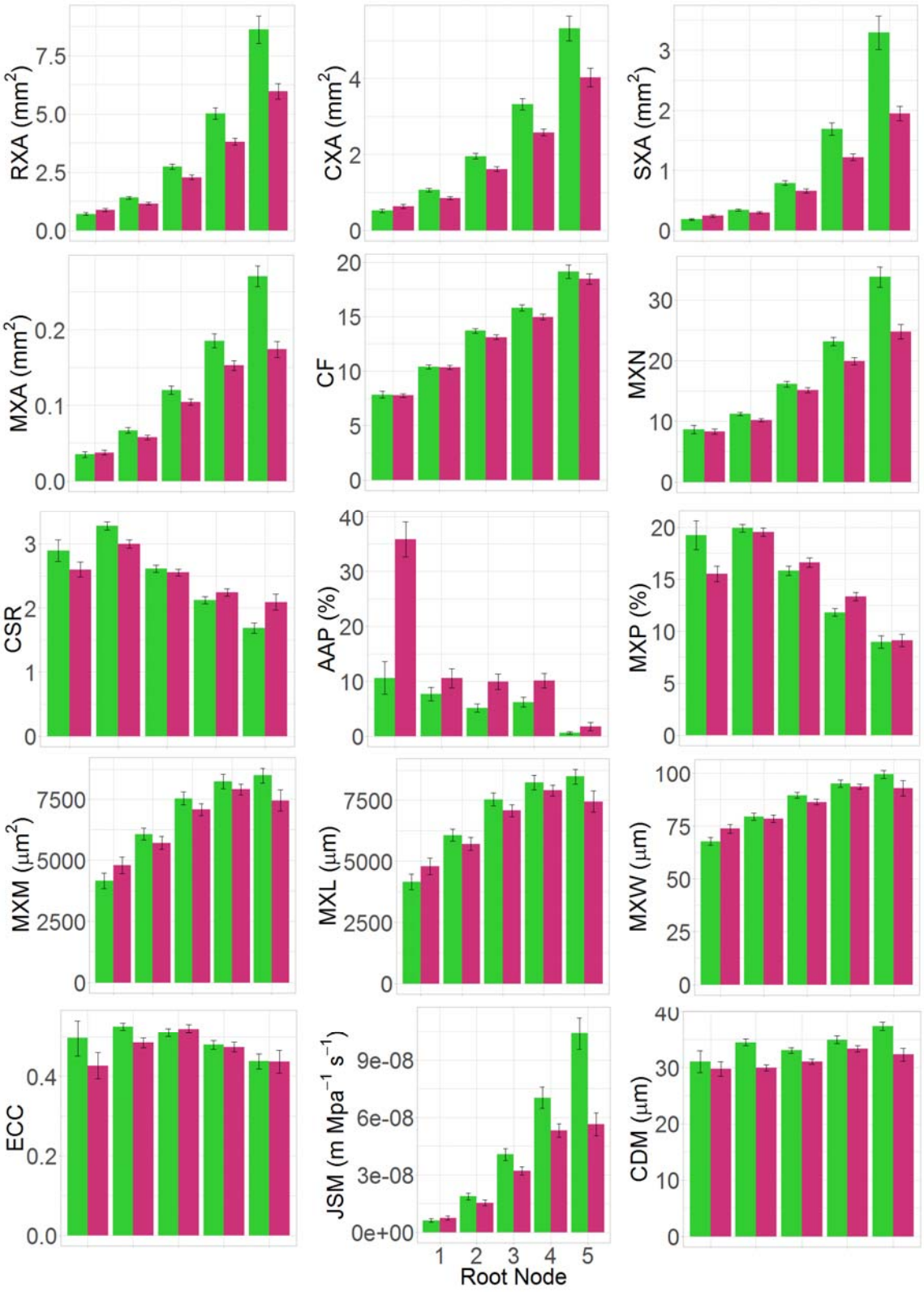
RXA (mm2)
CXA (mm2)
SXA (mm2)
MXA (mm2)
CF
MXN
CSR
AAP (%)
MXP (%)
MXM (µm2)
MXL (µm)
MXW (µm)
ECC
JSM (m Mpa−1 s−1)
CDM (µm)
Root Node

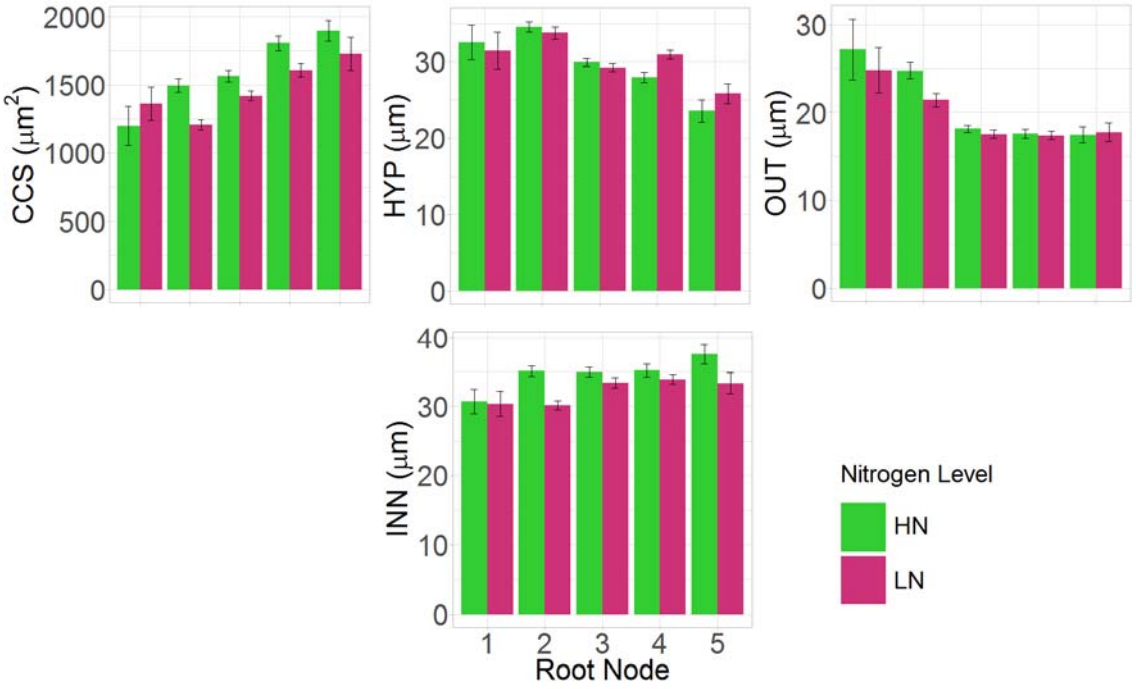

Figure 1-6. Node-specific root anatomy responses to nitrogen stress. Root trait means ± S.E. by node (x-axis) and nitrogen treatment (green, HN; pink, LN) in field-grown maize genotypes (PA16). Total n=469 roots per plot. See Table 1-1 for trait abbreviations and units. Percent change under LN by node are in Appendix A, Table S5.

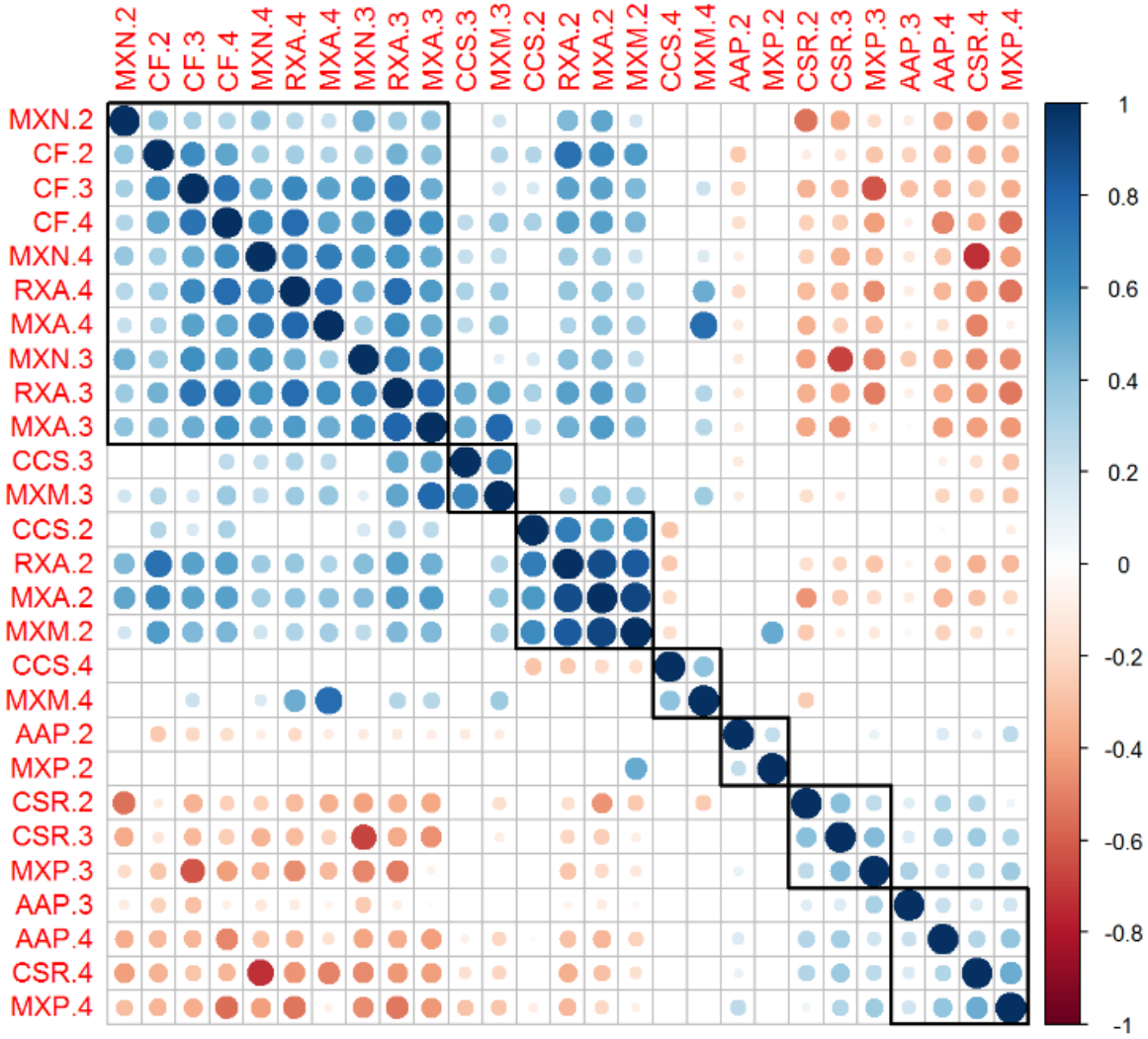

Figure 1-7. Maize root anatomy trait relationships across nodes. Correlation matrix of root anatomy traits evaluated in nodes 2, 3, 4 (numbered) in n=69 mean trait values per node from low-nitrogen field-grown maize hybrids (PA16). Color scale indicates Spearman's ranked correlation coefficient. Larger circle size reflects smaller p-value; blank cells indicate correlation was not significant at $p<0.05$. Most strongly related traits are ordered and grouped in black boxes according to hierarchical clustering. See Table 1-1 for trait abbreviations.

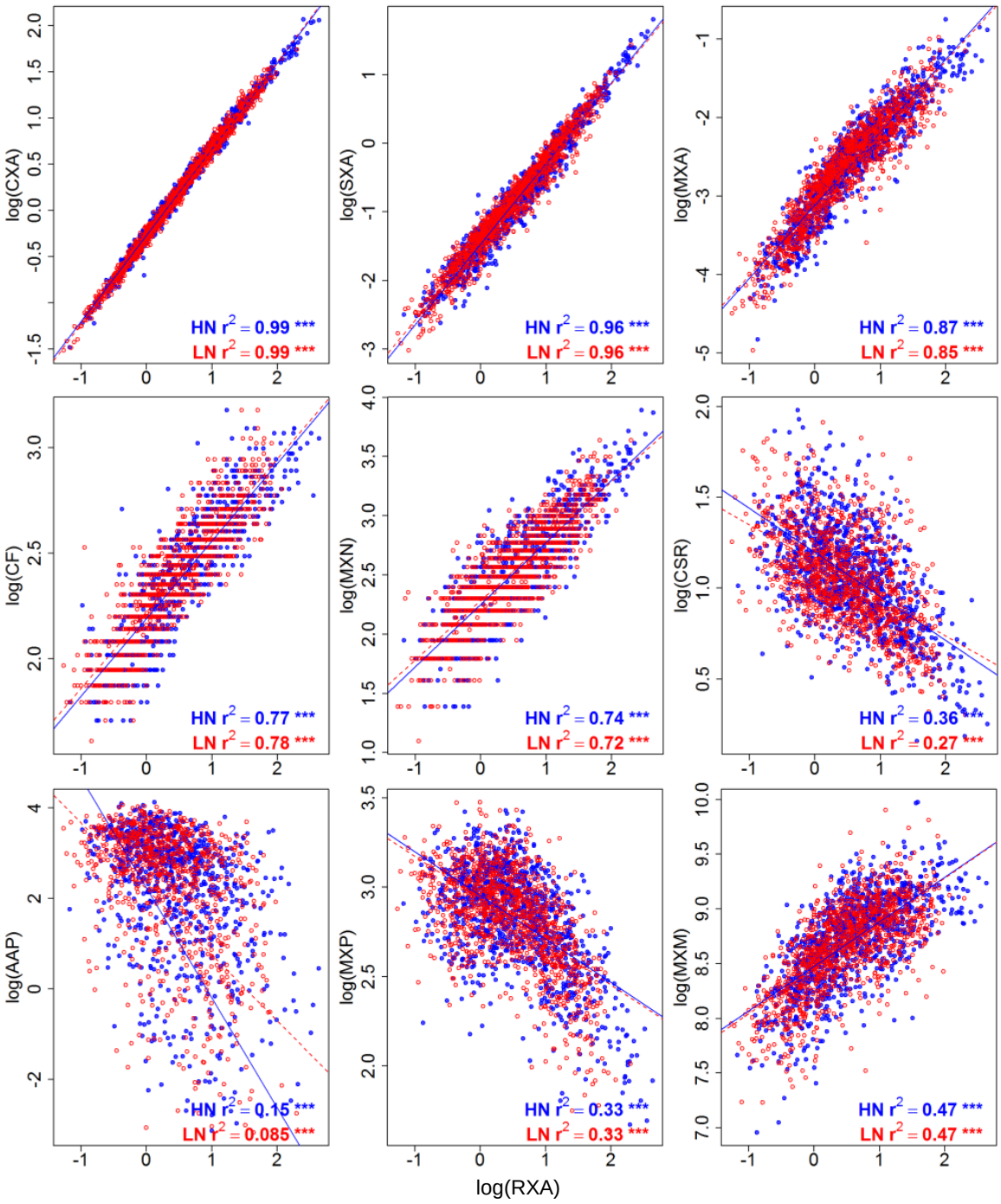
log(CXA)
HN r2 = 0.99 ***
LN r2 = 0.99 ***
log(SXA)
HN r2 = 0.96 ***
LN r2 = 0.96 ***
log(MXA)
HN r2 = 0.87 ***
LN r2 = 0.85 ***
log(CF)
HN r2 = 0.77 ***
LN r2 = 0.78 ***
log(MXN)
HN r2 = 0.74 ***
LN r2 = 0.72 ***
log(CSR)
HN r2 = 0.36 ***
LN r2 = 0.27 ***
log(AAP)
HN r2 = 0.15 ***
LN r2 = 0.085 ***
log(MXP)
HN r2 = 0.33 ***
LN r2 = 0.33 ***
log(MXM)
HN r2 = 0.47 ***
LN r2 = 0.47 ***
log(RXA)

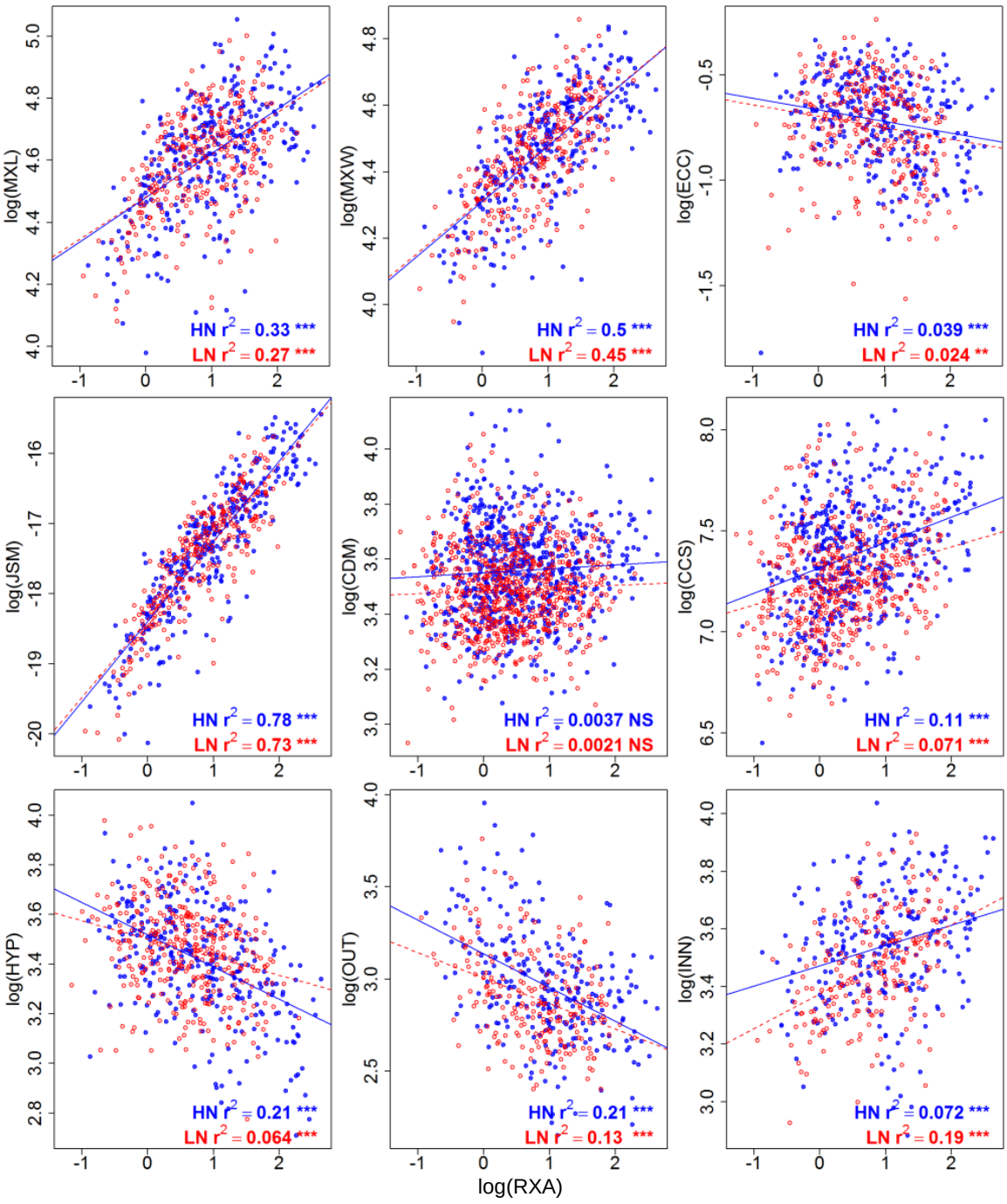
log(MXL)
HN r2 = 0.33 ***
LN r2 = 0.27 ***
log(MXW)
HN r2 = 0.5 ***
LN r2 = 0.45 ***
log(ECC)
HN r2 = 0.039 ***
LN r2 = 0.024 **
log(JSM)
HN r2 = 0.78 ***
LN r2 = 0.73 ***
log(CDM)
HN r2 = 0.0037 NS
LN r2 = 0.0021 NS
log(CCS)
HN r2 = 0.11 ***
LN r2 = 0.071 ***
log(HYP)
HN r2 = 0.21 ***
LN r2 = 0.064 ***
log(OUT)
HN r2 = 0.21 ***
LN r2 = 0.13 ***
log(INN)
HN r2 = 0.072 ***
LN r2 = 0.19 ***
log(RXA)

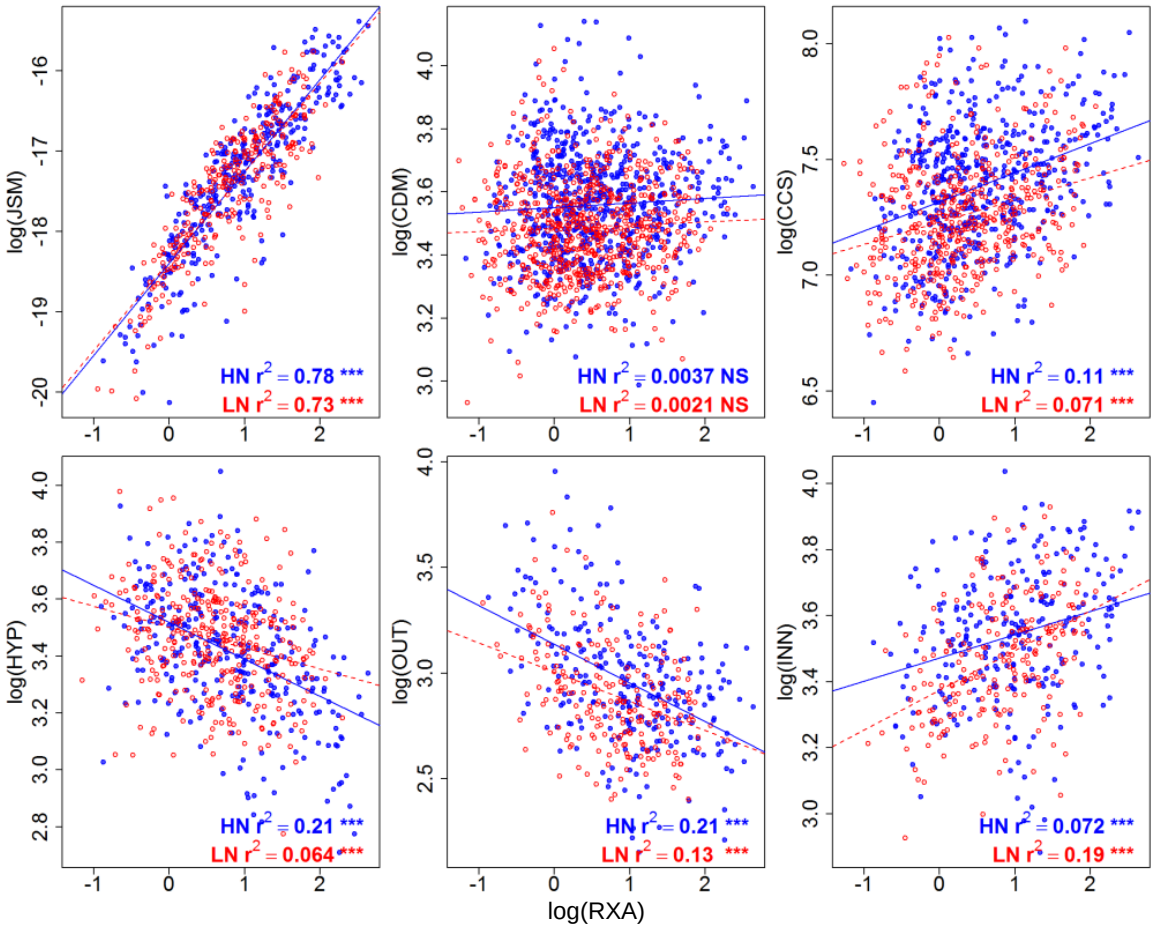

Figure 1-8. Scaling relationships between root anatomy traits and root diameter. The natural logarithm of each root anatomy trait is plotted against the natural logarithm of root cross-sectional area (RXA, mm^2), including up to 5 root nodes from field-grown maize inbreds and hybrids (PA13, PA14, SA14, PA15, PA16), with nitrogen (N) treatment indicated with colors (high N, blue; low N, red). R^2 and p-values (significance levels of p<0.1., 0.05*, 0.001**, 0.0001***, not significant >0.1 NS) are given in each plot. Each plot has n=472 to 2217 depending on trait; not all traits were evaluated in all studies. See Table 1-1 for abbreviations and units.

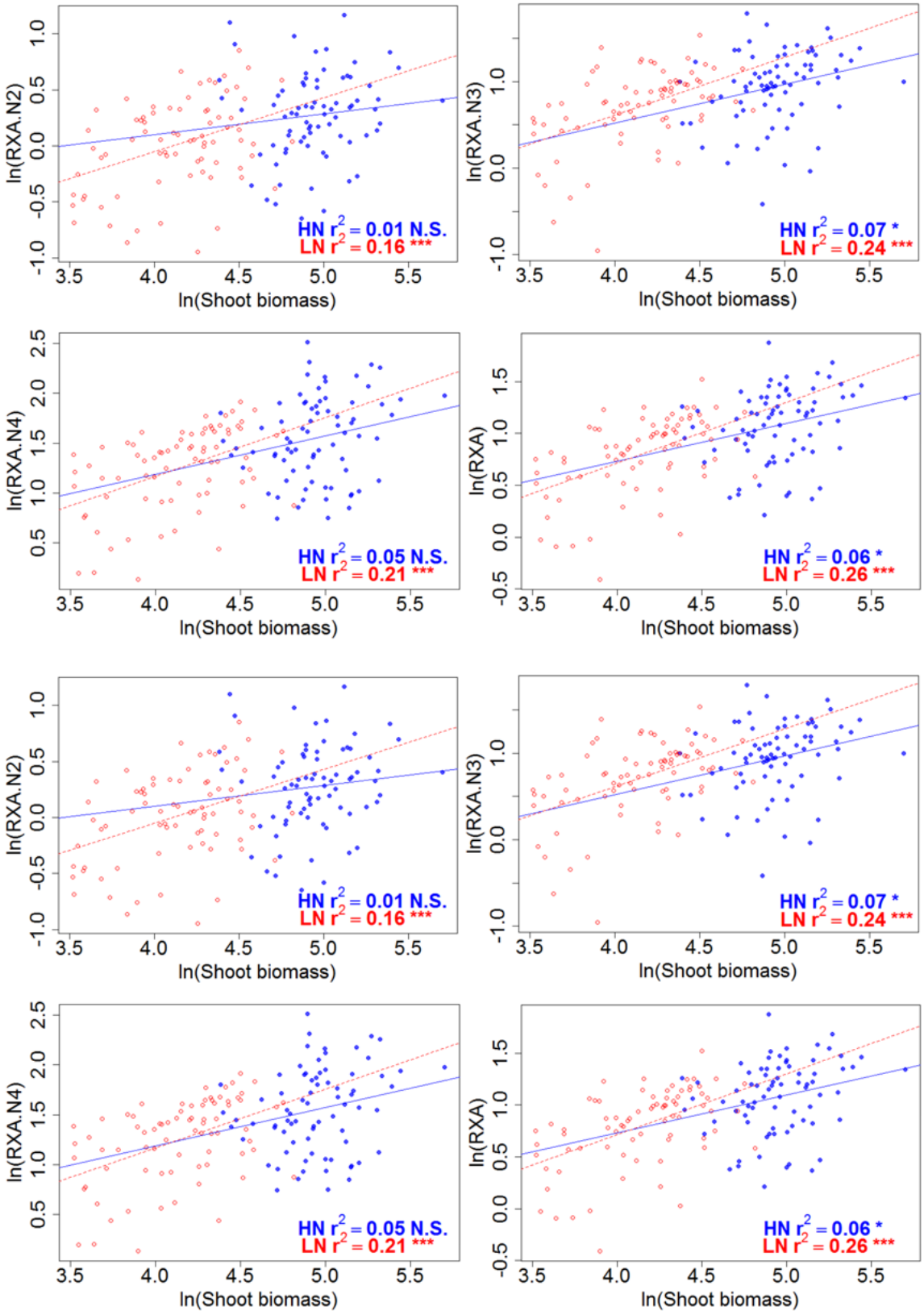
ln(RXA.N2)
ln(Shoot biomass)
HN r2 = 0.01 N.S.
LN r2 = 0.16 ***
ln(RXA.N3)
ln(Shoot biomass)
HN r2 = 0.07 *
LN r2 = 0.24 ***
ln(RXA.N4)
ln(Shoot biomass)
HN r2 = 0.05 N.S.
LN r2 = 0.21 ***
ln(RXA)
ln(Shoot biomass)
HN r2 = 0.06 *
LN r2 = 0.26 ***
ln(RXA.N2)
ln(Shoot biomass)
HN r2 = 0.01 N.S.
LN r2 = 0.16 ***
ln(RXA.N3)
ln(Shoot biomass)
HN r2 = 0.07 *
LN r2 = 0.24 ***
ln(RXA.N4)
ln(Shoot biomass)
HN r2 = 0.05 N.S.
LN r2 = 0.21 ***
ln(RXA)
ln(Shoot biomass)
HN r2 = 0.06 *
LN r2 = 0.26 ***

Figure 1-9. Allometric relationships of root diameter by node. The natural logarithm of root cross-sectional area (RXA, mm^2) is plotted against the natural logarithm of dry shoot biomass (g) weighed at anthesis from maize hybrids (PA16), with nitrogen (N) treatment indicated with colors (high N, blue; low N, red) and each node indicated on the y-axis (N2, N3, N4, and averaged across nodes). R^2 and p-values (significance levels of p<0.1., 0.05*, 0.001**, 0.0001***, not significant >0.1 N.S.) are given in each plot. Allometric scaling coefficients for nodes 2, 3, 4, and averaged across nodes were, respectively: 0.20, 0.45, 0.37, 0.36 for high N, and 0.48, 0.67, 0.59, 0.59 for low N. An isometric relationship between RXA and shoot biomass would be approximated by a scaling coefficient of 0.67. Nitrogen treatment did not have a statistically significant effect in the analysis of covariance models of ln(RXA) ~ ln(Shoot biomass)*TRT for any of the nodes.

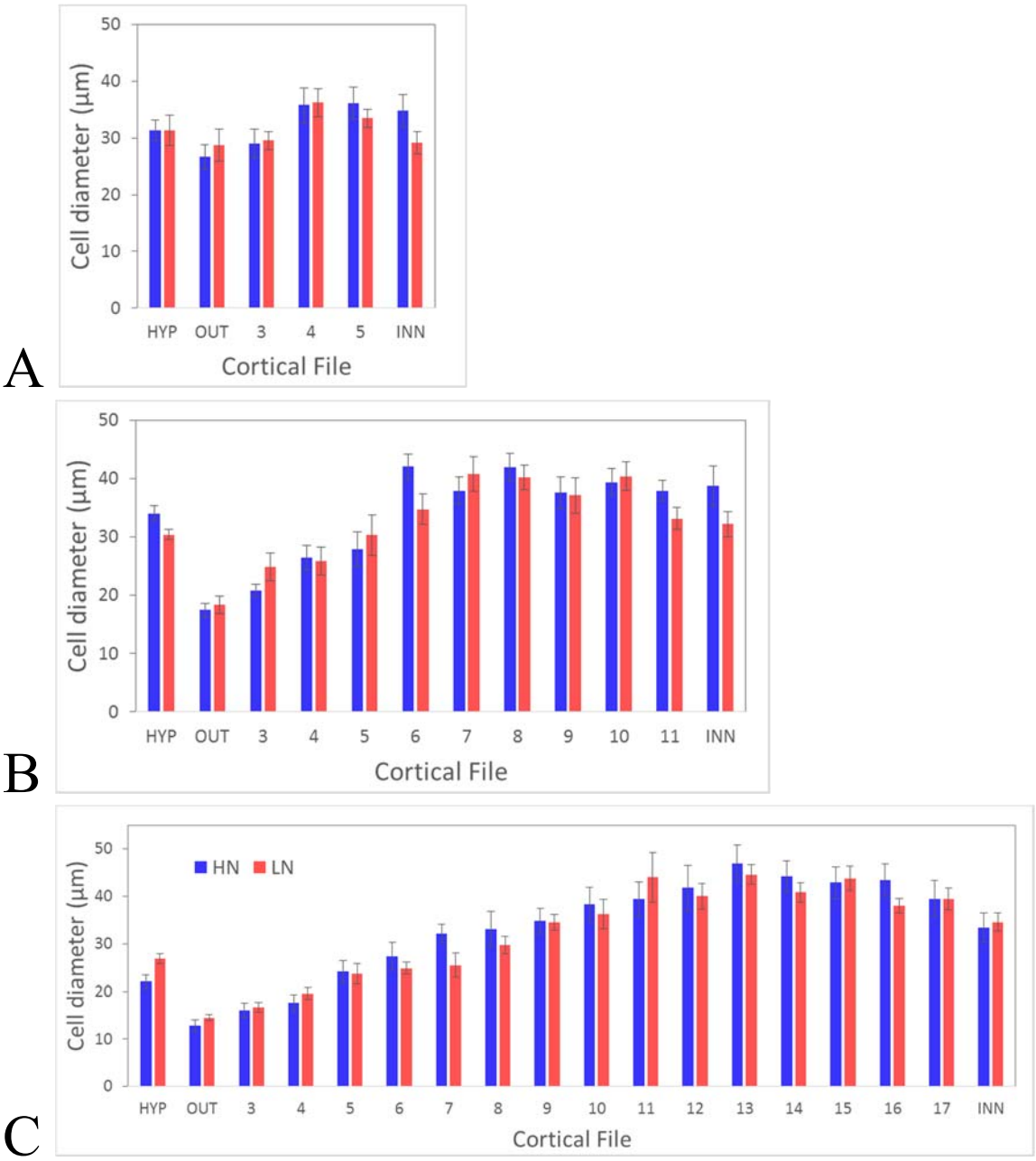

Figure 1-10. Cortical cell sizes in roots of different cell file numbers. Mean ± SE cortical cell diameters (n=20 per file, per plot) in each cell file, for roots with 7 (from nodes 1 and 2), 13 (from nodes 3 and 4), and 19 (from nodes 4 and 5) total cell files (top to bottom) from field-grown maize hybrids (PA16). HYP is the hypodermis, OUT indicates the outermost cortical file, and INN indicates the second innermost cortical cell file; the remaining cell files are numbered. The innermost cortical cell file adjacent to the stele was not measured due to high variability in the occurrence of cells in this file, depending on stele shape. High nitrogen (blue, HN) and low N (red, LN) treatments are indicated.

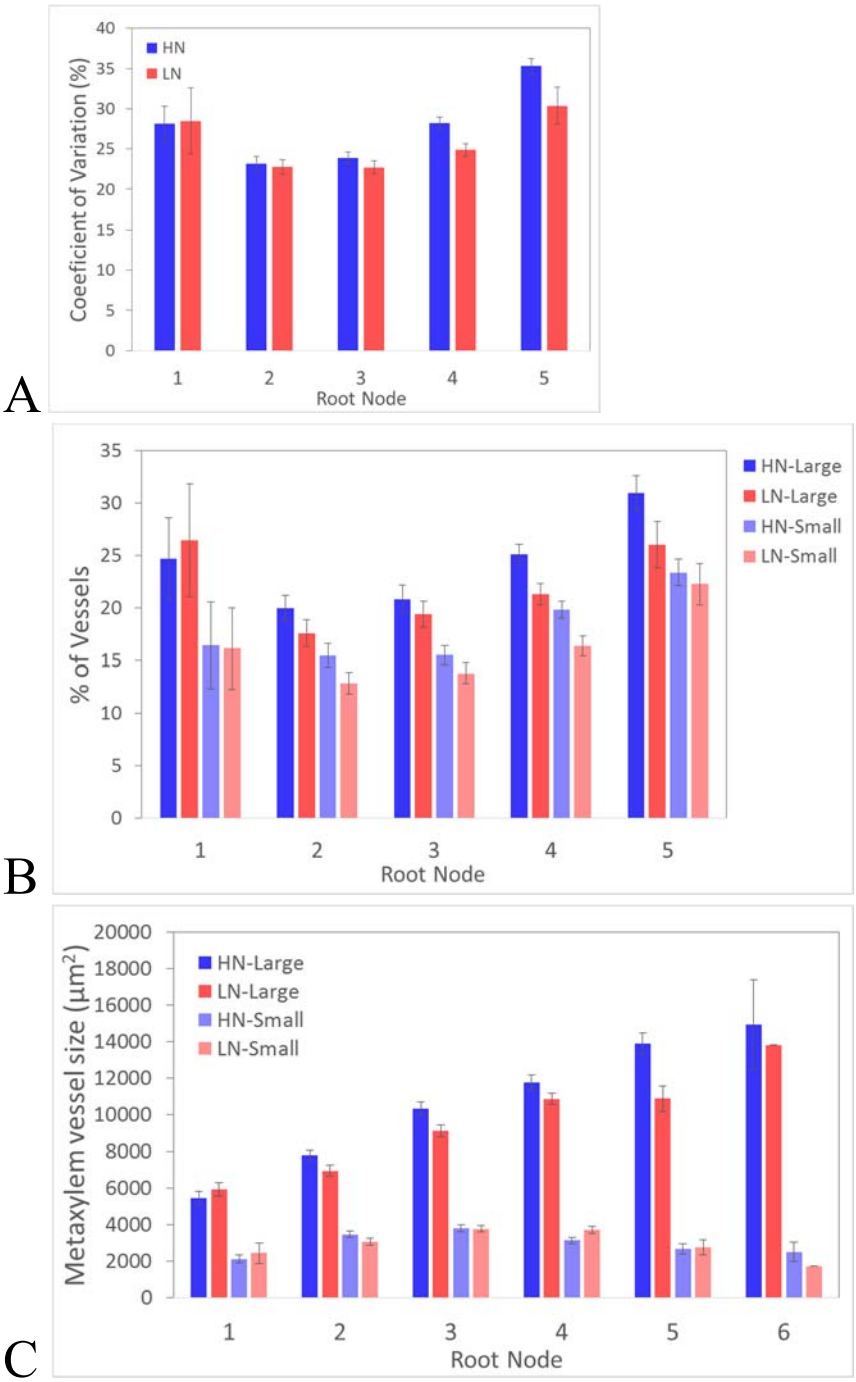

Figure 1-11. Metaxylem vessel size distribution across nodes. (A) Mean ± SE coefficient of variation in metaxylem vessel sizes within a root cross-section for each node, (B) mean ± SE relative number of very large (left two bars, per node) and very small (right two bars, per node) metaxylem vessels, and (C) mean ± SE maximum metaxylem vessel size (left two bars, per node) and minimum metaxylem vessel size (right two bars, per node) from field-grown maize hybrids (PA16). High nitrogen (red, n=276 per plot) and low N (blue, n=276 per plot) treatments are indicated. The thresholds for relatively large (>1.14*MXM) and small (<0.75*MXM) vessels were determined empirically on a subset of root cross-sections.

Table 1-1. Description of maize root anatomy traits.

Trait	Measurement
RXA	Root cross-section area (mm^2)
CXA	Cortex cross-section area (mm^2)
SXA	Stele cross-section area (mm^2)
CSR	Cortex-to-stele ratio (CXA/SXA)
CF	Number of cortical cell files
CCS	Median cortical cell size, from the mid-section of the cortex (μm^2)
MXN	Number of metaxylem vessels
MXA	Total metaxylem vessel area in cross-section (mm^2)
MXP	Percent of total metaxylem vessel area in the stele (100*MXA/SXA)
AA	Total aerenchyma area in cross-section (mm^2)
AAP	Percent of aerenchyma area in the cortex (100*AA/CXA)
MXL, MXW	Median metaxylem vessel diameter (μm) – major axis (MXL) and minor axis (MXW)
MXM	Median metaxylem single vessel cross-section area (μm^2)
CDM	Median cortical cell diameter across all cortical cell files (μm)
HYP, OUT, INN	Median cortical cell diameter of hypodermis, outermost and innermost cortical cell file (μm)
ECC	Median metaxylem vessel eccentricity
JSM	Estimated conductance rate of all metaxylem vessels in cross-section (m Mpa^{-1} s^{-1})

Table 1-2. ANOVA table of genotype, nitrogen level, node, and interaction effects on maize root anatomy traits. Analysis of variance results from 39 genotypes (G) x 2 nitrogen treatments (T) x 3 nodes (N) x 2 replicates (n=468) from PA16. F-values and significance levels (p <0.1., 0.05*, 0.001**, 0.0001***, not significant (>0.1), N.S.) are given for each trait (see Table 1-1 for abbreviations) for each main factor (G, T, N) and all factor interactions (G:T, G:N, T:N, G:T:N). Data from root nodes 2, 3, 4 were included. Five genotypes were excluded due to missing data.

	Root diameter related traits						Proportion traits		
	RXA	**CXA**	**SXA**	**MXA**	**CF**	**MXN**	**CSR**	**AAP**	**MXP**
G	3.1***	3.1 ***	2.6***	3***	5***	4.7***	1.9**	1.7**	4.7***
T	14.9 NS	25.5NS	6.7 NS	8.2 NS	15.8***	30.9 NS	0.7 NS	3.6 NS	4.4*
N	361***	341.7 ***	318.3***	253.5***	404.1***	389.6***	123.7***	1.9 NS	182.4***
G:T	1.8**	1.8 **	1.8**	2.1***	2.6***	2.2***	1.6*	1.3 NS	1.3 NS
G:N	1.2 NS	1.2 NS	1.2 NS	1.5*	1 NS	1.3.	1.1 NS	0.8 NS	1 NS
T:N	10.9***	7.8***	14.4***	4.7**	2.4.	7.7***	8***	0 NS	5.4**
G:T:N	0.7 NS	0.8 NS	0.7 NS	1 NS	0.6 NS	0.7 NS	0.8 NS	0.8 NS	0.8 NS

	Metaxylem vessel related traits					Cortical cell related traits				
	MXM	**MXL**	**MXW**	**ECC**	**JSM**	**CDM**	**CCS**	**HYP**	**OUT**	**INN**
G	2.5***	2.8 ***	2.2 ***	2.9***	2.5 ***	1.8 **	1.7**	1.5 *	1.8 **	1.8 **
T	12.6***	10.0**	10.1**	1 NS	8.0 NS	49.3***	40.6***	0.0 NS	10.2**	10.0 .
N	51.3***	43.9 ***	66.0 ***	8.9***	131.0 ***	7.0 **	24.1***	30.7 ***	40.7 ***	4.3 *
G:T	1.5*	1.5 *	1.6 *	1 NS	1.8 **	1.2 NS	1.3 NS	1.3 NS	0.9 NS	1.2 NS
G:N	1.2 NS	1.3 .	1.2 NS	1.1 NS	1.4 *	1.2 NS	1 NS	1.1 NS	0.9 NS	1.0 NS
T:N	0.1 NS	0.3 NS	0.5 NS	2.7.	5.2 **	5.3**	0.8 NS	6.9**	3.3*	5.5**
G:T:N	1 NS	1.0 NS	0.7 NS	1.2 NS	1.1 NS	0.9 NS	1.1 NS	0.9 NS	0.7 NS	1.0 NS

Table 1-3. Effect size of genotype, nitrogen treatment, and node on maize root anatomy traits. Effect sizes (%) for genotype (G), nitrogen treatment (T), and root node (N) and their interactions for each anatomical trait in PA16 (n=468). Effect sizes are the proportion of variation in the trait explained by the given factor, interaction, or other sources (residuals). See Table 1-1 for trait abbreviations. Root nodes 2, 3, 4 included. For each traits, the maximum source of variation is in bold; if this source is an interaction or residual, the maximum main factor source of variation is underlined.

	Root diameter related traits						Proportion traits		
	RXA	**CXA**	**SXA**	**MXA**	**CF**	**MXN**	**CSR**	**AAP**	**MXP**
G	9.5	10	8.8	11	13	13	9.7	14	19
T	4.2	4.8	3.1	2.9	1	2.4	0.5	2.8	0.4
N	**50**	**49**	**49**	**41**	**52**	**52**	**34**	0.3	**38**
G:T	5	5	5.4	6.8	6.4	5.7	8.2	11	5.3
G:N	6.6	6.7	7.4	9.4	4.8	7	11	14	8.3
T:N	1.4	1.1	2	0.6	0.3	0.9	2	0.1	1.2
G:T:N	3.9	4.2	4.4	6.1	2.8	3.5	7.9	13	6.8
Resid	19	20	20	22	20	16	27	**45**	21

	Metaxylem vessel traits					Cortical cell related traits				
	MXM	**MXL**	**MXW**	**ECC**	**JSM**	**CDM**	**CCS**	**HYP**	**OUT**	**INN**
G	15.9	18	14	21	13	13	12	9.8	13	13.5
T	1.6	1.3	1.3	0.3	3	9	7	0	2.3	5.7
N	16	13	20	3.4	**28**	2.5	8.3	12	15	1.9
G:T	8.7	8.4	9.3	6.9	8	8.4	9	9.3	6.9	8.5
G:N	14	15	14	15	12	18	14	16	13	15.6
T:N	0	0.1	0.1	1.2	0.8	1.9	0.4	2.6	1.5	2.0
G:T:N	11	12	8.4	17	9.2	13	15	13	10	15.0
Resid	**32**	**33**	**32**	**35**	27	**35**	**34**	**38**	**37**	**37.9**

Table 1-4. Genotypic variation in maize root anatomy traits by node. Genotypic coefficients of variation (G.C.V., %) for each trait, where [CV = 100*(standard deviation of trait value)/(mean trait value)] using mean trait values for each genotype, by node (N2, N3, N4) and nitrogen treatment (HN, LN) in field-grown maize hybrids (PA16, n=39 genotypes; 5 genotypes excluded due to missing data). Mean G.C.V. across nodes and nitrogen treatments in bold. See Table 1-1 for trait abbreviations.

		Root-diameter related traits						**Proportion traits**		
		RXA	**CXA**	**SXA**	**MXA**	**CF**	**MXN**	**CSR**	**AAP**	**MXP**
N2	HN	28.1	28.4	31.2	35.6	9.9	16.7	16.3	107.4	14.4
	LN	30.7	30.1	34.5	36.4	10.7	16.7	18	90	13.4
N3	HN	31.4	31.2	33.7	36.7	12.3	17.2	12.4	101.9	21.6
	LN	30.4	28.4	37.2	29.3	12.3	21.5	13.3	82.1	17.8
N4	HN	32.6	30.8	38.6	37.3	11.6	21	17.7	104	22.8
	LN	29.7	28	35.8	30.8	12.7	23.4	19.7	93	20.8
	Mean	**30.5**	**29.5**	**35.2**	**34.4**	**11.6**	**19.4**	**16.2**	**96.4**	**18.5**

		Metaxylem vessel traits					**Cortical cell related traits**				
		MXM	**MXL**	**MXW**	**ECC**	**JSM**	**CDM**	**CCS**	**HYP**	**OUT**	**INN**
N2	HN	28.9	15.4	14.7	13.1	59.5	15.3	25.8	17.7	29	15.2
	LN	29.6	15.9	14.8	15.5	63.5	11.8	21.2	15	21	13.9
N3	HN	28.4	16	11.6	17.1	68.3	13.5	29.5	15	22.1	15.3
	LN	22	12.2	9.8	14.2	44.6	9.9	18.4	11.4	21.5	13.2
N4	HN	27.5	16	12.9	16.7	58.4	16.2	24.8	17.5	20.3	20.5
	LN	19.5	11.2	9.7	17.8	47.7	11.4	20.4	13.6	16.7	13.6
	Mean	**26**	**14.5**	**12.3**	**15.7**	**57**	**13**	**23.4**	**15**	**21.8**	**15.3**

Table 1-5. Anatomical response to nitrogen stress among genotypes. The percent of evaluated maize genotypes which showed significant trait response ($p<0.05$) under low N stress ("Plasticity") for the indicated anatomical trait, averaged across nodes 2, 3, and 4 ("All") and for each node (N) individually; the percent of plastic genotypes which showed a negative response (i.e. decreased trait value) under low N ("Direction"); and the percent of plastic genotypes which showed a strong response (greater than 50% change in trait value, "Strength") among field-grown hybrids (PA16, n=140 per trait, per node). See Table 1-1 for trait abbreviations.

	Percent of genotypes with				**Percent of plastic genotypes with**							
	Plastic response ($p<0.05$)				Strong response (>50%)				Negative response (-)			
Trait	**All**	**N2**	**N3**	**N4**	**All**	**N2**	**N3**	**N4**	**All**	**N2**	**N3**	**N4**
RXA	31.4	2.9	8.6	8.6	63.6	0	66.7	66.7	90.9	0	66.7	66.7
SXA	11.4	2.9	8.6	2.9	75	100	100	100	75	100	66.7	100
MXA	20	2.9	5.7	5.7	71.4	100	50	50	85.7	100	50	50
CF	25.7	14.3	17.1	11.4	0	0	0	0	77.8	60	66.7	50
MXN	25.7	2.9	11.4	5.7	11.1	0	0	0	88.9	100	75	0
CSR	11.4	5.7	8.6	5.7	0	0	0	0	75	50	66.7	0
AAP	5.7	2.9	0	8.6	100	100	—	100	50	0	—	66.7
MXP	8.6	5.7	0	0	0	0	—	—	0	50	—	—
MXM	8.6	5.7	5.7	5.7	33.3	50	50	0	100	100	100	50
ECC	0	0	5.7	2.9	—	—	0	0	—	—	50	0
JSM	11.4	5.7	8.6	8.6	75	100	0	66.7	100	100	33.3	100
CDM	22.9	17.1	0	5.7	0	16.7	—	0	100	100	—	0
CCS	20	8.6	0	5.7	42.9	0	—	50	100	66.7	—	100
HYP	5.7	2.9	5.7	5.7	0	0	0	0	0	0	100	0
OUT	5.7	8.6	2.9	2.9	50	0	100	0	100	100	100	0
INN	14.3	5.7	2.9	8.6	20	0	100	0	100	100	100	66.7
Mean	14.3	5.9	5.7	5.9	36.2	31.1	38.9	28.9	76.2	68.4	72.9	43.3

Chapter 3

Nodal root diameter and node number in maize (*Zea mays* L.) interact to influence nitrogen stress tolerance

Abstract

Plants preferentially allocate resources to root construction and metabolism, as opposed to shoot growth, when nitrogen is limiting. The benefits of investing in various root architectural and anatomical structures for nitrogen acquisition are not well understood. Nodal root number (NRN) and diameter (i.e. root cross-sectional area, RXA) were evaluated in maize IBM RILS in field and greenhouse experiments, and found to be inversely correlated under high and low nitrogen conditions. Slower development of root nodes, as opposed to differences in the number of roots per node, resulted in substantially reduced NRN and increased RXA. At two phenotypic extremes were M201 which produced few, thick axial roots, and M277 which produced many, thin roots, in high and low nitrogen conditions across field and greenhouse experiments. M201 had deeper root distribution and less spatial overlap among axial roots, suggesting less intra-plant competition. M201 also had less total axial root volume than M277 despite similar root biomass, suggesting greater investment in other root classes. Fewer, thicker axial roots was correlated with better shoot growth under moderate nitrogen stress, but not under severe stress, which reduced root diameter substantially across genotypes. Fewer axial roots offset respiratory and nitrogen costs of thicker diameter roots. Further exploration of root trait interactions among different root classes may reveal novel strategies for trait-based breeding of crop stress tolerance.

Highlight

Nodal root diameter and number are interacting traits in maize. Genotypes with slower nodal root emergence produced fewer, thicker axial roots, and performed better under moderate nitrogen stress.

Key words and abbreviations

Maize, nitrogen stress, root diameter, root number, trait interactions

IBM, intermated B73 x Mo17
RIL, recombinant inbred line

Introduction

Developing stress tolerant, resource efficient crops is a key strategy for addressing the challenges of climate change, global food security, and land degradation (Blum and Jordan, 1985; IPCC, 2014; Mickelbart et al., 2015; Hunter et al., 2017). Maize is a critical global crop, cultivated for food, fuel, and industrial uses (FAO, 2014). In intensive agriculture systems, nitrogen (N) fertilizers are over-applied to maximize grain yield, yet over half of the applied nitrate leaches beyond the root zone and pollutes waterways, or is volatilized as harmful greenhouse gases (Hirel et al., 2011; Dhital and Raun, 2016). In low-input subsistence agriculture, which sustains half of the global population, maize is grown on marginal soils where nitrogen availability is a primary constraint on yield (Gibbon et al., 2007). Breeding nitrogen-efficient and nitrogen-stress tolerant maize varieties would therefore have substantial economic and environmental benefits.

Plant root systems are responsible for the acquisition of water and nutrients, and have evolved specialized structural and physiological traits to forage for resources in complex, heterogeneous soil environments (Kenrick, 2002). Plants preferentially allocate assimilated carbon to root construction and metabolism, as opposed to shoot growth, when nitrogen becomes limiting (Brouwer, 1962; Bloom, 1985). However, the relative advantages of investing in different root system strategies are difficult to comprehensively assess. For example, maize develops spatiotemporally and genetically distinct classes of embryonic and post-embryonic roots, each composed of specialized axial (supportive, conducting) and lateral (branching, absorptive) roots (Hoppe et al., 1986; Demotes-Mainard and Pellerin, 1992; Hochholdinger et al., 2004). Each root varies from base to apex (root tip) in anatomical composition and metabolic

activities, including the degree of root exudation, nutrient translocation and assimilation, soil penetration strength, root hair density and length, and mycorrhizal associations.

Several root ideotypes, or select combinations of root traits defined as breeding targets, have been proposed for improving nitrogen acquisition efficiency (for ideotype breeding, see Donald, 1968; Clarke and McCaig, 1993; for root system ideotypes, see White et al., 2013; Lynch, 2013; Schmidt and Gaudin, 2017). To understand how different root traits contribute to nitrogen stress adaptation, whole root system responses to nitrogen stress, as well as the utility of individual traits, have been explored. Individually, traits such as steep crown root angle, fewer nodal roots, and reduced lateral root branching have been associated with rapid, deep rooting and better yield under nitrogen stress in select IBM RILs (Trachsel et al., 2013; Zhan and Lynch, 2014; Saengwilai et al., 2014a), although modeling results suggest that traits which maximize deep rooting may only provide benefits under certain precipitation regimes and soil textures (Dathe et al., 2016). Maize acquires (N uptake per unit N supplied) and utilizes (biomass produced per unit N supplied) nitrogen more efficiently under nitrogen stress (Gaudin et al., 2011a). Under low nitrogen conditions, select maize genotypes reduced the number and diameter of nodal roots, but increased individual axial root length, increased lateral to axial root length ratio, and increased expression of nitrate transporters, among other changes (Gaudin et al., 2011a, b; Gao et al., 2015). Increased root cortical aerenchyma was also found to be adaptive under nitrogen stress (Gao et al, 2015; Saengwilai et al., 2014b).

Recent work has shown that maize breeding has indirectly resulted in increasing nitrogen use efficiency (Ciampitti and Vyn, 2012; York et al., 2015; DeBruin et al., 2017). York and colleagues (2015) evaluated root architecture and anatomical traits (from the second root node) of a set of commercial hybrids representing different "eras" of cultivation were assessed under varying nitrogen levels and planting densities, and found that the most recent varieties had multiple changes in root system structure, including fewer (per node) but shallower axial roots, delayed lateral branching, and increased metaxylem vessel number, although this was offset by narrower vessel diameter resulting in no change in vessel area.

To understand the effects of combining potentially adaptive root traits, this study primarily evaluated the relationship of two root traits – the number of nodal roots (a combination of the number of developed root nodes, and the number of roots per node), and nodal root diameter. While fewer nodal roots have been shown to improve N stress tolerance, the utility of anatomical traits, such as RXA, within the context of different NRN has not been studied. Previous work has suggested a benefit of maintaining larger RXA under low N (see Chapter 2),

despite increased carbon costs; however, interactions with other root traits, such as a simultaneous reduction in NRN, could potentially offset carbon costs while enabling greater hydraulic conductance, soil penetration strength, and resilience of thicker roots, which could be beneficial for N acquisition. To investigate this interaction, this study compared maize IBM RILs which contrasted in both NRN and RXA, and evaluated combined trait effects on root respiration, nitrogen content, root length, root depth distributions, and shoot growth, in greenhouse and field experiments under high and low nitrogen conditions.

Materials & Methods

Plant material

Two greenhouse experiments (GH1 and GH2) were performed in 2015, using maize recombinant inbred lines (RILs) from the intermated B73 x Mo17 population (IBM). GH1 and GH2 included 8 RILs each: 30, 126, 178, 201, 277, 323, 352, plus 365 (GH1) and 181 (GH2). PA15 included 11 IBM RILs: 59, 129, and all RILs from GH1 and GH2. Seeds were provided by Dr. Shawn M. Kaeppler from U-Wisconsin, Madison, USA.

Five field experiments were performed (PA13, PA14, SA14, PA15, PA16). The 2013 (PA13) and 2014 (PA14) field studies in PA included 30 and 27 RILs, respectively, from the IBM, NYH (Ny821 x H99) and OWRI (Oh43 x W64a) populations. The 2014 field study in South Africa (SA14) included 25 IBM and NYH genotypes. The 2015 field study (PA15) included 11 IBM RILs. The 2016 field study (PA16) included 44 maize hybrid genotypes. The Genomes to Fields (G2F) Consortium curated and provided seeds for the hybrid genotypes. IBM, NYH, and OWRI RIL maize seeds were provided by Dr. Shawn Kaeppler from U-Wisconsin, Madison, USA. Genotypes from all field studies are listed in Appendix C, Table S1.

Growth conditions

GH1 and GH2 were conducted in the same greenhouse at University Park, PA (40° 45' 36.0" N, 73° 59' 2.4" W), with 14 h photoperiod, maintained at approximately 28°C/26°C day/night, 40% RH, PPFD of 500 μmol m^{-2} s^{-1} at the sixth leaf (Growmaster Procom, Micro

Grow, Temecula, CA, USA). GH1 seeds were germinated on April 28, 2015, and plants were harvested June 4-5, 2015. GH2 seeds were germinated Sept 26, 2015, and plants were harvested November 3-4, 2015.

Seeds were surface-sterilized with 25% (v/v) commercial bleach for 3 min, rinsed with distilled water, then soaked in the seed fungicide Captan (0.2 g/L) for at least 10 min. Seeds were germinated using the paper roll-up method. Seeds were placed 2.5 cm apart in a row, 4 cm from the top edge, between two sheets of heavy weight seed germination paper (Anchor Paper Co., St. Paul, MN, USA), then rolled up and placed vertically in an imbibing solution of 0.5 mM $CaSO_4$, and dark-incubated at 28°C for 2 days (Imperial II, Lab-line, Dubuque, IA, USA). Representative seedlings from each genotype were transplanted at about 5 cm depth and thinned after 4 days.

Plants were grown in individual mesocosms. Each mesocosm consisted of a PVC pipe with an inner diameter of 15.5 cm (outer diameter 16 cm) and height of 1.54 m, set vertically within a PVC socket cap (17 cm inner diameter, 18.5 cm outer diameter) with a single drainage hole drilled in the bottom. A layer of plastic mesh was laid over the drainage hole. Mesocosms were secured about 30 cm apart (center to center) against vertical wooden frames. Each mesocosm was fitted with a bottom-draining plastic liner bag constructed from 6 mil polyethylene sheets (USP Corp, Lima, OH, USA) using a heat sealer (Model H-1254, U-line, Pleasant Prairie, WI, USA). Details on mesocosm construction are available at this link: http://plantscience.psu.edu/research/labs/roots/methods/rootbox-greenhouse-methods/cylinders-for-root-evaluation.

Each mesocosm was filled with a 30 L mixture consisting of 50% commercial grade medium sand (Quikrete, Harrisburg, PA, USA), 27% horticultural grade fine vermiculite (D3, Whittemore Companies Inc., Lawrence, MA, USA), 18% field soil, and 5% horticultural grade super coarse perlite (Whittemore Companies Inc.), by volume. Soil was collected from the top 20 cm of low-nitrogen fields (Hagerstown silt loam) maintained at the Russell E. Larson Agricultural Research Center at Rock Springs, PA, air dried, crushed and sieved through a 4 mm mesh. A thin surface layer of perlite was added to each mesocosm to help retain moisture and reduce compression of media.

Plants were fertigated using individual 12.7 cm diameter drip rings (Dramm, Manitowoc, WI, USA) with 2 mm diameter poly tubes inserted into a PolyFlex pipe (1.9 cm inner, 2.5 cm outer diameter), which was connected to a submersible pump (Little Giant, Fort Wayne, IN, USA) in a 100 L Rubbermaid tub, containing one of two nutrient solutions. The high nitrogen (HN) solution contained (in µM): 6500 NO_3, 80 NH_4, 500 P, 2000 Mg, 3500 S, 3500 Ca, 3010 K,

10 Cl, 14 B, 3 Mn, 1 Zn, 0.5 Mo, 0.4 Cu, 110 Fe. The low nitrogen (LN) solution contained (in μM): 130 NO_3, 10 NH_4, 500 P, 2000 Mg, 4500 S, 2310 Ca, 1500 K, 500 Cl, 14 B, 3 Mn, 1 Zn, 0.5 Mo, 0.4 Cu, 110 Fe. Iron was applied as 5.85 mg/L Fe-DTPA (Dissolvine D-Fe-11, Akzonoble, Amsterdam, Netherlands). Nutrient solutions were adjusted to pH 6.0 using KOH pellets, and maintained at this pH with KOH or HCl as needed. A dilute micronutrient foliar spray was applied uniformly as needed. Each mesocosm was saturated with 2.5 L of nutrient solution one day prior to transplant, then fertigated 200 mL per mesocosm every other day.

The PA13, PA14, PA15, and PA16 field trials were conducted in 0.4 ha fields maintained with split high and low nitrogen treatments (field #87, 85, 105, 103 in 2013; 105, 85 in 2014; 103 in 2015; 105, 85 in 2016) at The Pennsylvania State University's Russell Larson Research Farm (40°42'40.915"N, 77°,57'11.120"W, central coordinate between field #105 and 85), which has Hagerstown silt loam soil (fine, mixed, semi-active, mesic Typic Hapludalf). To generate low N conditions, approximately 2.5 cm of sawdust was applied to fields #85, 103, 105 in May 2011 and 2012, and applied to field #87 in 2012 only. The high-nitrogen sides of the fields were fertilized with 146 kg N ha^{-1} applied as urea (46-0-0) in 2013 and 2014; 157 kg N ha^{-1} in 2015; and 213 kg N ha^{-1} in 2016 while no N fertilizer was applied on the low-nitrogen sides. Fields received drip irrigation, nutrients other than N, and pest management as needed.

Seeds were planted using hand jab planters in rows with 76 cm row spacing, 91 cm alleys, 23 cm plant spacing, 4.6 m plot length with 3.7 m planted, or approximately 56,800 plants ha^{-1}. In PA13, PA14, and PA15, each genotype was planted in 3-row plots, and plants from the middle row of each 3-row plot were sampled; in PA16, single-row plots were used, and plants were sampled from the middle section of the plot.

Planting dates for PA13, PA14, PA15, and PA16 were: May 18, 2013, May 31, 2014, June 14, 2015, and May 25, 2016, respectively. Following anthesis, root and biomass harvest began on: Aug 21, 2013, Aug 25, 2014, Sept 3, 2015, and Aug 8, 2016, respectively. Soil coring began on: Sept 9, 2013, Aug 20, 2014, Sept 9, 2015, and were not taken for PA16. Yield was collected at physiological maturity. Physiological measurements and sampling, such as for photosynthesis rate, SPAD, leaf chlorophyll content, leaf specific weight, plant height, ear height and number, leaf area, leaf number, and stand counts were completed approximately one week prior to root and biomass harvest (see "Plant harvest and measurements").

SA14 was conducted at the Ukulima Root Biology Center in Alma, Limpopo, South Africa in the Nebraska Farm pivot (24°33'0.12" S, 28°7'25.84 E, 1235 m asl), which has Clovelly loamy sand (Typic Ustipsamment). A total of 184 kg N ha^{-1} was applied to high N plots,

through five applications of fertigation and granular urea. A total of 23 N ha^{-1} was applied to the low N plots at planting via fertigation. Pivot irrigation, nutrients and pesticides were applied as needed. Hand-planting was completed November 26, 2013 and plant harvest and root sampling began Feb 10, 2014. Planting density was approximately 80,000 plants ha^{-1} with 76 cm row spacing. Genotypes were planted in 3-row plots, and plants were sampled from the middle row of each plot.

The average percent reduction in shoot biomass and yield from all experiments is listed in Appendix C, Table S2. The soil nitrate distribution by depth under high and low nitrogen treatments is shown for GH2, SA14, and PA15 in Appendix C, Fig S1.

Experimental design

GH1 and GH2 were two-way factorial randomized complete block designs, with four replicates (blocks) containing randomized combinations of 8 genotypes x 2 nitrogen treatments (high and low nitrogen).

Field experiments were split-plot randomized block designs with different configurations. In PA13 and PA14, 30 genotypes were randomized in each of 4 replicates (blocks) of 2 nitrogen treatments (sub-plots within blocks), totaling 240 plots. In PA15, 11 genotypes were randomized in 4 blocks within 2 N treatments, totaling 88 plots. In PA16, 44 genotypes were randomized in 2 blocks with 2 nitrogen treatments, totaling 178 plots. In SA14, 25 genotypes were randomized into each of 4 high N and 4 low N blocks, totaling 208 plots. In PA13 and PA16, separate 1-acre fields were used for each block; in PA14 two 1-acre fields were sub-divided into 8 blocks; in PA15, one 1-acre field was sub-divided into 8 blocks. In SA14, blocks were randomly assigned within a center pivot and split N treatments were applied.

Plant harvest and measurements

In greenhouse studies, plants were harvested over two days, with two replicates harvested per day. Shoots were removed, dried at approximately 70^0C, and stem and leaves were weighed separately. Whole root systems in media were removed intact within polyethylene liner bags. Liner bags were placed on a tray, sliced open vertically, and media was gently washed off with a

hose. Nodal axial roots were counted manually, with root counts recorded by node. The number of roots per node was defined as its "nodal occupancy". The length of each axial root was measured from base to tip with a meter stick, with lengths recorded by node; broken roots were measured as possible and recorded separately to obtain the most accurate average lengths possible. Two representative root segments each were excised from 2 to 4 cm from the stem base from the second and third nodes (GH1) and from the second, third, and fourth nodes (GH2), and preserved in 75% ethanol for anatomical analysis. Root respiration rate was measured on three 2-cm axial root segments (4 to 6 cm from the stem base) from each of these nodes, using a LI-COR 6400XT (LI-COR Biosciences, Lincoln, NE, USA) fitted with a closed custom chamber. A subset of these roots were dried at about 70^0C, weighed to determine specific root length, and manually ground, homogenized, and a 2 mg subsample was analyzed for carbon and nitrogen content using a CHN elemental analyzer (2400 CHNS/O Series II, PerkinElmer, Waltham, MA, USA). Each 30 cm of the entire root system, beginning at the stem base, was collected and dried at about 70^0C to obtain total root biomass. The depth above which a given percent of the root system biomass was located (e.g. 95% for D95) was calculated using linear interpolation of cumulative root mass at each depth. Dried leaves were ground, homogenized, and a 2 mg subsample was analyzed for total nitrogen content with a CHN elemental analyzer (2400 CHNS/O Series II, PerkinElmer, Waltham, MA, USA) using the Dumas combustion method.

In field studies, representative plants from each plot were excavated using a shovel (Trachsel et al., 2011). In PA13, PA14, and SA14, two plants were plot were sampled; in PA15 and PA16, one plant per plot was sampled. Root crowns were separated from the shoots, soaked in water with detergent, and hosed to remove remaining soil. Each node of roots was excised, and up to 3 representative roots from select nodes for each study (see Appendix C, Table S1) were sampled at 2 to 4 cm from the base of the stem and preserved in 75% ethanol for anatomical processing. In PA13, two root crowns from the low nitrogen treatment were dried, and a 2 cm basal segment from each node and the primary root were excised, weighed to determine specific root length, manually ground and homogenized, and a 2 mg subsample was used to determine carbon and nitrogen content using a CHN elemental analyzer. In SA14, for all plants, an additional representative axial root from each node was excised from 2 to 4 cm from the base, dried at about 70^0C, and weighed to determine specific root length. These roots were then ground manually and homogenized, and a 2 mg subsample was analyzed for carbon and nitrogen content using a CHN elemental analyzer. In PA16, all nodal roots were counted by node, and recorded as crown or brace roots; roots less than 2 cm were noted as emerging. In PA13, PA14, SA14, and

PA15, for a subset of plants, nodal roots were counted by node and roots less than 2 cm emerged were noted separately. In PA13, PA14, and PA16, all root crowns were also imaged to check for variation in root angle; a subset of root crowns were imaged in SA14. Shoot biomass was separated into stem, leaves, and ears, dried at approximately 70°C, and weighed. Ears from eight plants per plot (PA16) and five plants per plot (PA15) were collected at physiological maturity, dried to approximately 15% moisture content, shelled and weighed. Dried leaves were ground, homogenized, and a 2 mg subsample was analyzed for total nitrogen content with a CHN elemental analyzer.

To determine relative root lengths and depths, soil cores 60 cm in depth and 5 cm in diameter were taken manually with a sledgehammer and farm jack, using a steel coring tube with quick relief soil coring bit, drive head, and plastic liner (Giddings Machine Co., Windsor, CO, USA), between two plants from all plots in PA15, and a subset of plots in PA13, PA14, and PA15. Soil cores were separated into 10 cm segments, and fine roots were extracted using a custom root washer. Roots were placed in water on a clear plastic tray, scanned (Epson Perfection V700 Photo, Epson America, Inc., Long Beach, CA, USA) at 600 dpi and analyzed for root length separated by diameter classes (e.g. 0.2, 0.5, 1 mm) to estimate lateral versus axial root lengths using Winrhizo Pro software (Regent Instruments, Québec City, Quebec, Canada). Linear interpolation of cumulative root lengths by depth was used to calculated the depth at which a given percent of root length occurred (e.g. for 95%, this is reported as D95).

For GH2, media samples were collected at different depths in the mesocosm, air-dried, homogenized, and samples of equal mass were tested for nitrate content was using a LAQUA nitrate meter (Spectrum Technologies, Aurora, IL, USA) according to manufacturer's instructions. For PA15, soil cores were taken, separated by depth, homogenized, dried at 70°C, and extracted as above. Soil nitrate content was determined spectrophotometrically in SA14.

Image analysis

For GH1 and field experiments, the middle portion of two representative root segments per node of each plant were ablated and imaged using laser ablation tomography (LAT). This technique employs a nanosecond pulsed UV laser (Avia 355-7000, Coherent, Santa Clara, CA, USA) focused into a single-line scanning beam with a HurryScan 10 galvanometer (Scanlab, Puchheim, Germany) to ablate the cross-sectional surface of a root secured to a three-axis

motorized stage (ATS100-100, Aerotech Inc, Pittsburgh, PA, USA). The root is moved into the laser beam at about 30 μm s^{-1} (rate is adjusted according to root quality), and as each surface is ablated and exposed, images lit by the laser UV light are captured using a stage-mounted (#62-009, Edmund Optics, Barrington, NJ, USA) camera and 5X macro lens (Canon EOS Rebel T3i camera with 65mm MP-E 1-5x variable magnification, Canon USA Inc, Melville NY, USA). Image scale was 1.173 pixels per micron. Select greenhouse-grown root segments required pre-processing in a critical point dryer (Leica EM CPD300, Leica Microsystems, Wetzlar, Germany) to prevent sample dessication during laser ablation. Roots were placed in histo prep tissue capsules (29 mm x 6 mm) (Fisherbrand, Fisher Scientific, Waltham, MA, USA) and gradually dehydrated 75% to 100% ethanol prior to critical point drying.

For GH2, two ethanol-preserved roots from each node (2, 3, and 4) were manually sectioned using fresh double-edged razor blades (American Safety Razor Company, Verona, VA, USA), wet-mounted and visualized using a Diaphot inverted light microscope (Nikon Inc., Melville, NY, USA) under 4X magnification with a mounted CCD camera (Nikon DS-Fi1 camera with DS-U2 USB controller, Nikon, Inc.). Images were captured using NIS Elements F 4.30.00 software (Nikon, Inc.) at a scale of 390.7 pixels per mm, using 1280 x 920 pixel resolution. Two representative cross-sections images per root were selected for analysis.

Images were analyzed using one of two workflows. Images from GH1, GH2, PA13, SA14, PA15, and PA16 were analyzed using custom macros created with the open-source ObjectJ plug-in (https://sils.fnwi.uva.nl/bcb/objectj/) in ImageJ (https://imagej.nih.gov/ij/index.html), in which cortex, stele, aerenchyma, vessel and cell outlines were manually traced, and cell files manually counted (Appendix C, Fig S2). This allowed careful quantification of cell and vessel sizes. Images from PA14 were analyzed using the open-source Java program RootScan2 (code by Cleoniki Kesidis, http://plantscience.psu.edu/research/labs/roots/methods/computer/rootscan), which is based on RootScan (Burton et al., 2012) but optimized for LAT images, and is under development. Cortical cell file and metaxylem vessel numbers were manually confirmed. Trait descriptions and abbreviations are provided in Table 2-1 (see Chapter 2 for additional details).

Statistical analysis

Statistical analysis and visualizations were generated using R version 3.3.1 (R Core Team, 2016). Bar plots were generated using data aggregation functions from the package *plyr* and plotting functions from the package *ggplot2* (Wickham, 2009; Wickham, 2011).

Results

Nodal root number and diameter were inversely related among maize RILs

Nodal root diameter (RXA), averaged from axial roots in the second and third nodes, was inversely related to nodal root number (NRN) among maize IBM RILs in high and low nitrogen conditions in the greenhouse (**Fig 2-1 A, B**; see Table 2-1 for trait descriptions) and under low nitrogen in the field (Appendix C, Fig S3). The relationship was strongest under severe nitrogen stress in GH1 (**Fig 2-1A**; nitrogen stress levels for each experiment are given in Appendix C, Table S2). Of the first three root nodes in field-grown IBM RILs, RXA from the third root node was most correlated with NRN, while RXA in the first node was not correlated (Appendix C, Fig S3). In GH2, there was also a stronger relationship between NRN and RXA from the third and fourth nodes, compared to the second node; however, in GH1, the second node RXA was most strongly related to NRN (not shown).

Number of root nodes, rather than nodal occupancy, was related to root diameter

There was an inverse relationship between the number of developed root nodes (NN) and average RXA under high and low nitrogen conditions in GH1 and GH2, and under low nitrogen only in PA15 and PA16 (**Fig 2-2 A, B, C, D**). By contrast, the average number of roots per node, or nodal occupancy (NO), in the first four nodes was not strongly correlated with RXA in either high and low nitrogen conditions in the field and greenhouse, except in GH1 under severe nitrogen stress (Appendix C, Fig S4 A, B, C, D).

RILs M201 and M277 consistently contrasted in nodal root number and diameter, with similar root biomass

IBM RILs M201 and M277 showed the strongest phenotypic contrast in NRN and RXA, across greenhouse and field experiments, (**Fig 2-3 A, B**; Appendix C, Fig S5 A, B and S6 A, B) with over two-fold variation in each trait under high and low nitrogen conditions in GH2 (**Fig 2-3 A, B**). Trait relationships and physiological contrasts among IBM RILs (in the following sections) were well represented by M201 and M277. For example, M201 and M277 did not differ in NO across developed nodes, but M277 produced up to two more nodes of roots (**Fig 2-3 C, D;** Appendix C, Figs S5 C, D and S6 C, D). The youngest two nodes in M277 had the greatest NO, resulting in contrasting NRN (Appendix C, Fig S7 A, B, C). Despite strong differences in NRN and RXA, M201 and M277 did not differ significantly in total root biomass under high and low nitrogen conditions in GH2 (**Fig 2-4**).

Genotypic differences in root diameter were associated with cortical cell file number, stele area, and cortical cell size

Contrasts in RXA among IBM RILs were most strongly related to cortical cell file number and stele area, rather than cortical cell diameter (**Fig 2-5 A, B, C, D**). Cortical cell diameter was strongly positively correlated to RXA under low nitrogen, but not high nitrogen conditions (**Fig 2-5B**). M201 produced the most cortical cell files, but had similar cortical cell diameter as M277, and M201 had the largest stele area, both in total area and proportion relative to cortical area (Appendix C, Fig S8 A, B, C, D). M201 had the greatest number of metaxylem vessels and total metaxylem vessel area, but similar median vessel size as M277 (Appendix C, Fig S8 E, F, G). M201 produced less cortical aerenchyma in high and low nitrogen conditions than M277 (Appendix C, Fig S8H). Stele cell diameters and file numbers were not evaluated.

Fewer, thicker nodal roots were associated with better shoot growth under moderate nitrogen stress in maize inbreds

Fewer nodal roots was correlated with greater shoot mass under mild to moderate nitrogen stress in maize IBM RILs, in GH2 and PA15 (**Fig 2-6A** and Appendix C, Fig S9A). By

contrast, there was no significant relationship between nodal root number and shoot mass under high nitrogen in these studies (**Fig 2-6A** and Appendix C, Fig S9A). Larger root diameter was positively correlated with shoot biomass under low nitrogen in both studies, but was also positively correlated with shoot biomass in high nitrogen in GH2 (**Fig 2-6B** and Appendix C, Fig S9B). Under severe nitrogen stress in GH1, there was no relationship between NRN and shoot mass (Appendix C, Fig S10A). Root diameter was positively correlated with shoot mass in high nitrogen only in GH1 (Appendix C, Fig S10B).

Among field-grown hybrids, NRN was weakly positively correlated with shoot mass under low nitrogen, but there was no relationship in high nitrogen (Appendix C, Fig S11A). Root diameter was positively correlated with shoot mass under both high and low nitrogen, although the relationship was stronger under low nitrogen (Appendix C, Fig S11B). The relationship between NRN and shoot mass varied by node among hybrids; for example, the number of roots in the first node was negatively correlated with shoot mass under high nitrogen, while the NO of the fifth node was significantly positively correlated with shoot mass under low nitrogen. (Appendix C, Fig S11 C, D).

Genotypes with fewer nodal roots produced less total axial root length and volume

The total axial root length produced (TRL, the product of NO and ARL, the average axial root length in each node, for all developed nodes) was most strongly related to NRN under high and low nitrogen conditions, whereas RXA was only significantly negatively correlated with TRL under low nitrogen (**Fig 2-7 A, B**). M277 produced the greatest TRL among IBM RILs, while M201 produced the least (**Fig 2-8**).

Total axial root volume (TRV) was calculated as the product of RXA, NO, and ARL for each node, summed across nodes. Several M201 plants did not produce fourth node roots by harvest, and these values were included as ‘zero’ investment in TRV for this node. M277 produced more nodes but invested less TRV in each node compared to M201, under high and low nitrogen conditions (Appendix C, Fig S12 A, B, C; first node not shown). However, M277 produced greater TRV than M201 when summed across nodes (Appendix C, Fig S12D; TRV not shown beyond node 4).

Thicker axial roots resulted in deeper distribution of root mass and less spatial overlap

Larger RXA was significantly correlated with deeper relative root distribution among RILs in both high and low nitrogen conditions (**Fig 2-9A**). NRN was less related to root depth distribution (**Fig 2-9B**). M201 had the deepest relative root distribution in among RILs in high nitrogen conditions, while M277 had relatively more shallow root mass, although the two genotypes were similar in root depth distribution under low nitrogen (Appendix C, Fig S13 A, B, C, D). M201 also showed the least spatial overlap in the average root depth occupied by axial roots in each node, and M277 had the greatest overlap in depths of axial roots across nodes (**Fig 2-10**).

Nitrogen stress had node-specific effects on root system structure and physiology

In greenhouse grown plants, nitrogen stress reduced average axial root length (ARL), RXA, and NO overall, with effects differing by node (ARL and NO in the sixth node represent only a few plants) (**Fig 2-11 A, B, C**). In high nitrogen conditions, ARL decreased in each node; the first two nodes typically reached the bottom of the mesocosm (150 cm) by harvest, five weeks after germination (**Fig 2-11A**). RXA increased with each younger root node across genotypes, and NO increased from the third node onward (**Fig 2-11 B, C**).

Nitrogen stress significantly decreased specific root respiration (per gram of root) in fourth node axial roots, and decreased root nitrogen content (percent, by mass) across nodes (**Fig 2-12 A, B**). Nitrogen stress significantly decreased axial root respiration per unit of root length, and in combination with reductions in axial root length, resulted in substantial reductions in total axial root respiration per plant (Appendix C, Fig S14 A, B). Similarly, reduced root nitrogen content combined with decreased root biomass resulted in substantial reduction in total root nitrogen (grams per plant) across genotypes (Appendix C, Fig S14 C, D).

Under nitrogen stress, a greater proportion of the root system became deeply distributed. The percent of roots in the shallowest 20 cm decreased, while the percent of roots in the deepest layers increased (in field, **Fig 2-12C**; in greenhouse, Appendix C, Fig S13 A, B). Additionally, while total root mass and total axial root length decreased under nitrogen stress (Fig 2-4; Fig 2-8), the ratio of root to shoot mass increased under nitrogen stress across genotypes, reflecting a

decrease in allometric coefficient (from 1.17 to 0.83) under nitrogen stress (Appendix C, Fig S15 A, B; allometric coefficients for each genotype not evaluated separately).

The extent to which nitrogen stress affected axial root lengths, nodal occupancy, root anatomy, root mass, root depth distribution, axial root volume, root to shoot ratio, root respiration rates and nitrogen content differed among genotypes in the greenhouse and field (e.g. Figs 2-3, 2-4, 2-8, 2-10; Appendix C, Figs S5, S6, S7, S8, S12, S13, S14, S15, S16).

Fewer nodal roots offset increased carbon and nitrogen costs of thicker axial roots

Root respiration per unit of root length was significantly positively related to RXA in high and low nitrogen conditions (**Fig 2-13A**). However, total axial root respiration (root respiration rate multiplied by total axial root length) was not significantly related to RXA (**Fig 2-13B**). M201 had greater axial root respiration (per unit of root length) and slightly greater root nitrogen content (percent by mass) than M277 (Appendix C, Fig S14 A, C). However, when multiplied by the total number and length of axial roots, total axial root respiration was similar for M201 and M277; total root nitrogen content also did not significantly differ when multiplied by root mass for the two genotypes (Appendix C, Fig S14 B, D). Total root nitrogen was similar across genotypes under nitrogen stress (Appendix C, Fig S14D).

Maize hybrids showed greater contrast in nodal occupancy than number of developed root nodes

In a diverse collection of maize hybrids almost two-fold variation in NRN among 44 genotypes was associated with two-fold variation in NO (average 3.1 to 6.2 roots per node) and a range of 6 to 8 developed root nodes at harvest under high nitrogen conditions (Appendix C, Fig S16 A, B, C). Under low nitrogen, NN was inversely correlated with RXA, but NO was not correlated; as a result, NRN and RXA had a weak correlation (Fig 2-2D; Appendix C, Fig S17). There was a stronger relationship between NRN and RXA in the third and fourth nodes, compared to the second node (Appendix C, Fig S17).

Discussion

The maize root system is comprised of many interacting traits

The maize root system is developmentally complex, and forms primary, seminal, and nodal axial roots with several orders of lateral branching. These root classes are structurally and spatiotemporally distinct, exhibit different genetic and transcriptional regulation for specialized functions (Hochholdinger et al., 2004; Tai et al., 2016). The formation of the primary root and other embryonic structures are genetically patterned in the embryo, whereas post-embryonic axial and lateral root development are strongly mediated by environmental sensing and hormone signals (e.g. Hetz et al., 1996). Few monogenic root mutants have been described for maize (reviewed in Hochholdinger and Tuberosa, 2009) and root morphogenesis of different root classes is poorly understood, compared to dicotyledonous species such as *Arabidopsis thaliana*, which has served as a model for the study of root morphogenesis and environmental sensing (e.g. Schiefelbein and Somerville, 1990; Birnbaum et al., 2003; Benfey and Scheres, 2000; Brady et al., 2007; Hochholdinger and Zimmermann, 2008; Richter et al., 2009; Benková and Bielach, 2010; Bouguyon et al., 2012).

Maize nodal roots are responsible for the majority of water and nutrient uptake contributing to grain yield, and develop in successive acropetal nodes with axial roots of increasing diameter and number (detailed in Chapter 2). Several studies have sought to test the functional utility of individual root traits, in order to develop a "root system ideotype", or a group of target traits, for drought and nutrient stress tolerance (e.g. Donald, 1968; Clarke and McCaig, 1993; Lynch, 2013; Schmidt and Gaudin, 2017). However, "stacking" traits successfully requires an understanding of trait interactions, including trade-offs, synergism, or pleiotropy (e.g. York et al., 2013). This study evaluated nodal root architecture and anatomical traits in maize recombinant inbred lines (RILs) in the greenhouse and field, and a diverse collection of field-grown maize hybrids, in order to evaluate potential root trait interactions and their impact on nitrogen acquisition efficiency.

Among IBM RILs, we found a significant inverse relationship between total nodal root number (NRN) and the axial root diameter averaged from multiple nodes (RXA), which was primarily driven by a difference in the rate of nodal root emergence. Two RILs exemplified this contrast, showing stable phenotypes across field and greenhouse experiments: M201 produced

few, thick axial roots, and M277 produced many, thinner axial roots. M201 had a particularly stable axial root phenotype, and maintained the same NRN and RXA under high and low nitrogen. As shown across multiple IBM RILs, the phenotypic contrasts between M201 and M277 were driven by a difference in the number of root nodes developed during a similar maturation period, rather than the number of roots per node, or "nodal occupancy" (NO). M277 consistently produced about two more root nodes than M201, resulting in a two-fold difference in the number of nodal roots, since younger nodes have more roots.

Anatomically, greater cortical cell file number (CCFN) and stele area (SXA) strongly influenced RXA, while cortical cell diameter contributed to differences in RXA under low nitrogen only. M277 and M201 were reflective of this pattern; M201 had the greatest CCFN and SXA among IBM RILs, but did not have a larger median cortical cell diameter (CDM) in high nitrogen conditions. However, M201 maintained a larger CDM under low nitrogen, resulting in greater RXA under high and low nitrogen conditions. By contrast, M277 had the least CCFN among RILs in both high and low nitrogen conditions.

Nodal root number and diameter were strongly related to the total axial root length produced in greenhouse-grown IBM RILs. Greater NRN and thinner RXA were strongly associated with increased total axial root length (TRL), in high nitrogen conditions. Under low nitrogen, only NRN was strongly predictive of TRL. Greater TRL indicated greater investment in axial root growth, but not necessarily deeper relative root distribution. In greenhouse-grown maize plants, axial roots in the first two nodes reached the bottom of the mesocosm by harvest, at about five weeks after transplant. Given the sandy media and constrained pot diameter, differences in root angle and penetration strength likely did not contribute much to differences in axial root depth; instead, differences in root elongation rate and investment in axial root growth likely determined the axial root length.

Axial root growth patterns in M201 and M277 were representative of this relationship between NRN, RXA, and TRL. By harvest, in high nitrogen conditions, M277 had produced three nodes of axial roots reaching the bottom of the mesocosm, and the depth of its fourth node axial roots was equivalent to M201's third node. M277 had also developed a fifth node of roots at half the depth of its fourth node, and roots from its sixth node were emerging, just as roots from M201's fourth node emerged. As a result, across nodes, M277 produced double the total axial root length of M201, with twice as many nodal roots and about half of the average RXA. When summed across nodes, M277 produced substantially greater total axial root volume (TRV; the product of axial root number, diameter and lengths for each node) than M201.

While the relationship between NRN and RXA was strong among IBM RILs, it was less evident among a set of genetically diverse maize hybrids, which were evaluated at anthesis in the field. These hybrids contrasted strongly in nodal occupancy, rather than the number of root nodes developed at time of harvest. The relationship between NRN and RXA could be unique to the IBM RIL population; the IBM parent genotypes, B73 and Mo17, contrast in the rate of nodal root emergence and shoot node development, and in performance under nitrogen stress (e.g. as shown in **Chapter 2, Appendix A**), and have also been shown to contrast in root diameter, number, and length in QTL mapping studies (Burton et al., 2014; Burton et al., 2015). Interestingly, Mo17 has fewer, thicker nodal roots than B73, but produces more seminal roots and longer primary and seminal roots, with similar total root system diameter (a metric of root system angle) compared to B73 (Burton et al., 2014).

Seminal, primary, and lateral root classes were not evaluated in detail in this study, but the relative investment in these younger and finer root classes could account for the similarities in total root mass despite contrasting axial root production in M201 and M277. Increases in lateral to axial root length ratio have been suggested as a potential adaptation to nitrogen stress (Gaudin, 2011b; Postma et al., 2014; Gao et al., 2015; Zhan and Lynch, 2015). Additional study is needed to reveal whether M201 invested the additional carbon in other root classes, such as additional lateral root proliferation, which could result in greater specific root length overall and increased capacity for nitrate uptake.

Fewer, thicker nodal roots are associated with improved nitrogen acquisition in maize

Lynch (2013) proposed a root system ideotype referred to as the “steep, cheap, and deep” (SCD) hypothesis, which suggests that architectural and anatomical traits which result in metabolically efficient, deeper rooting and minimal intra-plant competition would improve acquisition of mobile resources such as water and nitrate, conveying yield benefits under drought and nitrogen stress. Steeper crown root angles (Trachsel et al., 2013), fewer, longer lateral roots (Zhan and Lynch, 2014; Zhan et al., 2015), and fewer nodal roots (Saengwilai et al., 2014a; Gao and Lynch, 2016) have been shown to correlate with deeper root distribution and improved nitrogen stress and drought tolerance.

Anatomically, increased cortical aerenchyma has been associated with metabolically cheaper axial roots, resulting in improved low nitrogen and drought tolerance (Zhu et al., 2010;

Saengwilai et al., 2014b; Chimungu et al., 2015), whereas reduced cortical burden (total living root cortical area) rather than cortical aerenchyma was more strongly associated with improved drought tolerance in another study (Jaramillo et al., 2013). Larger mid-cortical cell diameters and fewer cortical cell files were associated with reduced metabolic costs per root length, deeper rooting, and enhanced drought tolerance (Chimungu et al., 2014 a, b). Ten of these studies were conducted using maize IBM RILs.

Functional-structural modeling in *SimRoot* suggested that the effects of reduced nodal root number on nitrate uptake were similar regardless of whether this reduction came from delaying the emergence of roots (reduced time with a given number of roots), or producing fewer roots per node (York, 2014). The SCD hypothesis also suggested unresponsiveness to local nitrate would improve deeper growth and resource capture, but the direct benefit of plasticity in these root traits has not been tested. Separately (and conversely), increased secondary lateral root branching, and plastic responses of increasing root angle and length through the increase in cell elongation have been associated with nitrogen stress adaptation in maize (e.g. reviewed in Yu et al., 2014; Gaudin et al., 2011a; Gao et al. 2015). Thicker root diameter has been associated with better performance in hybrids, partly due to a positive allometric relationship with plant size (see Chapter 1). Increased RXA has also been associated with increased soil penetration strength, cortical area available for mycorrhizal colonization, resistance to pests, increased hydraulic conductance, and root longevity (as discussed in Chapter 2). The influence of soil penetration strength could be an important consideration for anatomical and architectural trait interactions in compacted soils, which were not investigated in this study.

This study suggests that a combination of fewer, thicker nodal roots could be beneficial under nitrogen stress. Among field- and greenhouse-grown IBM RILs, there was a significant, negative correlation between nodal root number and shoot mass under mild and moderate nitrogen stress (average of 50% biomass reduction), supporting the results of several studies which suggest that reducing nodal root number is adaptive for stress (Gaudin et al., 2011b; Saengwilai et al., 2014a; York et al., 2015; Gao et al. 2015; Gao and Lynch, 2016). This study also found consistent positive correlations between RXA and shoot mass under low nitrogen, among greenhouse-grown IBM RILs and field-grown IBM RILS and hybrids, suggesting a potential benefit of thicker axial roots (or, a benefit of thicker roots given concurrent decrease in root number, or other unknown linked traits) for nitrogen stress tolerance. Shoot mass was also weakly correlated to RXA under high nitrogen in some experiments, suggesting that a positive allometric relationship of RXA with plant size (see Chapter 2) should be accounted for. However,

under severe nitrogen stress (average 80% biomass reduction), there was little contrast in shoot growth among IBM RILs, and NRN and RXA were not correlated with performance under low nitrogen.

To understand the potential mechanisms underlying how the rate of nodal root emergence affects nitrogen uptake, the carbon and nitrogen costs, root depth distribution, and intra-plant competition were evaluated among IBM RILs. Among RILs, fewer NRN reduced carbon and nitrogen costs, offsetting the increased respiratory costs and nitrogen content of thicker RXA. Under high and low nitrogen, RXA was positively correlated with root respiration per unit root length; however, when respiration rates were multiplied by the total axial root length, RXA and total respiratory costs were not correlated. Similarly, total nitrogen content in the top 30 cm of the root system did not differ significantly among RILs under low nitrogen. M277 and M201 again reflected these patterns well: M201 had greater axial root construction costs in terms of carbon (specific root length; not shown) and nitrogen per unit length, as well as greater respiration rate per length. However, these costs were offset by the reduction in number of axial roots, resulting in total respiration and nitrogen which did not differ significantly from M277.

Fewer nodal roots was strongly correlated with deeper root distribution in both high and low nitrogen conditions, primarily through a reduction in the percent of shallow root mass. This suggests that greater root length was located at depth, where leaching nitrate could be captured efficiently. M201 showed the deepest root distribution among RILs, and had substantially less root mass in the top 30 cm, as well as greater root mass at depth compared to M277. M277 had greater maximum root lengths and total axial root length, but produced multiple nodes with axial root tips occupying similar depths. M201, by contrast, showed the least spatial overlap in the location of its axial root tips (shown as average root length per node). This suggests that M201 had less intra-plant competition, and may have acquired nitrate more efficiently with fewer overlapping root interception and diffusion zones, combined with greater hydraulic conductance rates due to greater total metaxylem vessel area per root.

Therefore, this study suggests that reducing the rate of nodal root emergence, which reduces the number of nodal roots and increases axial root diameter, allows a functional complementation; constructing fewer axial roots significantly reduced root carbon and nitrogen costs, offsetting costs incurred by increased root diameter. Thicker roots with slower elongation rates reduced spatiotemporal redundancy and increased root depth distribution, potentially without trade-offs in total hydraulic conductance capacity. Finally, reduced investment in axial root growth potentially enabled greater resource allocation toward other specialized root classes

(e.g. for nutrient absorption in lateral roots) and shoot growth. Altogether, slower nodal root emergence resulting in fewer, thicker axial roots was associated with improved shoot growth under moderate nitrogen stress. Additional study of shoot development (see Chapter 4) and the contribution of other root classes would be useful to for further understanding of how the timing of nodal root emergence can influence root system structure and nitrogen acquisition.

In terms of experimental design, this study also suggests that interactions between multiple root traits may confound conclusions of prior studies which used IBM RILs. The root architectural and anatomical trait studies cited above used IBM RILs with the assumption that genotypes could be compared due to the "isophenic" nature of the selected RILs. This experimental design has been suggested by York and colleagues (2015) as the optimal strategy for investigating trait utility: "[near] isophenic lines" were defined as genotypes which "differ primarily in the state of a single phene, or at least a small number of phenes", where phene refers to a unit of the phenotype (the observed organism).

Several experiments in this study were originally designed to test the hypothesis of whether larger cortical cell diameter and fewer cortical cell files were beneficial under nitrogen stress, as they were shown to be under drought (Chimungu et al., 2014 a, b). Therefore, many of the same RILs have been included; M201 and M277 were both drought-tolerant genotypes, purported to vary primarily in cortical cell size (M201 had "large cortical cells"), and cell file number (M277 had "few cell files"), as evaluated in the second root node only. Additional RILs such as M126 (large cells), M178 (few files and large cells), M181 (many files and small cells), M323 (small cells), and M365 (few files), were also included in this study. This study found substantial contrasts in RXA and NRN among these genotypes, which suggest that they are not isophenic for the anatomical traits studied previously.

Further study of interacting root system traits and functions would benefit from more holistic phenotyping efforts that can reveal underlying processes driving genotypic contrast (see Chapter 4 discussion), as well as continued phenotypic screening and development of mutant lines. The development of quantitative methods and terminology to better interpret the adaptive utility of complex, "infinite" phenotypes has also been proposed (e.g. Pieruschka and Poorter, 2012; Lynch and Brown, 2012; York et al., 2013; Bodner et al., 2013; Chitwood and Topp, 2015). For example, "phenes", "phene states", and "phene aggregates" have been proposed as more specific terms referring to biological traits (unique to a level of biological organization, e.g. a tissue or organ), attributes, and their composite metrics, respectively; for example, "root depth" is sometimes referred to inaccurately as a root system "trait" although it is a result of multiple

biological processes, and could instead be termed a "phene aggregate" (York et al., 2013). York and colleagues (2013) use this framework to suggest a "functional response landscape" approach for analyzing "phene synergisms", or trait interactions; each functional landscape is determined by whether each phene has either a linear effect on the response variable or a central optimum; when combined, additive, antagonistic (less than additive), or synergistic (greater than additive) phene interactions would be evident (e.g. Fig 5, York et al., 2013).

With a larger number of genotypes contrasting primarily in the traits explored in this study (e.g. possible elemental phenes could be the rate of nodal root emergence and the number of cortical cell files in crown axial roots), this approach could be used to identify additive, antagonistic or synergistic interactions. As shown in this study, however, nodal root number, length, and diameter could affect metabolic costs within the same "phene module", which limits the potential for synergistic interactions (as hypothesized in York et al., 2013).

Nitrogen stress effects on root traits depend on genotype, environment, and timing

Plants, as sessile organisms, have developed sophisticated sensing, signaling, and response mechanisms to acquire sufficient nitrogen for growth (reviewed in Bouguyon et al., 2012). Nitrogen is not only the mineral nutrient required in the greatest abundance, but assimilation of nitrogen is one of the most energy-intensive metabolic processes, intrinsically linking nitrogen status to carbon availability (Bloom et al., 1992; Crawford 1995; Stitt 1999). Therefore, nitrogen stress typically induces changes not only in root structure and metabolism, but also systemic changes in whole plant resource allocation and growth rate, mediated by phytohormones such as auxin and cytokinin, as well as other molecules (e.g. Takei et al., 2001; Gifford et al., 2008; Tian et al., 2008; Mi et al., 2008; Krouk et al., 2010; Bouguyon et al., 2016; Krouk, 2016; Ohkubo et al., 2017). Forde and Lorenzo (2001) collectively termed these alterations in response to nutrient distributions as "tropomorphogenesis", and noted that both direct (localized) and indirect (systemic) changes could differ among genotypes.

Across genotypes, this study found that nitrogen stress resulted in reduction of individual axial root lengths (and thus maximum depths reached) in each node, as well as total axial root length (Fig 2-8, Fig 2-9). Previous studies have found either increases in individual crown root length (Gaudin et al., 2011b; aeroponics), or increases in root elongation rate, with average crown root length decreasing under stress in the second and third nodes, but increasing in the first node

(Gao et al., 2015; hydroponics). These contrasting results could be due to differences in resistance and heterogeneity of the growth medium or other factors. Variability in the elongation rates of roots within a node was described by Hoppe and colleagues (1986) and was observed in this study (individual root lengths not shown). Variability in axial root lengths was similar across high and low nitrogen conditions (not shown), although increased variability in lateral root lengths under nitrogen stress has been reported (Gaudin et al., 2011b).

Nitrogen stress significantly decreased the number of roots per node in all nodes except the first two. However, genotypes varied in the node at which nodal occupancy began to decrease, and some genotypes (e.g. M181) showed no significant decrease in occupancy across nodes. Previous studies have shown that timing of root node primordia initiation is staggered, and all initiated primordia always elongate in the first five nodes (Sharman, 1942; Girardin et al., 1987; Aguirrezabal et al., 1993). Aguirrezabal and colleagues (1993) also suggested that in contrast to the first five nodes, subsequent nodes regularly initiated excess root primordia which did not elongate, increasing their sensitivity to carbon availability and the potential for plastic responses. If root initiation preceded onset of stress signaling, nodal occupancy would likely not be affected (e.g. Pellerin, 1994) (in contrast to elongation rate, which could therefore be considered more "plastic"). Therefore, the timing and level of N stress could directly impact the potential for decreased nodal root number.

As a result of changes in root number, diameter, and length, root systems became more deeply distributed under nitrogen stress in the field and greenhouse, which has been shown in previous studies (e.g. Trachsel et al., 2013; Saengwilai et al., 2014; Zhan and Lynch, 2015). The extent to which root depth distribution changed differed among genotypes, but all genotypes showed a substantial reduction in the proportion of root mass in the top 30 cm under low nitrogen in the greenhouse. Similarly, nitrogen stress induced a significant reduction in the percent of root length in the top 20 cm of soil in the field, and an increase in the percent of root length in the deepest 20 cm, among IBM RILs.

Nitrogen stress also decreased root respiration rates (per unit length) and root nitrogen content, with greater decreases in younger nodes. These reductions were associated with root diameter decreases under low N, depending on node, and changes in other anatomical traits which were similar to those described in Chapter 2. However, despite decreased RXA overall, genotypes maintained their relative "large" versus "small" RXA classifications under nitrogen stress.

Finally, nitrogen stress induced a well-established increase in root to shoot mass allocation, which can be observed generally as a shift in allometric scaling between root and

shoot mass across genotypes. However, within genotypes, the allometric scaling coefficients for both high and low nitrogen appeared to differ, and would be an important difference to characterize in further studies. The integration of root and shoot responses to nitrogen stress is maize, and the impacts of different anatomical, morphological, and architectural strategies on nitrogen uptake and utilization efficiency, remain to be explored.

Conclusions

This study explored the interaction of root anatomical and architectural traits in maize, and found substantial contrast in two nodal root traits in a set of IBM RILs: the number of developed root nodes (and thus total number of axial roots emerged in a given period) and nodal root diameter. Root diameter contrast was driven primarily by differences in cortical cell file number and stele area, with some differences in cortical cell diameter under low nitrogen. Genotypes with fewer, thicker roots developed root nodes more slowly, produced less total axial root length, and invested more carbon and nitrogen per unit of root length. Interesting, producing fewer roots appeared to offset these specific carbon and nitrogen costs, when calculated for the aggregate root system.

Fewer, thicker nodal roots was also associated with deeper root distribution and less intra plant competition, and resulted in greater shoot growth under mild and moderate nitrogen stress. The physiology of genotypes with thin axial roots supported elements of the “steep, cheap, and deep” hypothesis, producing significantly greater total root length and maximum depths in the same growth period, while respiring less and costing less nitrogen per unit root length. However, when combined with producing more nodal roots, the resulting greater total investment in axial root growth was not advantageous.

Together, the evaluation of RILs and hybrids highlight a novel root trait combination related to an integrated, developmental process (the rate of nodal root emergence) which may underlie phenotypic contrast and physiology. Contrast in nodal occupancy among hybrids, rather than in node development rate, suggests that trait combinations of nodal occupancy and root anatomy could be investigated in future studies. These relationships among root system traits are complex yet important to study further for the goal of developing and breeding for root system ideotypes, which requires the successful stacking of multiple, potentially interacting root traits.

Acknowledgements

We thank Shawn Kaeppler and the G2F consortium for providing plant materials.

For agronomic and technical support, we thank Qun Wang, Robert Snyder, Michael Williams, Johan Prinsloo, Ainiz Fauzi, Jonathan Wu, Pufan Wang, Ryan Burnett, Hannah Schneider, Tania Galindo-Castañeda, Stephanie Klein, Claire Lorts, Gustavo da Silveira, Andy Evensen, Xiyu Yang, Kirsten Lloyd, Larry York, and Joseph Chimungu.

We thank Benjamin Hall and support from the Edmund Optics Higher Education Grant for technical support and improvements to the LAT platform.

This work was supported by USDA NIFA's AFRI grant 2013-02682 to JPL, the Howard G. Buffett Foundation for research in South Africa, and the USDA National Institute of Food and Agriculture, Hatch project 4372. Any opinions, findings, conclusions, or recommendations expressed in this publication are those of the author(s) and do not necessarily reflect the view of the National Institute of Food and Agriculture (NIFA) or the United States Department of Agriculture (USDA).

References

Aguirrezabal LAN, Pellerin S, Tardieu F. 1993. Carbon nutrition, root branching and elongation: can the present state of knowledge allow a predictive approach at the whole-plant level? Environmental and Experimental Botany **33**, 121–130.

Barber SA. 1995. Soil nutrient bioavailability: a mechanistic approach. John Wiley and Sons, New York, USA. pp. 91.

Benfey PN, Scheres B. 2000. Root development. J. Current Biology 10, Abstract, R813-815.

Benková E, Bielach A. 2010. Lateral root organogenesis - from cell to organ. Current Opinion in Plant Biology **13**, 677–683.

Birnbaum K. 2003. A Gene Expression Map of the Arabidopsis Root. Science **302**, 1956–1960.

Bloom AJ, Sukrapanna SS, Warner RL. 1992. Root Respiration Associated With Ammonium and Nitrate Absorption and Assimilation By Barley. Plant Physiology **99**, 1294–1301.

Bloom AJ, Chapin FS, Mooney HA. 1985. Resource Limitation in Plants- An economic analogy. Ann. Rev. Ecol. Syst. **16**, 363–392.

Blum A, Jordan WR. 1985. Breeding crop varieties for stress environments. Critical Reviews in Plant Sciences **2**, 199–238.

Bodner G, Leitner D, Nakhforoosh A, Sobotik M, Moder K, Kaul H. 2013. A statistical approach to root system classification. Frontiers in Plant Science **4**, 292.

Bouguyon E, Gojon A, Nacry P. 2012. Nitrate sensing and signaling in plants. Seminars in Cell and Developmental Biology **23**, 648–654.

Bouguyon E, Perrine-Walker F, Pervent M, *et al.* 2016. Nitrate Controls Root Development through Post-Transcriptional Regulation of the NRT1.1/NPF6.3 transporter/sensor. Plant Physiology **172**, 1237–1248.

Brouwer R. 1962. Nutritive influences on the distribution of dry matter in the plant. Netherlands Journal of Agricultural Science **10**, 399–408.

Burton AL, Johnson J, Foerster J, Hanlon MT, Kaeppler SM, Lynch JP, Brown KM. 2014. QTL mapping and phenotypic variation of root anatomical traits in maize (*Zea mays* L.). Theoretical and Applied Genetics **128**, 93–106.

Burton AL, Johnson JM, Foerster JM, Hirsch CN, Buell CR, Hanlon MT, Kaeppler SM, Brown KM, Lynch JP. 2014. QTL mapping and phenotypic variation for root architectural traits in maize (*Zea mays* L.). Theoretical and Applied Genetics **127**, 2293–311.

Chimungu JG, Maliro MFA, Nalivata PC, Kanyama-Phiri G, Brown KM, Lynch JP. 2015. Utility of root cortical aerenchyma under water limited conditions in tropical maize (*Zea mays* L.). Field Crops Research **171**, 86–98.

Chimungu JG, Brown KM, Lynch JP. 2014. Large root cortical cell size improves drought tolerance in maize. Plant Physiology **166**, 2166–2178.

Chimungu JG, Brown KM, Lynch JP. 2014. Reduced root cortical cell file number improves drought tolerance in maize. Plant Physiology **166**, 1943–1955.

Chitwood DH, Topp CN. 2015. Revealing plant cryptotypes: Defining meaningful phenotypes among infinite traits. Current Opinion in Plant Biology **24**, 54–60.

Ciampitti IA, Vyn TJ. 2012. Physiological perspectives of changes over time in maize yield dependency on nitrogen uptake and associated nitrogen efficiencies: A review. Field Crops Research **133**, 48–67.

Clarke JM, McCaig TN. 1993. Breeding for efficient root systems. In: Plant Breeding: Principles and prospects, eds. Hayward MD, Bosemark NO, Romagosa I. Dordrecht: Springer Netherlands, 485–499.

Crawford NM. 1995. Nitrate: nutrient and signal for plant growth. The Plant Cell **7**, 859–68.

Dathe A, Postma JA, Postma-Blaauw MB, Lynch JP. 2016. Impact of axial root growth angles on nitrogen acquisition in maize depends on environmental conditions. Annals of Botany **118**, 401–14.

DeBruin JL, Schussler JR, Mo H, Cooper M. 2017. Grain Yield and Nitrogen Accumulation in Maize Hybrids Released during 1934 to 2013 in the US Midwest. Crop Science **57**, 1–16.

Demotes-Mainard S, Pellerin S. 1992. Effect of mutual shading on the emergence of nodal roots and the root/shoot ratio of maize. Plant and Soil **147**, 87–93.

Dhital S, Raun WR. 2016. Variability in optimum nitrogen rates for maize. Agronomy Journal **108**, 2165–2173.

Donald CM. 1968. The breeding of crop ideotypes. Euphytica **17**, 385–403.

Edman JD, Taylor DJ. 1917. The American Association for the Advancement of Science. Nature **98**, 448–450.

FAO. 2014. FAOSTAT. Cited May 18, 2017. http://www.fao.org/faostat/en/#data

Forde BG, Lorenzo H. 2001. The nutritional control of root development. Plant and Soil **232**, 51–68.

Gao K, Chen F, Yuan L, Zhang F, Mi G. 2015. A comprehensive analysis of root morphological changes and nitrogen allocation in maize in response to low nitrogen stress. Plant, Cell and Environment **38**, 740–750.

Gao Y, Lynch JP. 2016. Reduced crown root number improves water acquisition under water deficit stress in maize (*Zea mays* L.). Journal of Experimental Botany **67**, 4545–4557.

Gaudin ACM, McClymont SA, Raizada MN. 2011. The nitrogen adaptation strategy of the wild teosinte ancestor of modern maize, *Zea mays* subsp. parviglumis. Crop Science **51**, 2780–2795.

Gaudin ACM, McClymont SA, Holmes BM, Lyons E, Raizada MN. 2011. Novel temporal, fine-scale and growth variation phenotypes in roots of adult-stage maize (*Zea mays* L.) in response to low nitrogen stress. Plant, Cell and Environment **34**, 2122–2137.

Gibbon D, Dixon J, Flores D. 2007. *Beyond Drought Tolerant Maize: Study of Additional Priorities in Maize. Report to Generation Challenge Program*.

Gifford ML, Dean A, Gutierrez RA, Coruzzi GM, Birnbaum KD. 2008. Cell-specific nitrogen responses mediate developmental plasticity. Proceedings of the National Academy of Sciences of the United States of America **105**, 803–8.

Girardin P, Jordan M, Picard D, Trendel R. 1986. Harmonisation des notations concernant la description morphologique d'un pied de maïs (*Zea mays* L.). Agronomie **6**, 873–875.

Hetz W, Hochholdinger F, Schwall M, Feix G. 1996. Isolation and characterization of rtcs, a maize mutant deficient in the formation of nodal roots. The Plant Journal **10**, 845–857.

Hirel B, Tétu T, Lea PJ, Dubois F. 2011. Improving nitrogen use efficiency in crops for sustainable agriculture. Sustainability **3**, 1452–1485.

Hochholdinger F, Tuberosa R. 2009. Genetic and genomic dissection of maize root development and architecture. Current opinion in plant biology **12**, 172–7.

Hochholdinger F, Woll K, Sauer M, Dembinsky D. 2004. Genetic dissection of root formation in maize (Zea mays) reveals root-type specific developmental programmes. Annals of Botany **93**, 359–68.

Hochholdinger F, Zimmermann R. 2008. Conserved and diverse mechanisms in root development. Current Opinion in Plant Biology **11**, 70–4.

Hoppe DC, McCully ME, Wenzel CL. 1986. The nodal roots of *Zea* : their development in relation to structural features of the stem. Canadian Journal of Botany **64**, 2524–2537.

Hunter MC, Smith RG, Schipanski ME, Atwood LW, Mortensen DA. 2017. Agriculture in 2050: Recalibrating targets for sustainable intensification. BioScience **67**, 386–391.

IPCC, 2014: Climate Change 2014: Synthesis Report. Contribution of Working Groups I, II and III to the Fifth Assessment Report of the Intergovernmental Panel on Climate Change [Core Writing Team, R.K. Pachauri and L.A. Meyer (eds.)]. IPCC, Geneva, Switzerland, 151 pp.

Jaramillo RE, Nord EA, Chimungu JG, Brown KM, Lynch JP. 2013. Root cortical burden influences drought tolerance in maize. Annals of Botany **112**, 429–437.

Kenrick. 2002. The Origin of Roots. In: Plant Roots: The Hidden Half, Third Edition, eds. Waisel Y, Eshel A, Kafkafi. Basel, New York: Marcel Dekker, Inc., 1–19.

Krouk G. 2016. Hormones and nitrate: a two-way connection. Plant Molecular Biology **91**, 599–606.

Krouk G, Lacombe B, Bielach A, *et al.* 2010. Nitrate-regulated auxin transport by NRT1.1 defines a mechanism for nutrient sensing in plants. Developmental Cell **18**, 927–937.

Lynch JP. 2013. Steep, cheap and deep: an ideotype to optimize water and N acquisition by maize root systems. Annals of Botany **112**, 347–57.

Lynch JP, Brown KM. 2012. New roots for agriculture: exploiting the root phenome. Philosophical transactions of the Royal Society of London. Series B, Biological sciences **367**, 1598–604.

Mi G, Chen F, Zhang F. 2008. Multiple signaling pathways control nitrogen-mediated root elongation in maize. Plant signaling & behavior **3**, 1030–1032.

Mickelbart MV, Hasegawa PM, Bailey-Serres J. 2015. Genetic mechanisms of abiotic stress tolerance that translate to crop yield stability. Nature Reviews Genetics **16**, 237–251.

Ohkubo Y, Tanaka M, Tabata R, Ogawa-Ohnishi M, Matsubayashi Y. 2017. Shoot-to-root mobile polypeptides involved in systemic regulation of nitrogen acquisition. Nature Plants **3**, 17029.

Pellerin S. 1994. Number of maize nodal roots as affected by plant density and nitrogen fertilization : relationships with shoot growth. European Journal of Agronomy **3**, 101–110.

Pieruschka R, Poorter H. 2012. Phenotyping plants: Genes, phenes and machines. Functional Plant Biology **39**, 813–820.

Postma JA, Dathe A, Lynch JP. 2014. The Optimal Lateral Root Branching Density for Maize Depends on Nitrogen and Phosphorus Availability. Plant Physiology **166**, 590–602.

Richards RA, Passioura JB. 1981. Seminal Root Morphology and Water Use of Wheat II. Genetic Variation1. Crop Science **21**, 253–255.

Richter GL, Monshausen GB, Krol A, Gilroy S. 2009. Mechanical Stimuli Modulate Lateral Root Organogenesis. Plant Physiology **151**, 1855–1866.

Saengwilai P, Nord E a, Chimungu JG, Brown KM, Lynch JP. 2014. Root cortical aerenchyma enhances nitrogen acquisition from low-nitrogen soils in maize. Plant Physiology **166**, 726–735.

Saengwilai P, Tian X, Lynch JP. 2014. Low crown root number enhances nitrogen acquisition from low-nitrogen soils in maize. Plant Physiology **166**, 581–9.

Schiefelbein J, Somerville C. 1990. Genetic Control of Root Hair Development in *Arabidopsis thaliana*. The Plant Cell **2**, 235–243.

Schmidt JE, Gaudin ACM. 2017. Toward an Integrated Root Ideotype for Irrigated Systems. Trends in Plant Science **22**, 433–443.

Sharman BC. 1942. Developmental anatomy of the shoot of *Zea mays* L. Annals of Botany **6**, 245–282.

Stitt M. 1999. Nitrate regulation of metabolism and growth. Current opinion in plant biology **2**, 178–186.

Tai H, Lu X, Opitz N, Marcon C, Paschold A, Lithio A, Nettleton D, Hochholdinger F. 2016. Transcriptomic and anatomical complexity of primary, seminal, and crown roots highlight root type-specific functional diversity in maize (*Zea mays* L.). Journal of Experimental Botany **67**, 1123–1135.

Takei K, Sakakibara H, Taniguchi M, Sugiyama T. 2001. Nitrogen-Dependent Accumulation of Cytokinins in Root and the Translocation to Leaf: Implication of Cytokinin Species that Induces Gene Expression of Maize Response Regulator. Plant and Cell Physiology **42**, 85–93.

Tian F, Bradbury PJ, Brown PJ, Hung H, Sun Q, Flint-Garcia S, Rocheford TR, McMullen MD, Holland JB, Buckler ES. 2011. Genome-wide association study of leaf architecture in the maize nested association mapping population. Nature Genetics **43**, 159–162.

Tian Q, Chen F, Liu J, Zhang F, Mi G. 2008. Inhibition of maize root growth by high nitrate supply is correlated with reduced IAA levels in roots. Journal of Plant Physiology **165**, 942–951.

Trachsel S, Kaeppler SM, Brown KM, Lynch JP. 2013. Maize root growth angles become steeper under low N conditions. Field Crops Research **140**, 18–31.

Trachsel S, Kaeppler SM, Brown KM, Lynch JP. 2011. Shovelomics: High throughput phenotyping of maize (*Zea mays* L.) root architecture in the field. Plant and Soil **341**, 75–87.

Wickham H. 2009. ggplot2: Elegant Graphics for Data Analysis. Springer-Verlag New York

Wickham H. 2011. The Split-Apply-Combine Strategy for Data Analysis. Journal of Statistical Software, 40(1), 1-29. URL http://www.jstatsoft.org/v40/i01/.

White PJ, George TS, Dupuy LX, Karley AJ, Valentine TA, Wiesel L, Wishart J. 2013. Root traits for infertile soils. Frontiers in plant science **4**, 193.

York LM. 2014. Integration of root phenes affecting nitrogen acquisition in maize. PhD thesis, Pennsylvania State University.

York LM, Galindo-Castaneda T, Schussler JR, Lynch JP. 2015. Evolution of US maize (*Zea mays* L.) root architectural and anatomical phenes over the past 100 years corresponds to increased tolerance of nitrogen stress. Journal of Experimental Botany **66**, 2347–2358.

York LM, Nord EA, Lynch JP. 2013. Integration of root phenes for soil resource acquisition. Frontiers in plant science **4**, 355.

Yu P, White PJ, Hochholdinger F, Li C. 2014. Phenotypic plasticity of the maize root system in response to heterogeneous nitrogen availability. Planta **240**, 667–678.

Zhan A, Lynch JP. 2015. Reduced frequency of lateral root branching improves N capture from low-N soils in maize. Journal of Experimental Botany **66**, 2055–2065.

Zhan A, Schneider H, Lynch JP. 2015. Reduced Lateral Root Branching Density Improves Drought Tolerance in Maize. Plant Physiology **168**, 1603–15.

Zhu J, Brown KM, Lynch JP. 2010. Root cortical aerenchyma improves the drought tolerance of maize (*Zea mays* L.). Plant, Cell and Environment **33**, 740–749.

Figures and Tables

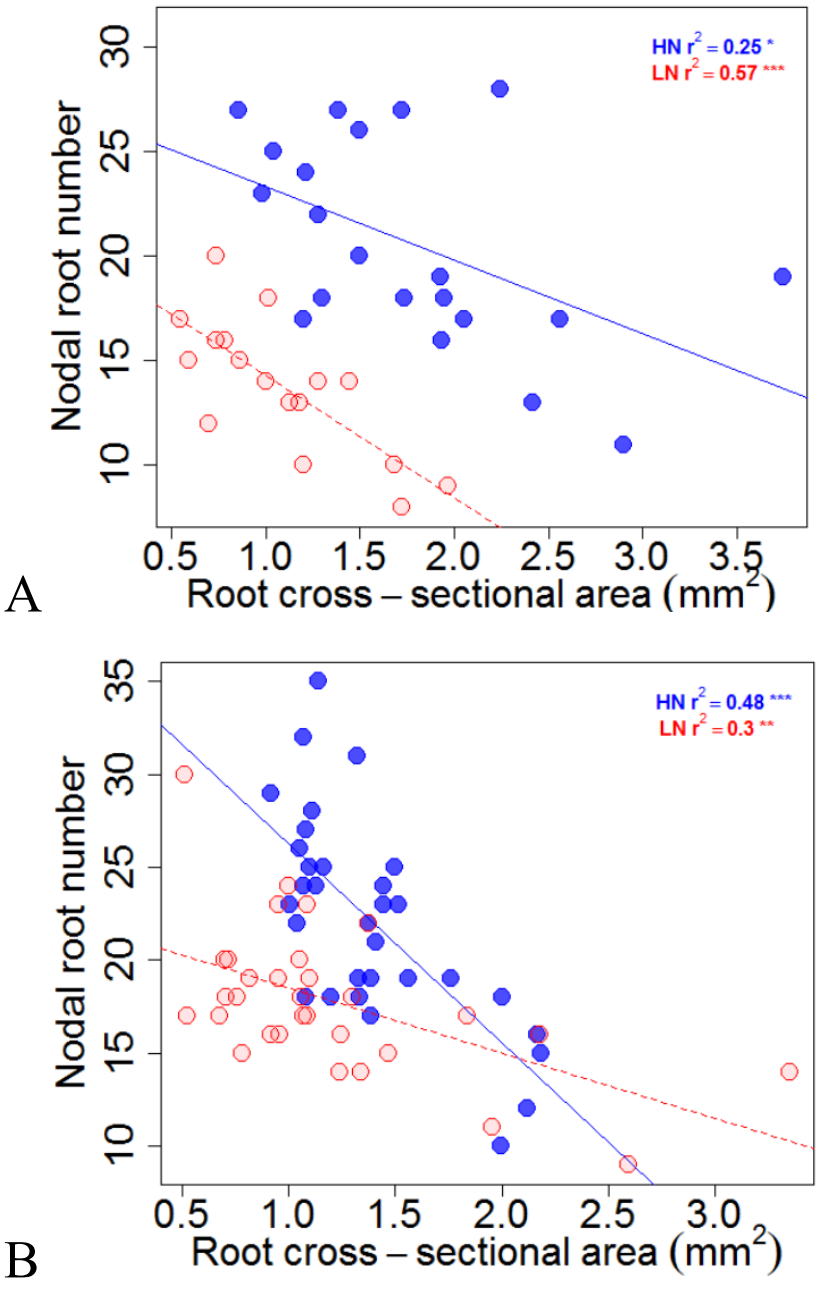

Figure 2-1. Relationship between nodal root number and diameter among maize inbreds. Linear regression of number of nodal roots (NRN) emerged at harvest and root cross-sectional area (RXA) averaged from two second and third node roots (fully developed in all genotypes at harvest), from individual plants of eight maize IBM RILs grown in high (HN, blue) or low nitrogen (LN, red) treatments in two greenhouse studies: (A) in GH1 (A), LN reduced biomass by 80% and in GH2 (B), LN reduced biomass by 50% (see Appendix C, Table S2). R^2 value and significance ($p< 0.05$*, 0.01**, 0.001***) are indicated.

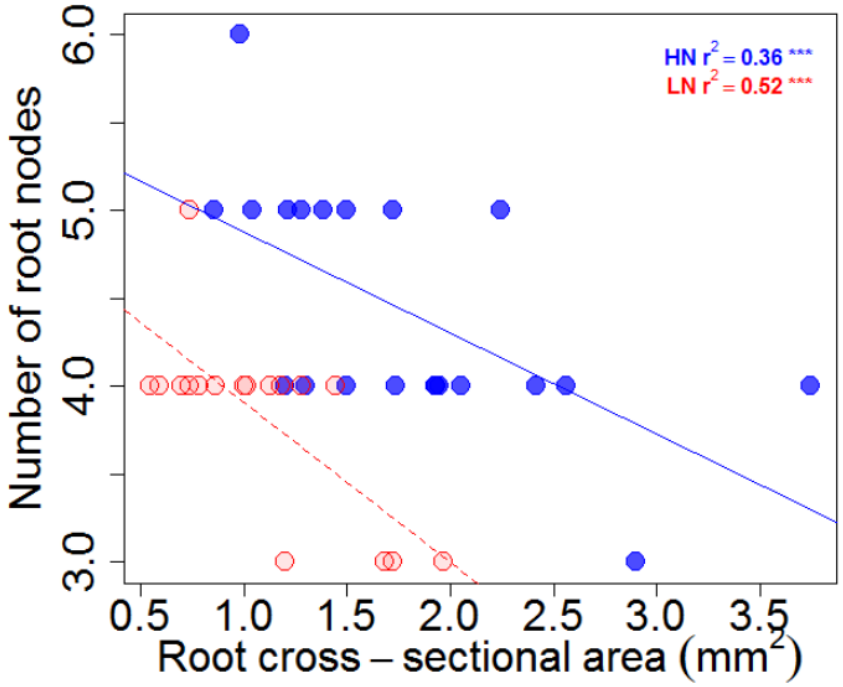
HN r2 = 0.36 ***
LN r2 = 0.52 ***
Number of root nodes
3.0
4.0
5.0
6.0
0.5
1.0
1.5
2.0
2.5
3.0
3.5
Root cross – sectional area (mm2)

A

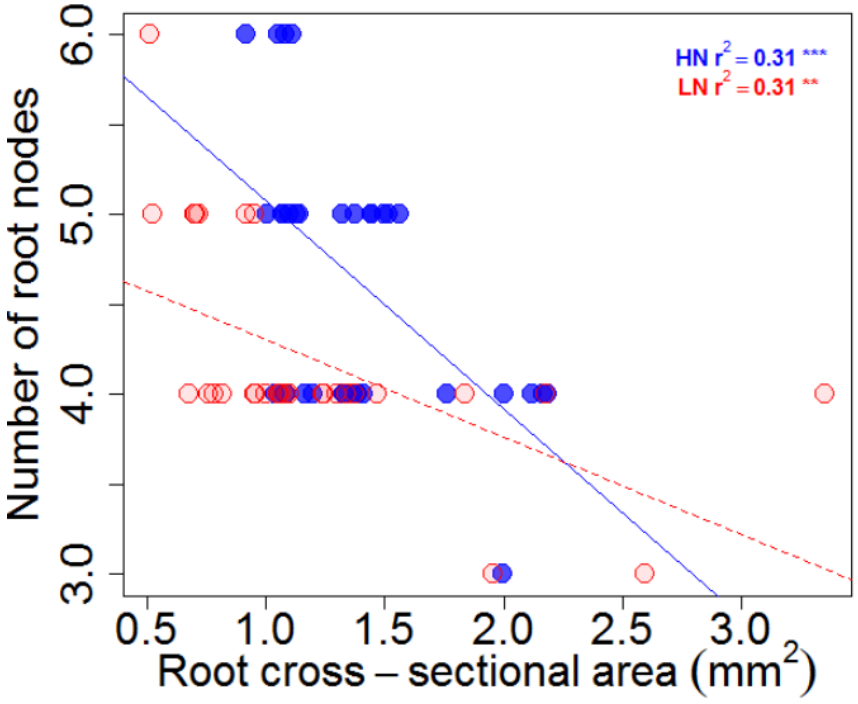
HN r2 = 0.31 ***
LN r2 = 0.31 **
Number of root nodes
3.0
4.0
5.0
6.0
0.5
1.0
1.5
2.0
2.5
3.0
Root cross – sectional area (mm2)

B

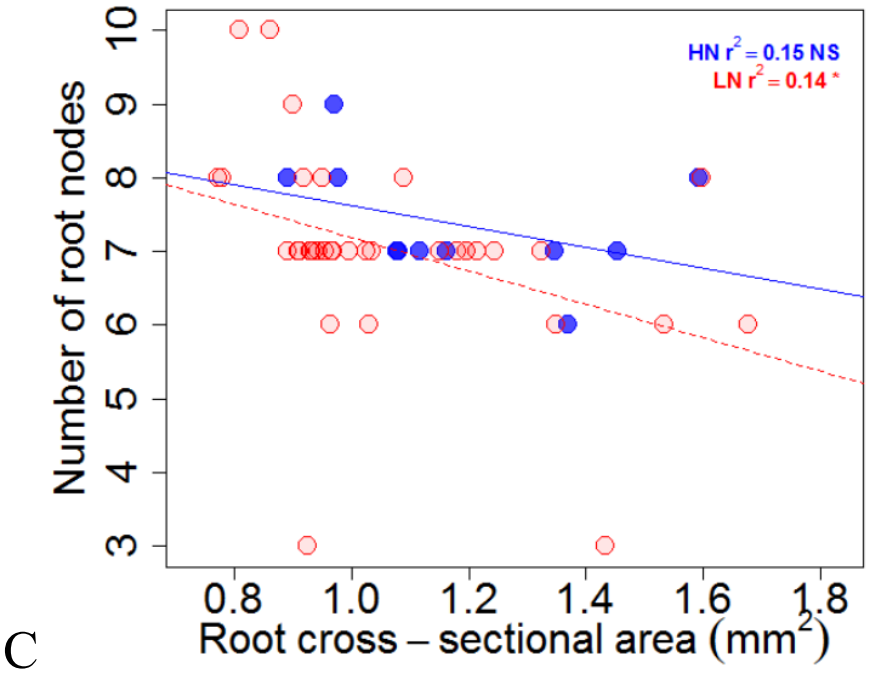

C

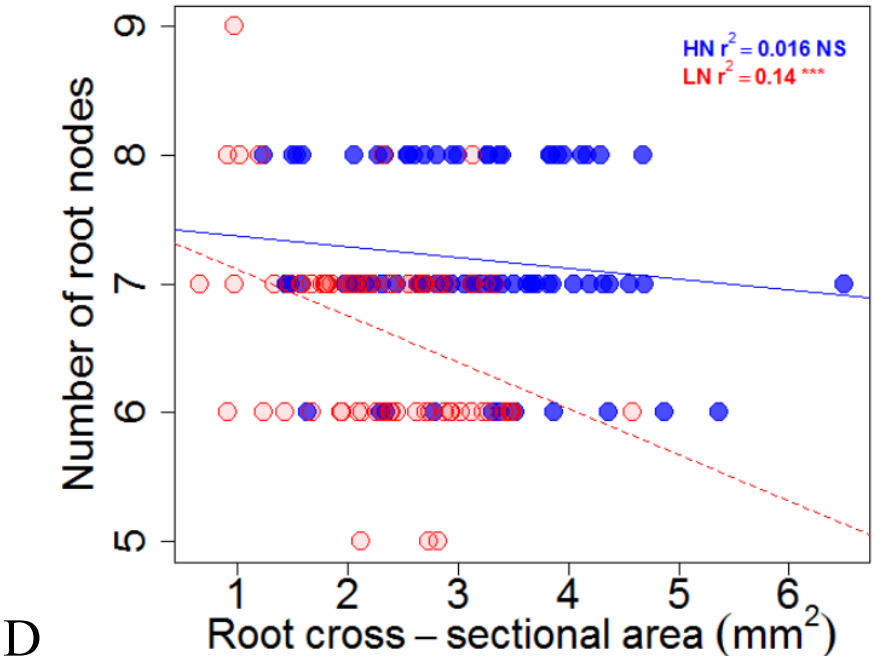

D

Figure 2-2. Relationship between number of root nodes and nodal root diameter among maize inbreds and hybrids. Linear regression of total number of developed root nodes (NN) at harvest and root cross-sectional area (RXA) averaged from two roots from each of the indicated nodes from individual plants in (A) GH1 (RXA from nodes two and three), (B) GH2 (RXA from nodes 2 and 3), (C) PA15 (RXA from nodes 1, 2, 3), and (D) PA16 (RXA from nodes 2,3,4) grown in high (HN, blue) or low nitrogen (LN, red) conditions (for stress levels and genotypes, see Appendix C, Tables S1 and S2). R^2 value and significance ($p< 0.1.$, 0.05*, 0.01**, 0.001***; NS, not significant) are indicated. For PA15, the number of nodes was evaluated in four replicates in LN and one replicate in HN.

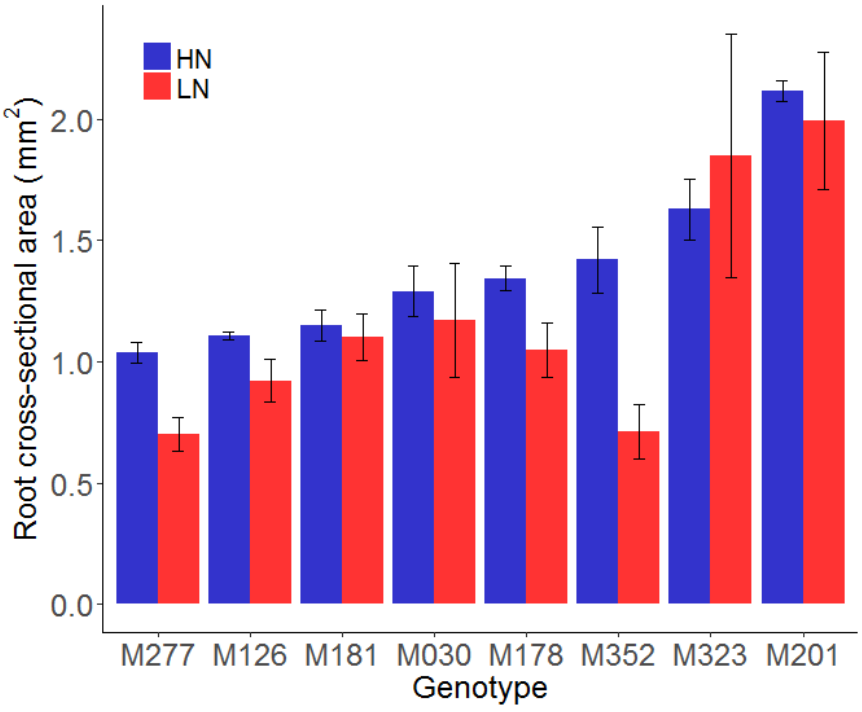
HN
LN
Root cross-sectional area (mm^2)
2.0
1.5
1.0
0.5
0.0
M277 M126 M181 M030 M178 M352 M323 M201
Genotype

A

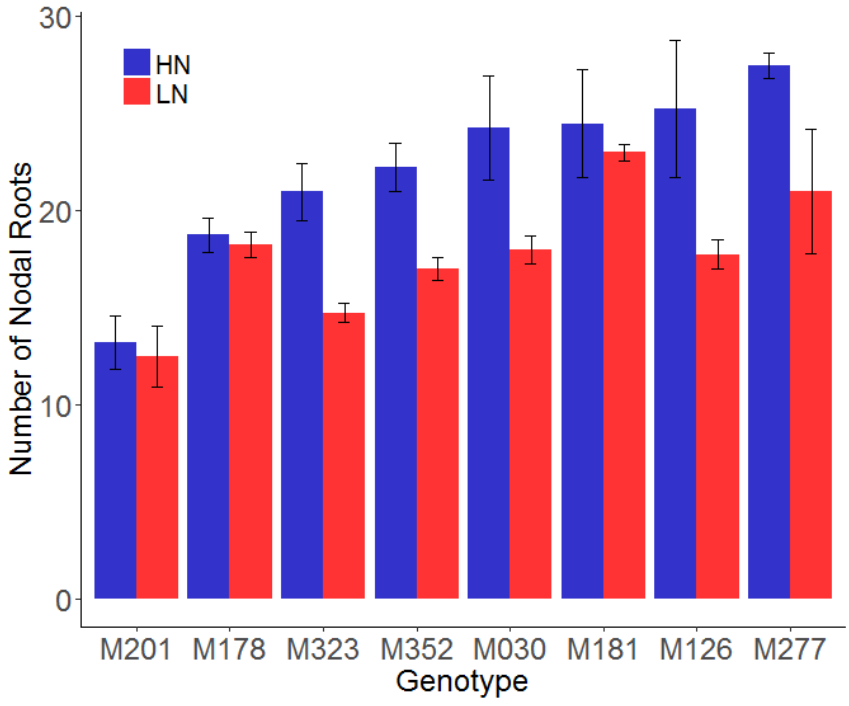
HN
LN
Number of Nodal Roots
30
20
10
0
M201 M178 M323 M352 M030 M181 M126 M277
Genotype

B

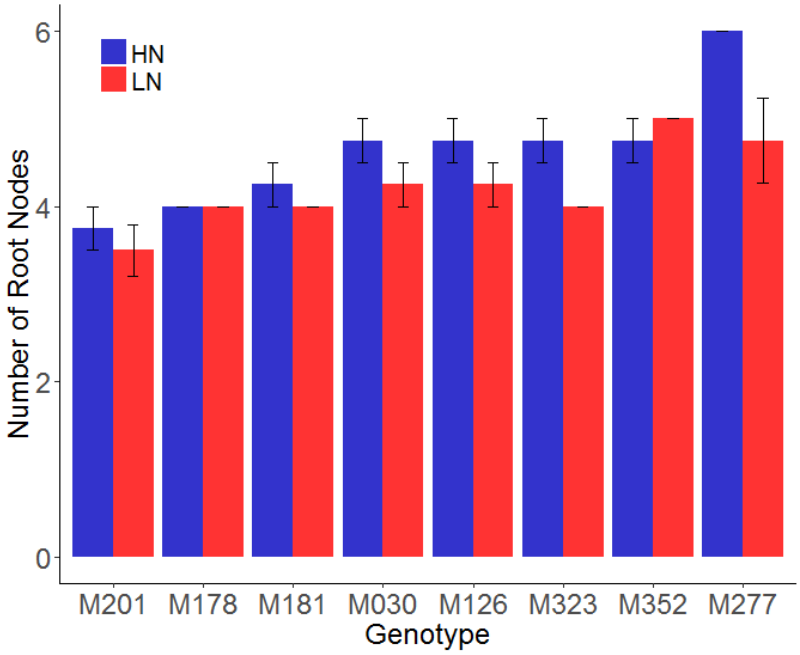

C

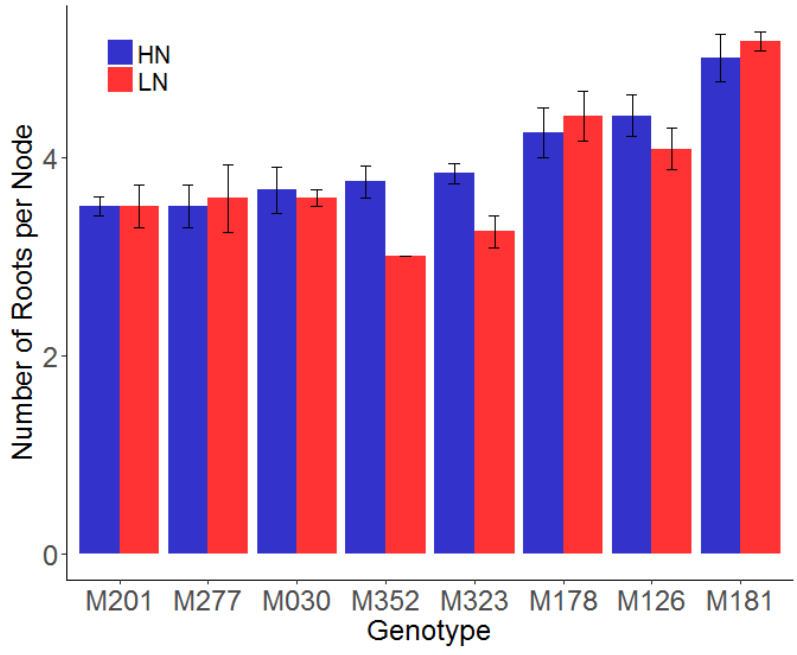

D

Figure 2-3. Genotypic contrast in nodal root number and diameter among maize inbreds. Means ± SE of (A) total number of nodal roots (NRN) emerged at harvest, and (B) root cross-sectional area (RXA), averaged from two roots each from nodes 2 and 3, (C) number of nodal roots per node (NO), averaged from the first three nodes, and (D) number of developed root nodes at harvest (NN), for maize RILs in GH2 (n=4 plants per RIL per nitrogen treatment). Genotypes are IBM RIL numbers indicated as M# and arranged in ascending order by high nitrogen trait values. High and low nitrogen treatments are indicated (HN, blue; LN, red).

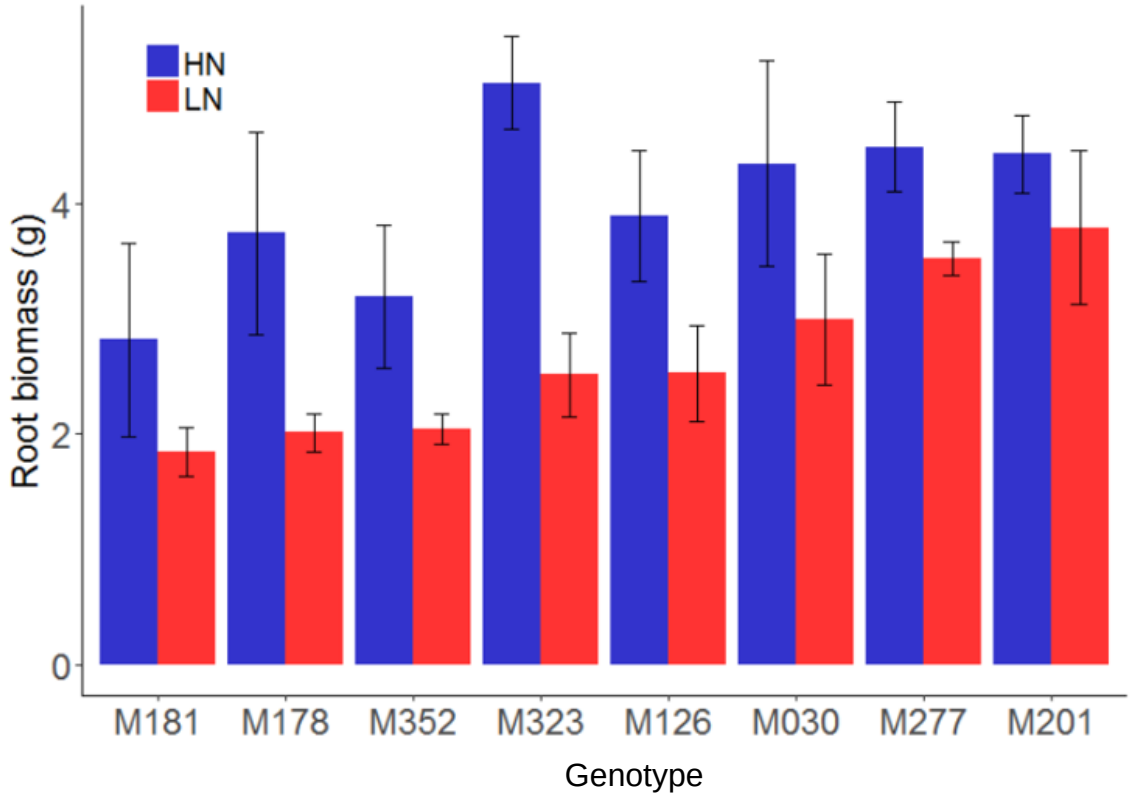

Figure 2-4. Root biomass at harvest in IBM RILs. Means ± SE of total dry root biomass among IBM RILs in GH2 (n=4 plants per RIL per nitrogen treatment. IBM RIL number is indicated as M# and are arranged in ascending order according to mean trait value under low nitrogen. High and low nitrogen treatments are indicated (HN, blue; LN, red).

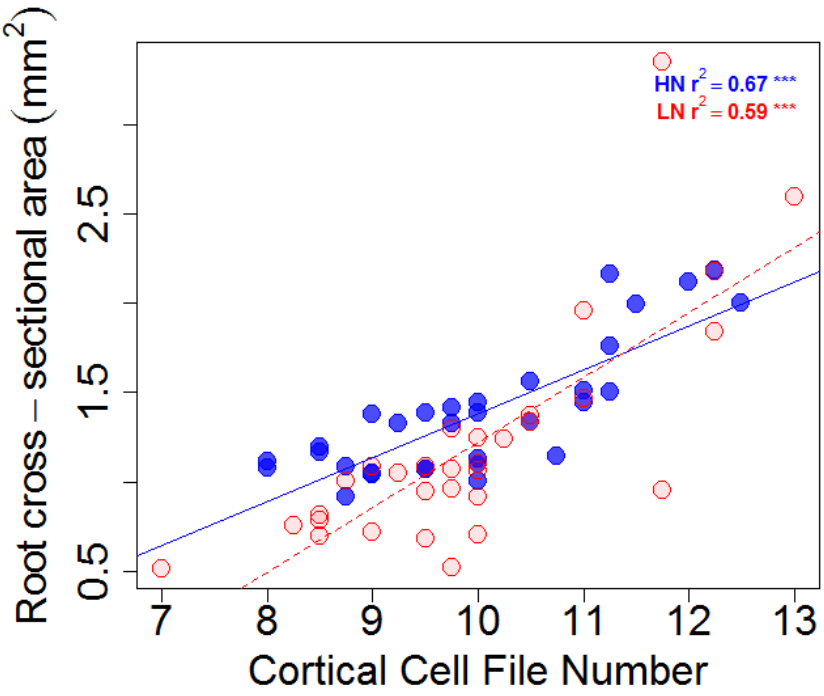
HN r2 = 0.67 ***
LN r2 = 0.59 ***
Root cross – sectional area (mm2)
0.5
1.5
2.5
7
8
9
10
11
12
13
Cortical Cell File Number

A

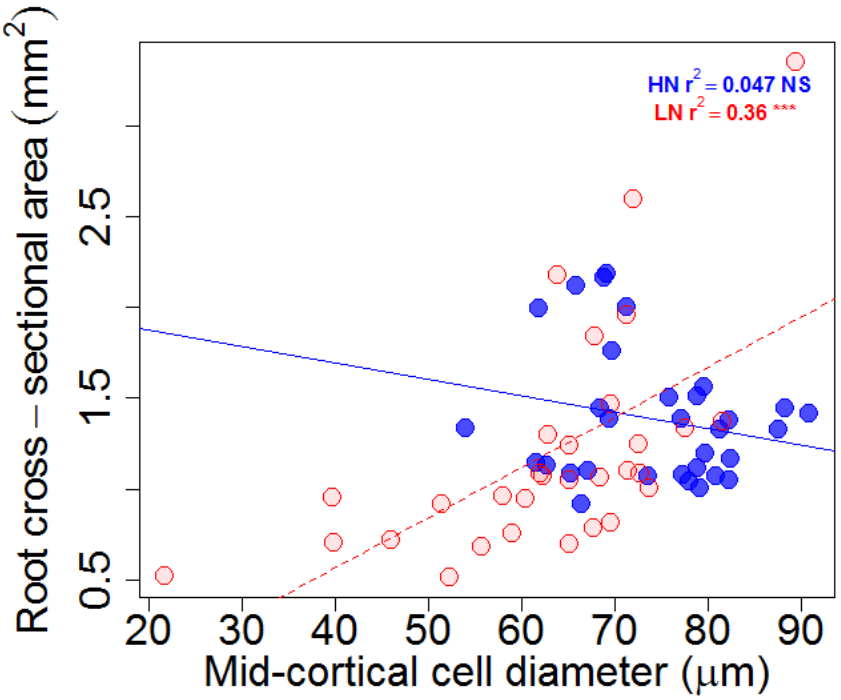
HN r2 = 0.047 NS
LN r2 = 0.36 ***
Root cross – sectional area (mm2)
0.5
1.5
2.5
20
30
40
50
60
70
80
90
Mid-cortical cell diameter (μm)

B

C

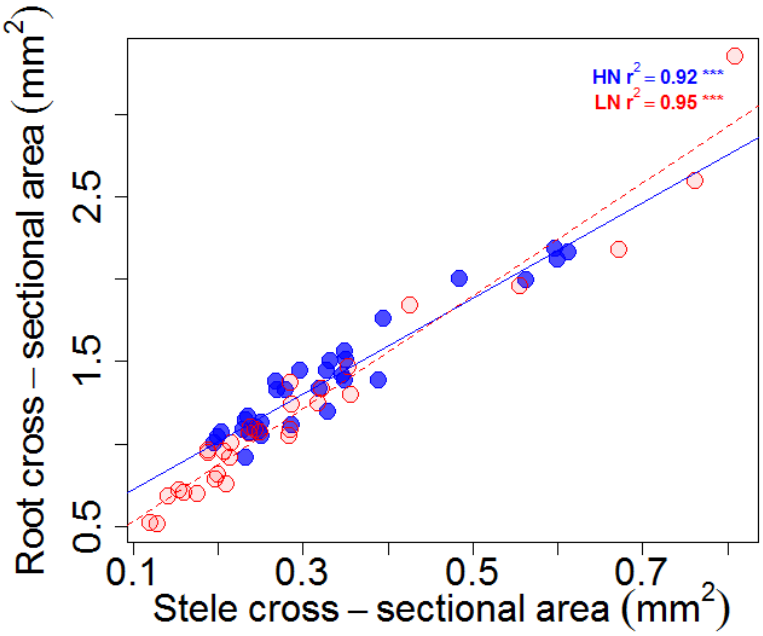

D

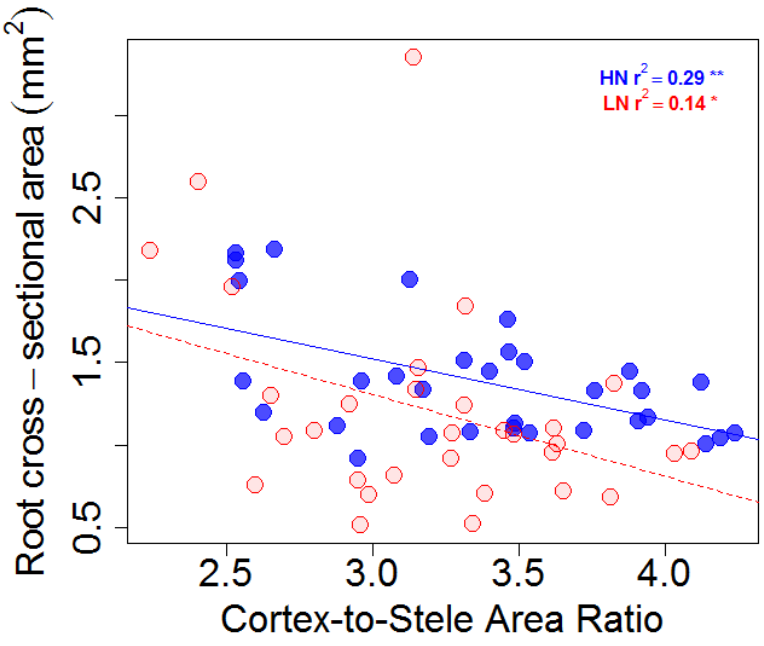

Figure 2-5. Relationship between nodal anatomical traits and diameter among maize IBM RILs. Linear regression of the following nodal anatomical traits against root cross-sectional area (RXA) averaged from two second and third node roots (fully developed in all genotypes at harvest), from individual plants of maize IBM RILs grown in high (HN, blue) or low nitrogen (LN, red) treatments in GH2: (A) cortical cell file number, (B) mid-cortical cell diameter, (C) stele cross-sectional area, and (D) cortex to stele area ratio. R^2 value and significance ($p< 0.05$*, 0.01**, 0.001***; $p>0.1$ not significant, NS) are indicated.

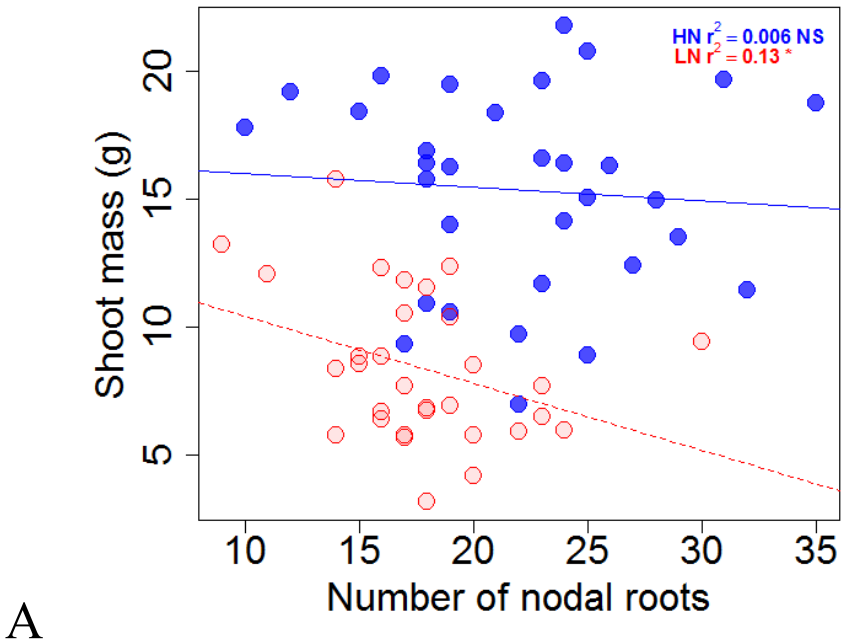

A

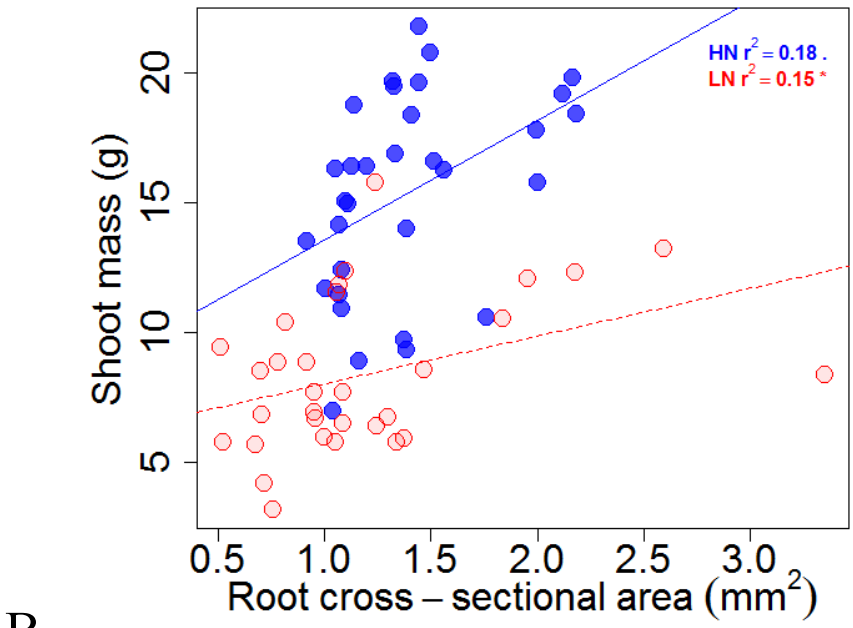

B

Figure 2-6. Relationship between shoot biomass, nodal root number and diameter in maize IBM RILs. Linear regression of (A) total number of nodal roots at harvest (NRN) and (B) root cross-sectional area (RXA) averaged from two second and third node roots, against total dry shoot biomass, from individual plants of eight maize IBM RILs grown in high (HN, blue) or moderate low nitrogen (LN, red) treatments in GH2. R^2 value and significance (p< 0.1., 0.05*, NS, not significant) are indicated. Plants with missing values were excluded.

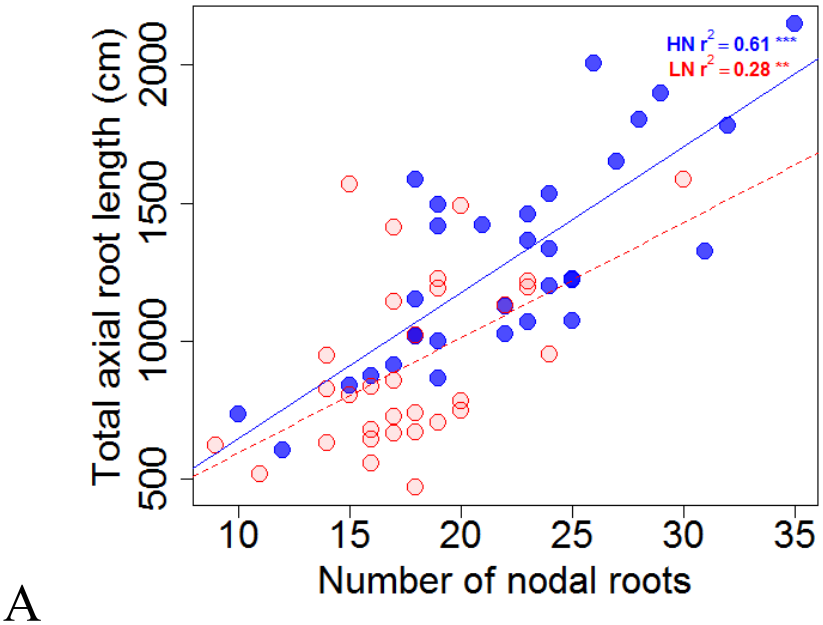

A

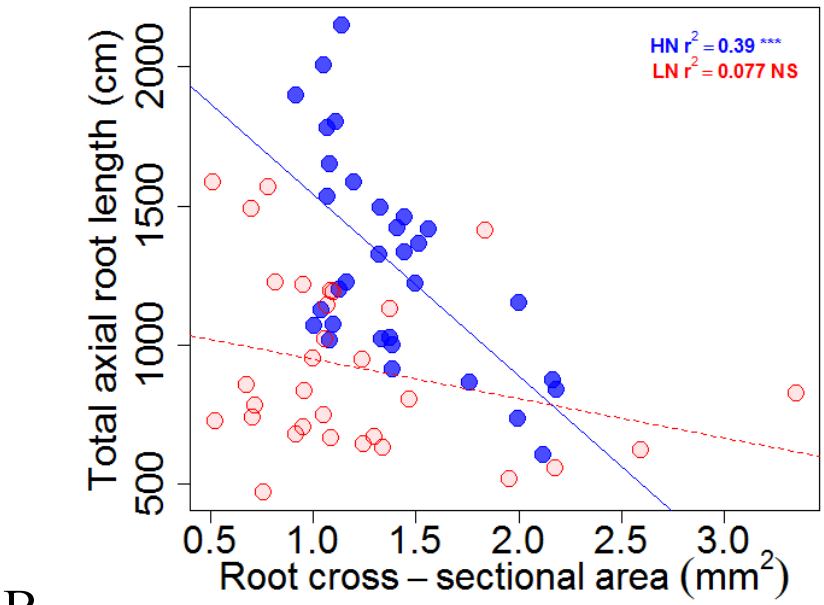

B

Figure 2-7. Relationship between total axial root length, root number and diameter among maize RILs. Linear regression of (A) total number of nodal roots at harvest (NRN) and (B) root cross-sectional area (RXA) averaged from two second and third node roots, against total axial root length summed from node 2 through all developed root nodes, from individual plants of eight maize IBM RILs grown in high (HN, blue) or moderate low nitrogen (LN, red) treatments in GH2. R^2 value and significance (p< 0.1., 0.05*, 0.01**, 0.001***, NS, not significant) are indicated. Plants with missing values were excluded.

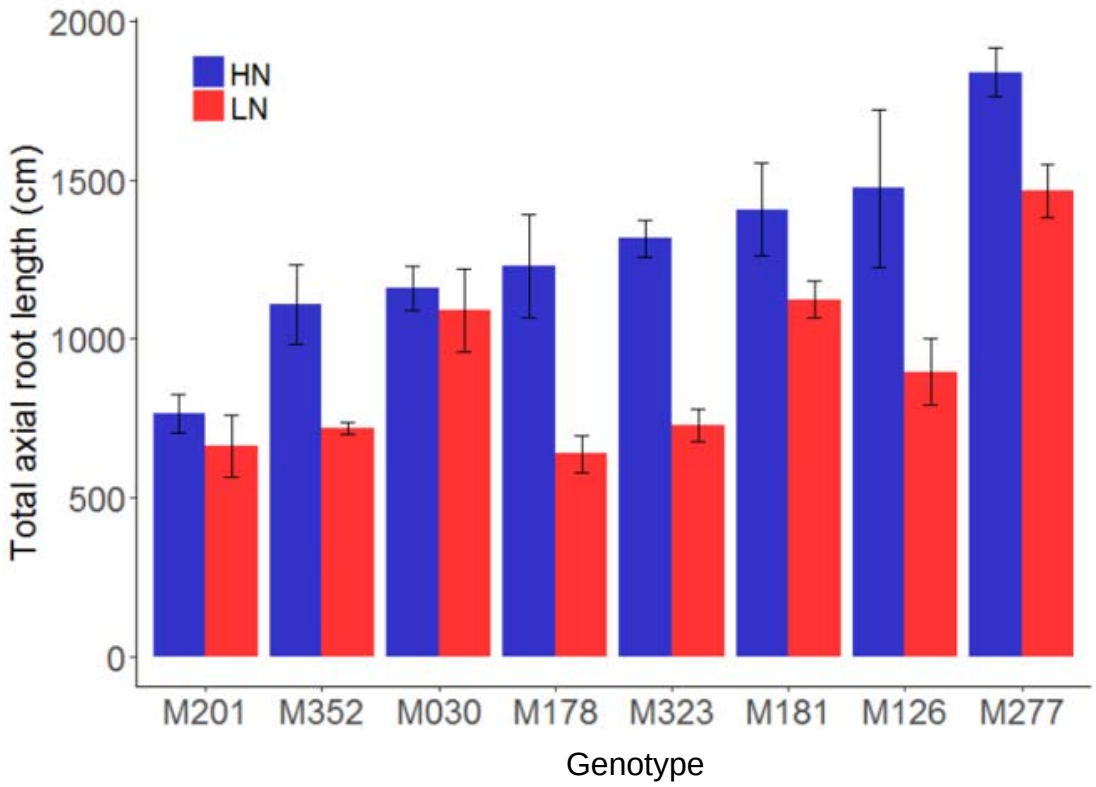

Figure 2-8. Total axial root length produced in IBM RILs. Means ± SE of the total axial root length (TRL), summed for nodes two through all developed nodes, at harvest for each IBM RIL in GH2. IBM RIL number is indicated as M# and arranged in ascending order by high nitrogen trait values. High and low nitrogen treatments are indicated (HN, blue; LN, red).

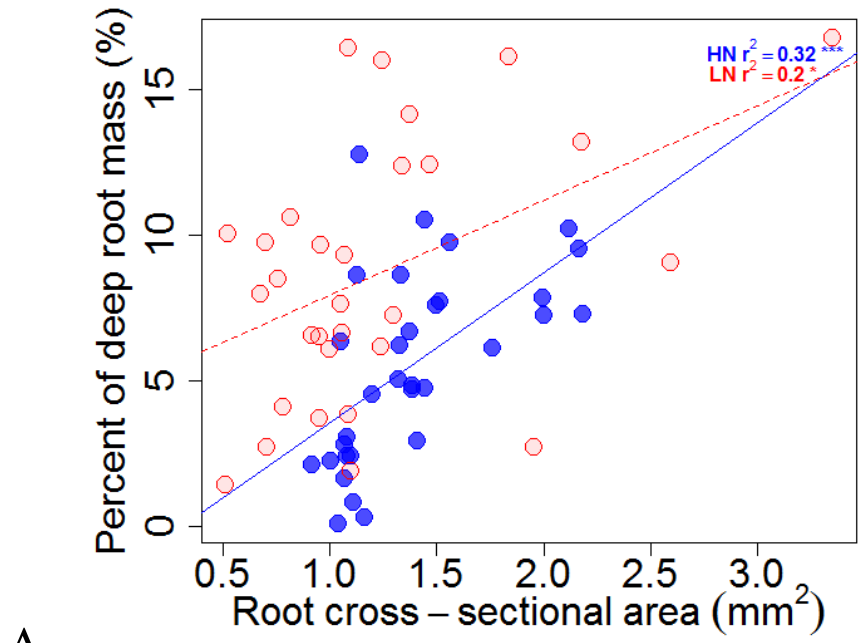

A

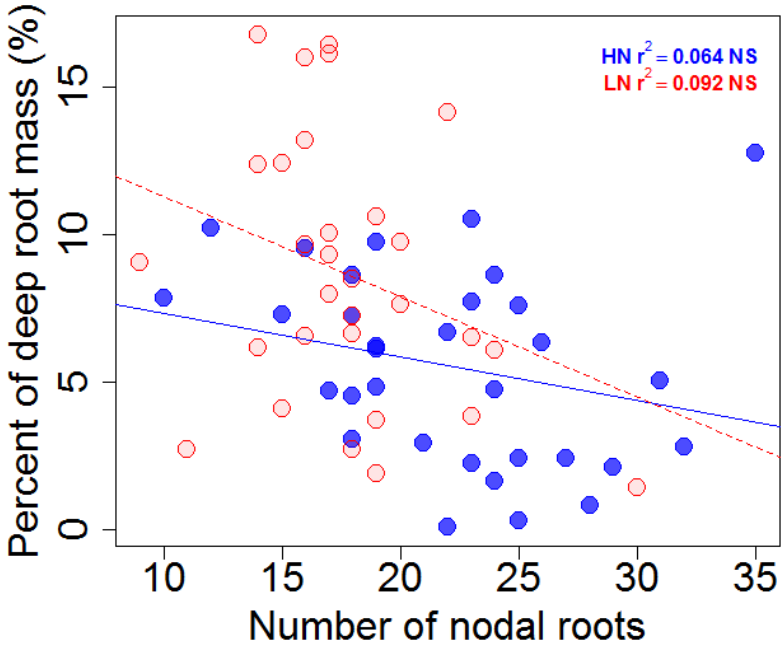

B

Figure 2-9. Relationship between total axial root length, root number and diameter among maize RILs. Linear regression of (A) root cross-sectional area (RXA) averaged from two second and third node roots and (B) total number of nodal roots at harvest (NRN) against the percent of total root biomass in the deepest 30 cm of the root system, from individual plants of eight maize IBM RILs grown in high (HN, blue) or moderate low nitrogen (LN, red) treatments in GH2. R^2 value and significance (p< 0.1., 0.05*, 0.01**, 0.001***, NS, not significant) are indicated. Plants with missing values were excluded.

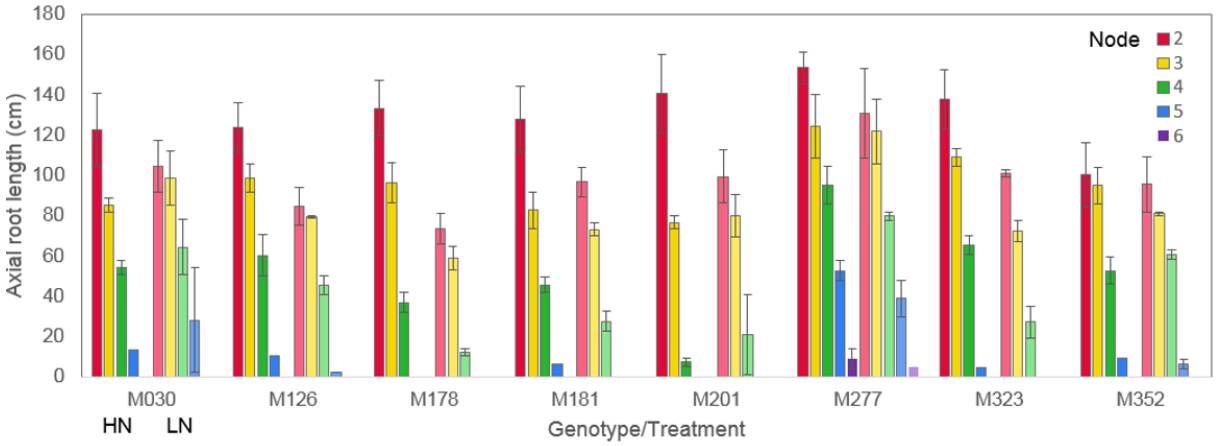

Figure 2-10. Axial root lengths by node in IBM RILs. Means ± SE of the average axial root length (ARL) in each node, for nodes two through all developed nodes (in sequence left to right, indicated by color), at harvest for IBM RILs (M#) under high (HN, left bars for each genotype) and low (LN, right bars for each genotype) nitrogen in GH2.

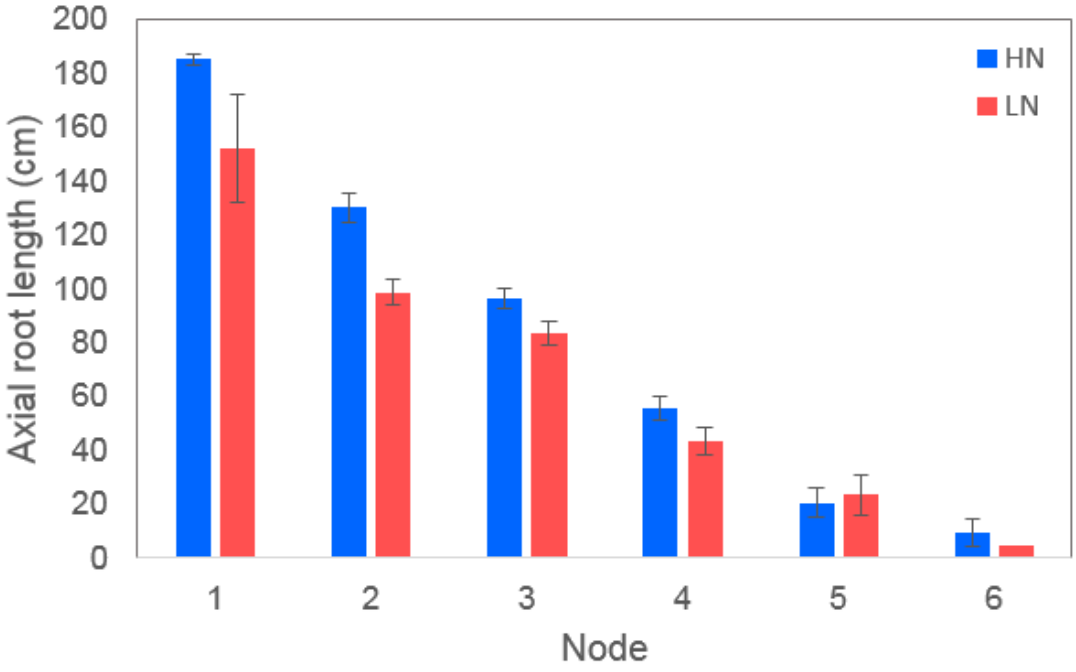
Axial root length (cm)
200
180
160
140
120
100
80
60
40
20
0
HN
LN
1
2
3
4
5
6
Node

A

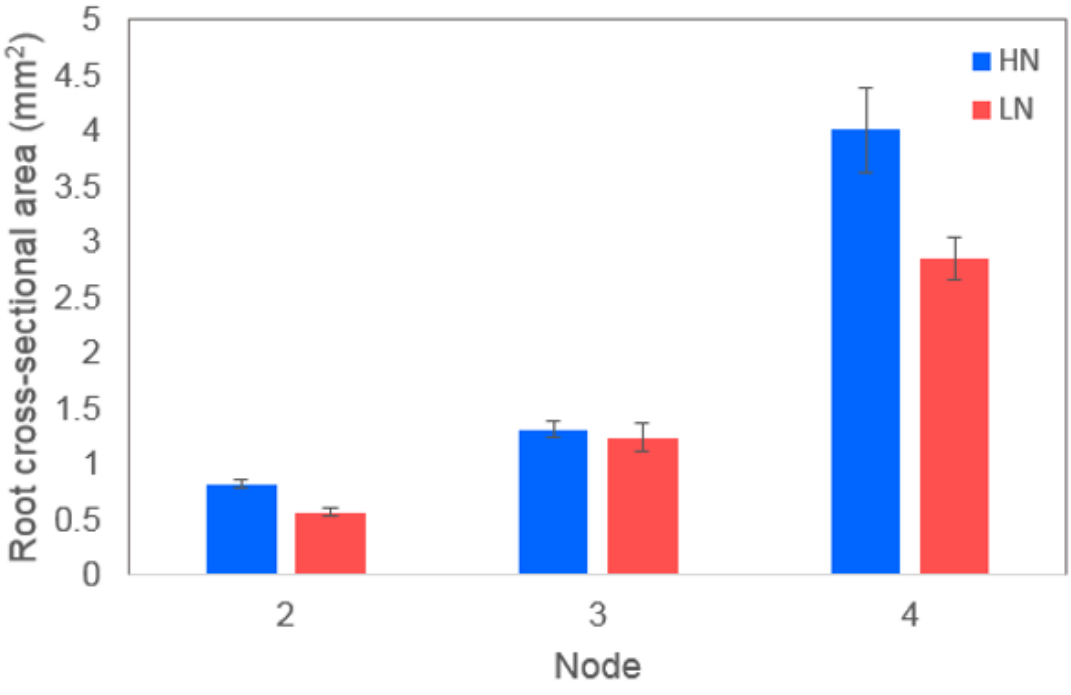
Root cross-sectional area (mm²)
5
4.5
4
3.5
3
2.5
2
1.5
1
0.5
0
HN
LN
2
3
4
Node

B

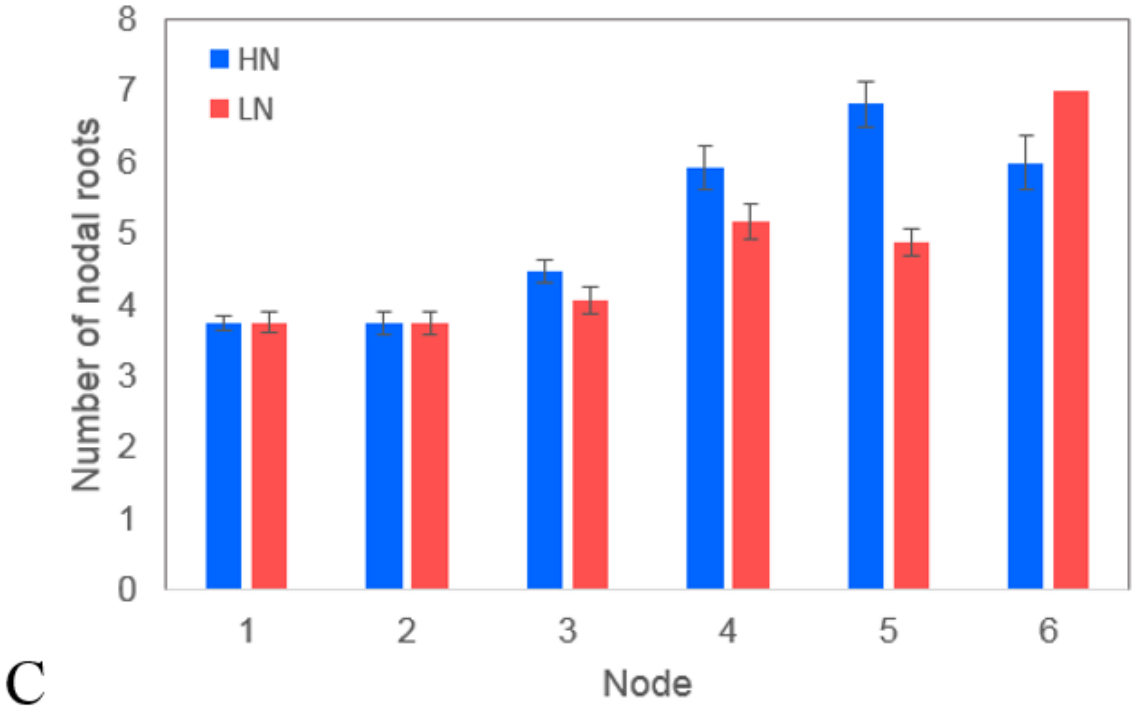

Figure 2-11. Axial root lengths, diameters, and occupancy by node under low nitrogen in IBM RILs. Means ± SE of (A) the average axial root length (ARL) by node at time of harvest, and (B) average RXA by node, and (C) average number of roots per node (NO), in GH2. ARL was evaluated in all plants for nodes 2 through 6, and only a subset of plants in node 1. High and low nitrogen treatments are indicated (HN, blue; LN, red).

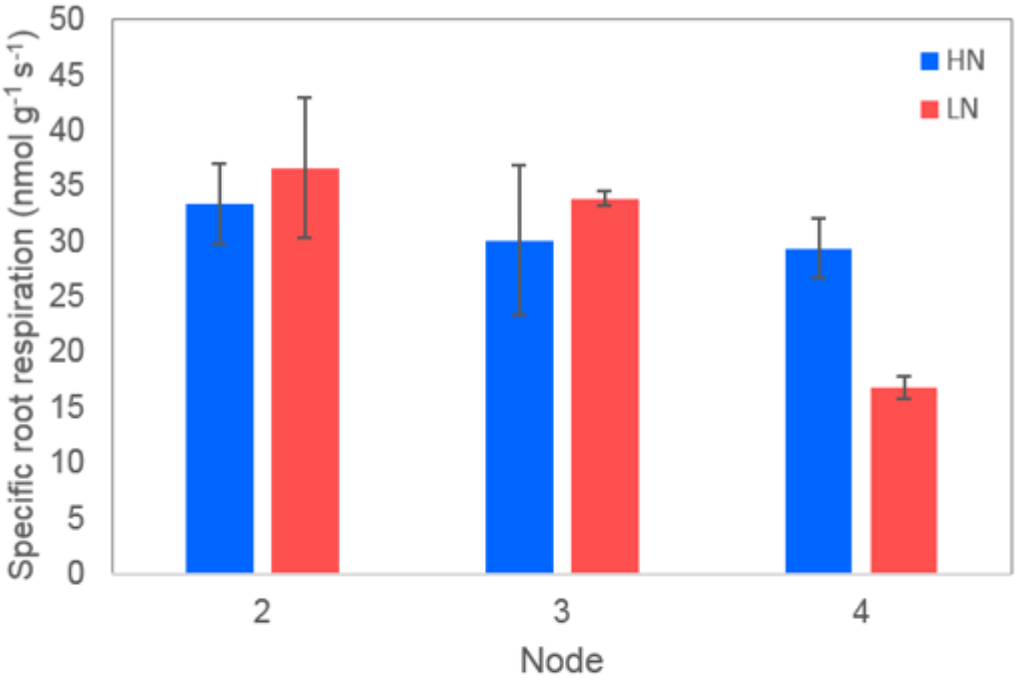
Specific root respiration (nmol g-1 s-1)
50
45
40
35
30
25
20
15
10
5
0
HN
LN
2
3
4
Node

A

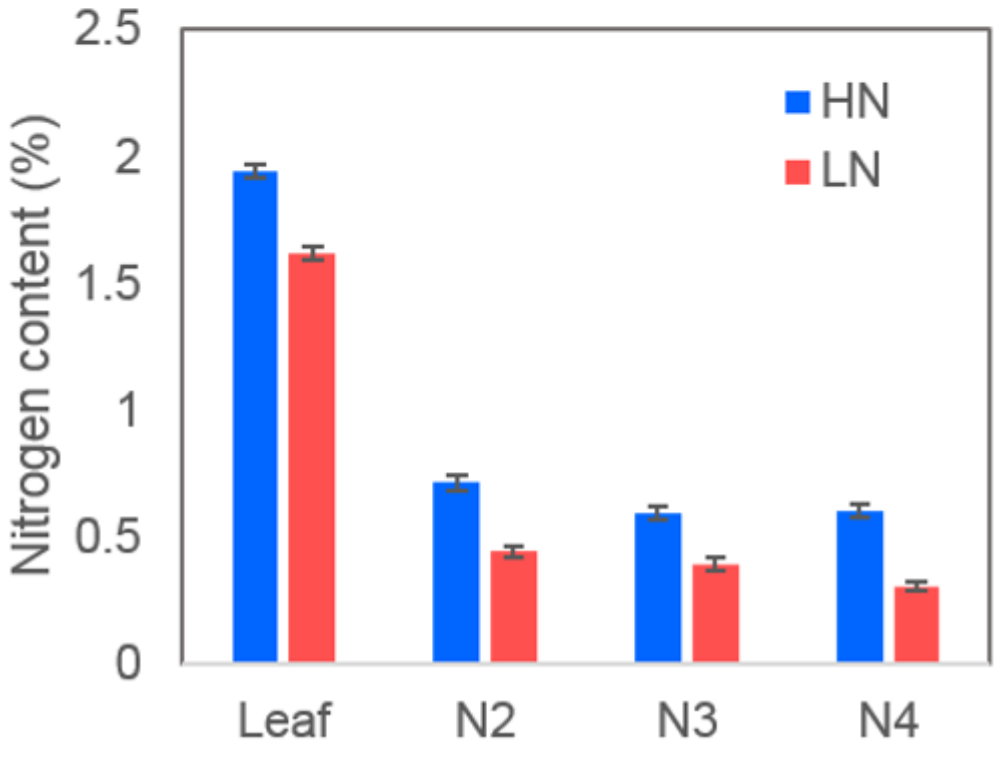
Nitrogen content (%)
2.5
2
1.5
1
0.5
0
HN
LN
Leaf
N2
N3
N4

B

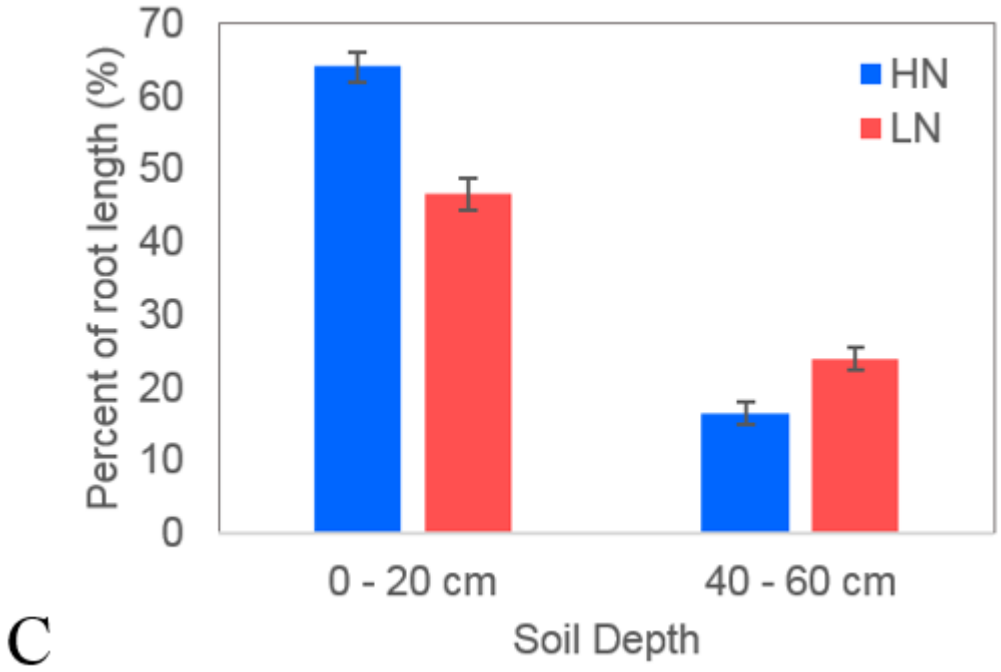

C

Figure 2-12. Effect of nitrogen stress on root respiration, nitrogen, and root length distribution in IBM RILs. Means ± SE of (A) specific root respiration averaged across genotypes, by root node in GH2, (B) percent of nitrogen in the nodal root 2-4 cm from base, across field-grown IBM and NYH RILs in SA14, and (C) percent of total root length in the shallowest and deepest 20 cm obtained from soil cores, averaged across field-grown IBM RILs in PA15. High and low nitrogen treatments are indicated (HN, blue; LN, red).

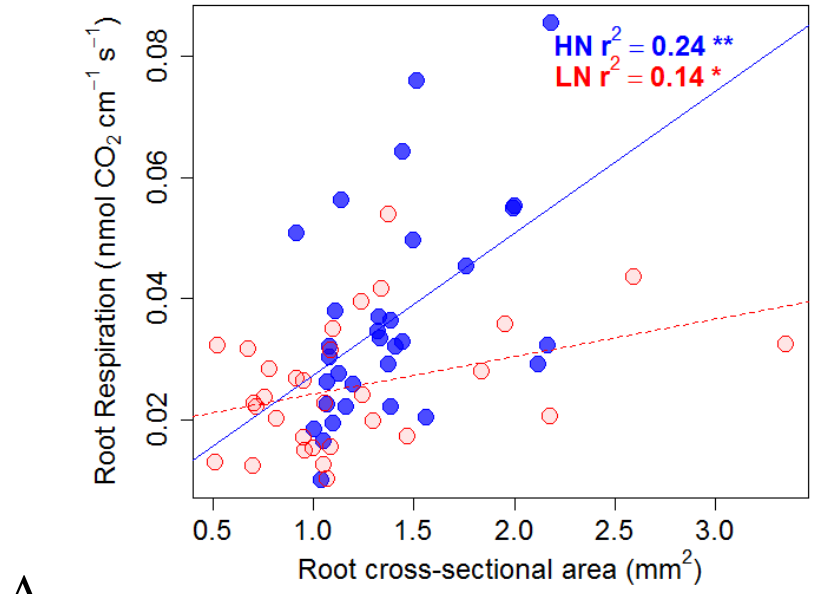

A

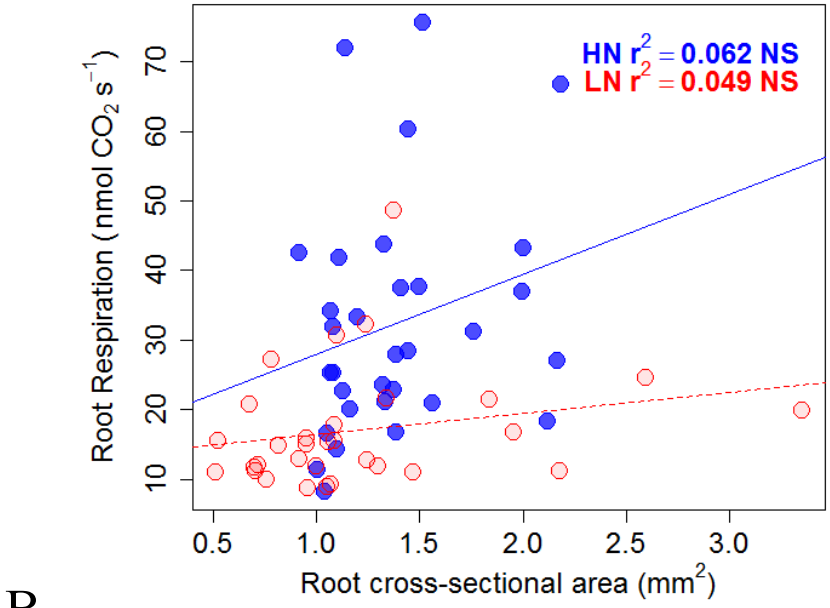

B

Figure 2-13. Relationship between axial root diameter and respiration among maize RILs. Linear regression of root cross-sectional area (RXA) averaged from two second and third node roots against (A) root respiration per unit root length averaged from three roots each from nodes 2 and 3, and (B) total axial root respiration (root respiration rate multiplied by axial lengths of all developed nodes expect the first node), from individual plants of maize IBM RILs grown in high (HN, blue) or moderate low nitrogen (LN, red) treatments in GH2. R^2 value and significance ($p< 0.05$*, 0.01**, $p>0.1$ NS, not significant) are indicated.

Table 2-1. Description of maize root system measurements.

Trait	Measurement and Unit
RXA	Axial root cross-section area, mm^2
NRN	Total number of nodal roots emerged at time of harvest
NN	Total number of root nodes developed at time of harvest
NO	Number of nodal roots per node ('nodal occupancy')
ARL	Root length of a single axial root (e.g. averaged across roots within a node), cm
TRL	Total root length of axial roots (e.g. summed across roots within a node), cm; TRL = NO*ARL for the indicated node(s).
TXA	Total cross-section root area in indicated node(s), mm^2; TXA = RXA * NO
TRV	Total axial root volume in indicated node(s), mm^3; TRV = RXA * (ARL*10) * NO
D95	Depth above which 95% of the root system is located (e.g. by length or mass, as specified)

Chapter 4

Integrating nodal root and leaf traits to enhance nitrogen use efficiency in maize (*Zea mays* L.)

Abstract

Breeding crops for improved nitrogen acquisition and utilization requires the integration of efficient shoot and root architecture, morphology, and anatomy. Yet shoot and root phenotyping often occur in isolation, and relationships between leaf and root traits are poorly understood. This study evaluated leaf traits among maize IBM RILs which were previously found to contrast in nodal root number and diameter, and found substantial contrast in leaf size, number, specific leaf area, stomatal density and index, interveinal distance, and midrib anatomy under high nitrogen. Leaf anatomy traits were strongly inter-related, but did not show a strong linkage to root traits with a few exceptions; for example, stomatal density was positively related to the percent of root cortical aerenchyma under both high and low nitrogen conditions. However, there was strong genotypic contrast in leaf thickness and other leaf anatomical traits under moderate nitrogen stress, associated with root traits; genotypes that maintained thicker roots also maintained thicker leaves, which had more mesophyll tissue, larger cells and vessels, and less vein and stomatal density. Leaf thickness was related to total shoot nitrogen, but not carbon assimilation per leaf area or leaf nitrogen content, suggesting it was related to improved nitrogen status as a result of efficient nitrogen uptake, rather than independently contributing to nitrogen use efficiency. Thus, there is potential to integrate root and shoot traits which improve nitrogen acquisition and utilization efficiency, respectively, and combined ideotypes which consider carbon and nitrogen costs in addition to hydraulic flow should be considered.

Highlight

The relationship between leaf and root phenotypes was explored among maize IBM RILs. Leaf anatomy varied with leaf thickness, but there was no contrast in leaf thickness under high nitrogen, despite contrasting root phenotypes. Genotypes with improved nitrogen stress tolerance maintained thicker nodal roots and leaves under nitrogen stress. Integrated root and leaf ideotypes for nitrogen use efficiency are discussed.

Key words and abbreviations

Leaf anatomy, leaf thickness, maize, nodal root number, nitrogen uptake, nitrogen use efficiency, root diameter

IBM, intermated B73 x Mo17
RIL, recombinant inbred line

Introduction

Breeding crop varieties with improved nitrogen acquisition and utilization efficiency is a key strategy for sustaining the growing human population, while mitigating effects of climate change and land degradation (Moll et al., 1982; Tilman et al., 2002; Zhang et al., 2015). Nitrogen deficiency is a major limitation to crop yield in subsistence agriculture, which is essential for food security (Sanchez, 2002; Vitousek et al., 2009). By contrast, over half of applied nitrogen fertilizer in commercial agricultural operations is not captured by plants, either leaching beyond the root zone, polluting waterways and creating hypoxic zones, or volatizing into harmful greenhouse gases such as nitrogen oxides and ammonia (Hirel et al., 2011; Liu et al., 2016). Nitrogen fertilizer is often the most expensive input in these operations; more efficient nitrogen use would yield both economic and environmental benefits (FAO 2014; Lassaletta et al., 2016).

Improvements in genetic material and agronomic practices have resulted in increasing maize yields, and has indirectly improved nitrogen acquisition and utilization efficiency (Wu et al., 2011; Ciampitti and Vyn, 2012; York et al., 2015; Dhital and Raun, 2016; DeBruin et al.,

2017). Tollenaar and Lee (2002) suggested that yield gains have been a result of the interaction of genetics and management due to the selection environment; modern varieties have a suite of shoot and root traits optimal for high density monocultures, including vertical leaf angle and shorter leaf length, fewer nodal roots, reduced stem and root lodging, increased pest resistance, delayed leaf senescence and increased post-silking nutrient uptake (Boomsma et al., 2009; York et al., 2015; DeBruin et al., 2017). However, direct selection for beneficial root and leaf traits have largely been independent efforts, and potential genetic linkages between root and leaf traits are not well understood.

Several root system ideotypes have been proposed for optimizing nitrogen acquisition efficiency (White et al., 2013; Lynch, 2013; Yu et al., 2015; Schmidt and Gaudin, 2017). For example, root phenotypes which reduce metabolic costs and enable rapid, deep rooting under nitrogen stress, such as reduced nodal root number and reduced lateral branching, have been associated with improved nitrogen acquisition (Lynch, 2013; Saengwilai et al., 2014a; Zhan and Lynch, 2015). Slower nodal root development, resulting in both reduced nodal root number and increased axial root diameter, has been associated with improved nitrogen stress tolerance (see Chapter 2). Increased axial root length, secondary lateral branching, and nitrate transporter expression have also been associated with improved nitrogen uptake (Gaudin et al., 2011), and advantages of root plasticity for acquiring heterogeneous soil nitrogen have been explored (Yu et al., 2014).

By contrast, improvements in nitrogen utilization efficiency have been associated with aboveground traits and optimizing source-sink metabolism in maize, including increased activity of nitrate assimilation and remobilization enzymes in leaves (e.g. glutamine synthetase), increased leaf longevity and chloroplast retention (i.e. “stay green”), and greater post-silking nitrogen assimilation (Moll et al., 1982; Rajcan and Tollenaar, 1999a, b; Borrell et al., 2001; Hirel et al., 2001; Mu et al., 2016). Additionally, maize is a NADP-ME C4 plant; small changes in leaf anatomy and enzyme activity have been shown to substantially influence the efficiency of C4 photosynthesis (Ghannoum et al., 2005; Covshoff et al., 2008; Slewinski et al., 2012; Lundgren et al., 2014), which enables greater carbon assimilation per unit of leaf nitrogen, as well as improved water use efficiency (Schmidt and Edwards, 1981; Sage and Pearcy, 1987; Oaks, 1994). Greater specific leaf area (either decreased leaf thickness, leaf tissue density, or both) and leaf nitrogen content have also been associated with improved photosynthetic nitrogen use efficiency (e.g. Donovan et al., 2011).

The optimal combination of both above- and belowground traits, or potential trade-offs of these utilization and acquisition strategies under varying nitrogen conditions, is unclear. The relationship between architectural, morphological, and anatomical traits between roots and leaves, and their responses to nitrogen levels, is poorly understood, yet important for identifying trait combinations which could enhance both nitrogen uptake and utilization efficiency under high and low nitrogen conditions. Furthermore, root and shoot development are regulated by many shared genes and signaling pathways, suggesting traits may be correlated through pleiotropy or close linkage (Byrne et al., 2003; Laux et al., 2004; Chen and Lubberstedt, 2010; Seago, Jr. and Fernando, 2013). To understand the relationship of root and leaf traits, their plasticity under nitrogen stress, and potential combinations of root and leaf traits for nitrogen stress tolerance, we evaluated leaf anatomy, morphology, and physiology among maize IBM RILs which contrasted in nodal root number and diameter, in the greenhouse and field, under multiple nitrogen conditions.

Methods

Plant materials

Two greenhouse experiments (GH1 and GH2) were performed in 2015, using maize recombinant inbred lines (RILs) from the intermated B73 x Mo17 population (IBM). GH1 and GH2 included 8 genotypes each: M0 30, 126, 178, 201, 277, 323, 352, plus M0 365 (GH1) and M0 181 (GH2). PA15 included 11 genotypes: M0 59, 129, and all genotypes from GH1 and GH2. Seeds were provided by Dr. Shawn M. Kaeppler from U-Wisconsin, Madison, USA. Genotypes and additional details are listed in Appendix D, Table S1.

Experimental conditions

Greenhouse experiments

GH1 and GH2 were conducted in the same greenhouse at University Park, PA (40° 45' 36.0" N, 73° 59' 2.4" W), with 14 h photoperiod, maintained at approximately 28°C/26°C day/night, 40% RH, PPFD of 500 μmol m^{-2} s^{-1} at the sixth leaf (Growmaster Procom, Micro Grow, Temecula, CA, USA). GH1 seeds were germinated on April 28, 2015, and plants were harvested June 4-5, 2015. GH2 seeds were germinated Sept 26, 2015, and plants were harvested November 3-4, 2015.

Seeds were surface-sterilized with 25% commercial bleach for 3 min, rinsed with distilled water, then soaked in the seed fungicide Captan (0.2 g/L) for at least 10 min. Seeds were germinated using the paper roll-up method. Seeds were placed 2.5 cm apart in a row, 4 cm from the top edge, between two sheets of heavy weight seed germination paper (Anchor Paper Co., St. Paul, MN, USA), then rolled up and placed vertically in an imbibing solution of 0.5 mM $CaSO_4$, and dark-incubated at 28°C for 2 days (Imperial II, Lab-line, Dubuque, IA, USA). Representative seedlings from each genotype were transplanted at about 5 cm depth and thinned after 4 days.

Plants were grown in individual mesocosms. Each mesocosm consisted of a PVC pipe with an inner diameter of 15.5 cm (outer diameter 16 cm) and height of 1.54 m, set vertically within a PVC socket cap (17 cm inner diameter, 18.5 cm outer diameter) with a drainage hole drilled in the bottom. A layer of plastic mesh was laid over the drainage hole. Mesocosms were secured about 30 cm apart (center to center) against vertical wooden frames. Each mesocosm was fitted with a bottom-draining plastic liner bag constructed from 6 mil polyethylene sheets (USP Corp, Lima, OH, USA) using a heat sealer (Model H-1254, U-line, Pleasant Prairie, WI, USA).

Each mesocosm was filled with a 30 L mixture consisting of 50% commercial grade medium sand (Quikrete, Harrisburg, PA, USA), 27% horticultural grade fine vermiculite (D3, Whittemore Companies Inc., Lawrence, MA, USA), 18% field soil, and 5% horticultural grade super coarse perlite (Whittemore Companies Inc.), by volume. Soil was collected from the top 20 cm of low-nitrogen fields (Hagerstown silt loam) maintained at the Russell E. Larson Agricultural Research Center at Rock Springs, PA, air dried, crushed and sieved through a 4 mm mesh. A thin surface layer of perlite was added to each mesocosm to help retain moisture and reduce compression of media.

Plants were fertigated using individual 12.7 cm diameter drip rings (Dramm, Manitowoc, WI, USA) with 2 mm diameter poly tubes inserted into a PolyFlex pipe (1.9 cm inner, 2.5 cm outer diameter), which was connected to a submersible pump (Little Giant, Fort Wayne, IN, USA) in a 100 L Rubbermaid tub, containing one of two nutrient solutions. The high nitrogen (HN) solution contained (in μM): 6500 NO_3, 80 NH_4, 500 P, 2000 Mg, 3500 S, 3500 Ca, 3010 K, 10 Cl, 14 B, 3 Mn, 1 Zn, 0.5 Mo, 0.4 Cu, 110 Fe. The low nitrogen (LN) solution contained (in μM): 130 NO_3, 10 NH_4, 500 P, 2000 Mg, 4500 S, 2310 Ca, 1500 K, 500 Cl, 14 B, 3 Mn, 1 Zn, 0.5 Mo, 0.4 Cu, 110 Fe. Iron was applied as 5.85 mg/L Fe-DTPA (Dissolvine D-Fe-11, Akzonoble, Amsterdam, Netherlands). Nutrient solutions were adjusted to pH 6.0 using KOH pellets, and maintained at this pH with KOH or HCl as needed. A micronutrient foliar spray was applied as needed. Each mesocosm was saturated with 2.5 L of nutrient solution one day prior to transplant, then fertigated 200 mL per mesocosm every other day.

Field experiment

The PA15 field trial was conducted in a 0.4 ha field maintained with split high and low nitrogen treatments (field #103) at The Pennsylvania State University's Russell Larson Research Farm (40°42'40.915"N, 77°,57'11.120"W), which has Hagerstown silt loam soil (fine, mixed, semi-active, mesic Typic Hapludalf). To generate low N conditions, about 2.5 cm of sawdust was applied in May 2011 and 2012. The high-nitrogen side of the field was fertilized with 157 kg N ha^{-1} applied as urea (46-0-0) while no N fertilizer was applied on the low-nitrogen side. Drip irrigation, nutrients other than N, and pest management were applied as needed. Seeds were planted on June 14, 2015 using hand jab planters in rows with 76 cm row spacing, 91 cm alleys, 23 cm plant spacing, 4.6 m plot length with 3.7 m planted, or approximately 56,800 plants ha^{-1}. Each genotype was planted in 3-row plots, and plants from the middle row of each 3-row plot were sampled.

Experimental design

GH1 and GH2 were two-way factorial randomized complete block designs, with four replicates (blocks) containing randomized combinations of 8 genotypes x 2 nitrogen treatments

(high and low nitrogen). PA15 was a split-plot randomized block design, with 11 genotypes were randomized in 4 blocks within 2 N treatments, totaling 88 plots. One 1-acre field was sub-divided into 8 blocks.

Plant measurements and harvest

Greenhouse experiments

In GH1 and GH2, plant height, leaf number and length and width of each leaf were measured prior to harvest. Leaf area was estimated using LL x LW x 0.75 (Montgomery, 1911). Stomatal imprints were collected and a representative leaf was preserved in 75% ethanol for anatomical analysis (see next section) and to collect leaf punches (five 2.5-cm diameter circles along leaf blade, excluding midrib) which were dried and weighed for specific leaf area. An entire leaf was also dried and weighed separately for a second measurement of specific leaf area. SPAD (SPAD 502Plus, Konika Minolta, Tokyo, Japan) and photosynthesis measurements (LI-COR 6400XT, LI-COR Biosciences, Lincoln, NE, USA) were taken on a sixth and seventh leaves in low and high nitrogen, respectively, with PAR set at 500 μmol m^{-2} s^{-1}, about one week prior to harvest.

Plants were harvested over two days, with two replicates harvested per day. Shoots were removed, dried at approximately 70^0C, and stem and leaves were weighed separately. Dried leaves were ground, homogenized, and a 2 mg subsample was analyzed for total nitrogen content with a CHN elemental analyzer (2400 CHNS/O Series II, PerkinElmer, Waltham, MA, USA) using the Dumas combustion method.

Whole root systems were removed intact within polyethylene liner bags. Liner bags were sliced open and media was gently washed off with a hose. Nodal axial roots were counted manually and recorded by node. The number of roots per node was defined as its “nodal occupancy”. The length of each axial root was measured from base to tip, with lengths recorded by node; broken roots were measured as possible and recorded separately to obtain the most accurate average lengths possible. Two representative root segments each were excised from 2 to 4 cm from the stem base from the second and third nodes (GH1) and from the second, third, and fourth nodes (GH2), and preserved in 75% ethanol for anatomical analysis.

Field experiment

In PA15, physiological measurements and sampling, including photosynthesis rate, SPAD, leaf chlorophyll content, specific leaf area, plant height, leaf area of each leaf and total leaf number, and stand counts were completed approximately one week prior to harvest. See above section for methods; eight leaf punches were taken for specific leaf area in PA15. Manually ground leaf tissue with a total fresh weight of about 0.25 g was extracted in ethanol, and chlorophyll a and b content was determined spectrophotometrically (Wintermans and DeMots, 1965).

Following anthesis, root and biomass harvest began on Sept 3, 2015. A representative plant from each plot was excavated using a shovel (Trachsel et al., 2011). Root crowns were separated from the shoots, soaked in water with detergent, and hosed to remove remaining soil. Each node of roots was excised, and up to 3 representative roots from nodes 1, 2, and 3 were sampled at 2 to 4 cm from the base of the stem and preserved in 75% ethanol for anatomical processing. For a subset of plants, nodal roots were counted by node and roots less than 2 cm emerged were noted separately. Shoot biomass was separated into stem, leaves, and ears, dried at approximately 70°C, and weighed. Ears from five plants per plot were collected at physiological maturity, dried to approximately 15% moisture content, shelled and weighed. Dried leaves were ground, homogenized, and a 2 mg subsample was analyzed for total nitrogen content with a CHN elemental analyzer.

The average percent reduction in shoot biomass and yield under nitrogen stress from all experiments are listed in **Appendix D, Table S1**. Soil nitrate distributions are in **Chapter 3, Appendix C, Fig S1.**

Image analysis

Leaf anatomy

For GH1 and GH2, anatomical samples were taken from leaf 7 or the largest expanded leaf; for PA15, the ear leaf was sampled. Stomatal imprints were taken on intact leaves prior to harvest on the adaxial and abaxial surface in the middle region of the leaf, between the midrib and margin. Clear super glue was applied in a thin layer on the leaf, pressed against a glass cover slip,

and allowed to dry on the leaf. The cover slips were then removed and images were captured with a Diaphot inverted light microscope (Nikon Inc., Melville, NY, USA) with a mounted CCD camera (Nikon DS-Fi1 camera with DS-U2 USB) using NIS Elements F 4.30.00 software (Nikon, Inc.) using 1280 x 920 pixel resolution. The following pixel conversions were used for the indicated objective lens: 4X, 781 pixels/mm; 10X, 2062 pixels/mm; 20X, 4115 pixels/mm; 40X, 8155 pixels/mm.

Basal leaf sections were preserved and cleared in 75% ethanol for at least 24 hours. For anatomical analysis, a basal section of the leaf approximately 2 cm from the midrib was removed, and several thin slices perpendicular to the midrib were made using fresh double-edged razor blades (American Safety Razor Company, Verona, VA, USA). These cross-sections were mounted in water and imaged as described above. Separately, the adaxial and abaxial surfaces of the leaf section were mounted and imaged. Finally, thin cross-sections of the leaf midrib were manually sliced, mounted and imaged. Leaf anatomical traits were quantified using custom macros created with the ObjectJ plug-in (https://sils.fnwi.uva.nl/bcb/objectj/) in ImageJ (https://imagej.nih.gov/ij/index.html). See **Appendix D, Table S1 and Fig S1** for sampling details and detailed image analysis protocol. See **Table 3-1** for trait descriptions.

Root anatomy

For GH1 and PA15, the middle portion of two representative root segments per node of each plant were ablated and imaged using laser ablation tomography (LAT). This technique employs a nanosecond pulsed UV laser (Avia 355-7000, Coherent, Santa Clara, CA, USA) focused into a single-line scanning beam with a HurryScan 10 galvanometer (Scanlab, Puchheim, Germany) to ablate the cross-sectional surface of a root secured to a three-axis motorized stage (ATS100-100, Aerotech Inc, Pittsburgh, PA, USA). The root is moved into the laser beam at about 30 μm s^{-1} (rate is adjusted according to root quality), and as each surface is ablated and exposed, images lit by the laser UV light are captured using a stage-mounted (#62-009, Edmund Optics, Barrington, NJ, USA) camera and 5X macro lens (Canon EOS Rebel T3i camera with 65mm MP-E 1-5x variable magnification, Canon USA Inc, Melville NY, USA). Image scale was 1.173 pixels per micron. Select greenhouse-grown root segments required pre-processing in a critical point dryer (Leica EM CPD300, Leica Microsystems, Wetzlar, Germany) to prevent sample dessication during laser ablation. Roots were placed in histo prep tissue capsules (29 mm

x 6 mm) (Fisherbrand, Fisher Scientific, Waltham, MA, USA) and gradually dehydrated 75% to 100% ethanol prior to critical point drying.

For GH2, two ethanol-preserved roots from each node (2, 3, and 4) were manually sectioned using fresh double-edged razor blades (American Safety Razor Company, Verona, VA, USA), wet-mounted and visualized using a Diaphot inverted light microscope (Nikon Inc., Melville, NY, USA) under 4X magnification with a mounted CCD camera (Nikon DS-Fi1 camera with DS-U2 USB controller, Nikon, Inc.). Images were captured using NIS Elements F 4.30.00 software (Nikon, Inc.) at a scale of 390.7 pixels per mm, using 1280 x 920 pixel resolution. Two representative cross-sections images per root were selected for analysis.

Images were analyzed using custom macros created with ObjectJ plug-in in ImageJ, in which cortex, stele, aerenchyma, vessel and cell outlines were manually traced, and cell files and vessel numbers recorded. Trait descriptions and abbreviations are provided in Table 3-1. See **Chapter 2, Appendix A, Fig S2,** and **Chapter 3, Appendix C, Fig S2** for image analysis details.

Statistical analysis

Statistical analysis and visualizations were generated using R version 3.3.1 (R Core Team, 2016). Analysis of variance and effect sizes were determined using *aov* and the *etasq* function in the *heplots* package (Fox et al., 2016), with genotype, nitrogen treatment, block, and the interaction of genotype and nitrogen treatment as factors. Bar plots were generated using data aggregation and processing functions from the *plyr* and *tidyr* packages and plotting functions from the package *ggplot2* (Wickham, 2009; Wickham, 2011; Wickham, 2016). Correlation matrices of scaled, centered data were generated with the gg*corrplot* package (Kassambara, 2016). Color coded values are Spearman's rank coefficient, and circle size scales with p-value, with blank cells (zero) when correlations were not significant at $p<0.05$. Trait arrangement was based on hierarchical clustering.

Results

IBM RILs with contrasting root traits had contrasting leaf anatomy and morphology

Among IBM RILs found to contrast in nodal root phenotypes (RXA and NRN, see **Chapter 3**), we found genotypic differences in leaf number (LN) and size (LAmed), specific leaf area (SLA), interveinal distance (IVD), stomatal density (SD.AB, SD.AD), stomatal index (abaxial only) (SI.AB), epidermal cell size (EpiCCS), and leaf midrib anatomy, including thickness (MidribLT), vascular size (MidribVascA), cell size (MidribCCS) and file number (number of parenchyma cells across the central axis of the midrib) (MidribCF) across nitrogen treatments in the greenhouse (Table 3-2; see Table 3-1 for trait descriptions).

Genotypic contrast was the strongest source of variation for leaf length (LL), interveinal distance, stomatal density, and epidermal cell size, relative to nitrogen and interaction effects (Table 3-3). Nitrogen stress had the strongest effects on leaf number, total leaf area (LA), specific leaf area, vascular bundle size (VascA), and median leaf length to width ratio (LWR), relative to other factors (Table 3-3). Genotype-dependent nitrogen stress effects were strongest for leaf thickness (LT), stomatal size (StomA), stomatal index, and mesophyll cell density (MesoDens) (Table 3).

Leaf thickness had strong genotypic contrast under moderate nitrogen stress in the greenhouse (Appendix D, Fig S2A; see Appendix D, Table S1 for stress levels), but not under severe nitrogen stress (all genotypes had a substantial decrease in leaf thickness; nitrogen treatment was the only significant effect; Appendix D, Fig S2B, ANOVA table not shown) or mild nitrogen stress in the field (no genotype or nitrogen treatment effect on leaf thickness; Appendix D, Fig S2C, ANOVA table not shown). The following results focus on the moderate stress experiment (GH2).

Leaf and root trait relationships differed under high and low nitrogen conditions

Root diameter related traits were related to leaf midrib anatomy, but not other leaf anatomy or stomatal traits, under high nitrogen (Fig 3-1; root diameter related traits refers to RXA, SXA, MXA, CF, MXN, with only RXA shown in Fig 3-1 and Fig 3-2). For example, the number of cell files across the midrib was positively correlated with RXA, and the average cell

size was negatively correlated with RXA, under high nitrogen (Fig 3-1). Stomatal density was positively correlated with median metaxylem vessel size, and root cortical cell size, and mid-cortical cell diameter was positively correlated with interveinal distance, under high nitrogen (Fig 3-1).

Under low nitrogen, RXA was positively correlated with leaf thickness, epidermis and mesophyll cell size, and midrib vascular size, and negatively correlated with stomatal density and stomatal index (Fig 3-2). Root cortical cell size (CMD and MMD) was similarly positively correlated with leaf epidermal and mesophyll cell size, and negatively correlated with stomatal density, under low nitrogen (Fig 3-2). Stomatal density was positively correlated with percent of root cortical aerenchyma under both high and low nitrogen conditions (Fig 3-1, Fig 3-2).

Nitrogen stress had genotype-specific effects on leaf morphology and anatomy

Nitrogen stress reduced the number of leaves at harvest, total leaf area, and leaf width, and increased specific leaf area across IBM RILs (Fig 3-3; Table 3-2). Median leaf length, area, and thickness, as well as midrib thickness and vascular bundle size in the midrib, decreased overall, but nitrogen effects differed among genotypes (Fig 3-3; Table 3-2). Across RILs, percent of vascular tissue and average vascular bundle size decreased, while percent of epidermis tissue increased under low nitrogen (Fig 3-3; Table 3-2). Nitrogen stress also reduced adaxial stomatal density across RILs, but had genotype-specific effects on stomatal size and index (Fig 3-3; Table 3-2).

Thicker leaves were associated with greater shoot growth under nitrogen stress

Leaf thickness was positively correlated with shoot biomass under low nitrogen, but not high nitrogen conditions, across IBM RILs (Fig 3-4A). In contrast, shoot mass was positively correlated with median leaf area and plant height under both high and low nitrogen conditions (Fig 3-4 B, C). The number of developed leaves had a weaker positive correlation with shoot mass under low nitrogen, and was not correlated under high nitrogen (Fig 3-4D). Total shoot nitrogen was positively correlated with leaf thickness under low nitrogen, but not high nitrogen conditions (Fig 3-4E).

Thicker leaves had larger cells, vascular bundles, interveinal distance, and more mesophyll tissue

Thicker leaves had a larger percent of mesophyll tissue (relative to epidermis and vasculature), larger mesophyll and epidermal cell sizes, reduced mesophyll density, larger vascular bundles and greater interveinal distance under high and low nitrogen (Fig 3-2, Fig 3-3). Leaf midrib thickness and vascular bundle size were also strongly positively correlated under both high and low nitrogen (Fig 3-2, Fig 3-3). Leaf thickness was negatively correlated with stomatal density under low nitrogen, but not high nitrogen conditions (Fig 3-2, Fig 3-3).

Specific leaf area decreased as leaf thickness increased, but the correlation was weak for both high and low nitrogen, indicating other traits (e.g. tissue density) influenced specific leaf area (Appendix D, Fig S3A). Leaf thickness was negatively correlated with carbon assimilation and conductance rates, and not strongly correlated with specific leaf nitrogen content and the number of leaves (Appendix D, Fig S3 B, C, D, E).

Leaf and nodal root morphology were associated under certain nitrogen conditions

The number of leaves and the number of nodal roots produced in a growth period were positively correlated across IBM RILs in high nitrogen, but were not related under low nitrogen conditions (Fig 3-5A). In contrast, the total axial volume per node (TRV, averaged across nodes 2 and 3) was positively correlated with leaf thickness under low nitrogen, but not high nitrogen conditions (Fig 3-5B). This relationship was stronger than the positive correlation between RXA and leaf thickness, also under low nitrogen only (Fig 3-2).

Leaf growth patterns in high and low nitrogen conditions differed among maize RILs

Genotypes showed contrasting leaf sizes from base to apex, under both high and low nitrogen (Fig 3-6 A, B, C). M201 and M277 had the greatest contrast in root phenotypes (compared in Fig 3-6A), while M323 and M126 had moderate contrast in root phenotypes (compared in Fig 3-6B) and M178 and M181 had less contrast (compared in Fig 3-6C). M201 produced larger leaves in the first eight leaves compared to M277, while the two genotypes had similar leaf sizes in the upper leaves (i.e. higher leaf numbers), under high nitrogen conditions

(Fig 3-6A). Under low nitrogen, leaf sizes were not strongly affected in M201, whereas M277 showed progressively greater reductions in leaf size from base to apex (Fig 3-6A). Similarly, M126, M178, and M181 showed progressively greater reductions in leaf size under nitrogen stress, whereas M323 maintained relative leaf sizes from base to apex (Fig 3-6 B, C). M201 and M323 were previously shown to have few, thicker nodal roots, and M277 and M126 had many, thinner nodal roots. M178 had fewer roots than M181 (M181 had greater nodal occupancy), but the two genotypes did not differ strongly in RXA (see **Chapter 3, Fig 2-3**).

Discussion

Maize root and shoot traits can be integrated for enhanced nitrogen use efficiency

Shoot and root development in vascular plants is governed by a suite of common signaling pathways in their respective meristematic tissues, including epigenetic (Byrne et al. 2003) and essential cell patterning genes such as WUSCHEL, SHORTROOT and GLABRA (reviewed in Laux et al., 2004), due to shared evolutionary origins (Seago, Jr. and Fernando, 2013). For example, SCARECROW is an auxin-responsive transcription factor which regulates both root endodermal differentiation as well as the formation of bundle sheath cells and leaf veins required for C4 Kranz anatomy in maize leaves (Slewinski et al., 2012). In addition, cell size across organs has been related to genetic control of ploidy levels and structural constraints (surface-to-volume ratio) (Kondorosi et al., 2000).

In maize, the coordination of root and shoot development has been investigated with varying results. The timing of root emergence has been defined relative to leaf emergence, internode lengths, and leaf size (Sharman, 1942; Hebert et al., 1995; also see Chapter 1). Both shoot and root formation in earlier growth stages (e.g. primary and seminal roots, coleoptile node; lower leaves) versus later growth stages (upper nodal roots; upper leaves) have been shown to differ in terms of the degree of plasticity in response to environmental conditions (Sharman, 1942; Weaver, 1946; Heimsch and Stafford, 1952; Girardin et al., 1987; Aguirrezabal et al., 1993; Pellerin, 1994) and genetic regulation (Hochholdinger et al., 2004; Tai et al., 2016).

We evaluated the leaf anatomy of a representative mature leaf, as well as basal (mature) axial root anatomy from multiple nodes, and found generally weak associations between the leaf

and root traits evaluated under high nitrogen conditions. Multiple leaf anatomical traits were strongly and consistently associated with leaf thickness; similarly, many root anatomy traits were related to root diameter (see **Chapter 2**), under both high and low nitrogen conditions. However, root diameter was only related to two leaf anatomical traits under high nitrogen: a positive correlation with midrib cell file number, and negative correlation with midrib cell size. However, these relationships were weak, and not evident under nitrogen stress.

Interestingly, stomatal density was related to multiple root anatomy traits, and root cortical aerenchyma percent was related to several leaf anatomy traits, under both high and low nitrogen. Abaxial stomatal density was more strongly related to leaf thickness than adaxial stomatal density across nitrogen conditions. Adaxial stomatal density was strongly positively correlated with root mid-cortical cell size and median metaxylem vessel size under high nitrogen. However, under low nitrogen, adaxial stomatal density was strongly positively related to percent of root metaxylem vessel area in the stele, and weakly negatively related to median vessel size. Both adaxial and abaxial stomatal density were positively correlated with the percent of root cortical aerenchyma, across nitrogen conditions.

Several factors could result in these trait relationships, including genetic constraints and indirect selection. In general, trait correlations in a population are attributed to either genetic linkage, in which traits are controlled by different genes with similar physical locations on a chromosome, which promote their linked inheritance, or pleiotropy, in which one gene indirectly affects multiple processes (Chen and Lübberstedt, 2010). An example of pleiotropy would be a gene mutation in cell differentiation which alters both root and shoot morphogenesis, resulting in many downstream phenotypic effects.

Separately, selection (artificial or natural) for either specific trait combinations or multiple traits which independently enhance fitness in the selection environment could result in trait correlations among populations. This would include, broadly, selection against biophysically or biochemically unstable phenotype combinations or "phenotypic spaces" as well as finer-scale adaptive diversity (Donovan et al., 2011). Selection acts within genetic constraints; a lack of existing genetic diversity and heritability, or pleiotropy and linkage could result in sub-optimal or beneficial phenotype combinations. However, artificial selection and genetic modification can accelerate the disassociation of linked traits and generate novel combinations; for example, maize breeders have attempted to uncouple plant and ear height, to create low-eared, high-yielding tall plants (Helland, 2012).

The only stable relationship between mature leaf and nodal root traits among IBM RILs in this study was the association of stomatal density and root aerenchyma, which occurred despite a lack of consistent relationships among functionally related traits such as cell size and density in other leaf and root tissues. Increased stomatal density is associated with greater transpiration, which optimizes gas exchange and enhances nitrogen uptake in the absence of drought stress (Hepworth et al., 2015). Several cell patterning and cytokinin-related genes have been associated with stomatal patterning and development, which occurs late in leaf development (Casson and Gray, 2007). Plasticity in stomatal development has been observed in response to water availability, light, and other environmental factors (Casson and Gray, 2007).

By contrast, cortical aerenchyma is expressed independently of other root anatomy traits (Burton et al., 2013). Lysigenous aerenchyma forms through induced cell lysis rather than programmed differences in cell expansion (Jackson and Armstrong, 1999). Increased aerenchyma enhances oxygen diffusion through roots and is critical under water-logged conditions; ethylene accumulation and genes related to cell wall degradation and calcium signaling have been identified in regulating aerenchyma formation (Rajhi et al., 2010). However, aerenchyma formation is also induced under low nitrogen, phosphorus, sulphur, heat, and drought stress, and has been associated with enhanced stress tolerance due to the resulting reduction in root metabolic cost (Drew et al., 1989; Fan et al., 2003; Postma and Lynch, 2011; Saengwilai et al., 2014b). Conversely, increased aerenchyma formation can reduce root hydraulic conductivity and radial nutrient transport (Fan et al., 2007).

Given the independent developmental and hormone signaling pathways involved in stomatal density and root cortical aerenchyma formation, and their strong sensitivity to external conditions, it is possible that this trait relationship was due to other external factors (not related to nitrogen stress) rather than genetic constraints. The dearth of strong leaf and root trait correlations under high nitrogen conditions among these IBM RILs suggests these trait combinations are not subject to strong genetic constraints, and that there is potential for optimizing combinations of root and leaf phenotypes for both nitrogen acquisition and utilization (see next section). However, characterization of these traits across diverse maize genotypes would be necessary to elucidate the extent of genetic constraints versus adaptive strategies.

Future studies could combine root and shoot phenotyping and genetic mapping efforts. For example, genome-wide association studies have found loci associated with leaf dimensions and angle (Tian et al., 2011), root angle (Schneider et al., unpublished) and root anatomy (Saengwilai et al., unpublished), and carbon and nitrogen metabolites (Zhang et al., 2014).

Similarly, QTLs have been identified for leaf traits (Wassom, 2013), root traits (Burton et al., 2014; Burton et al., 2015), and enzyme activity related to carbon and nitrogen metabolism (Zhang et al., 2010) using the IBM population, in separate studies. Colocation of genetic loci for leaf and root traits could inform the discussion of genetic constraints. Furthermore, many leaf mutants in maize lack any study or annotation of root phenotypes (e.g. in MaizeGDB).

Thicker leaves were associated with slower root development and improved nitrogen status among IBM RILs

Enhancing nitrogen acquisition and utilization efficiency requires optimizing carbon and nitrogen metabolism to maximize growth and yield. Aboveground and belowground allocation of resources influences the efficiency of acquiring carbon and nitrogen, respectively, and are subject to allometric constraints (Poorter et al., 2012). Tradeoffs of particular combinations of leaf and root traits have generated phenotypic patterns shared across phylogenetic groups, which have been described in terms of an "economic spectrum" (Wright et al., 2004; Shipley et al., 2006; Diaz et al., 2016; Iversen et al., 2017; Valverde-Barrantes et al., 2017; Maherali et al., 2017). Leaves often fall into two categories: slow-growing and long-lived leaves with high specific leaf area (mass per area), low nitrogen content and low assimilation rate, and short-lived leaves with low specific leaf area, high nitrogen content and assimilation rate (Garnier and Laurent, 1994; Castro-Diez et al., 2000; Shipley et al., 2006; Donovan et al., 2010). Roots, similarly, can be generalized as either slow-growing, thick roots with low nitrogen content, or fast-growing, thin roots with high nitrogen content, although given differences in root classes it is more difficult to extrapolate results across species (e.g. Eissenstat et al., 2000; Iversen et al., 2017). Therefore effects of root architecture are difficult to separate from anatomical structure (see Chapter 2).

More recently, a "plant economic spectrum" was hypothesized linking leaf and root trait strategies, and the strength of trait correlations were among species differed according to clades and species sampled (Valverde-Barrantes et al., 2017). Trees and grasses broadly occupy opposite ends of the root economic spectrum, yet within monocots, leaf and root trait correlations were highly variable and less significant across species (Valverde-Barrantes et al., 2017). Therefore, maize generally occupies a lower quadrant of the spectrum which contains with species possessing thin roots (and high specific root length) with low root nitrogen content, and thin leaves with low leaf nitrogen content. Yet, we have found the range of root and leaf nitrogen

content among different maize root orders and leaf ages, among genotypes and within different nitrogen treatments, to vary in similar magnitude to the ranges compared across species – for example, maize root nitrogen content can vary from 0.5 to 3.5 percent of dry mass, depending on growth conditions and genotypes, and leaf nitrogen content can vary from 1 to 3.5 percent of dry mass, with greater ranges reported elsewhere. Therefore, the functional spectrum of root and leaf economic strategies among maize genotypes is worth exploring.

The extent of intraspecific genotypic variation found in leaf structure and its impact on nitrogen use efficiency varies depending on species and genotypes (e.g. Greef, 1994; Garnier et al., 1999; Moreno-Sotomayor et al., 2002; Brodribb et al., 2007; Retta et al., 2016), and few studies have characterized contrast in leaf anatomy in maize. Allometric relationships have been found among leaf thickness, cell size and cell wall thickness, but not vein size across angiosperms (John et al., 2013). Leaf thickness and tissue density can independently influence specific leaf area (Witkowski and Lamont, 1991). Interestingly, a study of rice genotypes found strong contrast in tissue density under low nitrogen, which drove differences in specific leaf area; reduced specific leaf area resulted in greater photosynthetic nitrogen use efficiency (Xiong et al., 2016).

We also suggest that the effects of leaf thickness should be considered separately from specific leaf area among maize genotypes; leaf thickness and specific leaf area were weakly inversely correlated, and genotypic contrast in other leaf anatomical traits was evident. Among these IBM RILs, leaf thickness did not differ significantly under high nitrogen, but showed strong contrast under moderate nitrogen stress; four RILs maintained thicker leaves under stress, while four RILs substantially decreased leaf thickness. Leaf thickness was positively related to shoot growth under moderate nitrogen stress, although the two were not related under high nitrogen. By contrast, average leaf area increased with shoot mass under both high and low nitrogen conditions, suggesting that leaf area was subject to an allometric effect with plant size among these genotypes, but leaf thickness was not. Interestingly, under mild nitrogen stress in the field (PA15), all RILs maintained leaf thickness and did not show contrast under stress, while under severe nitrogen stress in the greenhouse (GH1), all RILs significantly decreased in leaf thickness.

Among grass species, leaf thickness increased the proportion of mesophyll tissue relative to mechanically supportive tissues across a leaf area, allowing greater carbon assimilation rates, independent of the effect of leaf nitrogen content (Garnier et al., 1999). A detailed study of photosynthetic nitrogen use efficiency among and within tree species concluded that carbon assimilation per unit leaf mass, per unit leaf nitrogen, and per unit leaf area were reduced in

species with high leaf mass per area; this was due to a lower proportion of leaf nitrogen allocated to photosynthetic machinery, and possibly increased competition for CO_2 in the mesophyll (a lower internal CO_2 concentration) (Mediavilla et al., 2001). However, thicker leaves, less mesophyll density, and lower nitrogen per area was positively related to efficient carbon assimilation, for a given stomatal conductance within-species (Mediavilla et al., 2001).

Among these IBM RILs, leaf thickness was inversely related to carbon assimilation rate per unit leaf area, although the relationship was not significant under low nitrogen. Leaf thickness was more strongly associated with a reduction in stomatal conductance per unit leaf area, which could be related to the inverse correlation between leaf thickness and stomatal density. Additionally, there was no strong relationship between the leaf nitrogen content (percent by mass) and leaf thickness. Despite this, total shoot nitrogen was strongly positively associated with leaf thickness, suggesting that when leaf nitrogen content and photosynthesis rate per leaf area do not vary strongly among genotypes, leaf thickness can increase the nitrogen sink capacity of leaves although photosynthetic efficiency may not increase.

These genotypes contrasted strongly in the rate of nodal root emergence, which influences the number and diameter of nodal roots, as well as the total axial root length produced, and potentially the relative investment in axial root growth compared to other root classes (see **Chapter 3**). Unlike the contrast in leaf anatomy, contrast in root phenotypes was stable across nitrogen conditions, and genotypes with slower nodal root emergence and fewer, thicker nodal roots performed better under moderate nitrogen stress. These genotypes also had thicker leaves, and in some cases thicker stems (not shown); it is likely that maintaining leaf (and stem) thickness could be a response to nitrogen status. Genotypes with fewer, thicker roots had more efficient nitrogen uptake, allowing maintenance of leaf thickness and associated anatomical traits. These genotypes also contrasted in leaf size; M201, a genotype with the strongest performance, and few, thick nodal roots, also developed and maintained larger lower leaves across nitrogen conditions. Lower photosynthetic efficiency or nitrogen content could be offset by larger leaf area in early growth, which was optimally combined with greater carbon investment in each root node in early growth, when nitrogen availability relative to demand is typically greater.

Leaf hydraulics have also been proposed to influence trait relationships, although the interaction of root and leaf hydraulics is more complex (e.g. Rockwell and Holbrook, 2017). Brodribb and colleagues (2013) proposed that leaf cell size and stomatal size are coordinated to optimize hydraulic function, and cell sizes across leaf tissues inversely scale with density; slower growing species have larger cells, thicker leaves, fewer, larger stomates, and lower leaf vein

density, resulting in lower conductance overall. Greater vein density (and smaller veins) has been suggested as a primary mechanism to increase hydraulic efficiency, assuming no constraint in terms of stomatal and epidermal traits (Rockwell and Holbrook, 2017). The distance from vein to epidermis, however, mediates the effectiveness of increasing vein density; additionally, larger mesophyll cell size could reduce resistance to the symplastic transport of water from vein to leaf surface (Rockwell and Holbrook, 2017). Similarly, root cortical thickness has been suggested to impede hydraulic efficiency, but in absence of water deficit can promote nutrient absorption as well as mycorrhizal colonization important for maximizing nutrient uptake (Kong et al., 2017). Further work on the impact of root cortical anatomy and mycorrhizal associations is in progress (Tania Galindo-Castañeda, personal communication).

Many similar relationships were evident among these IBM RILs: thicker leaves had larger cells with reduced tissue density, as well as larger vascular bundles with greater interveinal distance, under both high and low nitrogen conditions. Stomatal density and leaf thickness were only negatively related under nitrogen stress. Optimizing hydraulic conductance through roots and leaves could enhance nitrogen acquisition and assimilation in the absence of water deficit, and is a useful functional perspective independent of construction costs relating directly to carbon and nitrogen. Therefore, developing integrated ideotypes of leaf and root trait combinations requires optimization of multiple distinct demands, as well as spatiotemporal or developmental context for the respective traits. In this study, combining "slow growth" modules such as thicker leaves and roots, as well as fewer nodal roots and larger leaves, resulted in greater nitrogen stress tolerance with no tradeoff under high nitrogen conditions.

Nitrogen stress affects maize leaf morphology, anatomy, and physiology in a genotype-specific manner

Nitrogen availability affects shoot and root development, including anatomy, morphology, and physiology. Nitrate deprivation responses include reallocating carbon to root growth, modification of root architecture and anatomy, induction of transporter activity and remobilization processes (e.g. reviewed in Krapp et al., 2011). In addition to its role as a building block for plant growth, nitrate acts as a signaling molecule, and can induce changes in gene expression and metabolism within minutes (Krapp et al., 2011); changes in nitrate supply have been shown to result in the reduction of active cytokinins, followed by reduced leaf growth rate

and both reduced cell size and number within hours, prior to changes in the leaf nitrogen content in tobacco (Walch-Liu et al., 2000; Krouk, 2016). However, nitrogen responses can vary among genotypes, and can be adaptive, neutral, or maladaptive for nitrogen uptake and utilization.

The effects of nitrogen stress on leaf cell size, number, and growth rates differ among species (e.g. Roggatz et al., 1999; Rademacher and Nelson, 2001; Vos et al., 2005). In maize, reduced nitrogen supply has been shown to reduce leaf area and leaf nitrogen content, while the leaf appearance rate and duration of leaf expansion were not affected; this reduced the photosynthesis capacity per leaf area (Vos et al., 2005). Another study found that nitrogen stress decreased leaf cell division and elongation rates in maize, but not average leaf cell lengths, resulting in reduced leaf length and growth rate (Jovanovic et al., 2004). Conversely, high nitrate has been shown to decrease epidermis pavement cell size and cell number in leaves, and inhibit apical dominance in roots and shoots in maize (Saiz-Fernandez et al., 2015). Burkholder and McVeigh (1940) found that the number of vascular bundles and size of parenchyma cells in the stem scaled with plant size across nitrogen levels, but scaling coefficients differed among genotypes.

We found that leaf length and leaf thickness varied under nitrogen stress in a genotype-specific manner among maize IBM RILs, but nitrogen stress decreased leaf number, width, area, and increased specific leaf area across genotypes. Under low nitrogen, leaf thickness and median leaf length decreased in four RILs, was maintained in three RILs, and increased in one (M201 for leaf thickness; M277 for leaf length, Appendix D, Fig S4A). Nitrogen stress did not have significant effects on interveinal distance, epidermis cell size, and parenchyma cell size in the leaf midrib. However, the adaxial to abaxial stomatal frequency ratio, the relative proportion of epidermis and vascular tissue compared to mesophyll tissue, and the size of vascular bundles in the leaf and midrib decreased under low nitrogen across genotypes. Adaxial stomatal density and index decreased under low nitrogen, but there were no abaxial effects. The average stomatal size also differed among genotypes but was more variable within-genotype; one RIL showed a strong increased in stomatal size under low nitrogen, while another RIL showed a decrease in stomatal size (Appendix D, Fig S4B). These results suggest that genotypic variation in leaf morphology and anatomy, as well as genetic control and physiological impact of differences in leaf morphological and anatomical plasticity in response to nitrogen stress, are worth further exploration.

Conclusions

The relationship between root and leaf anatomy and morphology has not been well studied in crops, yet improvements in yield require the integration of complex traits involved in both radiation and nutrient use efficiency. This study found substantial contrast in leaf morphology and anatomy among maize IBM RILs which have been previously shown to contrast in nodal root number and diameter, a combination related to the rate of nodal root emergence. One consistent relationship was found between stomatal density and root cortical aerenchyma, among root and leaf traits across nitrogen conditions. However, under low nitrogen only, there was a strong genotypic contrast in leaf thickness and associated anatomical traits. Genotypes with fewer, thicker nodal roots in combination with maintaining thicker leaves performed better under moderate nitrogen stress. However, carbon assimilation rates per unit leaf area and leaf nitrogen content per unit leaf mass did not vary strongly; leaf thickness was primarily related to an increase in total shoot nitrogen under nitrogen stress. This study suggests that thicker leaves were maintained as a result of improved nitrogen status from efficient nitrate uptake from fewer, thicker nodal roots. The development of larger lower leaves during early growth could also contribute to differences in nitrogen stress tolerance and remains to be explored. While a "slow growth" module in both roots and leaves resulted in enhanced nitrogen stress tolerance, this study offered promising preliminary correlations with only limited genetic diversity to explore root and leaf trait combinations, and future studies could address these gaps. Given the relative independence of root and shoot traits evaluated, many combined trait ideotypes for nitrogen acquisition and utilization efficiency are possible, and should consider not only carbon and nitrogen economy, but also hydraulic architecture and source-sink dynamics over development. Large scale phenotyping which targets multiple organs and scales of biological organization could improve understanding of genetic regulation, growth and development, and useful trait combinations for stress adaptation in crops.

Acknowledgements

We thank Shawn Kaeppler and the G2F consortium for providing plant materials.

For agronomic and technical support, we thank Robert Snyder, Michael Williams, Ainiz Fauzi, Jonathan Wu, Pufan Wang, Ryan Burnett, and Gustavo da Silveira. We thank Scott Diloretto for greenhouse management.

We thank Benjamin Hall and support from the Edmund Optics Higher Education Grant for technical support and improvements to the LAT platform. We thank the Nvidia Corporation for donation of a Tesla K40 GPU used in image processing which supported this research.

This work was supported by USDA NIFA's AFRI grant 2013-02682 to JPL, and the USDA National Institute of Food and Agriculture, Hatch project 4372. Any opinions, findings, conclusions, or recommendations expressed in this publication are those of the author(s) and do not necessarily reflect the view of the National Institute of Food and Agriculture (NIFA) or the United States Department of Agriculture (USDA).

References

Ågren GI, Franklin O. 2003. Root:shoot ratios, optimization and nitrogen productivity. Annals of Botany **92**, 795–800.

Aguirrezabal LAN, Pellerin S, Tardieu F. 1993. Carbon nutrition, root branching and elongation: can the present state of knowledge allow a predictive approach at the whole-plant level? Environmental and Experimental Botany **33**, 121–130.

Boomsma CR, Santini JB, Tollenaar M, Vyn TJ. 2009. Maize morphophysiological responses to intense crowding and low nitrogen availability: An analysis and review. Agronomy Journal **101**, 1426–1452.

Borrell AK, Mullet JE, George-Jaeggli B, Van Oosterom EJ, Hammer GL, Klein PE, Jordan DR. 2014. Drought adaptation of stay-green sorghum is associated with canopy development, leaf anatomy, root growth, and water uptake. Journal of Experimental Botany **65**, 6251–6263.

Borrell BA, Hammer G, van Oosterom E. 2001. Stay-green : A consequence of the balance between supply and demand for nitrogen during grain filling ? Annals of Applied Biology **138**, 91–95.

Brodribb TJ, Feild TS, Jordan GJ. 2007. Leaf Maximum Photosynthetic Rate and Venation Are Linked by Hydraulics. Plant Physiology **144**, 1890–1898.

Brodribb TJ, Jordan GJ, Carpenter RJ. 2013. Unified changes in cell size permit coordinated leaf evolution. New Phytologist **199**, 559–570.

Burkholder PR, McVeigh I. 1940. Growth and Differentiation of Maize in Relation to Nitrogen Supply. American Journal of Botany **27**, 414–424.

Burton AL, Lynch JP, Brown KM. 2013. Spatial distribution and phenotypic variation in root cortical aerenchyma of maize (Zea mays L.). Plant and Soil **367**, 263–274.

Burton AL, Johnson J, Foerster J, Hanlon MT, Kaeppler SM, Lynch JP, Brown KM. 2014. QTL mapping and phenotypic variation of root anatomical traits in maize (*Zea mays* L.). Theoretical and Applied Genetics **128**, 93–106.

Burton AL, Johnson JM, Foerster JM, Hirsch CN, Buell CR, Hanlon MT, Kaeppler SM, Brown KM, Lynch JP. 2014. QTL mapping and phenotypic variation for root architectural traits in maize (*Zea mays* L.). Theoretical and Applied Genetics **127**, 2293–311.

Byrne ME, Kidner CA, Martienssen RA. 2003. Plant stem cells: Divergent pathways and common themes in shoots and roots. Current Opinion in Genetics and Development **13**, 551–557.

Casson S, Gray JE. 2008. Influence of environmental factors on stomatal development. New Phytologist **178**, 9–23.

Castro-Diez P, Puyravaud JP, Cornelissen JHC. 2000. Leaf structure and anatomy as related to leaf mass per area variation in seedlings of a wide range of woody plant species and types. Oecologia **124**, 476–486.

Chen Y, Lübberstedt T. 2010. Molecular basis of trait correlations. Trends in Plant Science **15**, 454–461.

Ciampitti IA, Vyn TJ. 2012. Physiological perspectives of changes over time in maize yield dependency on nitrogen uptake and associated nitrogen efficiencies: A review. Field Crops Research **133**, 48–67.

Covshoff S, Majeran W, Liu P, Kolkman JM, van Wijk KJ, Brutnell TP. 2008. Deregulation of maize C4 photosynthetic development in a mesophyll cell-defective mutant. Plant physiology **146**, 1469–81.

DeBruin JL, Schussler JR, Mo H, Cooper M. 2017. Grain Yield and Nitrogen Accumulation in Maize Hybrids Released during 1934 to 2013 in the US Midwest. Crop Science **57**, 1–16.

Dhital S, Raun WR. 2016. Variability in optimum nitrogen rates for maize. Agronomy Journal **108**, 2165–2173.

Díaz S, Kattge J, Cornelissen JHC, *et al.* 2015. The global spectrum of plant form and function. Nature **529**, 1–17.

Donovan LA, Maherali H, Caruso CM, Huber H, de Kroon H. 2011. The evolution of the worldwide leaf economics spectrum. Trends in Ecology and Evolution **26**, 88–95.

Drew MC, He CJ, Morgan PW. 1989. Decreased Ethylene Biosynthesis, and Induction of Aerenchyma, by Nitrogen- or Phosphate-Starvation in Adventitious Roots of Zea mays L. Plant physiology **91**, 266–271.

Eissenstat DM, Wells CE, Yanai RD, Whitbeck JL. 2000. Building roots in a changing environment: Implications for root longevity. New Phytologist **147**, 33–42.

Fan M, Bai R, Zhao X, Zhang J. 2007. Aerenchyma formed under phosphorus deficiency contributes to the reduced root hydraulic conductivity in maize roots. Journal of Integrative Plant Biology **49**, 598–604.

Fan M, Zhu J, Richards C, Brown KM, Lynch JP. 2003. Physiological roles for aerenchyma in phosphorus-stressed roots. Functional Plant Biology **30**, 493–506.

FAO. 2014. FAOSTAT. Cited May 18, 2017. http://www.fao.org/faostat/en/#data

Fox J, Friendly M, Monette G. 2016. heplots: Visualizing Tests in Multivariate Linear Models. R package version 1.3-3. URL https://CRAN.R-project.org/package=heplots

Garnier E, Salager JL, Laurent G, Sonié L. 1999. Relationships between photosynthesis, nitrogen and leaf structure in 14 grass species and their dependence on the basis of expression. New Phytologist **143**, 119–129.

Garnier E, Laurent G. 1994. Leaf Anatomy, Specific Mass and Water-Content in Congeneric Annual and Perennial Grass Species. New Phytologist **128**, 725–736.

Gaudin ACM, McClymont SA, Raizada MN. 2011. The nitrogen adaptation strategy of the wild teosinte ancestor of modern maize, Zea mays subsp. parviglumis. Crop Science **51**, 2780–2795.

Ghannoum O, Evans JR, Chow WS, Andrews TJ, Conroy JP, von Caemmerer S. 2005. Faster Rubisco is the key to superior nitrogen-use efficiency in NADP-malic enzyme relative to NAD-malic enzyme C4 grasses. Plant Physiology **137**, 638–50.

Girardin P, Morel-fourrier B, Jordan M, Meyer J, Mercier J. 1987. Développement des racines adventives chez le maïs. Agronomie, EDP Sciences **7**, 353–360.

Greef JM. 1994. Productivity of Maize (Zea mays L.) in Relation to Morphological and Physiological Characteristics under Varying Amounts of Nitrogen Supply. Journal of Agronomy and Crop Science **172**, 317–326.

Hébert Y, Plomion C, Harzic N. 1995. Genotype x environment interaction for root traits in maize, as analysed with factorial regression models. Euphytica **81**, 85–92.

Heimsch C, Stafford HJ. 1952. Developmental Relationships of the Internodes of Maize. Bulletin of the Torrey Botanical Club **79**, 52–58.

Helland SJ. 2012. Effects of environment and planting density on plant stature, flowering time , and ear set in IBM populations of maize. PhD Thesis. Iowa State University.

Hepworth C, Doheny-Adams T, Hunt L, Cameron DD, Gray JE. 2015. Manipulating stomatal density enhances drought tolerance without deleterious effect on nutrient uptake. New Phytologist **208**, 336–341.

Hirel B, Bertin P, Quillere I, Bourdoncle W, Dellay C, Cadiou S, Retailliau C, Falque M. 2015. Towards a Better Understanding of the Genetic and Physiological Basis for Nitrogen Use Efficiency in Maize. Plant Physiology.

Hirel B, Tétu T, Lea PJ, Dubois F. 2011. Improving nitrogen use efficiency in crops for sustainable agriculture. Sustainability **3**, 1452–1485.

Hirel B, Martin A, Tercé-Laforgue T, Gonzalez-Moro MB, Estavillo JM. 2005. Physiology of maize I: A comprehensive and integrated view of nitrogen metabolism in a C4 plant. Physiologia Plantarum **124**, 167–177.

Hochholdinger F, Woll K, Sauer M, Dembinsky D. 2004. Genetic dissection of root formation in maize (Zea mays) reveals root-type specific developmental programmes. Annals of Botany **93**, 359–368.

Iversen CM, McCormack ML, Powell AS, *et al.* 2017. A global Fine-Root Ecology Database to address below-ground challenges in plant ecology. New Phytologist **215**, 15–26.

Jackson MB, Armstrong W. 1999. Formation of Aerenchyma and the Processes of Plant Ventilation in Relation to Soil Flooding and Submergence. Plant Biology **1**, 274–287.

John GP, Scoffoni C, Sack L. 2013. Allometry of cells and tissues within leaves. American Journal of Botany **100**, 1936–1948.

Jovanovic Z, Djakovic T, Stikic R, Prokic L, Hadzi-Taskovic Sukalovic V. 2004. Effect of N deficiency on leaf growth and cell wall peroxidase activity in contrasting maize genotypes. Plant and Soil **265**, 211–223.

Kassambara A. 2016. ggcorrplot: Visualization of a Correlation Matrix using 'ggplot2'. R package version 0.1.1. https://CRAN.R-project.org/package=ggcorrplot

Kondorosi E, Roudier F, Gendreau E. 2000. Plant cell-size control: growing by ploidy? Current Opinion in Plant Biology **3**, 488–492.

Krapp A, Berthomé R, Orsel M, *et al.* 2011. Arabidopsis Roots and Shoots Show Distinct Temporal Adaptation Patterns Toward Nitrogen Starvation. Plant Physiology **157**, 1255–1282.

Kong D, Wang J, Zeng H, Liu M, Miao Y, Wu H, Kardol P. 2017. The nutrient absorption-transportation hypothesis: optimizing structural traits in absorptive roots. New Phytologist **213**, 1569–1572.

Krouk G. 2016. Hormones and nitrate: a two-way connection. Plant Molecular Biology **91**, 599–606.

Lassaletta L, Billen G, Garnier J, Bouwman L, Velazquez E, Mueller ND, Gerber JS. 2016. Nitrogen use in the global food system: Past trends and future trajectories of agronomic performance, pollution, trade, and dietary demand. Environmental Research Letters **11**, 1–14.

Laux T, Würschum T, Breuninger H. 2004. Genetic regulation of embryonic pattern formation. The Plant cell **16 Suppl**, S190–S202.

Liu J, Ma K, Ciais P, Polasky S. 2016. Reducing human nitrogen use for food production. Scientific Reports **6**, 30104.

Lundgren MR, Osborne CP, Christin PA. 2014. Deconstructing Kranz anatomy to understand C4 evolution. Journal of experimental botany **65**, 3357–3369.

Lynch JP. 2013. Steep, cheap and deep: an ideotype to optimize water and N acquisition by maize root systems. Annals of Botany **112**, 347–57.

Mediavilla S, Escudero A, Heilmeier H. 2001. Internal leaf anatomy and photosynthetic resource-use efficiency: interspecific and intraspecific comparisons. Tree physiology **21**, 251–259.

Moll RH, Kamprath EJ, Jackson WA. 1982. Analysis and Interpretation of Factors Which Contribute to Efficiency of Nitrogen Utilization 1. Agronomy Journal **74**, 562–564.

Montgomery EG. 1911. Correlation studies in corn. 24th Annual Report: 108–159. Agricultural Experimental Station, Lincoln, NB.

Moreno-Sotomayor a, Weiss a, Paparozzi ET, Arkebauer TJ. 2002. Stability of leaf anatomy and light response curves of field grown maize as a function of age and nitrogen status. Journal of Plant Physiology **159**, 819–826.

Mu X, Chen Q, Chen F, Yuan L, Mi G. 2016. Within-Leaf Nitrogen Allocation in Adaptation to Low Nitrogen Supply in Maize during Grain-Filling Stage. Frontiers in Plant Science **7**, 1–11.

Oaks A. 1994. Efficiency of nitrogen utlization in C3 and C4 cereals. Plant Physiol. **106**, 407 414.

Pellerin S. 1994. Number of maize nodal roots as affected by plant density and nitrogen fertilization : relationships with shoot growth. European Journal of Agronomy **3**, 101–110.

Poorter H, Niklas KJ, Reich PB, Oleksyn J, Poot P, Mommer L. 2011. Biomass allocation to leaves, stems and roots: meta-analysis of interspecific variation and environmental control. New Phytologist **193**, 30–50.

Postma JA, Lynch JP. 2011. Root cortical aerenchyma enhances the growth of maize on soils with suboptimal availability of nitrogen, phosphorus, and potassium. Plant physiology **156**, 1190–1201.

Rademacher, I. F., Nelson CJ. 2001. Nitrogen Effects on Leaf Anatomy within the Intercalary Meristems of Tall Fescue Leaf Blades. Annals of Botany **88**, 893–903.

Rajcan I, Tollenaar M. 1999. Source : sink ratio and leaf senescence in maize: wII. Nitrogen metabolism during grain filling. Field Crops Research **60**, 255–265.

Rajcan I, Tollenaar M. 1999. Source : sink ratio and leaf senescence in maize: II. Nitrogen metabolism during grain filling. Field Crops Research **60**, 255–265.

Retta M, Yin X, van der Putten PEL, Cantre D, Berghuijs HNC, Ho QT, Verboven P, Struik PC, Nicola BM. 2016. Impact of anatomical traits of maize (Zea mays L.) leaf as affected by nitrogen supply and leaf age on bundle sheath conductance. Plant Science **252**, 205–214.

Rockwell FE, Holbrook NM. 2017. Leaf hydraulic architecture and stomatal conductance: a functional perspective. Plant Physiology **174**, pp.00303.2017.

Roggatz U, McDonald AJS, Stadenberg I, Schurr U. 1999. Effect of nitrogen deprivation on cell division and expansion of Ricinus communis L. Plant Cell Environ. **22**, 81.

Saengwilai P, Nord E a, Chimungu JG, Brown KM, Lynch JP. 2014. Root cortical aerenchyma enhances nitrogen acquisition from low-nitrogen soils in maize. Plant Physiology **166**, 726–735.

Saengwilai P, Tian X, Lynch JP. 2014. Low crown root number enhances nitrogen acquisition from low-nitrogen soils in maize. Plant Physiology **166**, 581–9.

Sage RF, Pearcy RW. 1987. The Nitrogen Use Efficiency of C3 and C4 Plants. II. Leaf nitrogen effects on the gas exchange characteristics of *Chenopodium album* (L) and *Amaranthus retroflexus* (L). Plant Physiol. **84**, 959–963.

Saiz-Fernandez, De Diego N, Sampedro MC, Mena-Petite A, Ortiz-Barredo A, Lacueta M. 2015. High nitrate supply reduces growth in maize, from cell to whole plant. Journal of Plant Physiology **173**, 120–129.

Sanchez P. 2002. Ecology. Soil fertility and hunger in Africa. Science (New York, N.Y.) **295**, 2019–2020.

Schmitt MR, Edwards GE. 1981. Photosynthetic capacity and nitrogen use efficiency of maize, wheat, and rice: A comparison between C3 and C4 photosynthesis. Journal of Experimental Botany **32**, 459–466.

Seago JL, Fernando DD. 2013. Anatomical aspects of angiosperm root evolution. Annals of Botany **112**, 223–238.

Sharman BC. 1942. Developmental anatomy of the shoot of Zea mays L. Annals of Botany **6**, 245–282.

Shipley B, Lechowicz MJ, Wright I, Reich PB. 2006. Fundamental trade-offs generating the worldwide leaf economics spectrum. Ecology **87**, 535–541.

Slewinski TL, Anderson AA, Zhang C, Turgeon R. 2012. Scarecrow plays a role in establishing Kranz anatomy in maize leaves. Plant and Cell Physiology **53**, 2030–2037.

Tai H, Lu X, Opitz N, Marcon C, Paschold A, Lithio A, Nettleton D, Hochholdinger F. 2016. Transcriptomic and anatomical complexity of primary, seminal, and crown roots highlight root type-specific functional diversity in maize (Zea mays L.). Journal of Experimental Botany **67**, 1123–1135.

Tian F, Bradbury PJ, Brown PJ, Hung H, Sun Q, Flint-Garcia S, Rocheford TR, McMullen MD, Holland JB, Buckler ES. 2011. Genome-wide association study of leaf architecture in the maize nested association mapping population. Nature Genetics **43**, 159–162.

Tilman D, Cassman KG, Matson PA, Naylor R, Polasky S. 2002. Agricultural sustainability and intensive production practices. Nature **418**, 671–677.

Tollenaar M, Lee EA. 2002. Yield potential, yield stability and stress tolerance in maize. Field Crops Research **75**, 161–169.

Valverde-Barrantes OJ, Freschet GT, Roumet C, Blackwood CB. 2017. A worldview of root traits: The influence of ancestry, growth form, climate and mycorrhizal association on the functional trait variation of fine-root tissues in seed plants. New Phytologist.

Vitousek PM, Naylor R, David MB, Drinkwater LE, Holland E, Johnes PJ, Katzenberger J, *et al*. 2009. Nutrient imbalances in agricultural development. Science **324**, 1519–1520.

Vos J, Van Der Putten PEL, Birch CJ. 2005. Effect of nitrogen supply on leaf appearance, leaf growth, leaf nitrogen economy and photosynthetic capacity in maize (Zea mays L.). Field Crops Research **93**, 64–73.

Walch-Liu P, Neumann G, Bangerth F, Engels C. 2000. Rapid effects of nitrogen form on leaf morphogenesis in tobacco. Journal of experimental botany **51**, 227–237.

Wassom JJ. 2013. Quantitative trait loci for leaf angle, leaf width, leaf length, and plant height in a maize (*Zea mays* L.) B73 × Mo17 population. Maydica **58**, 318–321.

Weaver HL. 1946. A Developmental Study of Maize with Particular Reference to Hybrid Vigor. American Journal of Botany **33**, 615–624.

Wickham H. 2009. ggplot2: Elegant Graphics for Data Analysis. Springer-Verlag New York

Wickham H. 2011. The Split-Apply-Combine Strategy for Data Analysis. Journal of Statistical Software, 40(1), 1-29. URL http://www.jstatsoft.org/v40/i01/.

Wickham H. 2016. tidyr: Easily Tidy Data with `spread()` and `gather()` Functions. R package version 0.6.0. https://CRAN.R-project.org/package=tidyr

Wintermans JF, de Mots A. 1965. Spectrophotometric characteristics of chlorophylls a and b and their pheophytins in ethanol. Biochimica et biophysica acta **109**, 448–453.

Witkowski ETF, Lamont BB. 1991. Leaf Specific Mass Confounds Leaf Density and Thickness. Oecologia **88**, 486–493.

Wright IJ, Westoby M, Reich PB, *et al.* 2004. The worldwide leaf economics spectrum. Nature **428**, 821–827.

Wu QP, Chen FJ, Chen YL, Yuan LX, Zhang FS, Mi GH. 2011. Root growth in response to nitrogen supply in Chinese maize hybrids released between 1973 and 2009. Science China Life Sciences **54**, 642–650.

Xiong D, Wang D, Liu X, Peng S, Huang J, Li Y. 2016. Leaf density explains variation in leaf mass per area in rice between cultivars and nitrogen treatments. Annals of Botany **117**, 963–971.

York LM, Galindo-Castaneda T, Schussler JR, Lynch JP. 2015. Evolution of US maize (*Zea mays* L.) root architectural and anatomical phenes over the past 100 years corresponds to increased tolerance of nitrogen stress. Journal of Experimental Botany **66**, 2347–2358.

Yu P, Li X, White PJ, Li C. 2015. A large and deep root system underlies high nitrogen-use efficiency in maize production. PLoS ONE **10**, 1–17.

Yu P, White PJ, Hochholdinger F, Li C. 2014. Phenotypic plasticity of the maize root system in response to heterogeneous nitrogen availability. Planta **240**, 667–678.

Zhan A, Lynch JP. 2015. Reduced frequency of lateral root branching improves N capture from low N soils in maize. Journal of Experimental Botany **66**, 2055–2065.

Zhang N, Gibon Y, Gur A, *et al.* 2010. Fine Quantitative Trait Loci Mapping of Carbon and Nitrogen Metabolism Enzyme Activities and Seedling Biomass in the Intermated Maize IBM Mapping Population. Plant physiology **154**, 1753–1765.

Zhang N, Gibon Y, Wallace JG, *et al.* 2015. Genome-wide association of carbon and nitrogen metabolism in the maize nested association mapping population. Plant physiology **168**, 575–83.

Zhang X, Davidson EA, Mauzerall DL, Searchinger TD, Dumas P, Shen Y. 2015. Managing nitrogen for sustainable development. Nature **528**, doi:10.1038/nature15743.

Figures and Tables

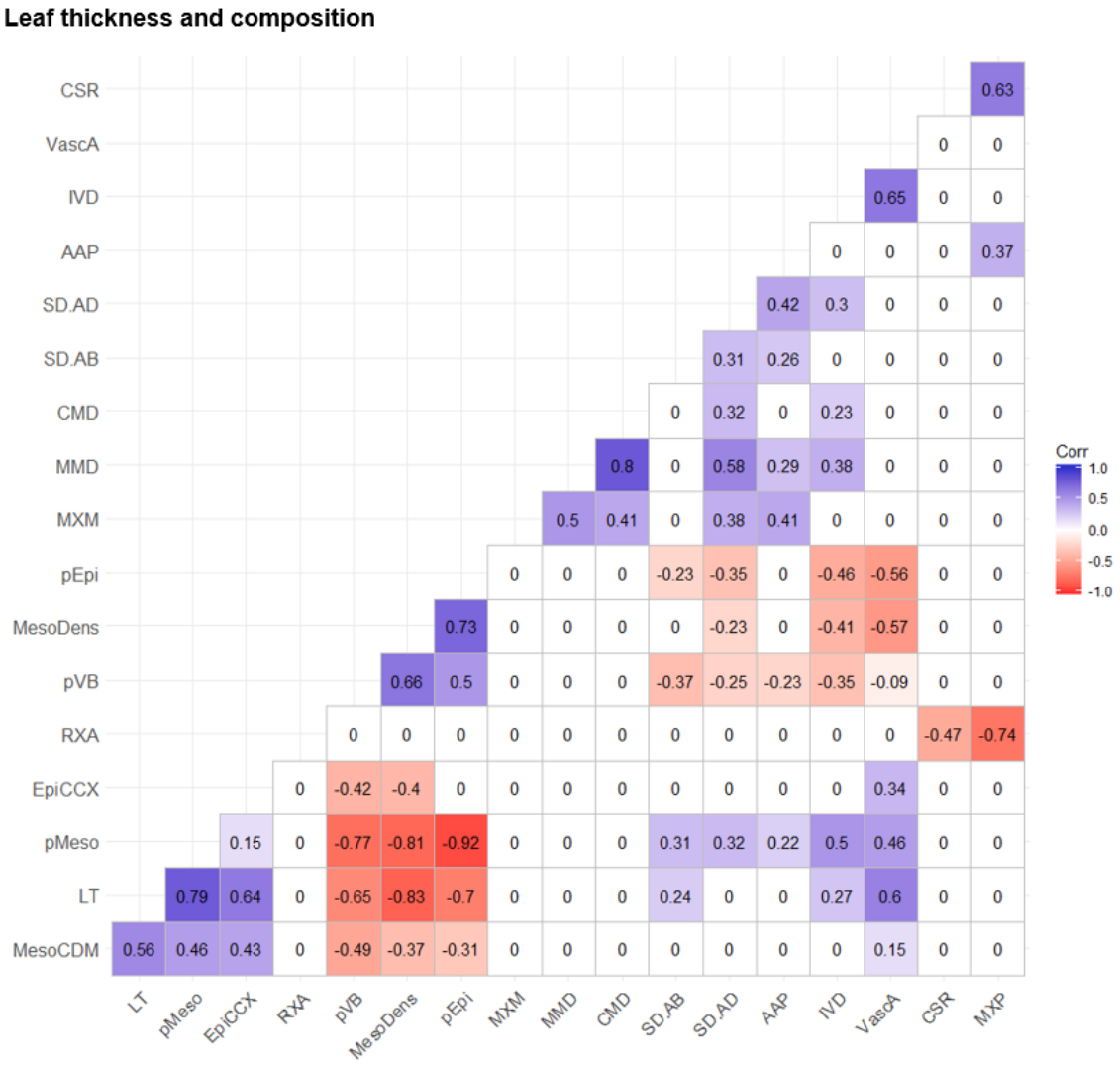

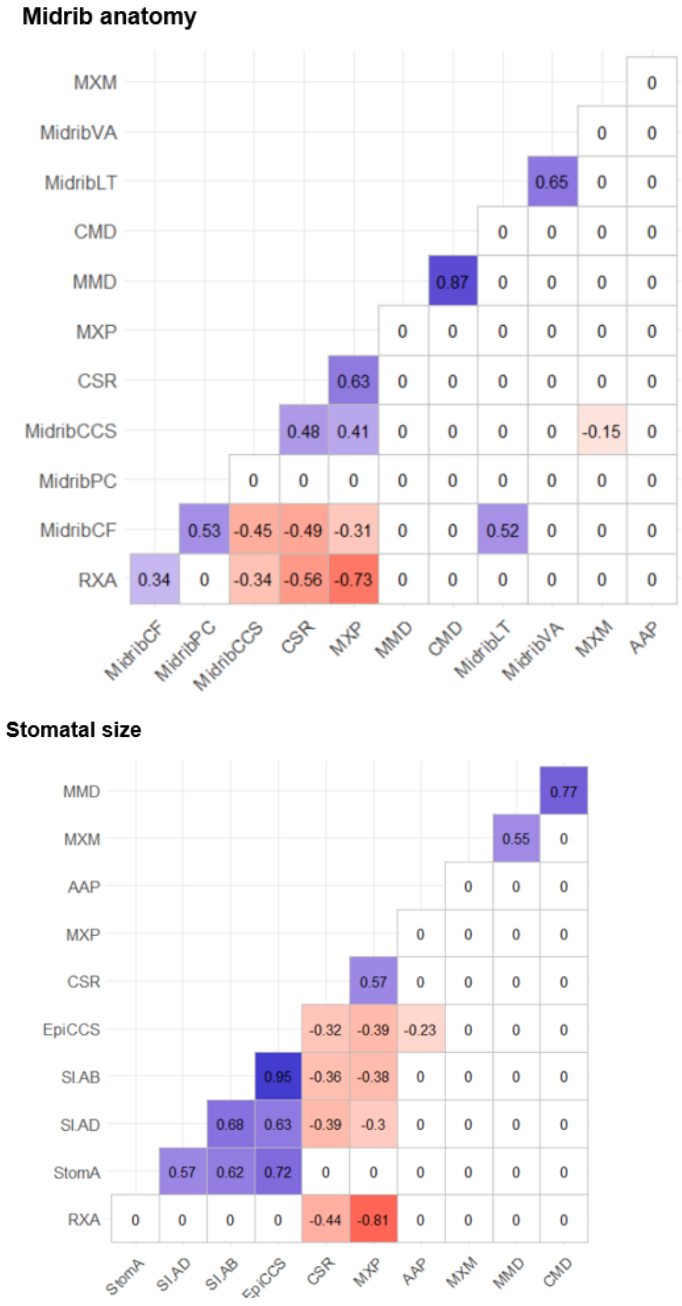

Figure 3-1. Relationships between maize leaf and root anatomy traits in high nitrogen. Correlation matrix of select leaf traits measured in a representative leaf and nodal root anatomy traits averaged from nodes 2 and 3 from greenhouse-grown maize RILs (GH2) in low nitrogen conditions. Color scale indicates Spearman's ranked correlation coefficient. Blank cells with "0" indicate the correlation was not significant at $p<0.05$ (correlation coefficient not shown in these cells). Traits are arranged in order according to hierarchical clustering. Cross-sectional leaf anatomy traits and stomatal density are in the main correlation matrix (n=30 for each trait); midrib traits (n=30) and stomatal size and index (n=26) are at bottom. See trait abbreviations in Table 3-1.

Leaf thickness and composition

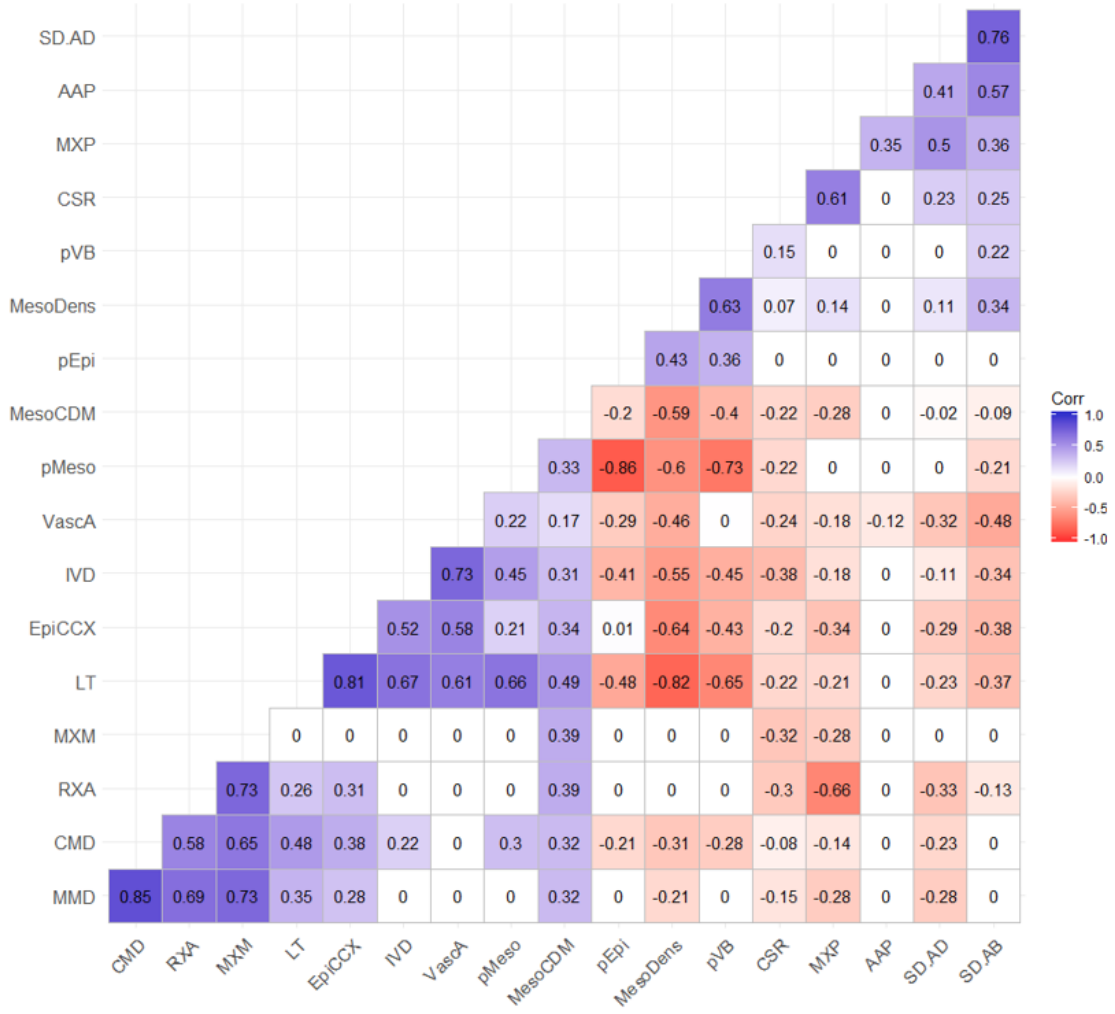

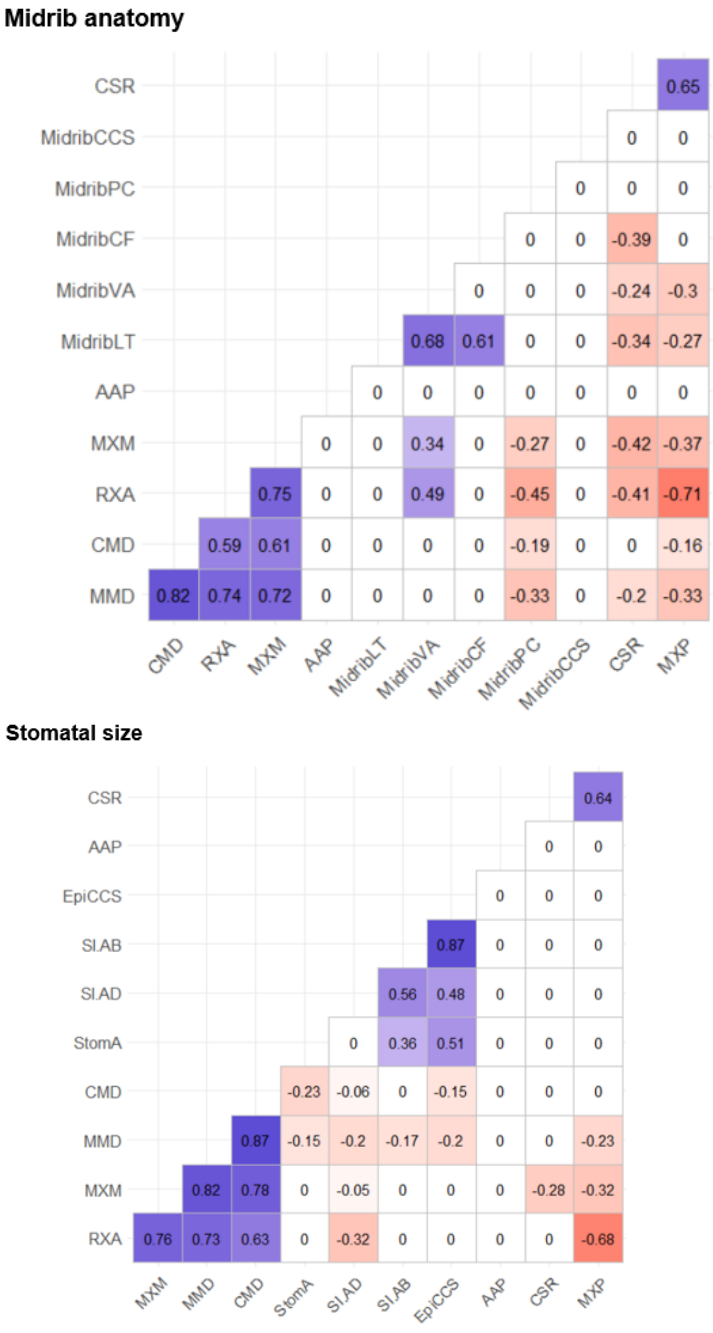

Figure 3-2. Relationships between maize leaf and root anatomy traits in low nitrogen. Correlation matrix of select leaf traits measured in a representative leaf and nodal root anatomy traits averaged from nodes 2 and 3 from greenhouse-grown maize RILs (GH2) in low nitrogen conditions. Color scale indicates Spearman's ranked correlation coefficient. Blank cells with "0" indicate the correlation was not significant at $p<0.05$ (correlation coefficient not shown in these cells). Traits are arranged in order according to hierarchical clustering. Cross-sectional leaf anatomy traits and stomatal density are in the main correlation matrix (n= 31 for each trait); midrib traits (n=26) and stomatal size and index (n=26) are at bottom. See trait abbreviations in Table 3-1.

Leaf number and size

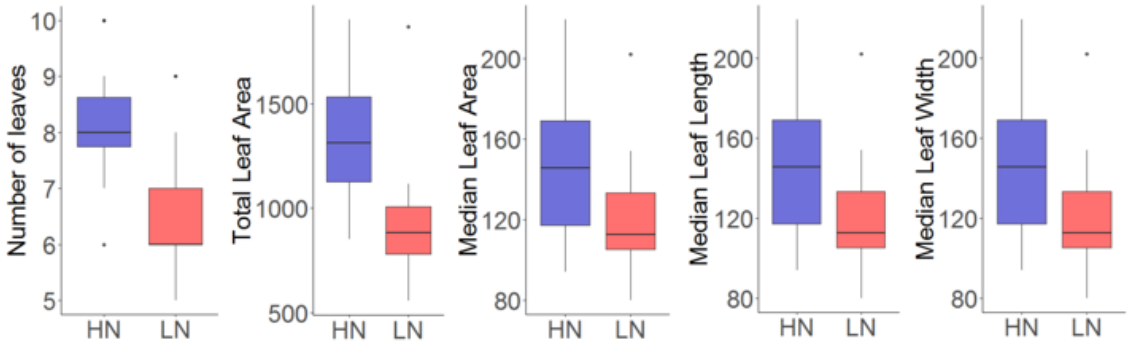

Leaf thickness and composition

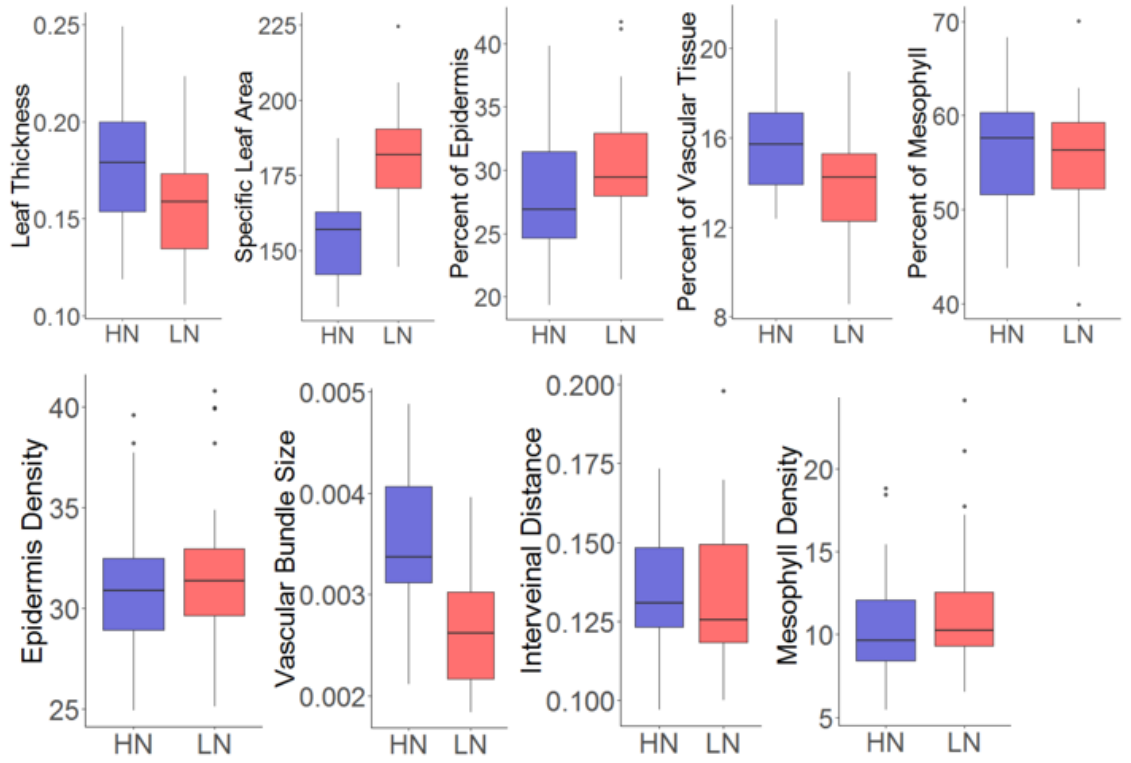

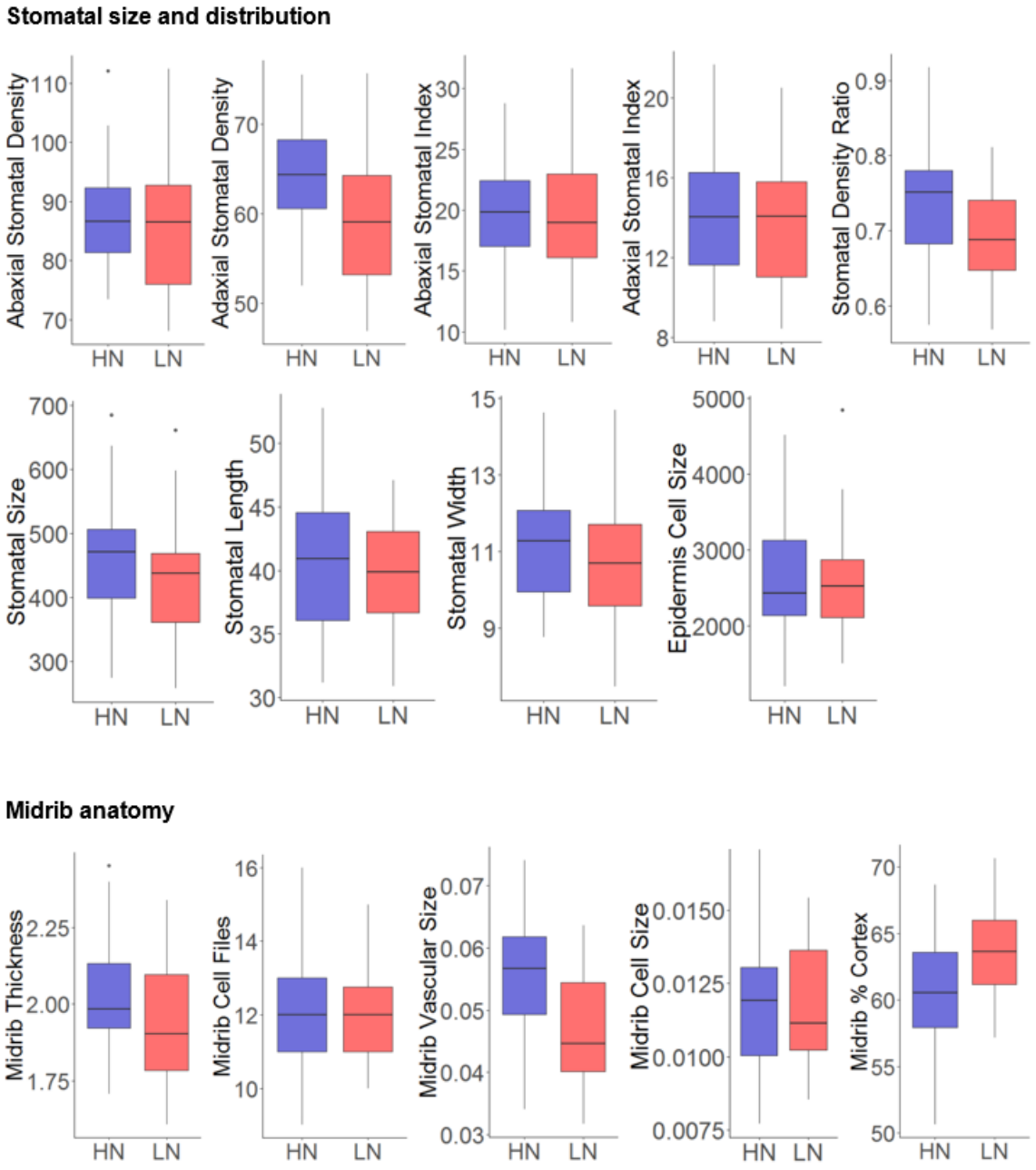

Figure 3-3. Leaf traits among IBM RILs in high and low nitrogen. Boxplots of leaf trait values under high (HN, blue) and low nitrogen (LN, red) conditions among IBM RILs (n=64) in GH2. Whiskers represent range not including outliers; dots represent outliers (above or below 1.5*IQR); box lines represent quartiles (25, 50, 75). See Table 3-1 for trait descriptions and units. See Table 3-2 for ANOVA of treatment effects.

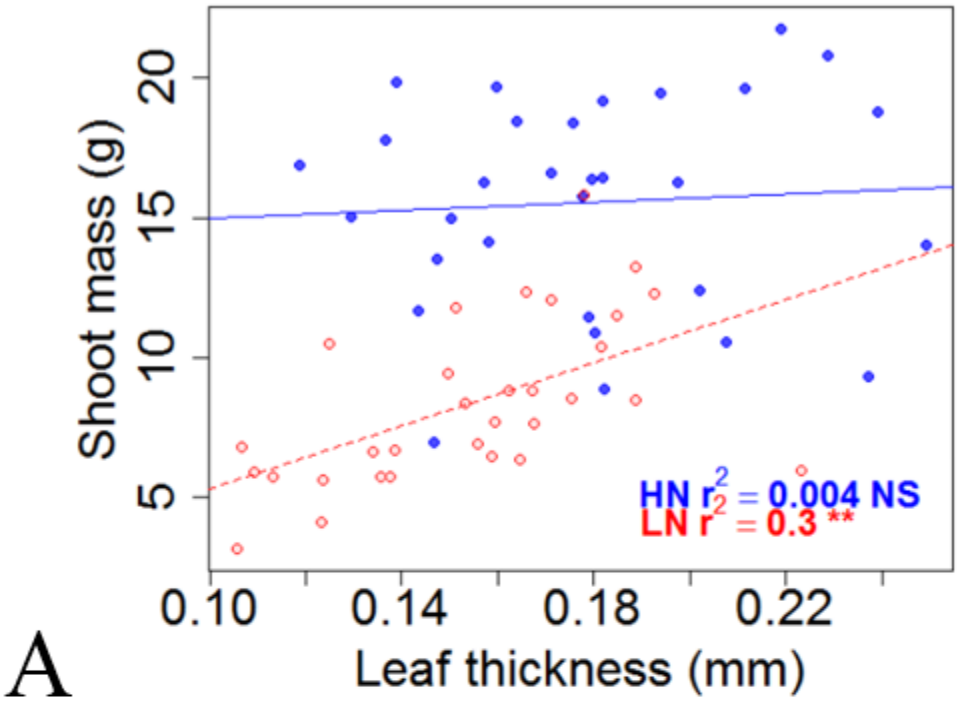
Shoot mass (g)
5
10
15
20
0.10
0.14
0.18
0.22
Leaf thickness (mm)
HN r2 = 0.004 NS
LN r2 = 0.3 **

A

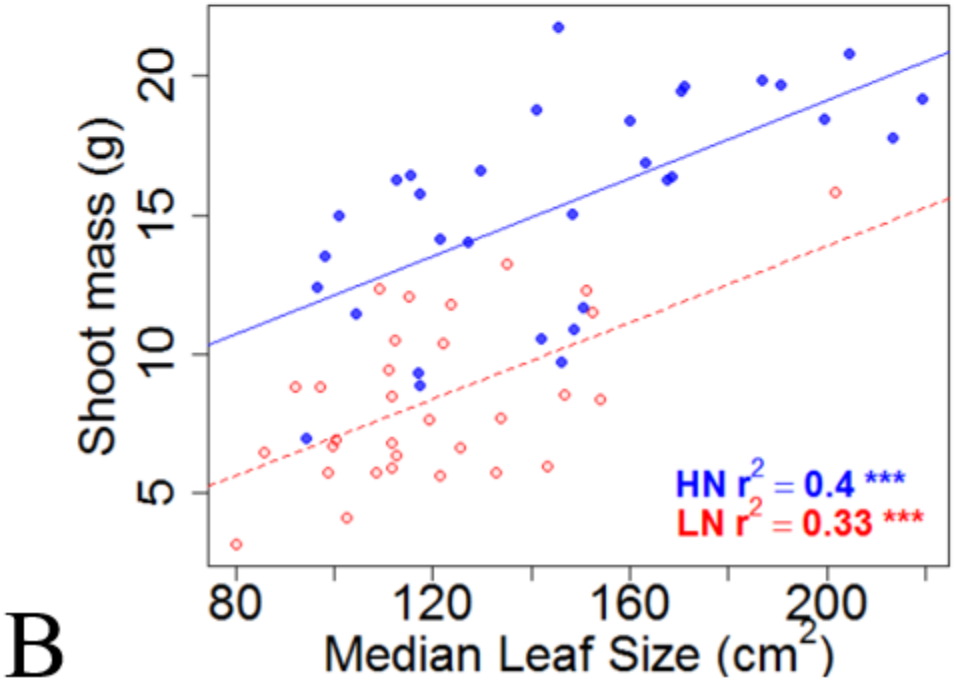
Shoot mass (g)
5
10
15
20
80
120
160
200
Median Leaf Size (cm2)
HN r2 = 0.4 ***
LN r2 = 0.33 ***

B

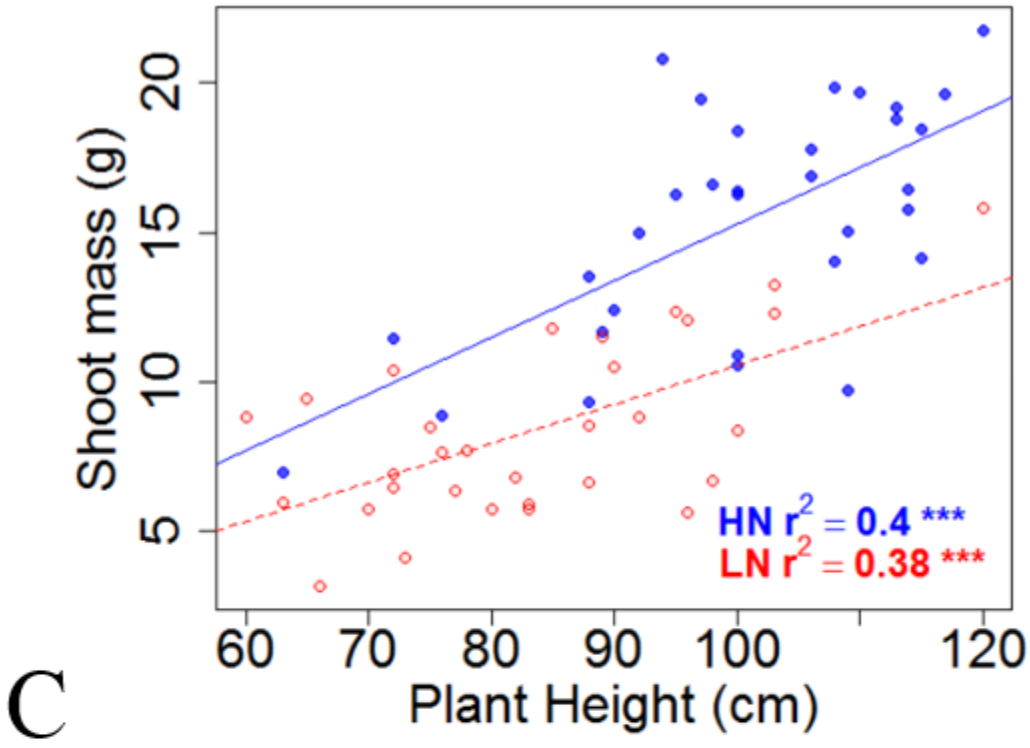
Shoot mass (g)
5
10
15
20
60
70
80
90
100
120
Plant Height (cm)
HN r2 = 0.4 ***
LN r2 = 0.38 ***

C

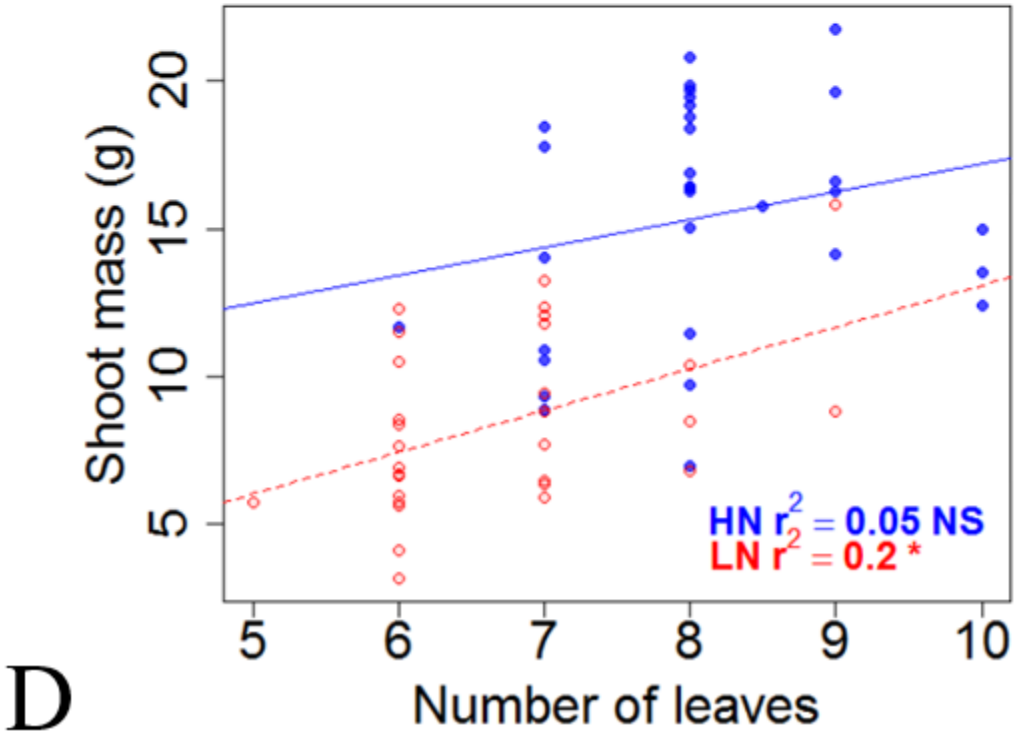
Shoot mass (g)
5
10
15
20
5
6
7
8
9
10
Number of leaves
HN r2 = 0.05 NS
LN r2 = 0.2 *

D

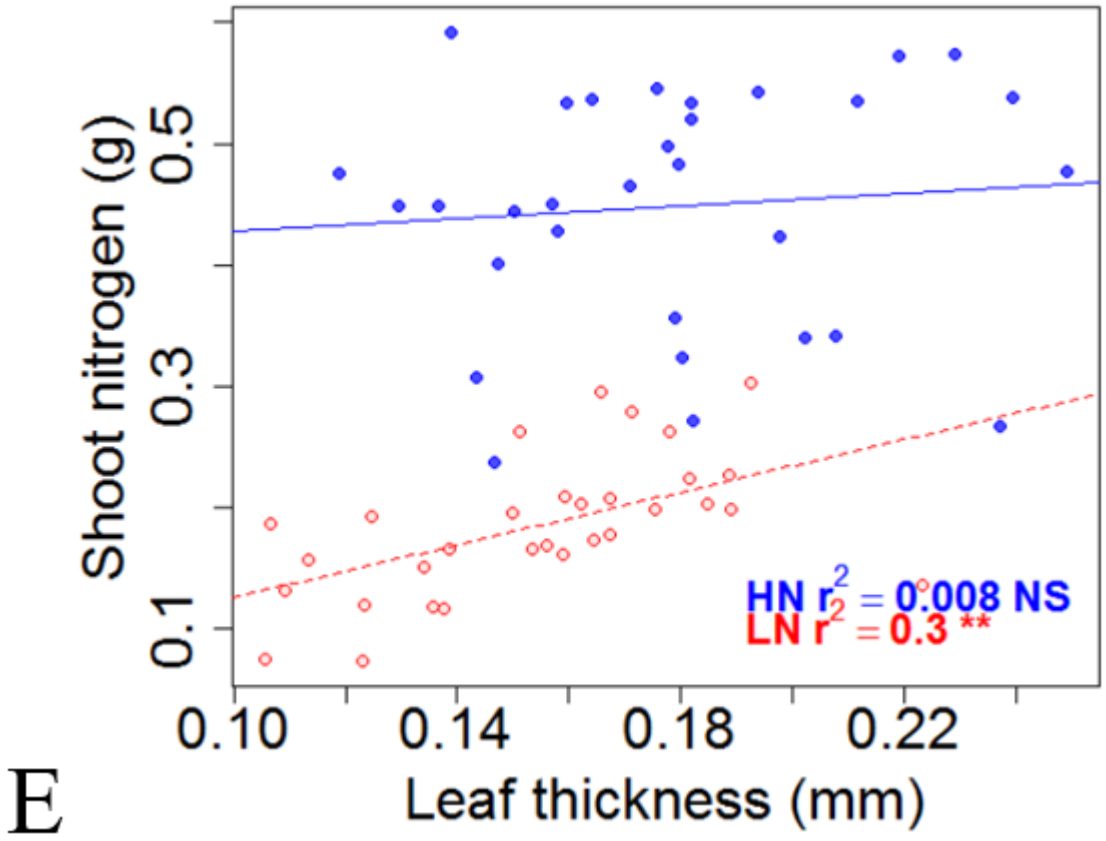

Figure 3-4. Relationships between leaf traits and shoot growth among maize inbreds. Linear regression of dry shoot mass against (A) leaf thickness, (B) median single leaf area, (C) plant height, (D) the number of expanded leaves at harvest, and (E) shoot nitrogen (stem and leaf mass multiplied by percent leaf nitrogen) under high (HN, blue) and low (LN, red) nitrogen conditions among IBM RILs in GH2. Each point is an individual plant (n=64 per plot, excluding missing values). R^2 value and significance ($p< 0.05$*, 0.01**, 0.001***; $p>0.1$ not significant, NS) are indicated.

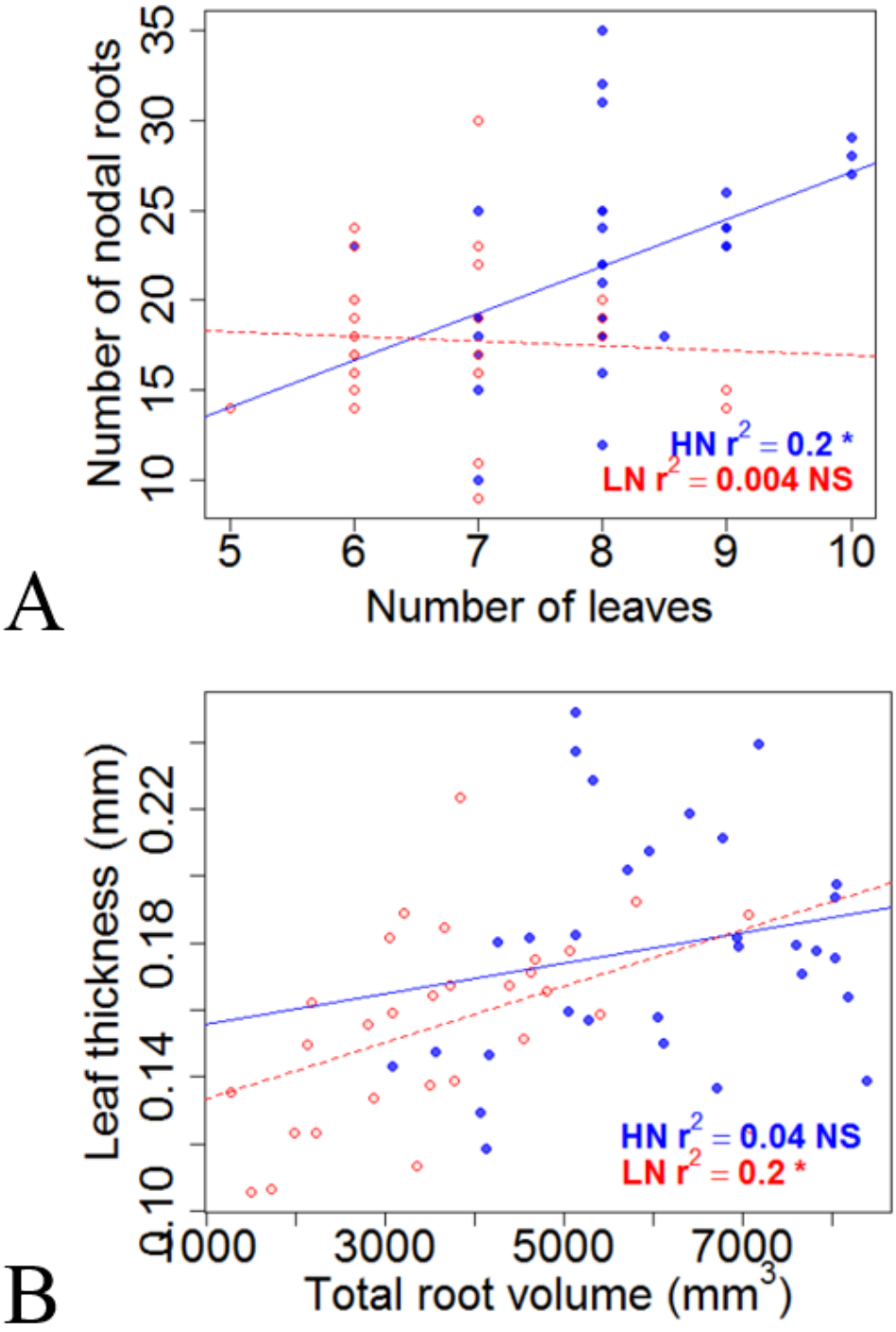

Figure 3-5. Relationships between leaf traits and root traits among maize inbreds. Linear regression of (A) number of nodal roots against number of leaves developed at harvest, and (B) leaf thickness of a representative leaf against the total axial root volume (TRV) averaged from nodes 2 and 3, under high (HN, blue) and low (LN, red) nitrogen among IBM RILs in GH2. Each point is an individual plant (n=64 per plot, excluding outliers). R^2 value and significance ($p< 0.05$*, 0.01**, 0.001***; $p>0.1$ not significant, NS) are indicated.

A

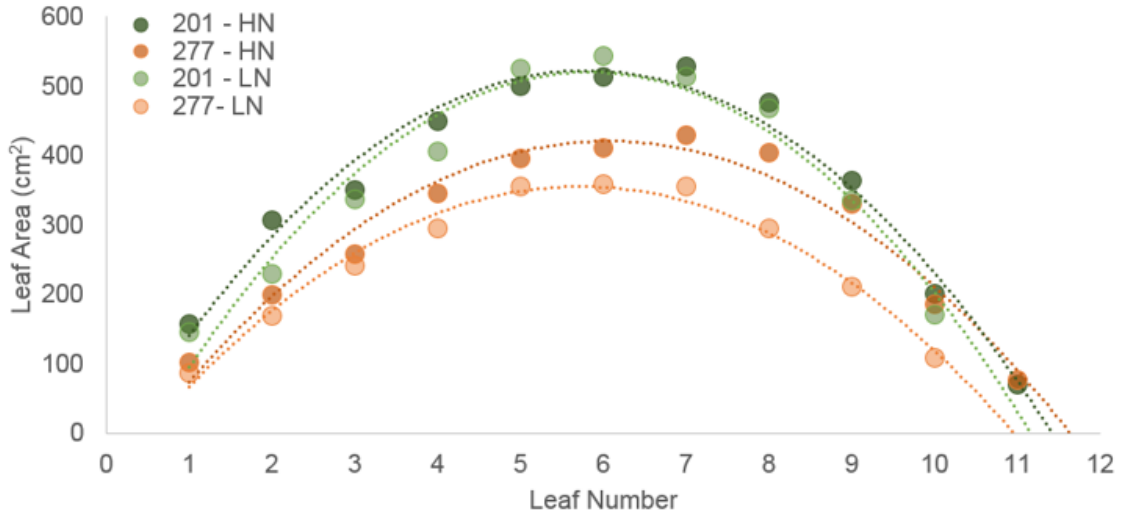
201 - HN
277 - HN
201 - LN
277- LN
Leaf Area (cm²)
Leaf Number
0
100
200
300
400
500
600
0
1
2
3
4
5
6
7
8
9
10
11
12

B

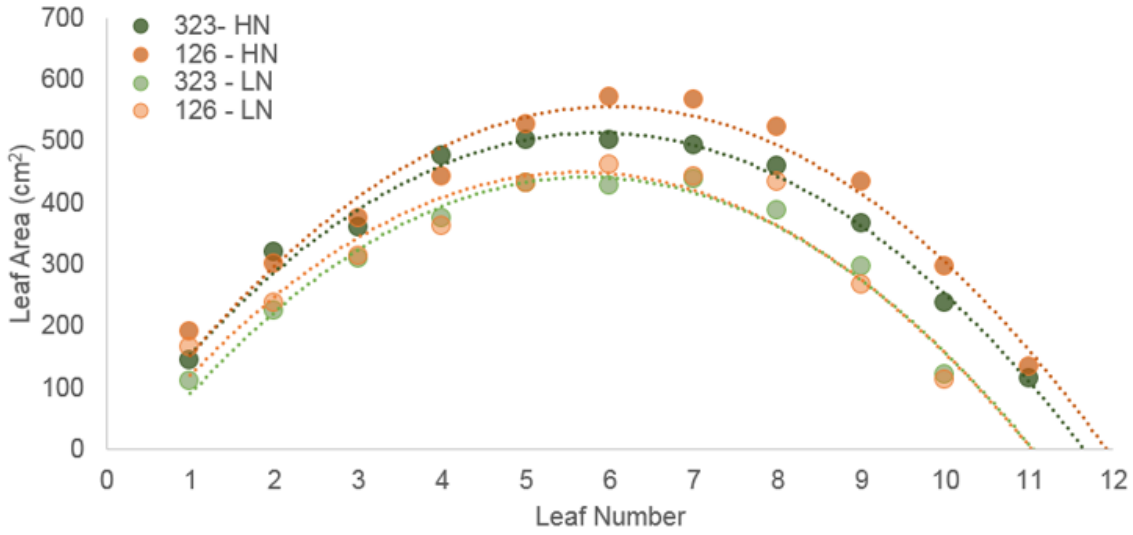
323- HN
126 - HN
323 - LN
126 - LN
Leaf Area (cm²)
Leaf Number
0
100
200
300
400
500
600
700
0
1
2
3
4
5
6
7
8
9
10
11
12

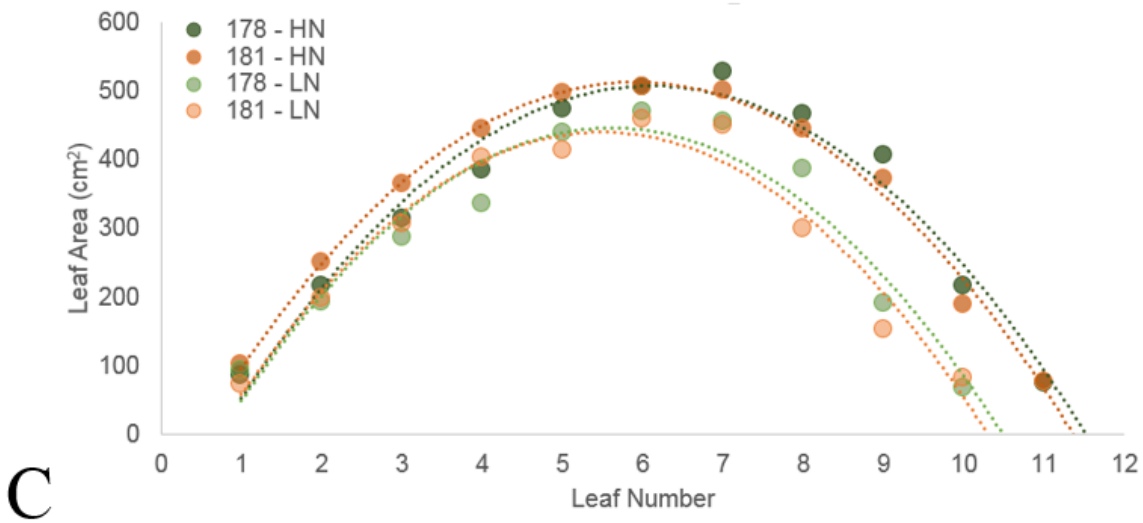

C

Figure 3-6. Leaf sizes among maize RILs under high and low nitrogen. Leaf area of each leaf as indicated by number (x-axis) for the indicated genotype (RIL number, in legend) and nitrogen treatment (high nitrogen, HN; low nitrogen, LN, in legend). Each point is the mean of four replicates from field-grown RILs in PA15. The following RILs are shown in each plot: (A) M201 and M277, (B) M323 and M126, (C) M178 and M181.

Table 3-1. Shoot and root system trait descriptions and measurements.

Trait	Description
Leaf number and size	
LN	Number of fully expanded leaves at harvest
LAtot	Total leaf area (cm^2)
LAmed	Median area of a single leaf (cm^2)
LLmed	Median length of a single leaf (cm)
LWmed	Median width of a single leaf (cm)
Leaf thickness and tissue composition	
LT	Leaf thickness (mm)
SLA	Specific leaf area ($cm^2\ g^{-1}$)
pEpi	Percent of leaf cross-section occupied by epidermis (sum of adaxial and abaxial) (%)
pVasc	Percent of leaf cross-section occupied by vascular bundles and bundle sheath cells (%)
pMeso	Percent of leaf cross-section occupied by mesophyll (%)
EpiDens	Density of epidermis cells across leaf section (average of adaxial and abaxial) (cells mm^{-1})
VascA	Cross-sectional area of vascular bundle and bundle sheath cells (μm^2)
IVD	Interveinal distance (mm)
MesoDens	Density of mesophyll cells in leaf cross-section (cells mm^{-2})
MesoCDM	Average diameter of mesophyll cell (μm)
EpiCCX	Cross-sectional area of epidermis cell (average of adaxial and abaxial, μm^2); 'height' x width
Stomatal size and distribution	
SD.AB	Stomatal density, abaxial (stomata mm^{-2})
SD.AD	Stomatal density, adaxial (stomata mm^{-2})
SI.AB	Stomatal index, abaxial (% of stomata), calculated as 100*(number of stomata)/(number of stomata + estimated number of epidermal cells) in a given area
SI.AD	Stomatal index, adaxial (% of stomata), calculated as 100*(number of stomata)/(number of stomata + estimated number of epidermal cells) in a given area
SD.R	Stomatal frequency ratio (SD.R = SD.AD / SD.AB)
StomA	Estimated stomatal size (μm^2), calculated as StomA = StomL*StomW
StomL	Stomatal length (μm)
StomW	Stomatal width (μm)
EpiCCS	Average epidermis cell size (μm^2) from epidermal peel (length x width)
Midrib anatomy	
MidribLT	Midrib thickness (mm)
MidribPC	Midrib cortical area (% of midrib, estimated as 100 * midrib cortical thickness / MidribLT)
MidribCF	Number of mesophyll cell files across the central axis of the midrib
MidribVA	Average cross-sectional area of vascular bundles in the midrib (μm^2)
MidribCCS	Average parenchyma cell size in midrib (mm^2)

Shoot measurements

Measurement	Description
PHT	Plant height (cm)
LNitro	Leaf nitrogen content (%)
Shootbiom	Dry shoot biomass (g)
Chl	Chlorophyll content (g g^{-1} DW)
Pn	Photosynthesis (assimilation) rate, µmol CO_2 m^{-2} s^{-1})
Cond	Leaf conductance rate (mmol m^{-2} s^{-1})

Root anatomy traits (measured in basal segments of axial crown roots)

Trait	Description
RXA	Root cross-section area, mm^2
SXA	Stele cross-section area (mm^2)
CXA	Cortex cross-section area (mm^2)
CSR	Cortex-to-stele ratio (CXA/SXA)
CF	Number of cortical cell files
CCS	Median cortical cell size, from the mid-section of the cortex (μm^2)
MXN	Number of metaxylem vessels
MXA	Total metaxylem vessel area in cross-section (mm^2)
MXP	Percent of total metaxylem vessel area in the stele (100*MXA/SXA)
AA	Total aerenchyma area in cross-section (mm^2)
AAP	Percent of aerenchyma area in the cortex (100*AA/CXA)
MXL, MXW	Median metaxylem vessel diameter (µm) - major axis (MXL) and minor axis (MXW) (Only measured if individual vessel areas were not traced or analyzed in RootScan2.)
MXM	Median metaxylem single vessel cross-section area (μm^2)
CMD	Median cortical cell diameter across all cortical cell files (µm)
MMD	Median mid-cortical cell diameter (µm)
HYP, OUT, INN	Median cortical cell diameter of hypodermis, outermost and innermost cortical cell file (µm) (In select cases, cross-sectional cell areas were traced; unit is μm^2.)
ECC	Median metaxylem vessel eccentricity

Root system traits and measurements

Trait	Description
NRN	Total number of nodal roots emerged at time of harvest
NN	Total number of root nodes developed at time of harvest
NO	Number of nodal roots per node ('nodal occupancy')
ARL	Root length of a single axial root (e.g. averaged across roots within a node), cm
TRL	Total root length of axial roots (e.g. summed across roots within a node), cm; TRL = NO*ARL for the indicated node(s).
TXA	Total cross-section root area in indicated node(s), mm^2; TXA = RXA * NO
TRV	Total axial root volume in indicated node(s), mm^3; TRV = RXA * (ARL*10) * NO
D95	Depth above which 95% of the root system is located (e.g. by length or mass, as specified)

Table 3-2. ANOVA table of leaf traits among maize IBM RILs. Analysis of variance (ANOVA) results from 8 genotypes x 2 nitrogen treatments x 4 replicates (n=64) of maize IBM RILs in GH2. F-values and significance levels (p <0.1., 0.05*, 0.001**, 0.0001***; not significant (p>0.1), NS) are given for the effect of genotypes (GT), nitrogen treatment (TRT), block (BL), and the interaction of GT and TRT (GxT) on each trait. See Table 3-1 for trait abbreviations.

Leaf number and size

	LN	LAtot	LAmed	LLmed	LWmed
GT	6.23 ***	4.34 ***	8.34 ***	15.38 ***	3.41 **
TRT	57.47 ***	62.25 ***	22.98 ***	0.69 NS	36.53 ***
BL	1.16 NS	0.6 NS	0.15 NS	1.32 NS	0.54 NS
G x T	1.78 NS	0.9 NS	2.5 *	2.39 *	0.83 NS

Leaf thickness and tissue composition

	LT	SLA	pEpi	pVasc	pMeso	EpiDens	VascA	IVD	MesoDens
GT	0.39 NS	4.37 ***	1.81 NS	0.56 NS	1.38 NS	1.36 NS	1.76 NS	3.07 *	1.5 NS
TRT	10.17 **	65.57 ***	5.22 *	7.9 **	0.39 NS	0.71 NS	33.07 ***	0.09 NS	3.08 .
BL	1.52 NS	7.32 ***	0.52 NS	1.94 NS	1 NS	9.22 ***	0.69 NS	1.37 NS	0.42 NS
G x T	2.65 *	1.32 NS	1 NS	1.08 NS	1.28 NS	2.13 .	1.22 NS	1.4 NS	2.93 *

Stomatal size and distribution

	SD.AB	SD.AD	SI.AB	SI.AD	SD.R	StomA	StomL	StomW	EpiCCS
GT	5.3 ***	3.93 **	2.51 *	0.77 NS	1.25 NS	1.25 NS	1.32 NS	0.69 NS	3.85 **
TRT	0.16 NS	11.93 **	0.3 NS	1.48 NS	5.46 *	2.38 NS	0.94 NS	2.95 .	0.05 NS
BL	1.58 NS	1.4 NS	10.02 ***	6.78 **	1.06 NS	8.45 ***	2.38 .	14.77 ***	13.03 ***
G x T	0.77 NS	1.42 NS	0.95 NS	2.89 *	0.99 NS	2.69 *	1.49 NS	3.84 **	1.16 NS

Midrib anatomy

	MidribLT	MidribCF	MidribVA	MidribCCS	MidribPC
GT	17.02 ***	9.93 ***	5.99 ***	5.99 ***	5.27 ***
TRT	10.73 **	0.49 NS	23.3 ***	0.07 NS	14.78 ***
BL	0.84 NS	5.95 **	0.78 NS	2.79 .	6.94 ***
G x T	3.85 **	1.29 NS	1.95 .	1.26 NS	0.95 NS

Table 3-3. Effect sizes of genotype and nitrogen treatment on leaf traits among maize IBM RILs. Effect sizes (%) for genotype (GT), nitrogen treatment (TRT), block (BL), and the interaction of GT and TRT (GxT) for each leaf trait in IBM RILs in GH2. Effect sizes are the proportion of variation in the trait explained by the given factor or interaction. See Table 1 for trait abbreviations. For each trait, the maximum source of variation (GT, TRT, or GxT) is in bold text.

Leaf number and size

	LN	LAtot	LAmed	LLmed	LWmed
GT	27.1	21	**40.7**	**62.2**	21.4
TRT	**35.7**	**43**	16	0.4	**32.7**
BL	2.2	1.2	0.3	2.3	1.4
G x T	7.7	4.4	12.2	9.7	5.2

Leaf thickness and tissue composition

	LT	SLA	pEpi	pVasc	pMeso	EpiDens	VascA	IVD	MesoDens
GT	3.4	17.8	**18.2**	5.8	**14.9**	10	12.4	**27.4**	13.4
TRT	12.9	**38.3**	7.5	**11.6**	0.6	0.7	**33.4**	0.1	3.9
BL	5.8	12.8	2.2	8.5	4.6	28.9	2.1	5.2	1.6
G x T	**23.5**	5.4	10.1	11.1	13.8	**15.6**	8.7	12.5	**26.2**

Stomatal size and distribution

	SD.AB	SD.AD	SI.AB	SI.AD	SD.R	StomA	StomL	StomW	StomLWR	EpiCCS
GT	**41.5**	**28.5**	**19.8**	6.6	13	9.5	14.3	4.1	**32**	**24.5**
TRT	0.2	12.4	0.3	1.8	8.1	2.6	1.5	2.5	0.8	0
BL	5.3	4.3	34	25	4.7	27.4	11	38.2	11.3	35.4
G x T	6	10.3	7.5	**24.8**	**10.3**	**20.4**	**16.1**	**23.2**	7.8	7.4

Midrib anatomy

	MidribLT	MidribCF	MidribVA	MidribCCS	MidribPC
GT	**61**	**52.3**	**36.1**	**44**	32
TRT	5.5	0.4	20	0.1	12.8
BL	1.3	13.4	2	8.8	18.1
G x T	13.8	6.8	11.7	9.3	5.8

Chapter 5

General Conclusions

Improving nitrogen acquisition and utilization efficiency in crops has the potential to address global challenges related to climate change, environmental degradation, and food security for a rapidly growing human population. Trait-based plant breeding requires (1) an understanding of physiological processes which may influence NUE, (2) an effective screening strategy to identify phenotypic variation in potentially useful traits, and (3) appropriate genetic material for assessing trait utility as well as identifying genetic loci for breeding purposes.

My research focused on anatomical phenotypes which could potentially enhance NUE in maize, and resulted in several novel contributions. Root system phenotyping, in the field or greenhouse, requires a nuanced approach grounded in developmental context. Maize axial root phenotypes as well as anatomical plasticity varied significantly across nodes, and phenotypes in the first two nodes were not representative of the bulk of the nodal root system. Interestingly, genotypes with greater NUE maintained thicker nodal roots in each node under nitrogen stress, an effect only partially attributable to allometry with plant size. The effects of nitrogen stress on root anatomy were generally strongest in later-developed nodes, coinciding with peak nitrogen demand. These results were consistent across multiple environmental conditions, with maize hybrid and inbred populations.

In exploring the utility of root anatomy traits, my research found that anatomical phenotypes are better assessed in context of root architectural variation. Specifically, the number and diameter of nodal roots showed a significant negative correlation among IBM RILs. Genotypes with slower nodal root emergence had fewer, thicker nodal roots, which in aggregate resulted in less axial root length, but improved the spatial distribution of roots, and reduced total carbon and nitrogen costs. The combination of fewer, thicker nodal roots resulted in improved nitrogen acquisition under low nitrogen conditions, and coincided with larger, thicker leaves in early growth. Thus, an updated root system ideotype should consider aggregate costs and benefits of root architecture, anatomy, and other important traits.

Finally, the integration of root and shoot traits for improving NUE has not been widely explored. My research found strong genotypic contrast in several leaf anatomy traits among IBM RILs, yet correlations between root and shoot anatomy traits were low, suggesting that trait combinations may not be subject to strong genetic constraints and there is potential for optimizing both shoot and root traits for NUE. The exception was a consistent positive association between the percent of root cortical aerenchyma and stomatal density, which remains to be explored. Additionally, cell size and density of various leaf tissues were inversely related and scaled strongly with leaf thickness, confirming results previously reported in literature.

Interestingly, among IBM RILs with contrast in nodal root traits, there was strong genotypic contrast in leaf thickness under moderate nitrogen stress, but not under mild or severe nitrogen stress. Under severe stress, all genotypes exhibited a substantial decrease in leaf thickness. Leaf thickness, particularly in relation to leaf mass per area, has been associated with interspecific differences radiation, water, and nitrogen use efficiency. Among IBM RILs, leaf thickness was inversely related to stomatal density, and weakly negatively correlated with conductance and carbon assimilation rate; there was no strong association with leaf nitrogen content. It will be useful to more thoroughly assess genotypic contrast in leaf phenotypes across development, and to develop integrated ideotypes of aboveground and belowground phenotypes to improve NUE.

Appendix A

Supplementary figures and tables for Chapter 2

Fig S1. **A maize root crown with different excised root nodes**. A field-excavated maize root crown (hybrid, high nitrogen) with nodal roots removed to show node 1 roots (left), node 6 roots (middle), and all roots removed, including the primary root; the mesocotyl is visible (right). The sixth node emerged at soil level, a transition from crown to brace root nodes. Scale bar is 2 cm.

Table S1. Plant materials and sampling details
See Tables S1.1 and S1.2 below.
Table S1.1 Root sampling - The following abbreviations are used: M# from IBM recombinant inbred line population, N# from NYH population.

Study	Root nodes sampled
PA13	2,3,4
PA14	1,2,3
PA15	1,2,3
PA16	2,3,4 all; 1,5,6 subset
SA14	1,2,3

Table S1.2 Plant materials - Inbred genotypes listed with (2) indicate an additional four replicates of the genotype were included as a check for field variability.
Hybrid genotypes were curated by the G2F Consortium. The full public dataset for G2F 2016 with details on seed sources will be released in March 2018 (doi will be made available).

Inbred genotypes				**Hybrid genotypes -** PA16	
PA13	**PA14**	**SA14**	**PA15**	Code	Pedigree
M001	M001	M001	M30	1	TX714/PHZ51
M021	M021	M021	M59	2	B73 X PHM49
M030	M030	M030	M126	3	PHW52 X PHN82
M062	M048	M131	M129	4	PHG39/Tx205
M090	M059	M146	M178	5	LH195/LH82
M126	M111	M178	M181	6	PHW52/Tx205
M131	M129	M201	M201	7	LH198/PHZ51
M146	M146	M263	M277	8	PHB47/PHZ51
M178	M178	M277	M323	9	2369 / LH123Ht
M201	M178 (2)	M323	M352	10	B73/PHZ51
M263	M181	M345	M365	11	PB80/PHZ51
M265	M181 (2)	M352		12	W10004_0216/PHZ51
M277	M201	M365		13	(CML442-B/CML343-B-B-B-B-B-B)-B-B-1-1-B-B-B-1-B12-1-B19/LH195
M323	M263	M379		14	TX714/Tx777
M345	M277	N015		15	B73/Tx777
M365	M317	N039		16	B14A X H95
N015	M323	N054		17	B14A X Oh43
N023	M344	N060		18	B37 X H95
N039	M352	N068		19	B37 X Oh43
N042	M365	N113		20	B73 X Mo17
N054	M365 (2)	N126		21	B73 X PHN82
N060	N015	N128		22	B97 X PHB47
N068	N039	N128 (2)		23	F42 X Mo17
N104	N060	N158		24	F42 X Oh43
N113	N068	N181		25	LH212Ht X LH195
N126	N113	N208		26	LH74 X PHN82

N128	N126			27	PHG39 X PHN82
N129	N128			28	PHG80 X PHZ51
N181	N181			29	PHP02 X PHB47
N208	OWRI-55			30	PHW52 X PHM49
				31	Wf9 X H95
				32	PHN11_PHG47_0251 X PHB47
				33	W10001_0022 X PHB47
				34	W10005_0107 X PHB47
				35	W37A X PHB47
				36	PHN11_Oh43_0001 X PHB47
				37	LH216 X LH195
				38	PHN11_PHW65_0323 X LH195
				39	B14A X Mo17
				40	B37 X Mo17
				41	F42 X H95
				42	PHG29 X PHG47
				43	2369 X 3IIH6
				44	LH123HT X 3IIH6

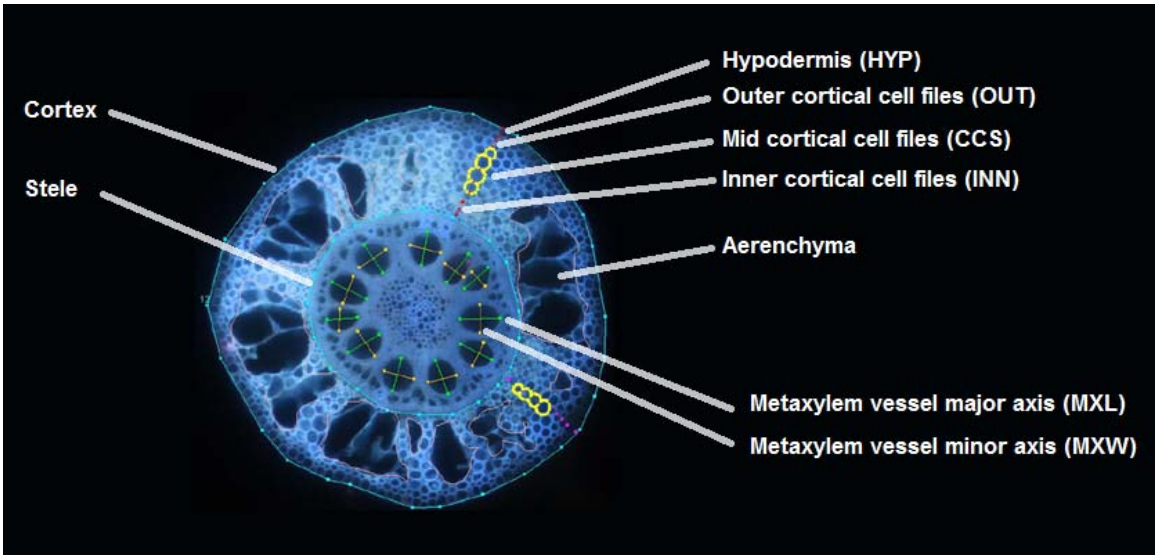

Fig S2. Maize root cross-section image analysis. An ObjectJ macro in ImageJ was created to semi-automate analysis of LAT images. An example of an analyzed image is below (S1 Fig 1); the outermost visible cell layer is the hypodermis, as the epidermis is typically degraded or not clearly visible in LAT images. Root (blue, outer), stele (blue, inner), and aerenchyma (pink) were outlined and total areas and ratios were calculated. Individual metaxylem vessels were estimated using the major (MXL, green) and minor axis (MXW, orange) lengths using the formula $((MXW+MXL)/2))^2/1.3$, derived empirically from testing manually traced vessel areas and various time-efficient methods of estimation (not shown). Images were zoomed in to allow accurate placement of MXL and MXW endpoints on the outer edge of each vessel. Cortical cell file number was manually counted in 4 axes to account for any asymmetry, then two representative axes across the cortex were selected to record a representative cell file count (the count of pink and red points) and measure cell diameters of each cell file (distance between every consecutive red/ pink point). The innermost cell layer was often incomplete and sporadic and the cell diameter (distance between innermost red or pink point and the stele outline) for this layer was not recorded. The cell diameters were used to calculate hypodermis (HYP), outermost (OUT) and innermost (INN). These cell diameters were also used to quantify file-specific cell diameter profiles. The median cortical cell size (CCS) was averaged from manually traced cell areas (yellow); for each image, the four largest consecutive cells in the cortex, typically in the mid-section, were traced in the two files. Images were zoomed in to allow careful tracing of the outer edge of the cells, excluding gaps between the cells; cell walls were included in the trace.

Table S2. ANOVA tables and effect sizes of genotype, nitrogen, and node on root traits in maize inbreds.
See Tables S2.1 and S2.2 below.

Table S2.1 ANOVA table of genotype, nitrogen level, node, and interaction effects on inbred maize root anatomy. Analysis of variance results from 11 inbred genotypes (G) x 2 nitrogen treatments (T) x 3 nodes (N) x 2 replicates (PA15, n=523, including 2 roots per node) from PA15. Nitrogen stress was mild. F-values and significance levels (p <0.1., 0.05*, 0.001**, 0.0001***, not significant (>0.1), N.S.) are given for each trait (see Table 1-1 for abbreviations) for each main factor (G, T, N) and all factor interactions (G:T, G:N, T:N, G:T:N). Data from root nodes 1,2,3 were included.

	RXA	CXA	SXA	MXA	CF	MXN
G	15.5***	12.2***	24.5***	12.4***	18.3***	22.9***
T	3.9*	5.6*	0.5 NS	0.3 NS	0.1 NS	0.5 NS
N	484.3***	410.8***	551.5***	579.2***	603.7***	413.9***
G:T	2.6**	2.5**	2.5**	2.3*	2.2*	2.1*
G:N	5.5***	4.1***	8.5***	5***	1.7*	3.5***
T:N	0.7 NS	0.9 NS	0.5 NS	1.3 NS	4.2*	1.4 NS
G:T:N	1.5.	1.4 NS	1.8*	1.2 NS	1.9**	1.3 NS

	CSR	AAP	MXP	MXM	ECC	CDM	CCS
G	19.6***	3.9***	15.9***	16.8***	5***	7.8***	5.4***
T	7**	0.1 NS	0.6 NS	2.2 NS	0.1 NS	16.5***	13.3***
N	181.8***	22.6***	0.8 NS	233.9***	48.2***	22.7***	13.4***
G:T	3.9***	2*	1.2 NS	1 NS	0.9 NS	2.3*	2.5**
G:N	2.1**	1.7*	2.8***	3.6***	1.3 NS	0.9 NS	1.5.
T:N	3.9*	2.6.	0.3 NS	3.2*	1.3 NS	1 NS	1.2 NS
G:T:N	1.2 NS	2.1**	1.6.	1 NS	0.7 NS	1 NS	1 NS

Table S2.2 Effect size of genotype, nitrogen treatment, and node on root anatomy. Effect sizes (%) for genotype (G), nitrogen treatment (T), and root node (N) and their interactions for each anatomical trait for 11 IBM maize inbred lines (PA15, n=523, including 2 roots per node). Nitrogen treatment was mild. Effect sizes are the proportion of variation in the trait explained by the given factor, factor interactions, or other random sources (residuals). See Table 1-1 for trait abbreviations. Root nodes 1, 2,3 included. The maximum source of variation is in bold for each trait; if the maximum source of variation is an interaction or residual, the greatest main effect is underlined.

	RXA	CXA	SXA	MXA	CF	MXN
G	8.7	7.9	11.9	6.5	9.4	14
T	0.2	0.4	0	0	0	0
N	**54.8**	**52.8**	**53.5**	**60.8**	**62**	**50.4**
G:T	1.5	1.6	1.2	1.2	1.1	1.3
G:N	6.2	5.3	8.2	5.2	1.8	4.2
T:N	0.1	0.1	0	0.1	0.4	0.2
G:T:N	1.7	1.7	1.7	1.3	2	1.6
Resid	26.8	30.2	23.5	24.9	23.3	28.3

	CSR	AAP	MXP	MXM	ECC	CDM	CCS
G	16.9	5.8	<u>21.8</u>	13.9	7.7	<u>11.8</u>	<u>8.5</u>
T	0.6	0	0.1	0.2	0	2.5	2.1
N	<u>31.4</u>	<u>6.7</u>	0.2	**38.5**	<u>14.7</u>	6.9	4.3
G:T	3.4	2.9	1.7	0.8	1.4	3.4	3.9
G:N	3.7	5.2	7.6	6	4.1	2.8	4.8
T:N	0.7	0.8	0.1	0.5	0.4	0.3	0.4
G:T:N	2.1	6.3	4.3	1.6	2.2	3.1	3.2
Resid	**41.2**	**72.3**	**64.2**	**38.5**	**69.5**	**69.2**	**72.8**

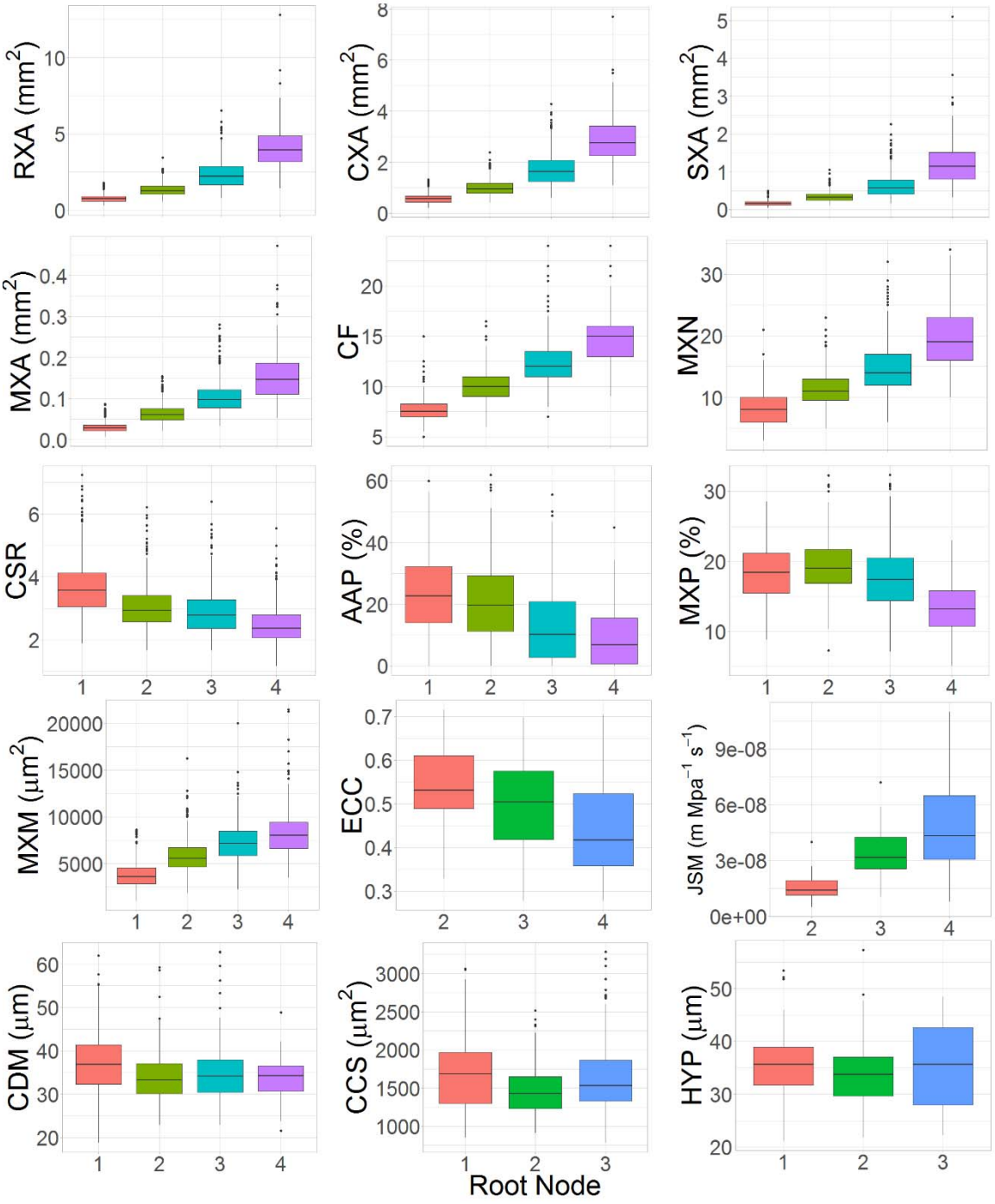

Fig S3. Root anatomy variation by node in field-grown maize inbreds. Boxplots of nodal root traits in nodes 1 (oldest) through 4 (left to right). Data aggregated from 4 field studies: PA13, PA14, PA15 in USA, and SA14 in South Africa, including both high and low nitrogen. For each plot, total n = 1739 to 1744, except AAP (n=1341), ECC and JSM (n=144, from nodes 2-4 only), and CCS (n=506, from nodes 1-3 only). See Table 1-1 for trait abbreviations and units.

Table S3. Genotypic variation in maize root anatomy traits by node. Genotypic coefficients of variation (G.C.V., %) for each trait, calculated as [CV = 100*(standard deviation of trait value)/(mean trait value)] using mean trait values for each genotype, by node (N2, N3, N4) and nitrogen treatment (HN, LN) in field-grown maize inbreds (top, PA15, n=11 IBM genotypes; bottom, PA14, 30 genotypes including 3 RIL populations). See Table 1-1 for trait abbreviations.

PA15

		RXA	CXA	SXA	MXA	CF	MXN	CSR	AAP	MXP
HN	N1	16.9	16.4	24.4	19.9	9.8	10.1	15.5	32.6	6.6
	N2	16.4	15.9	20.7	18.7	8.4	14.4	14.2	31.5	8.8
	N3	21.4	19.8	29.9	21.4	8.6	16.8	17	23.3	11.6
LN	N1	15.1	15.9	16.5	14.3	7.6	12.6	13.7	21.4	5.7
	N2	16.2	15.4	19.5	15.6	7.3	14.1	7.2	33.6	8.2
	N3	21.9	19.7	29.1	17.8	7	15.7	12.5	29.1	15.9
	Mean	**18**	**17.2**	**23.4**	**18**	**8.1**	**14**	**13.4**	**28.6**	**9.5**

		AA	MXM	MXL	MXW	ECC	CDM	CCS	OUT
HN	N1	43.6	17.1	8.3	9.7	2.3	9.6	18.7	14.2
	N2	30	15	8.4	8	2.1	8.2	13.3	14
	N3	24.8	18.2	10.1	10.6	4.1	9.9	17.1	19.3
LN	N1	34	17.1	7.6	9.2	1.8	6.1	10.1	7
	N2	32.2	12	6.1	6.5	2.1	6.1	9.5	9.5
	N3	26.8	18	9.4	10.5	3.3	7	13.8	9.7
	Mean	**31.9**	**16.2**	**8.3**	**9.1**	**2.6**	**7.8**	**13.8**	**12.3**

PA14

		RXA	CXA	SXA	MXA	MXN	CF	CSR	AAP	MXP	MXM	CCS	HYP
HN	N1	15.9	17	16	20.4	16.1	9.6	10.7	23.6	14	21.5	14.3	16.4
	N2	16.4	16.5	20.4	16.6	13.3	11.1	14.6	23.5	14.3	18.1	16.7	14.5
	N3	20.8	20.1	24.9	20.5	15.4	18.4	14.9	43.2	13.1	17.9	11	15.3
LN	N1	14.6	14.8	17.8	17.8	15.1	7.6	12.3	32.1	11.4	20.2	22.2	18.4
	N2	16.6	17.1	18.2	18	14.5	6.2	12.2	31.3	10.4	17	11.5	8.8
	N3	16.7	15.9	21.3	14.7	12.7	9.5	13.4	39.6	14.8	15.1	9.6	17
	Mean	**16.8**	**16.9**	**19.8**	**18**	**14.5**	**10.4**	**13**	**32.2**	**13**	**18.3**	**14.2**	**15.1**

Table S4. Within-genotype variation in maize root anatomy by node and N treatment. Coefficients of variation (C.V., %) were calculated as [CV= 100*(standard deviation of trait value)/(mean trait value)] for each genotype, then were averaged across genotypes for each node (N1, N2, N3, N4) and nitrogen treatment (HN, LN) among field-grown maize hybrids (PA16, 44 genotypes) and inbreds (PA15, 11 genotypes). See Table 1-1 for abbreviations.

PA16

		RXA	CXA	SXA	MXA	CF	MXN	CSR	AAP	MXP	AA
N2	**HN**	32.3	32.5	32	32.2	13.2	14.4	15	103	11.3	106.1
	LN	25.8	26.6	27.1	34	10.1	15.2	12.1	95.7	11.8	97.3
N3	**HN**	30.1	28.3	36.6	32.9	12.4	20.7	16.5	100.5	16.6	98.1
	LN	29.6	29.7	30.8	26.2	10.7	14.2	12.3	89.7	17.8	89.6
N4	**HN**	37	34.6	41.6	34	12.1	20.4	15	106.3	19.2	107.4
	LN	29.2	27.8	33.5	27	11.3	18.1	12.2	80.2	21.8	79.5
	Mean	**30.7**	**29.9**	**33.6**	**31.1**	**11.6**	**17.2**	**13.9**	**95.9**	**16.4**	**96.3**

		MXM	MXL	MXW	ECC	JSM	CDM	CCS	HYP	OUT	INN
N2	**HN**	24.4	13.3	12.4	12.4	49.9	12.1	20.5	15.4	25.1	14.2
	LN	27.9	15	14.4	17.4	55.1	11.2	20.1	12.3	20.1	13.3
N3	**HN**	21.7	11.6	10.2	11.4	48.1	12.1	16.2	12.9	21.6	13.4
	LN	21.5	12.8	11	14.9	39.4	10.9	19.2	12.7	14.9	15.8
N4	**HN**	25.3	13.2	12.2	15.6	49.2	10.9	19.9	16.4	20.8	15.5
	LN	18.3	11.1	8.6	15.3	38.7	8.7	14.4	11.4	17.5	15.8
	Mean	**23.2**	**12.8**	**11.5**	**14.5**	**46.7**	**11**	**18.4**	**13.5**	**20**	**14.7**

PA15

		RXA	SXA	CXA	CF	MXN	AAP	CSR	MXP	MXA	MXM	ECC	CCS	CDM
N1	**HN**	26.8	27	27.5	11.8	19.7	49.3	16.3	12.5	27.6	23.2	5.3	27.3	14.9
	LN	28.5	29.4	29.6	12.1	22.8	52.4	18.5	12.4	30.7	25.1	5.5	28.8	16.8
N2	**HN**	16.6	21.2	16.9	10.2	15.6	62.4	13.8	12.7	22.1	20	5.2	23.6	14.4
	LN	18.8	23.7	19	8	15.5	58.4	18.4	12.7	25.8	22.7	4.8	17.9	10.1
N3	**HN**	25.8	30.8	25.1	9.7	16.3	87.6	16.1	15.4	27.9	23	5.9	29	15
	LN	19.2	19.3	20.3	7.9	14.3	71.7	13	13.3	21.9	19.9	6.4	19.4	10.1
	Mean	**22.6**	**25.2**	**23.1**	**9.9**	**17.4**	**63.6**	**16**	**13.2**	**26**	**22.3**	**5.5**	**24.3**	**13.6**

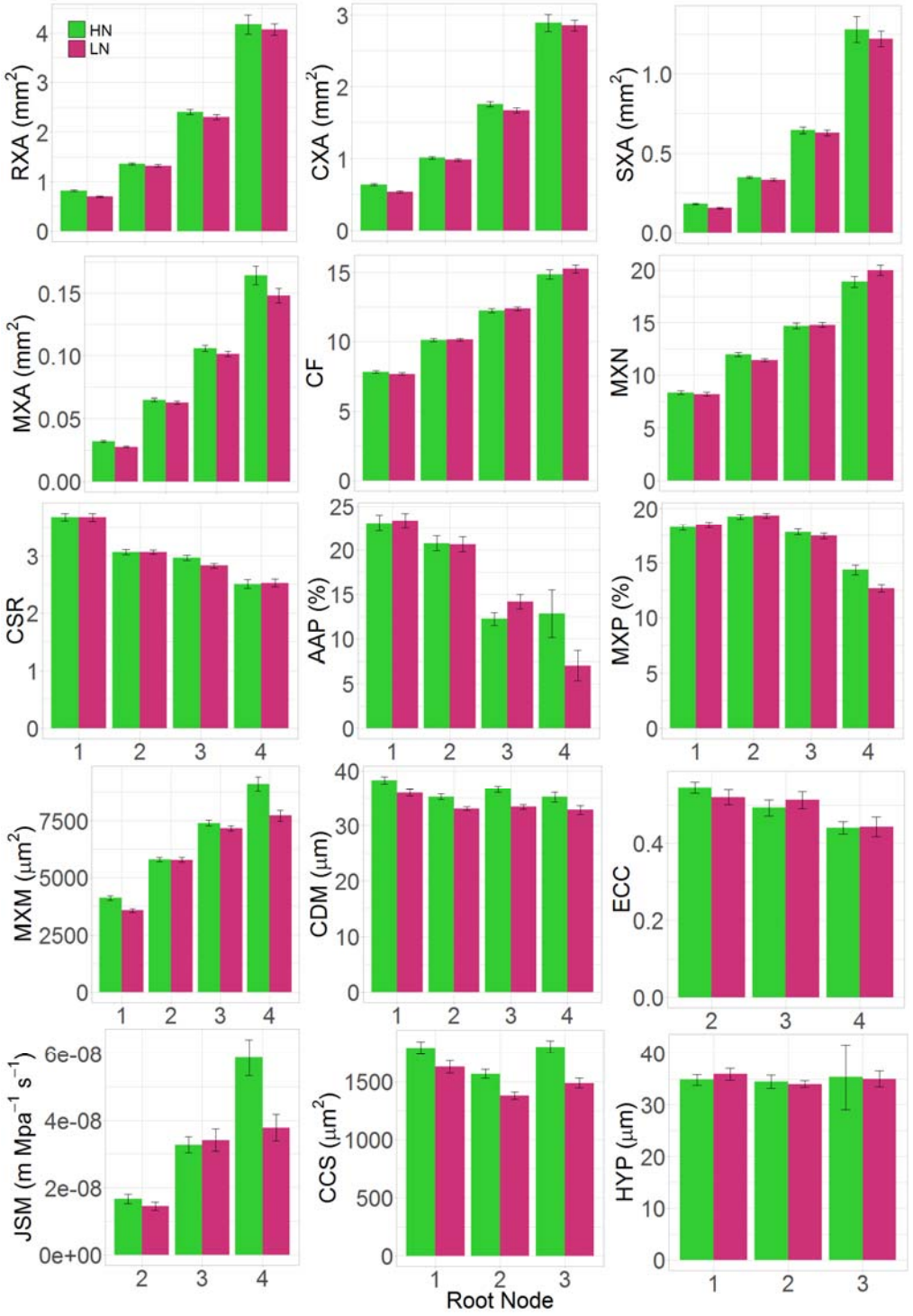

Fig S4. Node-specific root anatomy responses to nitrogen stress in maize inbreds. Root trait means ± S.E. per node (1-4) and nitrogen treatment (green, HN; pink, LN), total n=1739 roots per plot, except ECC, JSM, CCS, and HYP, which were evaluated on a subset. Data aggregated from 4 field studies (PA13, PA14, PA15, SA14). N stress was mild in PA studies and severe in SA. See Table 1-1 for trait abbreviations and units.

Table S5. Nitrogen stress induced change in root anatomy traits. Percent change in root trait values from high nitrogen to low nitrogen treatment (n=469 for each trait) for nodes 1-5 (N#) in PA16. These values are calculated from the same data in Fig 1-6.

	Root-diameter related traits						Proportion traits		
	RXA	**CXA**	**SXA**	**MXA**	**CF**	**MXN**	**CSR**	**AAP**	**MXP**
N1	24.2	20.8	34	7.3	-1.1	-3.8	-10.2	238.3	-19.5
N2	-18.1	-19.9	-12.3	-14.1	-0.5	-9.2	-8.5	37.7	-1.8
N3	-17	-17.2	-16.5	-13.1	-4.3	-6	-2.3	93.6	5.1
N4	-24.1	-22.3	-27.7	-17.6	-5.3	-14	5.7	63.4	12.9
N5	-30.6	-24.3	-40.8	-35.8	-3.6	-26.8	24.1	193.6	1.9

	Vessel related traits					Cortical cell related traits				
	MXM	**MXL**	**MXW**	**ECC**	**JSM**	**CDM**	**CCS**	**HYP**	**OUT**	**INN**
N1	15.5	6.4	8.7	-14	21.5	-4.1	13.6	-3.3	-8.8	-1
N2	-5.9	-3.8	-1.3	-7.9	-17.8	-13.3	-19.1	-2.4	-13.5	-14
N3	-6.2	-2.6	-3.6	2	-21.2	-6	-9.2	-2.2	-3.4	-4.5
N4	-4	-1.7	-1.6	-1.1	-24.4	-4.6	-11	10.8	-1	-3.7
N5	-12.1	-5.8	-6.8	-0.2	-45.8	-13.9	-9	9.7	1.8	-11.2

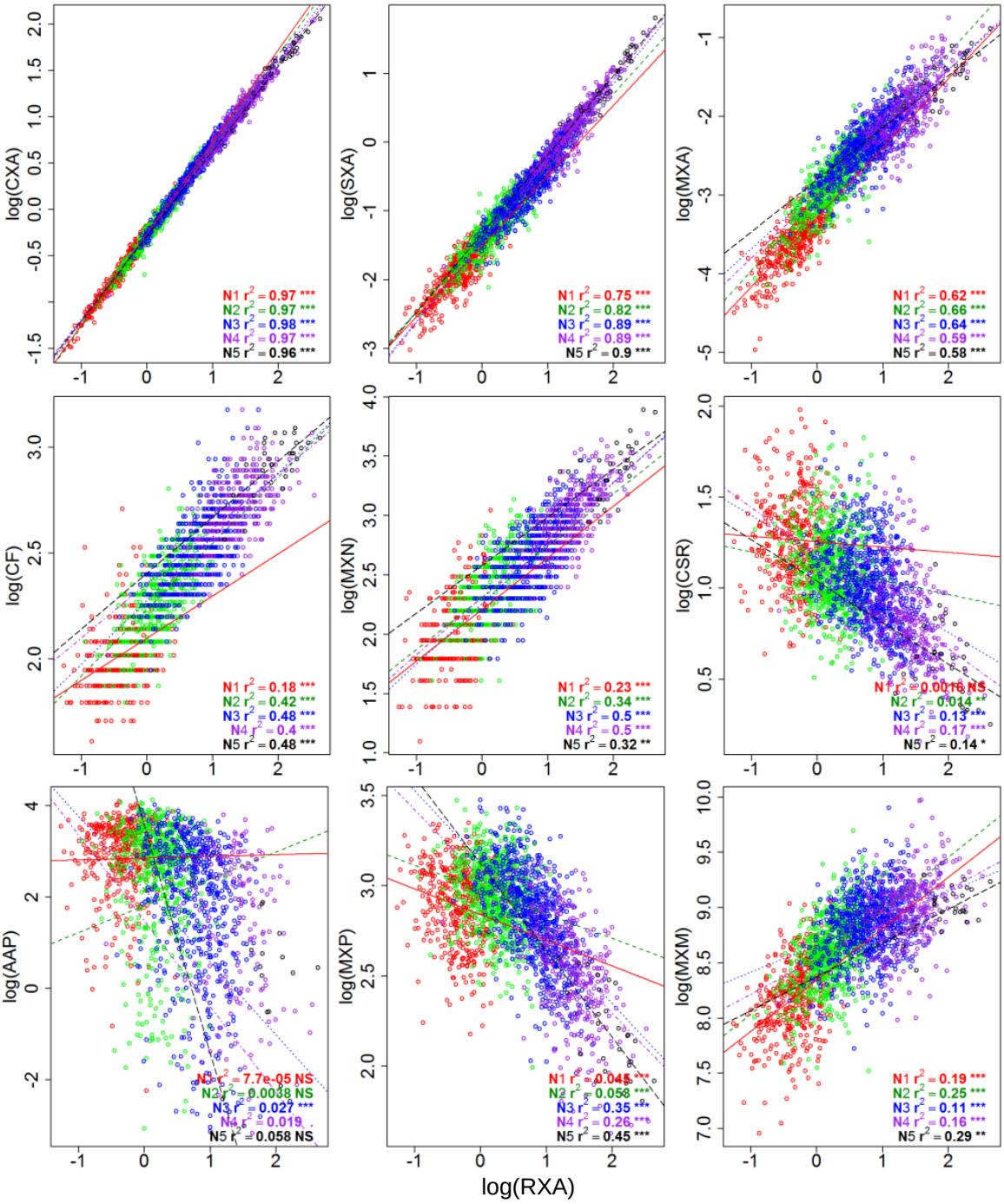
log(CXA)
N1 r² = 0.97 ***
N2 r² = 0.97 ***
N3 r² = 0.98 ***
N4 r² = 0.97 ***
N5 r² = 0.96 ***
log(SXA)
N1 r² = 0.75 ***
N2 r² = 0.82 ***
N3 r² = 0.89 ***
N4 r² = 0.89 ***
N5 r² = 0.9 ***
log(MXA)
N1 r² = 0.62 ***
N2 r² = 0.66 ***
N3 r² = 0.64 ***
N4 r² = 0.59 ***
N5 r² = 0.58 ***
log(CF)
N1 r² = 0.18 ***
N2 r² = 0.42 ***
N3 r² = 0.48 ***
N4 r² = 0.4 ***
N5 r² = 0.48 ***
log(MXN)
N1 r² = 0.23 ***
N2 r² = 0.34 ***
N3 r² = 0.5 ***
N4 r² = 0.5 ***
N5 r² = 0.32 **
log(CSR)
N1 r² = 0.0016 NS
N2 r² = 0.014 **
N3 r² = 0.13 ***
N4 r² = 0.17 ***
N5 r² = 0.14 *
log(AAP)
N1 r² = 7.7e-05 NS
N2 r² = 0.0038 NS
N3 r² = 0.027 ***
N4 r² = 0.019 .
N5 r² = 0.058 NS
log(MXP)
N1 r² = 0.045 ***
N2 r² = 0.058 ***
N3 r² = 0.35 ***
N4 r² = 0.26 ***
N5 r² = 0.45 ***
log(MXM)
N1 r² = 0.19 ***
N2 r² = 0.25 ***
N3 r² = 0.11 ***
N4 r² = 0.16 ***
N5 r² = 0.29 **
log(RXA)

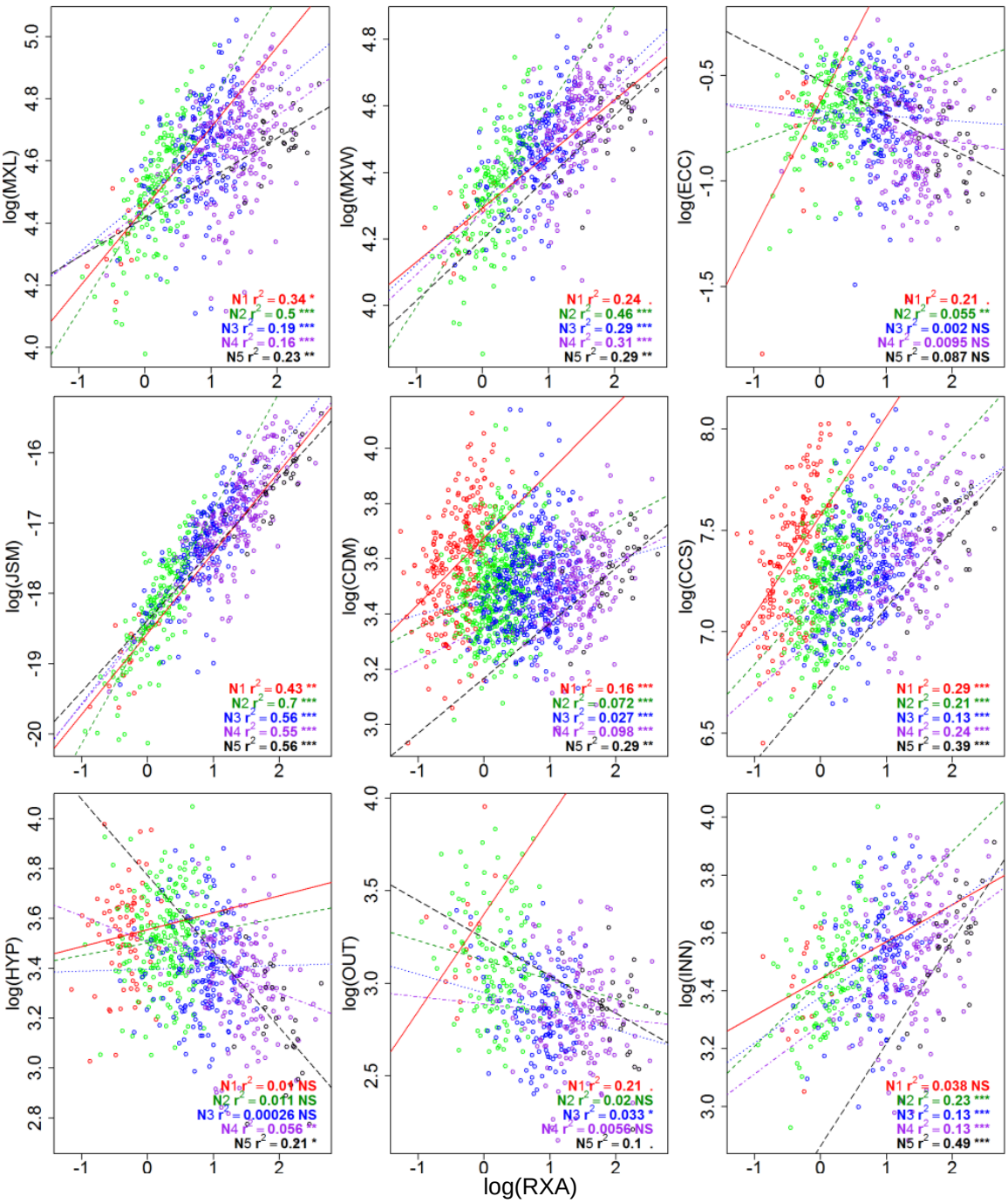

Fig S5. Scaling relationships between root anatomy traits and root diameter across nodes. The natural logarithm of each root anatomy trait is plotted against the natural logarithm of root cross-sectional area (RXA), including up to 5 root nodes from field-grown maize inbreds and hybrids (PA13, PA14, SA14, PA15, PA16) from both high and low nitrogen treatments, with node indicated with colors. R^2 and p-values (significance levels of p<0.1., 0.05*, 0.001**, 0.0001***, not significant >0.1 NS) are given in each plot for each node (N) number. Each plot has n=472 to 2217 depending on trait; not all traits were evaluated in all studies. See Table 1-1 for abbreviations and units.

Table S6. ANOVA table of genotype, nitrogen, and node effects on hybrid maize nodal metaxylem traits. Analysis of variance results from 44 hybrid genotypes (G) x 2 nitrogen treatments (T, high and low) x 3 nodes (N, from nodes 2,3,4) x 2 replicates (PA16, n=168, excluding missing values). F-values and significance levels (p <0.1., 0.05*, 0.001**, 0.0001***, not significant (>0.1), N.S.) are given for each main factor (G, T, N) and all factor interactions (G:T, G:N, T:N, G:T:N). Abbreviations: MIN, minimum cross-sectional area of a single metaxylem vessel; MAX, maximum cross-sectional area of a metaxylem vessel; RELS, RELL; percent of the number of very large or very small metaxylem vessels in a cross-section; CV, coefficient of variation of metaxylem vessel sizes in a cross-section; NUMS, NUML, total number of very small and very large metaxylem vessels in cross-section. The thresholds for relatively large (>1.14*median vessel size) and small (<0.75*median vessel size) vessels were determined empirically on a subset of root cross-sections.

	MIN	MAX	RELS	RELL	CV	NUMS	NUML
G	1.69**	3.01***	1.82**	1.46*	1.37.	2.67***	2.78***
T	0.039 N.S	20.85***	11.82***	7.31**	6.71*	26.10 ***	26.51***
N	4.43*	91.14***	9.53***	8.58***	11.22***	97.07 ***	110.76***
G:T	0.94 N.S.	1.56*	0.77 N.S.	1.13 N.S.	1.07 N.S.	0.86 N.S.	1.75**
G:N	1.35*	1.31.	1.22 N.S.	1.24 N.S.	1.10 N.S.	1.26.	1.28.
T:N	4.31*	0.41N.S.	0.30 N.S.	0.95 N.S.	1.72 N.S.	4.09*	6.81**
G:T:N	0.99 N.S.	1.13 N.S.	0.85 N.S.	1.41*	0.74 N.S.	0.77 N.S.	1.21 N.S.

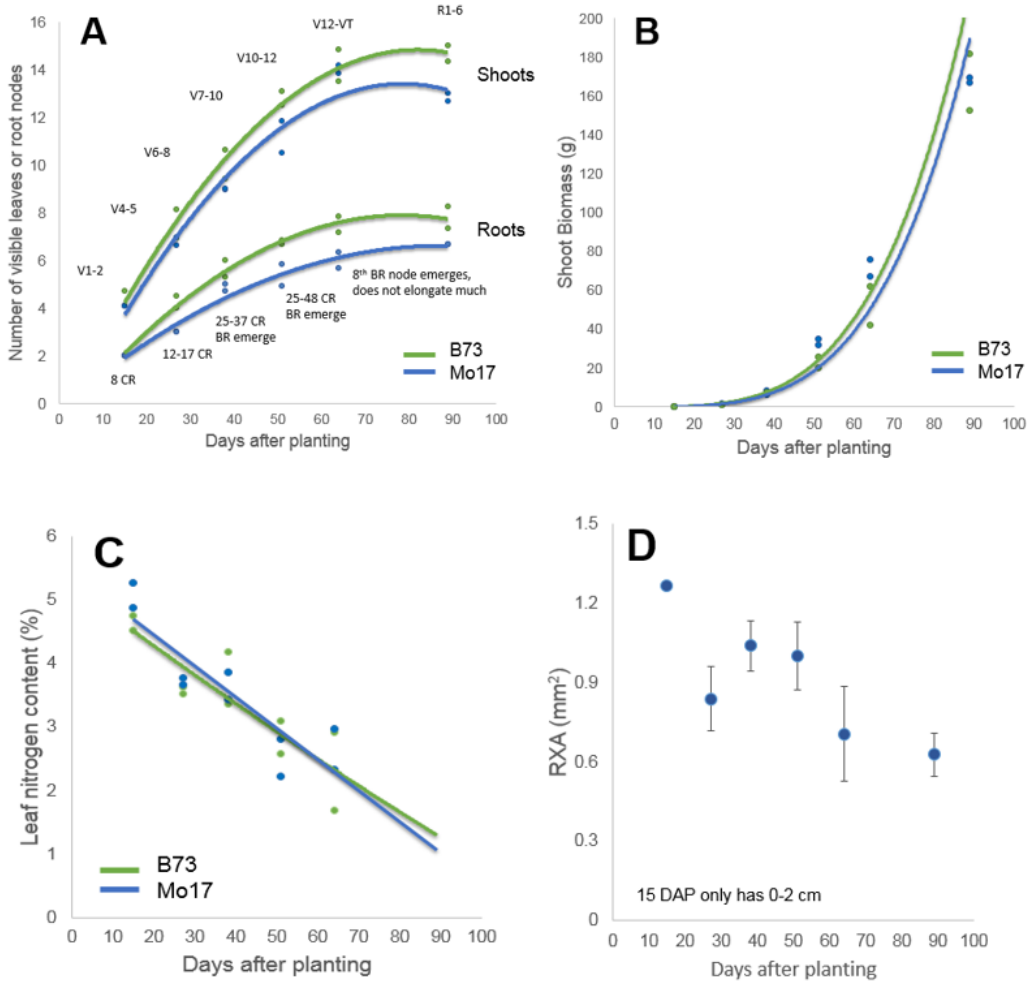

Fig S6. Relationship between maize shoot and root development. In (A), polynomial regression lines were fitted to the number of visible leaves (not collars; top) and number of adventitious root nodes (bottom) present at six time points. The approximate growth stage (V1 to R) and total number of crown roots (CR) and presence of brace roots (BR) are annotated, based on observed ranges in root number; the 7th and 8th brace root nodes have been observed with up to 22 roots per node, while 11 roots have been observed emerging from a 9th node, resulting in an observed range of 26 to 77 total nodal roots in field-grown maize at anthesis. In (B), power regression lines were fitted to the dry shoot biomass (g) measured at six time points. In (C), linear regression lines were fitted to the percent of leaf nitrogen at six time points. For (A), (B), and (C), points represent mean values of three plants each from high and low N treatments (the larger value is from high N) from maize inbred genotypes B73 (green) and Mo17 (blue). In (D), mean ± SE of root cross-sectional area (mm^2) were averaged from three positions collected 0 to 6 cm from the base of second node crown roots (except at the first time point, when only 0 to 2 cm of second node roots had emerged) from B73 plants in high N, at six time points; at 15 days after planting. All plants were harvested from high and low N fields at the Russell Larson Research Farm in PA in 2015.

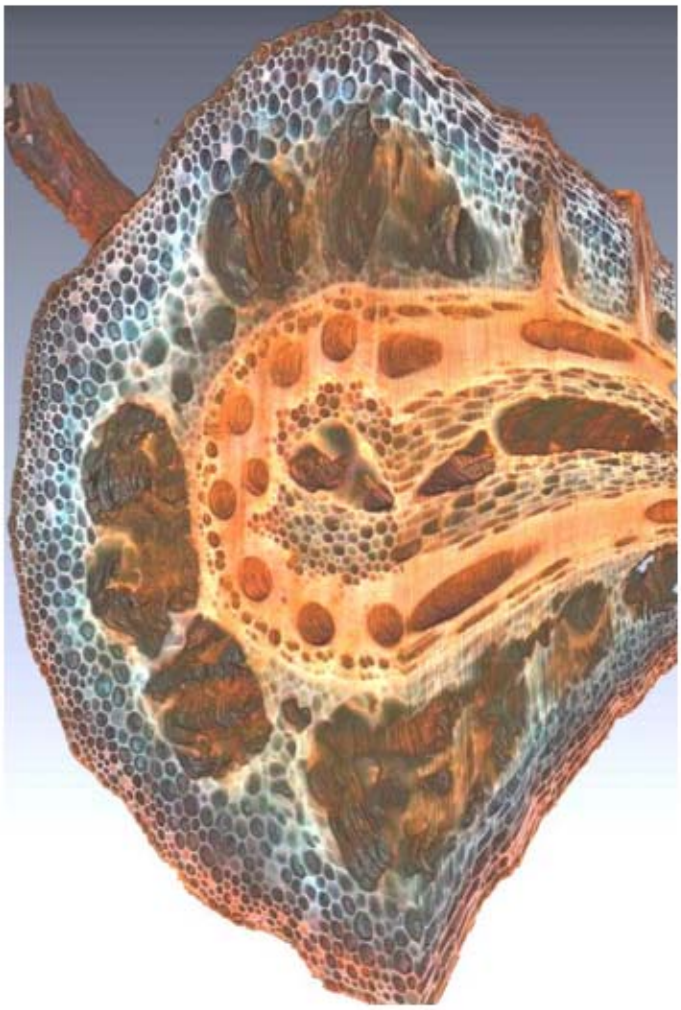

A

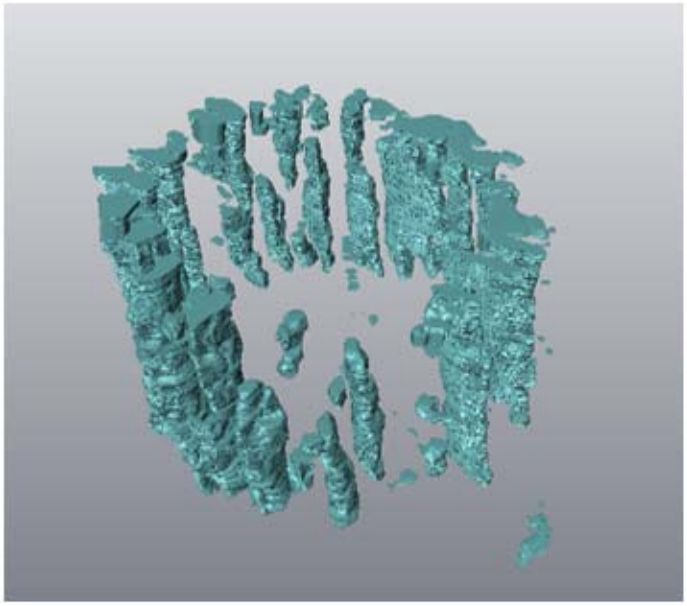

B

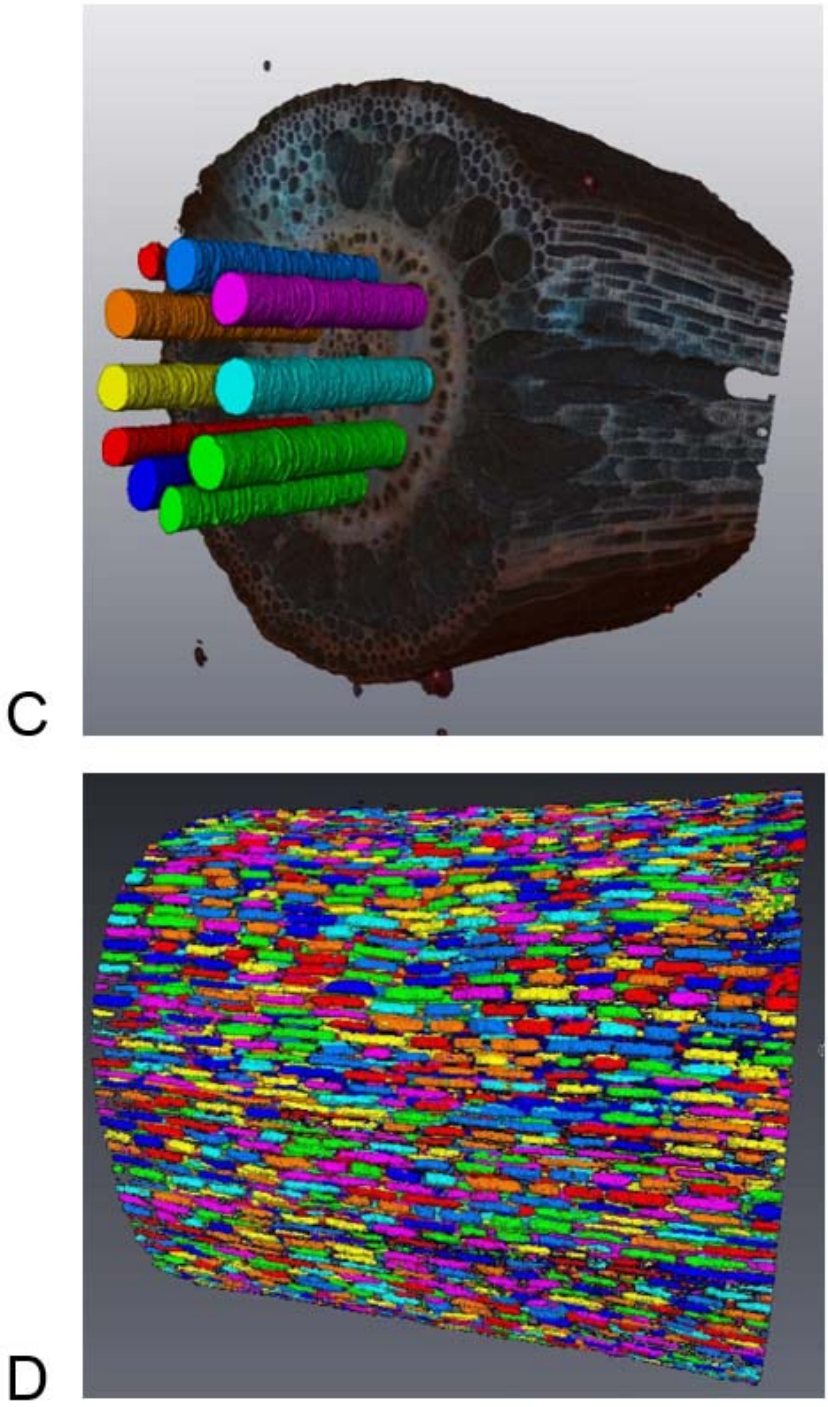

Fig S7. Three-dimensional reconstruction and segmentation of root anatomy. (A) Reconstructed image of a laser-ablated maize nodal root section (a 4 mm section near the base) using Avizo™. (B) Extracted volume of aerenchyma and (C) metaxylem vessels from maize nodal root (work of Dannielle Gibson) using MIPAR™ and visualized in Avizo. (D) Extracted volumes of cortical cells using Avizo™.

Appendix B

Root anatomy raw data for Chapter 2

Summary data associated with **Table 1-2**. Minimum, maximum, mean, median, and first and third quartile values from a balanced dataset of PA16 field-grown maize hybrids, i.e. with n=156 per root node (2, 3, and 4), n=234 per nitrogen treatment, and n=117 per replicate (plot; one plant per plot). See **Table 1-1** for trait abbreviations and units.

	RXA	SXA	CXA	MXA	CF	MXN	CSR	AAP	AA	MXP
Min.	0.38	0.06	0.29	0.01	6.5	2	1.2	0	0	5.32
Q1	1.32	0.32	0.99	0.06	10.5	11	2.18	0.48	0.01	13.07
Median	2.31	0.62	1.67	0.1	12.5	15	2.55	3.48	0.05	16.26
Mean	2.71	0.82	1.89	0.11	12.91	15.83	2.67	8.43	0.14	16.3
Q3	3.65	1.12	2.54	0.15	15	19	3.04	13.98	0.22	19.83
Max.	12.34	4.71	7.62	0.43	22	40	7.41	50.04	1.54	27.6

	MXM	MXL	MXW	ECC	JSM	CDM	CCS	HYP	OUT	INN
Min.	1649	48.6	43.09	0.15	9.59 E-10	19.69	662.9	16.73	8.6	15.95
Q1	5333	88.37	77.27	0.44	1.37 E-08	28.81	1202.4	26.89	15.55	28.85
Median	6949	102.21	86.54	0.51	2.91 E-08	32.2	1442.9	31.09	18.41	33.24
Mean	7072	101.42	86.64	0.5	3.85 E-08	32.92	1539	31.46	19.99	33.74
Q3	8523	114.23	96.65	0.57	4.84 E-08	35.9	1767.4	34.86	22.56	38.03
Max.	16752	170.87	134.34	0.79	2.19 E-07	69.59	5323.9	74.61	80.49	60.48

Summary data associated with **Table S2.1** in Appendix A. Minimum, maximum, mean, median, and first and third quartile values from a balanced dataset of PA15 field-grown maize inbreds, i.e. with n=174 per root node (1, 2, and 3), n=261 per nitrogen treatment. See **Table 1-1** for trait abbreviations and units. ECC (metaxylem vessel eccentricity) is reported here as median length to width ratio (LWR) of metaxylem vessels, from which eccentricity values were calculated.

	RXA	SXA	CXA	CSR	CF	CCS	MXN
Min.	0.2827	0.04901	0.22	1.866	5	783.4	4
Q1	0.7704	0.14641	0.6046	2.823	7.5	1289.1	7
Median	1.0476	0.24878	0.8016	3.298	9	1543.1	9
Mean	1.1424	0.27345	0.8697	3.51	8.985	1641.6	9.699
Q3	1.4071	0.35592	1.0597	4.005	10.5	1853.4	12
Max.	3.8396	1.03826	2.8013	7.243	14	4743.7	19

	AAP	MXA	MXP	MXM	ECC (LWR)	CDM
Min.	0	0.01115	10.8	1379	1.012	22.8
Q1	9.673	0.0314	18.68	4197	1.109	31.81
Median	20.059	0.0514	20.72	5373	1.156	35.57
Mean	20.597	0.05491	20.71	5637	1.165	36.36
Q3	30.316	0.07216	22.77	7030	1.21	39.41
Max.	61.904	0.15953	32.32	12485	1.499	62.8

The following raw datasets associated with Chapter 2 are available within this open-access ScholarSphere link, which contains the files listed below: https://doi.org/10.18113/S1GG93

Raw data associated with Table 1-2:
"pa16_hybrid_field_root_anatomy.csv"

Raw data associated with Appendix A, Table S2.1:
"pa15_inbred_field_root_anatomy.csv"

Raw data associated with Figure 1-8 and Appendix A, Figure S5:
"root_anatomy_across_nodes_in_field_studies.csv"

To cite raw data, use:
Yang, Jennifer T. (2017)."Integrating leaf and root phenotypes to enhance nitrogen use efficiency in maize (*Zea mays* L.)-Data". doi.org/10.18113/S1GG93

Appendix C

Supplementary figures and tables for Chapter 3

Table S1. Plant Materials.
See Tables S1.1 and S1.2 below.

Table S1.1 Root sampling
The following abbreviations are used: M# from IBM recombinant inbred line population, N# from NYH population.

Study	Root nodes sampled
GH1	2,3
GH2	2,3,4
PA13	2,3,4
PA14	1,2,3
PA15	1,2,3
PA16	2,3,4 all; 1,5,6 subset
SA14	2,3,4

Table S1.2 Plant materials

Inbred genotypes				**Hybrid genotypes** - PA16	
PA13	**PA14**	**SA14**	**PA15**	Code	Pedigree
M001	M001	M001	M30	1	TX714/PHZ51
M021	M021	M021	M59	2	B73 X PHM49
M030	M030	M030	M126	3	PHW52 X PHN82
M062	M048	M131	M129	4	PHG39/Tx205
M090	M059	M146	M178	5	LH195/LH82
M126	M111	M178	M181	6	PHW52/Tx205
M131	M129	M201	M201	7	LH198/PHZ51
M146	M146	M263	M277	8	PHB47/PHZ51
M178	M178	M277	M323	9	2369 / LH123Ht
M201	M178 (2)	M323	M352	10	B73/PHZ51
M263	M181	M345	M365	11	PB80/PHZ51
M265	M181 (2)	M352		12	W10004_0216/PHZ51
M277	M201	M365		13	(CML442-B/CML343-B-B-B-B-B-B)-B-B-1-1-B-B-B-1-B12-1-B19/LH195
M323	M263	M379		14	TX714/Tx777
M345	M277	N015		15	B73/Tx777
M365	M317	N039		16	B14A X H95
N015	M323	N054		17	B14A X Oh43
N023	M344	N060		18	B37 X H95
N039	M352	N068		19	B37 X Oh43
N042	M365	N113		20	B73 X Mo17
N054	M365 (2)	N126		21	B73 X PHN82
N060	N015	N128		22	B97 X PHB47
N068	N039	N128 (2)		23	F42 X Mo17
N104	N060	N158		24	F42 X Oh43
N113	N068	N181		25	LH212Ht X LH195
N126	N113	N208		26	LH74 X PHN82
N128	N126			27	PHG39 X PHN82
N129	N128			28	PHG80 X PHZ51
N181	N181			29	PHP02 X PHB47
N208	OWRI-55			30	PHW52 X PHM49
				31	Wf9 X H95
				32	PHN11_PHG47_0251 X PHB47
				33	W10001_0022 X PHB47
				34	W10005_0107 X PHB47
				35	W37A X PHB47
				36	PHN11_Oh43_0001 X PHB47
				37	LH216 X LH195
				38	PHN11_PHW65_0323 X LH195
				39	B14A X Mo17
				40	B37 X Mo17
				41	F42 X H95
				42	PHG29 X PHG47
				43	2369 X 3IIH6
				44	LH123HT X 3IIH6

Table S2. Nitrogen stress levels across experiments. Percent reduction refers to average across genotypes. Range refers to range among genotypes.

Study	No. of genotypes	Metric	% Reduction	Range
GH1	8	Dry shoot mass	80	69 – 88%
GH2	8	Dry shoot mass	46	29 – 60%
PA13	30	Yield	20	0 – 44%
		Dry shoot mass	4	0 – 40%
PA14	27	Yield	20	4 – 50%
		Dry shoot mass	23	0 – 37%
SA14	25	Dry shoot mass	55	32 – 72%
PA15	11	Yield	30	15 – 55%
		Dry shoot mass	20	12 – 31%
PA16	44	Yield	60	42 – 78%
		Dry shoot mass	53	23 – 74%

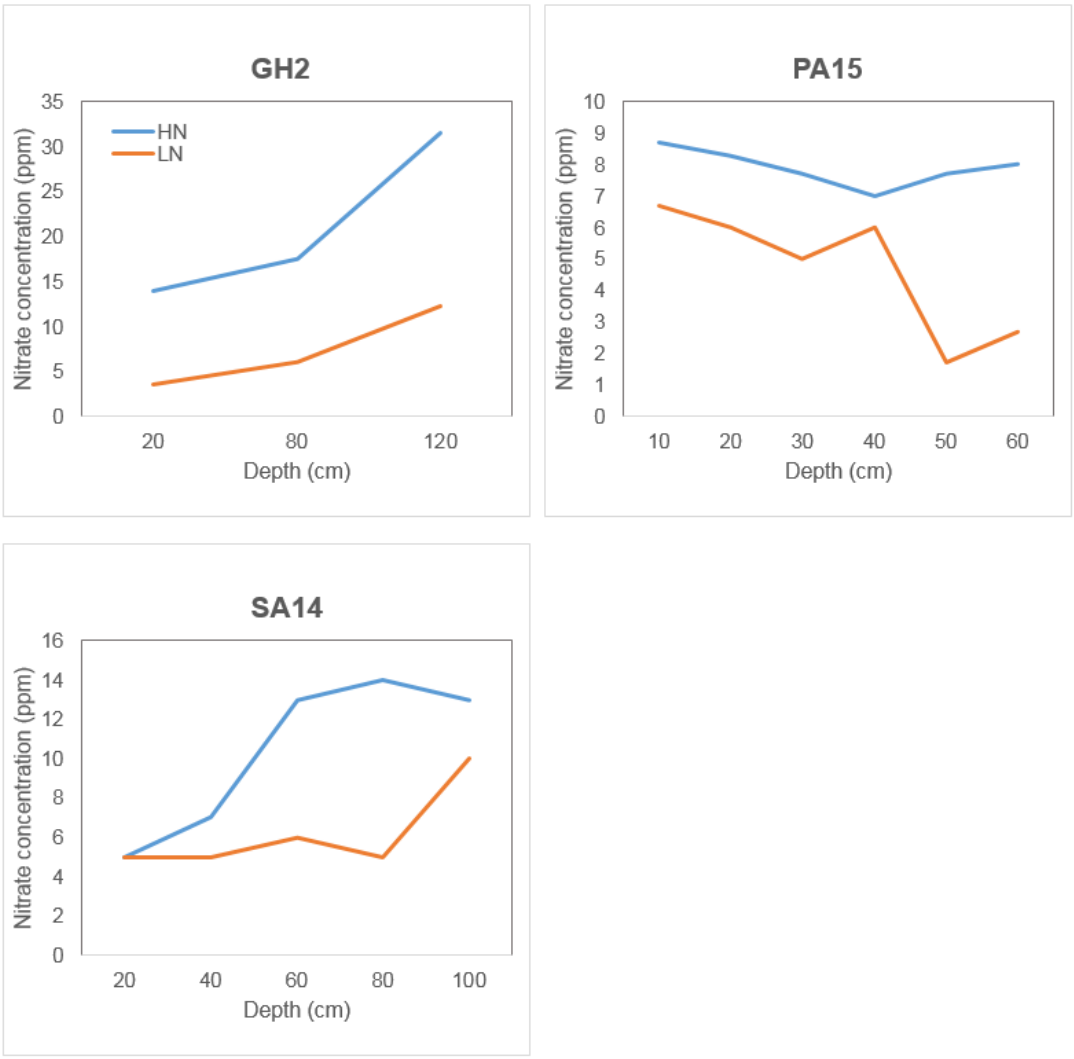

Fig S1. Nitrate concentrations by depth in greenhouse and field experiments. Nitrate concentration from soil or media extracts, averaged across soil or media samples from at least two replicates in GH2, PA15, and SA14, from the indicated depths in high (HN, blue) or low (LN, orange) nitrogen treatments.

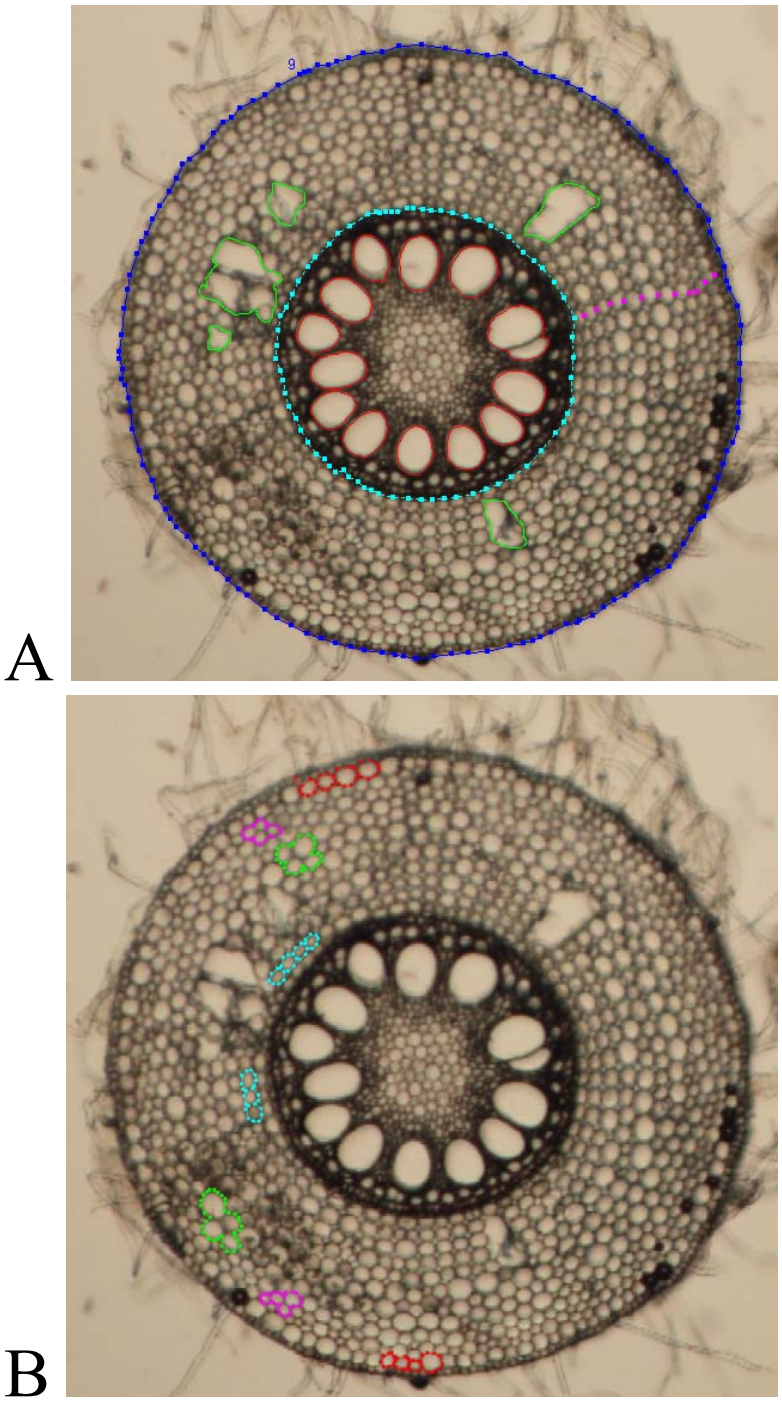

Fig S2. Maize root cross-section image analysis. An ObjectJ macro in ImageJ was created to semi-automate analysis of root-cross section images. The same anatomical traits were analyzed in LAT and manually sectioned roots, with minor differences in methodology. An example of an analyzed LAT image is given in Chapter 1. An example of an analyzed image from manual cross-sections is below. **(A)** The root (dark blue, outer), stele (cyan, inner), and aerenchyma (green) were outlined and total areas and

ratios calculated. Individual metaxylem vessels were traced (red) and individual and total areas determined. Vessels beginning to divide were traced as a single vessel (as seen below). Images were zoomed in to allow accurate tracing along the outer edge of each vessel. Cortical cell file number was manually counted in three positions to account for root asymmetry, and a representative axis across the cortex was selected to record a representative cell file count (the count of pink points) and measure cell diameters of each cell file (distance between every consecutive pink point). The innermost cell layer (i.e. distance between the innermost pink point and the stele boundary) was often incomplete and was not recorded. The cell diameters were used to calculate hypodermis (HYP), outermost (OUT) and innermost (INN). **(B)** For one full replicate, the inner (cyan), mid (green), outer (pink), and hypodermis (red) cortical cell sizes were determined and used to validate estimates from cell diameters as described above. Up to eight representative cells per layer were traced and average cell cross-sectional areas were calculated. Images were zoomed in to allow careful tracing of the outer edge of the cells; cell walls were included in the trace. Unlike LAT images, manual cross-sections from greenhouse-grown plants showed intact epidermis cells and root hairs.

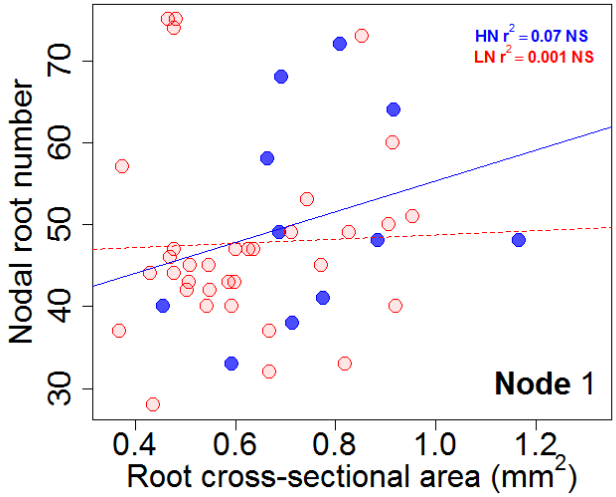
HN r2 = 0.07 NS
LN r2 = 0.001 NS
Node 1
Nodal root number
30
40
50
60
70
0.4
0.6
0.8
1.0
1.2
Root cross-sectional area (mm2)

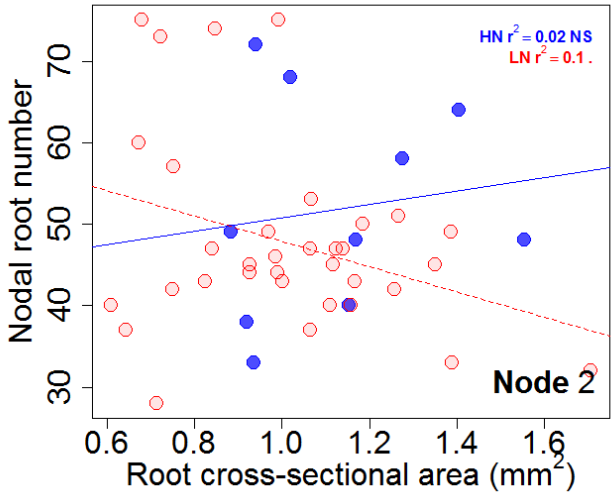
HN r2 = 0.02 NS
LN r2 = 0.1 .
Node 2
Nodal root number
30
40
50
60
70
0.6
0.8
1.0
1.2
1.4
1.6
Root cross-sectional area (mm2)

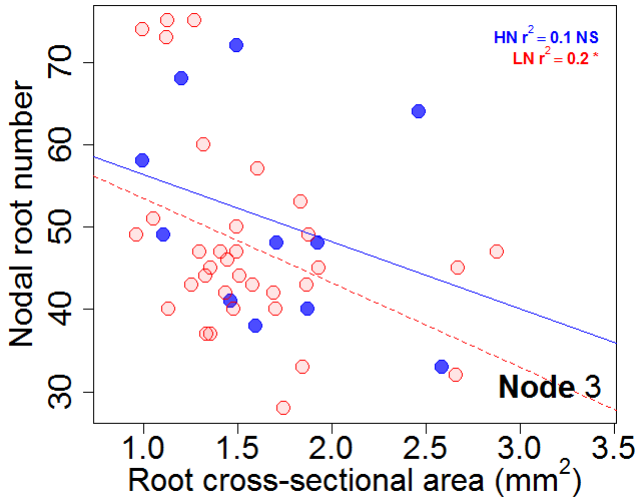
HN r2 = 0.1 NS
LN r2 = 0.2 *
Node 3
Nodal root number
30
40
50
60
70
1.0
1.5
2.0
2.5
3.0
3.5
Root cross-sectional area (mm2)

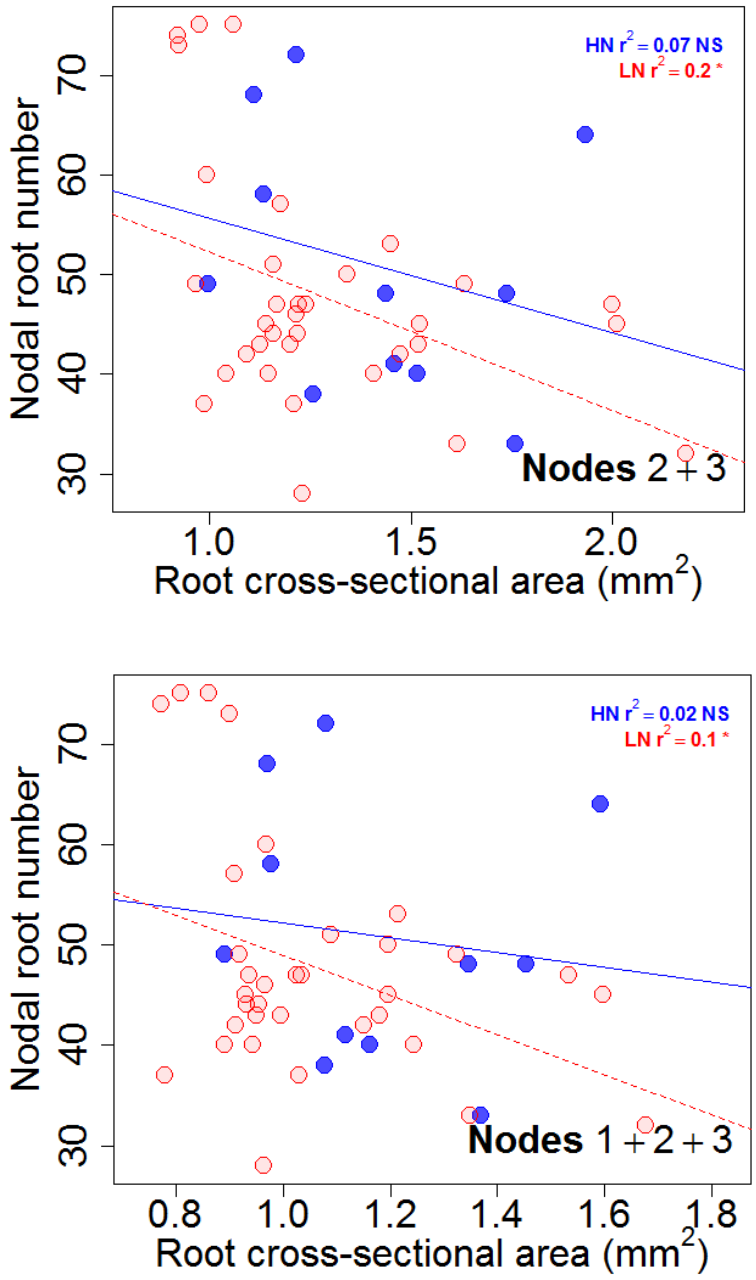

Fig S3. **Relationship between nodal root number and diameter among maize inbreds in the field**. Linear regression of total number of emerged nodal roots at harvest and root cross-sectional area averaged from two roots from each of the indicated nodes, from individual plants of 11 maize IBM RILs grown in high (HN, blue) or low nitrogen (LN, red) treatments in PA15 (see Appendix C, Tables S1 and S2). R^2 value and significance ($p < 0.1$., 0.05*, NS, not significant) are indicated. Nodal root number was evaluated in four replicates in LN and one replicate in HN.

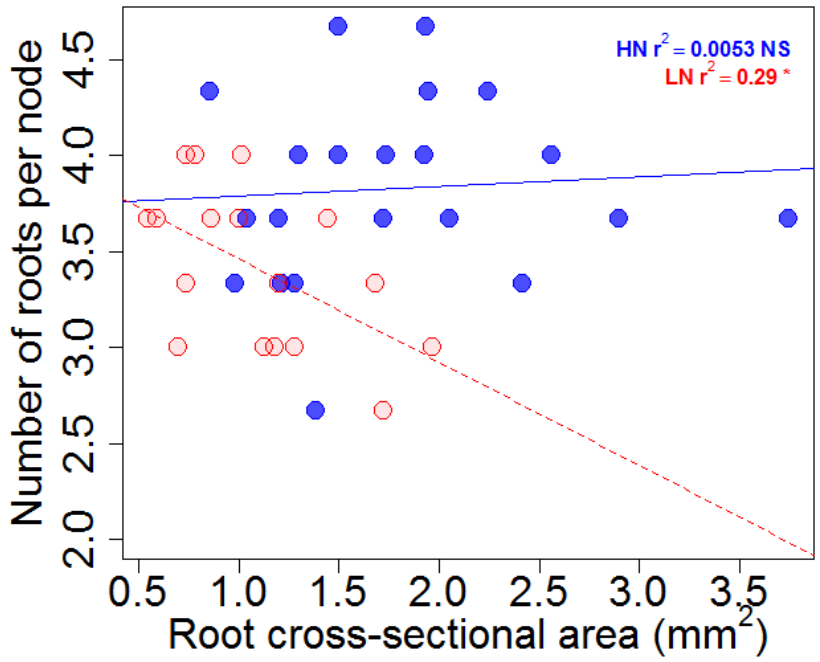
HN r2 = 0.0053 NS
LN r2 = 0.29 *
Number of roots per node
2.0
2.5
3.0
3.5
4.0
4.5
0.5
1.0
1.5
2.0
2.5
3.0
3.5
Root cross-sectional area (mm2)

A

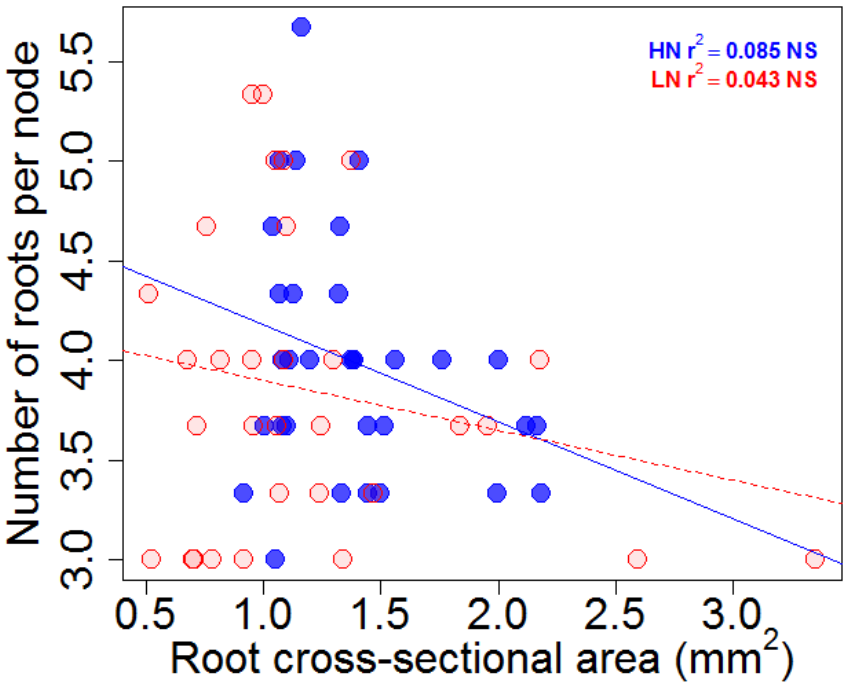
HN r2 = 0.085 NS
LN r2 = 0.043 NS
Number of roots per node
3.0
3.5
4.0
4.5
5.0
5.5
0.5
1.0
1.5
2.0
2.5
3.0
Root cross-sectional area (mm2)

B

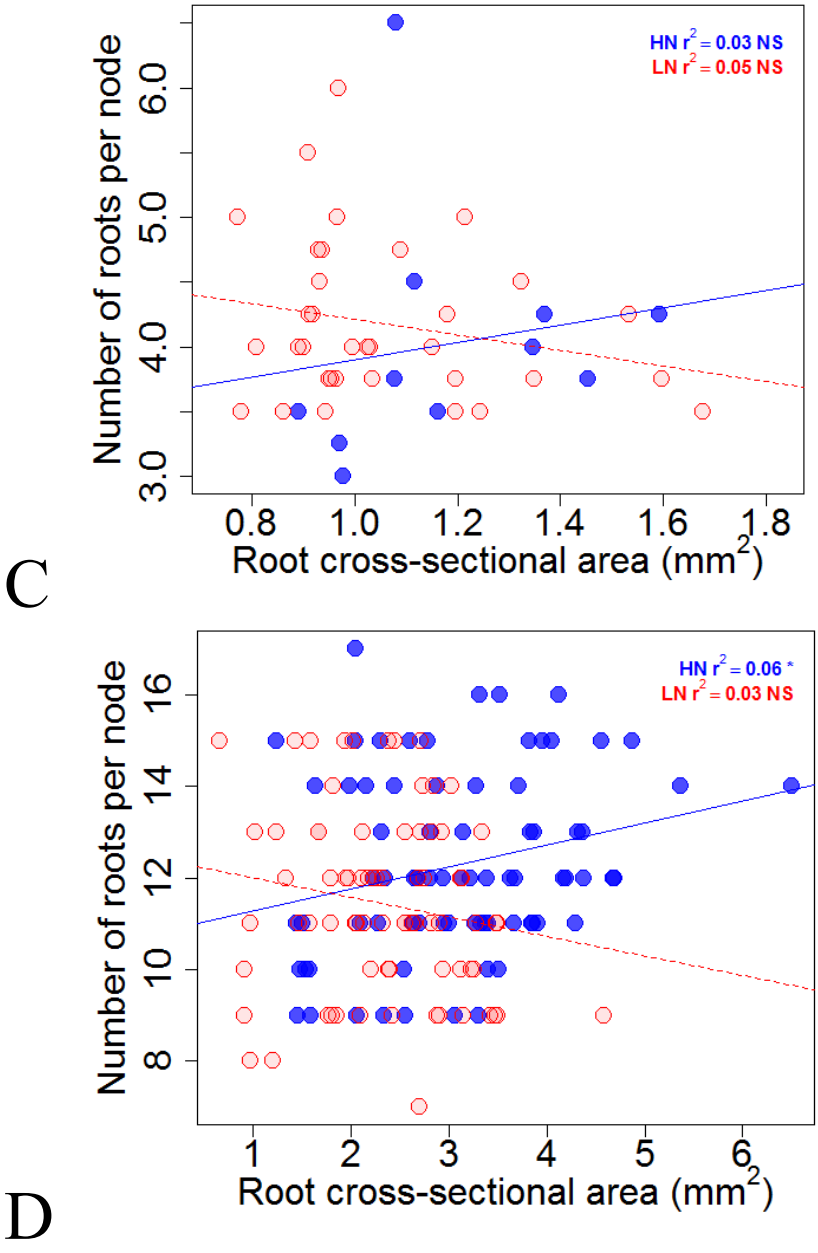

Fig S4. **Relationship between nodal root occupancy and diameter among maize genotypes**. Linear regressions of the average number of roots per node (NO) and root cross-sectional area (RXA) averaged from two roots from each of the indicated nodes from individual plants in **(A)** GH1 (RXA from nodes 2, 3; NO from nodes 1, 2, 3), **(B)** GH2 (RXA from nodes 2, 3; NO from nodes 1, 2, 3), **(C)** PA15 (RXA from nodes 1, 2, 3; NO from nodes 1, 2, 3, 4), and **(D)** PA16 (RXA from nodes 2,3,4; NO from nodes 1, 2, 3, 4) grown in high (HN, blue) or low nitrogen (LN, red) (see Appendix C, Tables S1 and S2). R^2 value and significance ($p< 0.1$., 0.05*, 0.01**, 0.001***; NS, not significant) are indicated. For PA15, the number of nodes was evaluated in four replicates in LN and one replicate in HN. Plants with missing values were excluded.

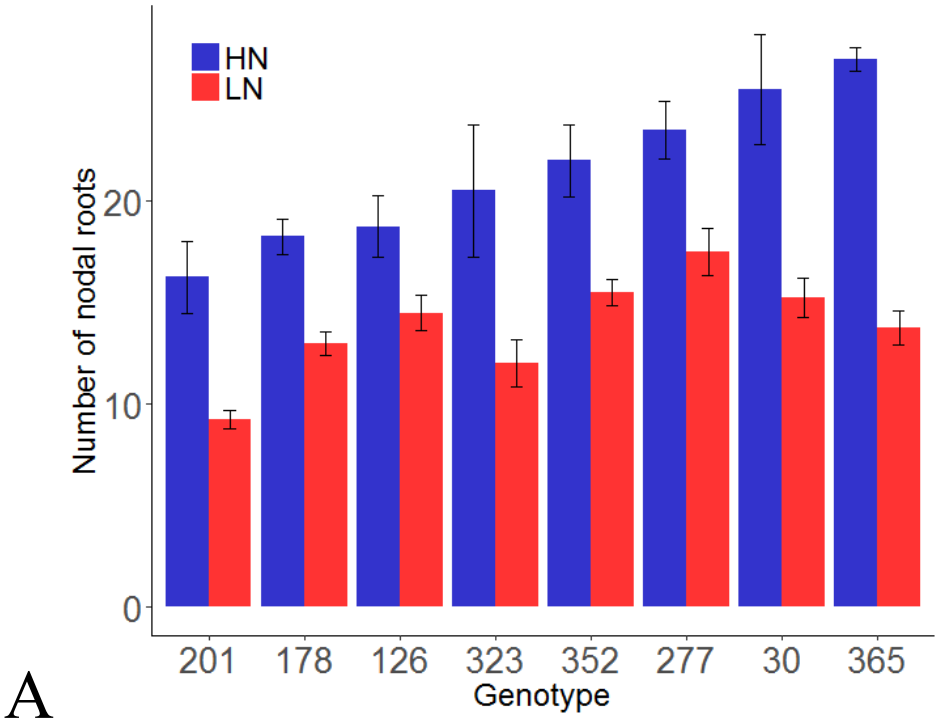
HN
LN
Number of nodal roots
0
10
20
201
178
126
323
352
277
30
365
Genotype

A

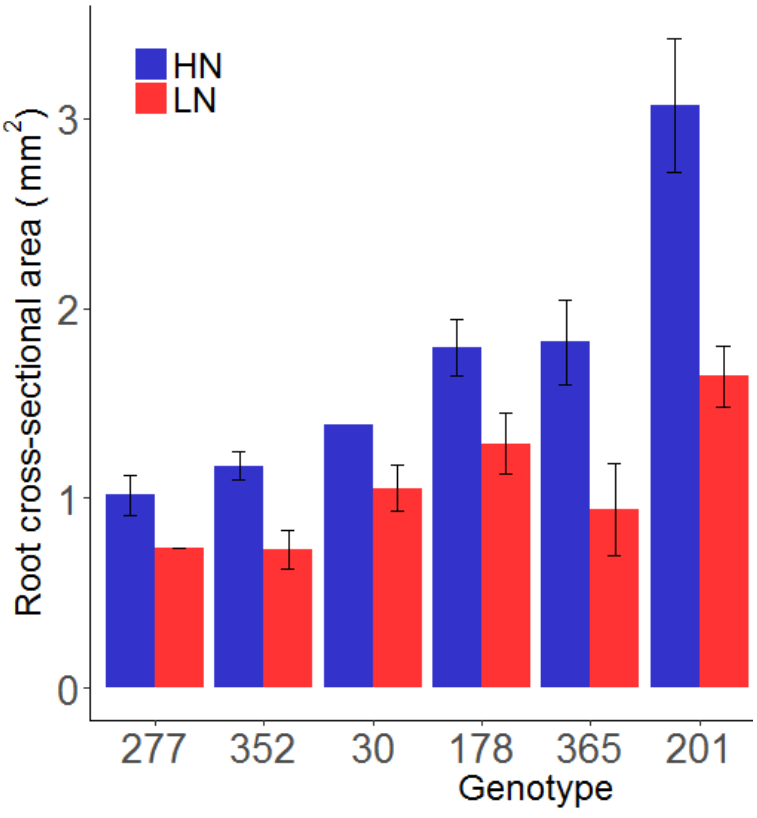
HN
LN
Root cross-sectional area (mm^2)
0
1
2
3
277
352
30
178
365
201
Genotype

B

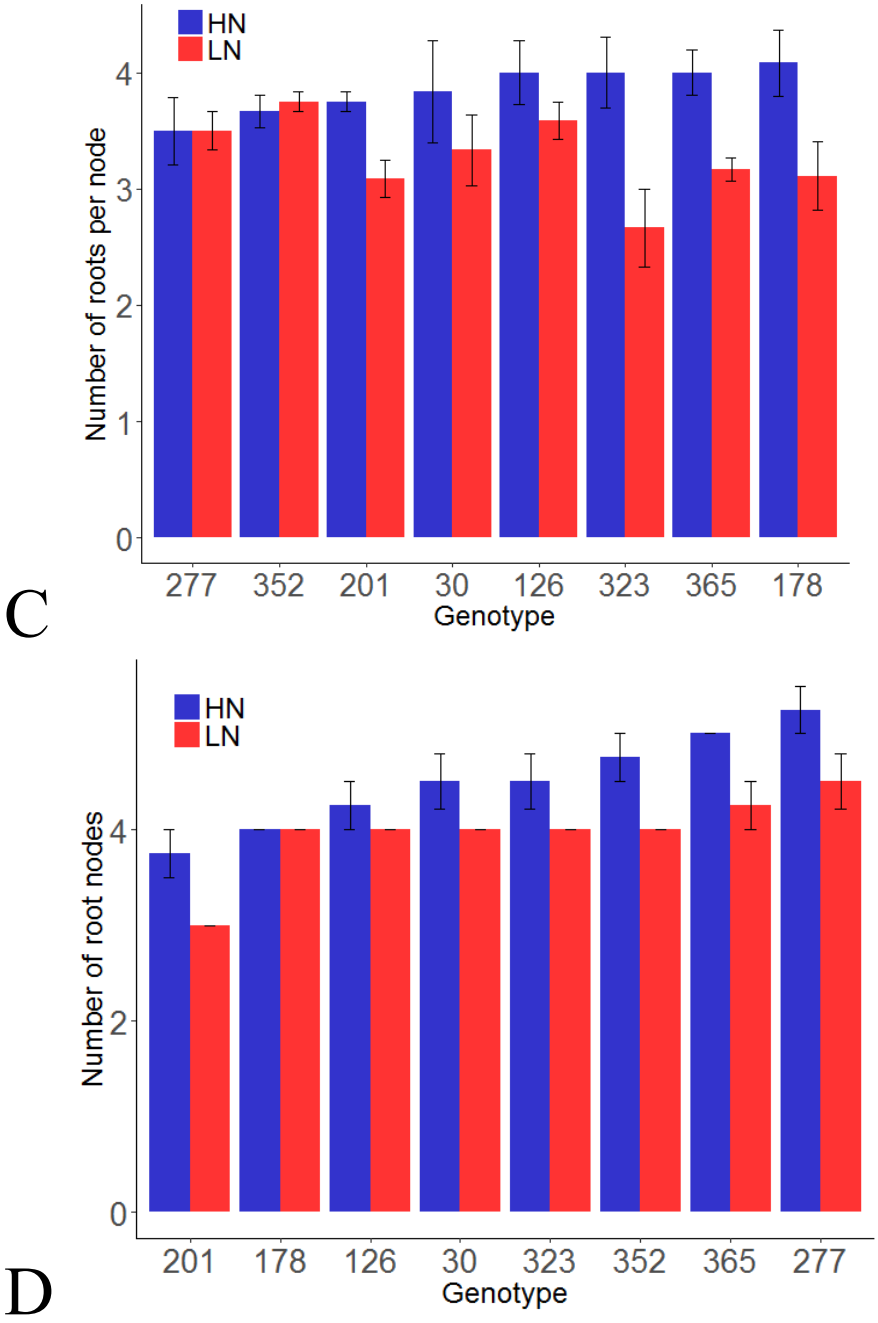

Fig S5. Genotypic contrast in nodal root number and diameter among maize inbreds. Means ± SE of **(A)** total number of nodal roots (NRN) emerged at harvest, and **(B)** root cross-sectional area (RXA), averaged from two roots each from nodes 2 and 3, **(C)** number of nodal roots per node (NO), averaged from the first three nodes, and **(D)** number of developed root nodes at harvest (NN), for maize RILs in GH1 (n=4 plants per RIL per nitrogen treatment). Genotypes are IBM RIL numbers and are arranged in ascending order by high nitrogen trait values. High and low nitrogen treatments are indicated (HN, blue; LN, red). M0 126 and M0 323 were excluded from (B) due to missing RXA data in low nitrogen.

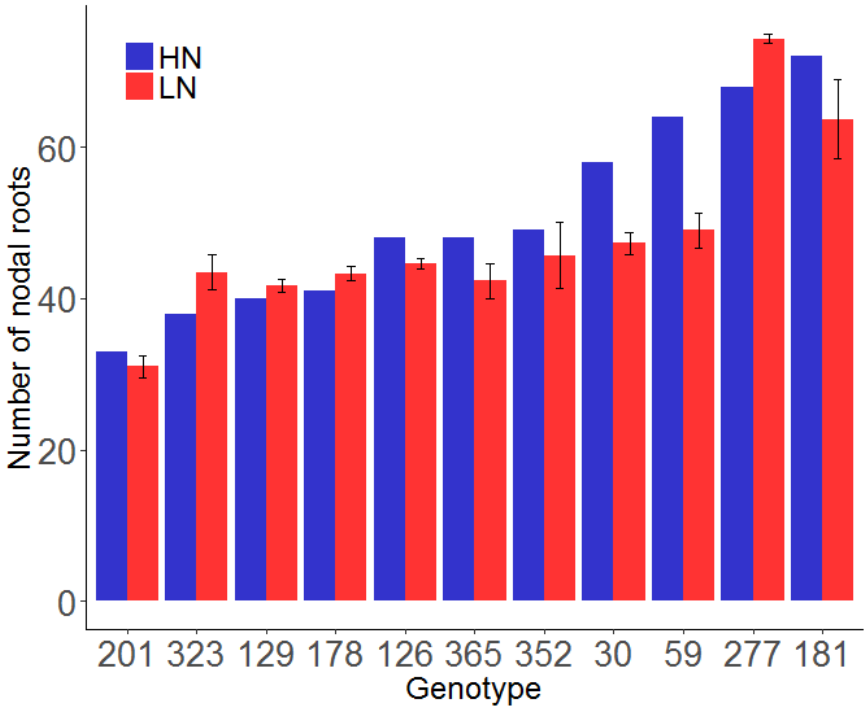
HN
LN
Number of nodal roots
0
20
40
60
201 323 129 178 126 365 352 30 59 277 181
Genotype

A

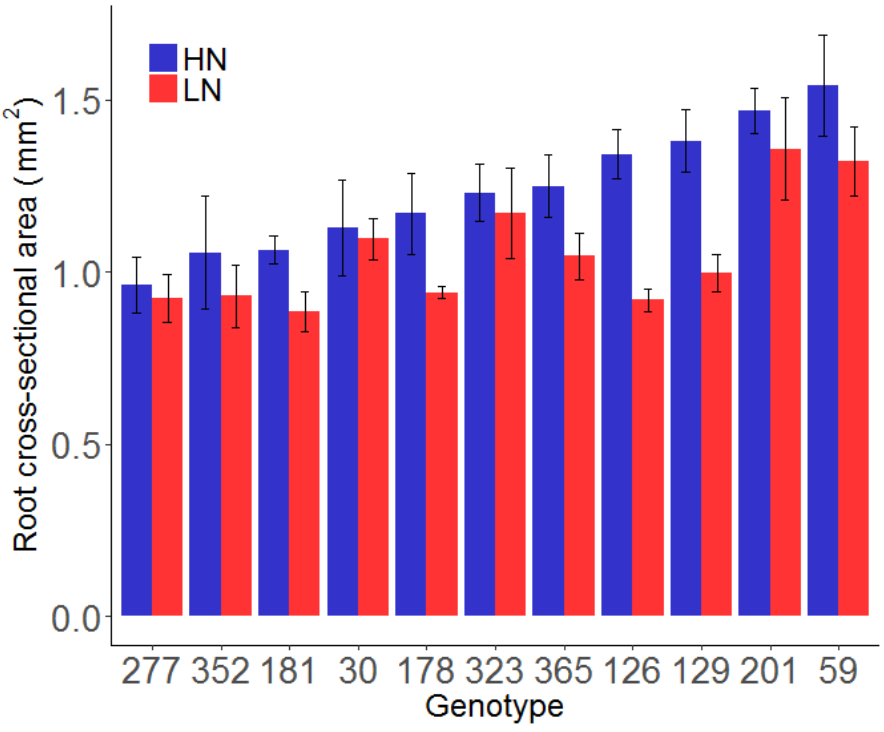
HN
LN
Root cross-sectional area (mm2)
0.0
0.5
1.0
1.5
277 352 181 30 178 323 365 126 129 201 59
Genotype

B

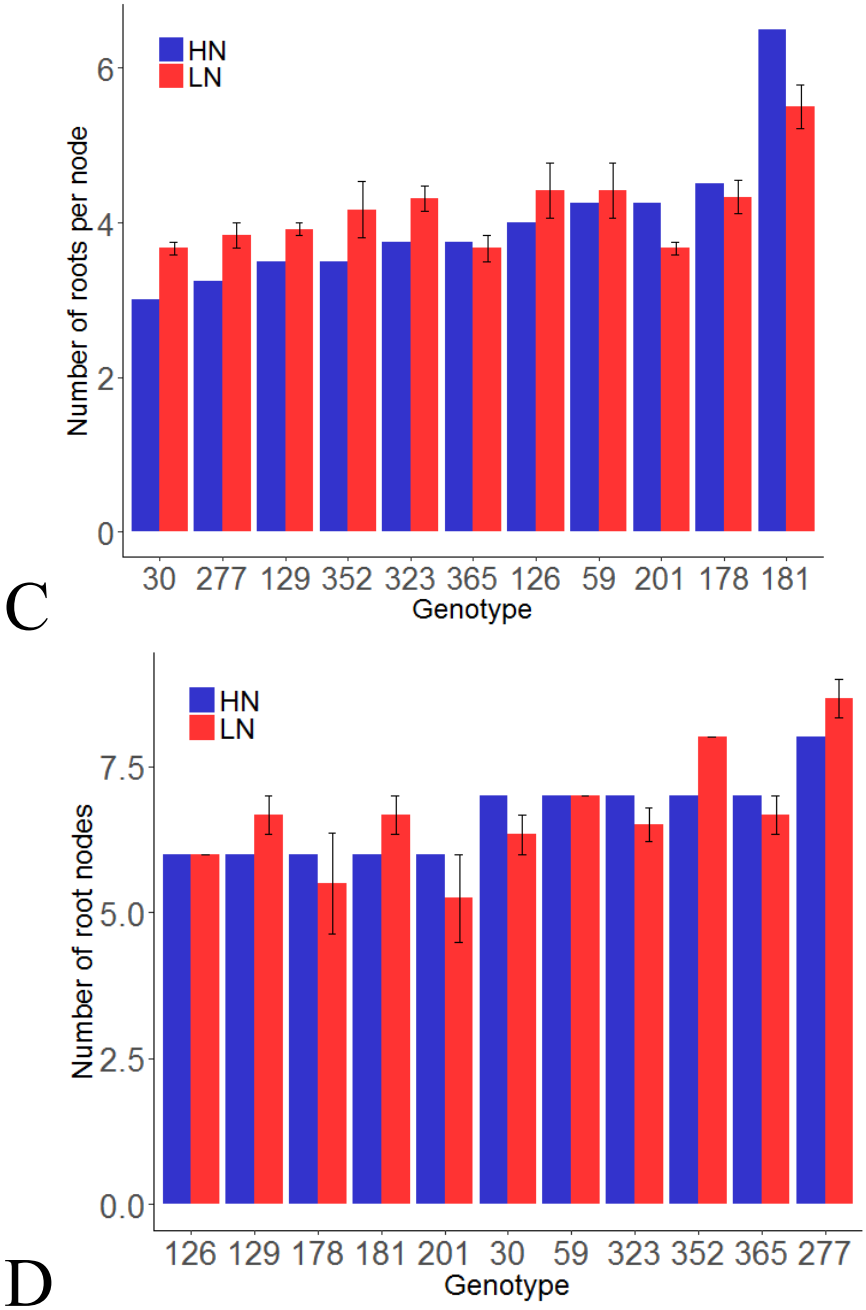

Fig S6. Genotypic contrast in nodal root number and diameter among maize inbreds. Means ± SE of **(A)** total number of nodal roots (NRN) emerged at harvest, and **(B)** root cross-sectional area (RXA), averaged from two roots each from nodes 1, 2 and 3, **(C)** number of nodal roots per node (NO), averaged from the first three nodes, and **(D)** number of developed root nodes at harvest (NN), for maize RILs in PA15 (n=4 plants per RIL per nitrogen treatment). Genotypes are IBM RIL numbers and are arranged in ascending order by high nitrogen trait values. High and low nitrogen treatments are indicated (HN, blue; LN, red). For NRN, NN, and NO, nodal roots were counted in four reps in LN and one rep in HN.

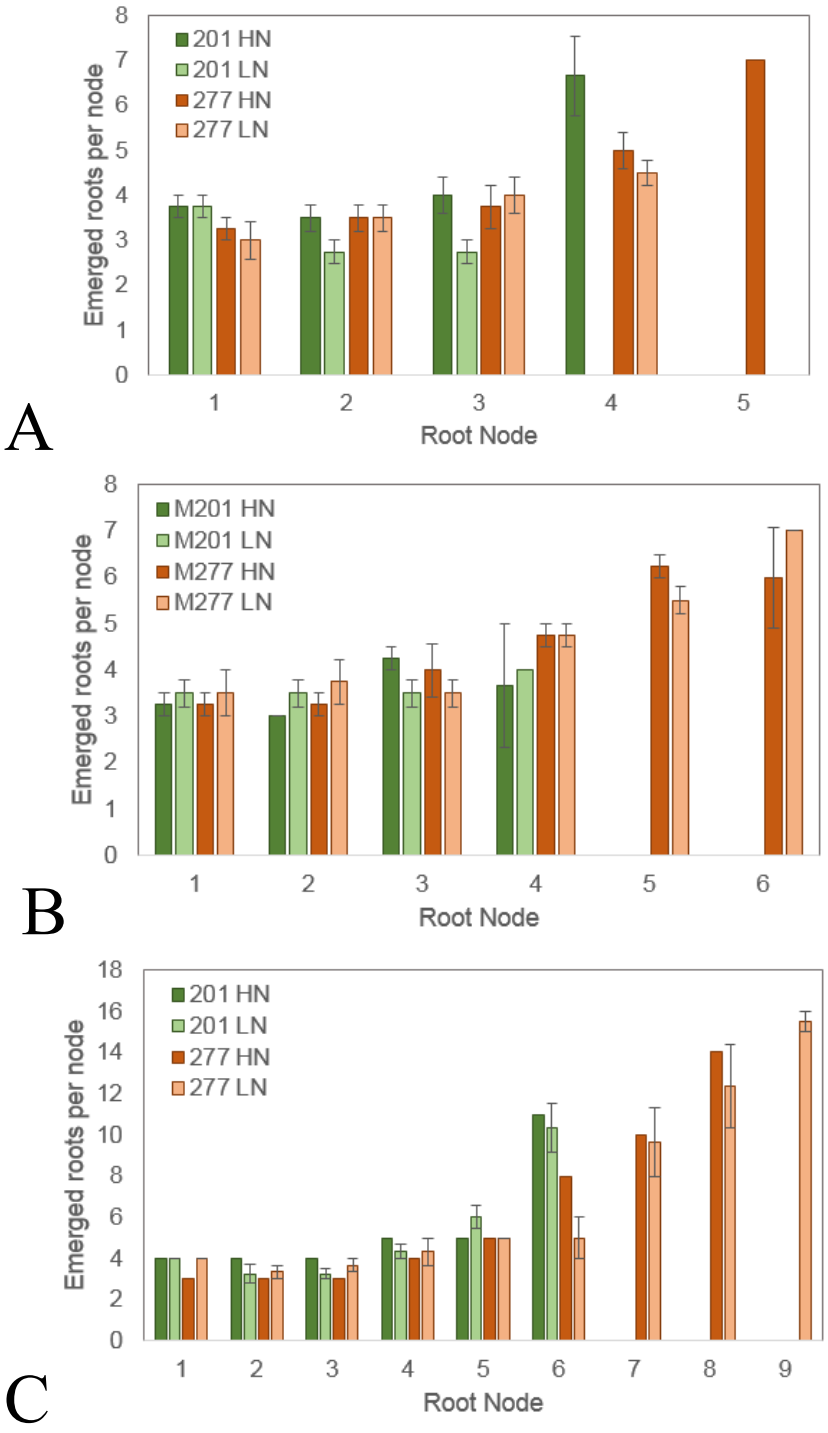

Fig S7. Nodal occupancy per node in IBM RILs M0 201 and M0 277. Means ± SE of number of emerged axial roots per node for M0 201 (green) and M0 277 (orange) in **(A)** GH1, **(B)** GH2, **(C)** PA15, under high (HN) and low nitrogen (LN) conditions as indicated in each legend. In PA15, nodal roots were counted in four reps in LN and one rep in HN, otherwise n=4 plants per RIL per nitrogen treatment.

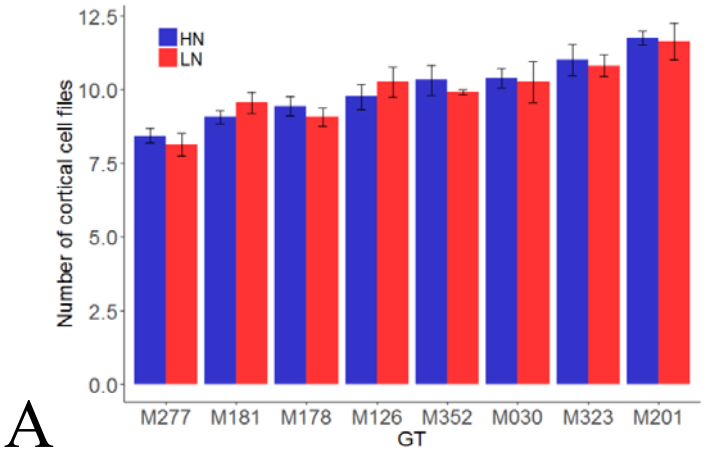
HN
LN
Number of cortical cell files
12.5
10.0
7.5
5.0
2.5
0.0
M277 M181 M178 M126 M352 M030 M323 M201
GT

A

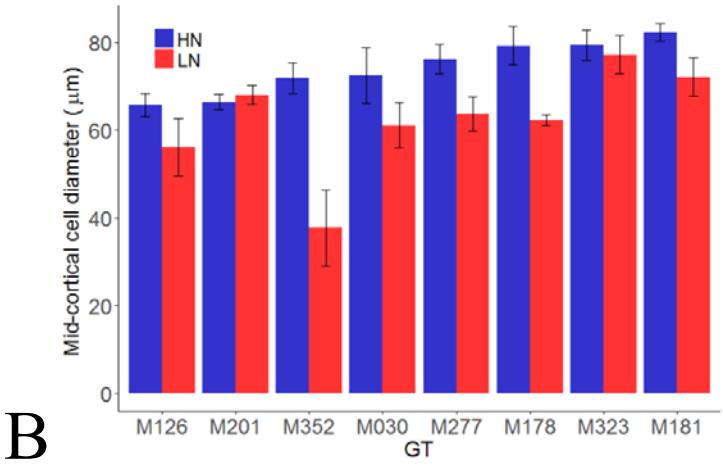
HN
LN
Mid-cortical cell diameter (μm)
80
60
40
20
0
M126 M201 M352 M030 M277 M178 M323 M181
GT

B

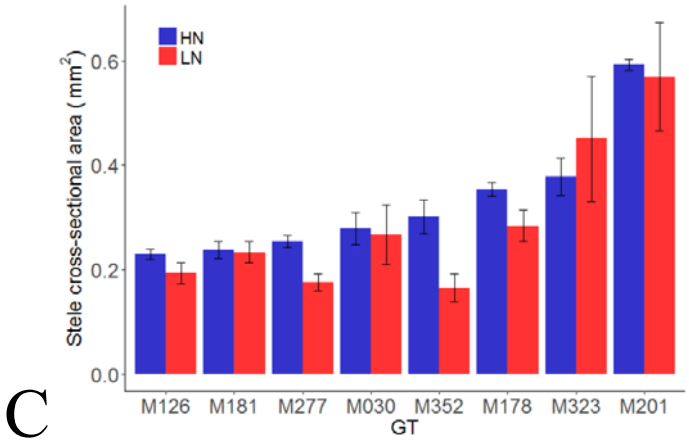
HN
LN
Stele cross-sectional area (mm²)
0.6
0.4
0.2
0.0
M126 M181 M277 M030 M352 M178 M323 M201
GT

C

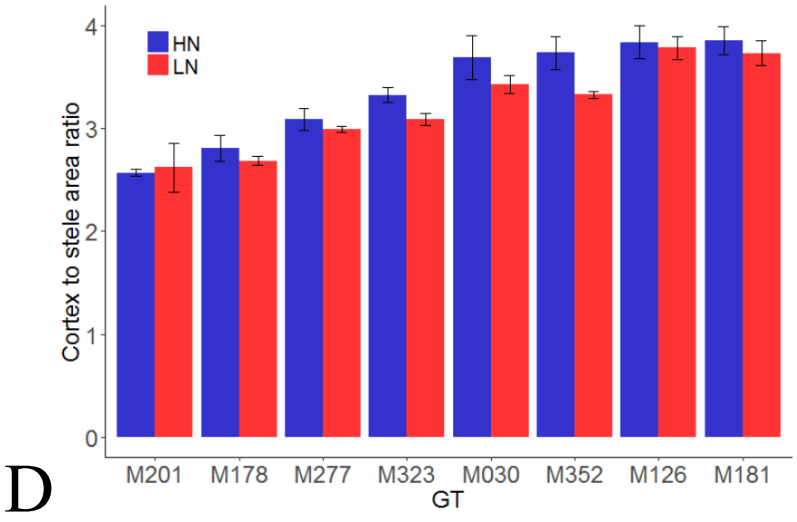
HN
LN
Cortex to stele area ratio
0
1
2
3
4
M201
M178
M277
M323
M030
M352
M126
M181
GT

D

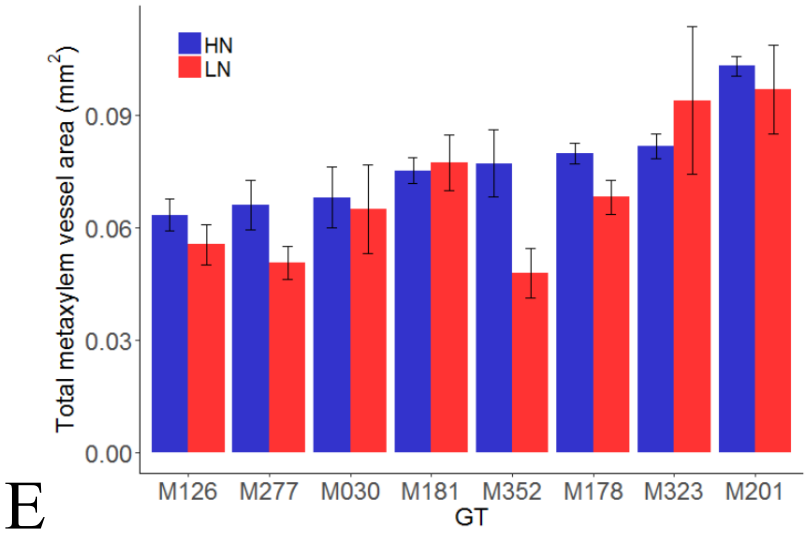
HN
LN
Total metaxylem vessel area (mm^2)
0.00
0.03
0.06
0.09
M126
M277
M030
M181
M352
M178
M323
M201
GT

E

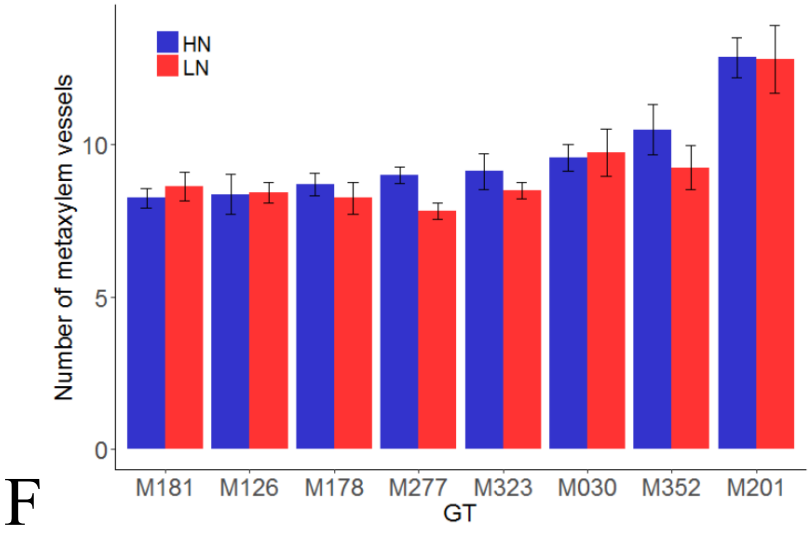
HN
LN
Number of metaxylem vessels
0
5
10
M181
M126
M178
M277
M323
M030
M352
M201
GT

F

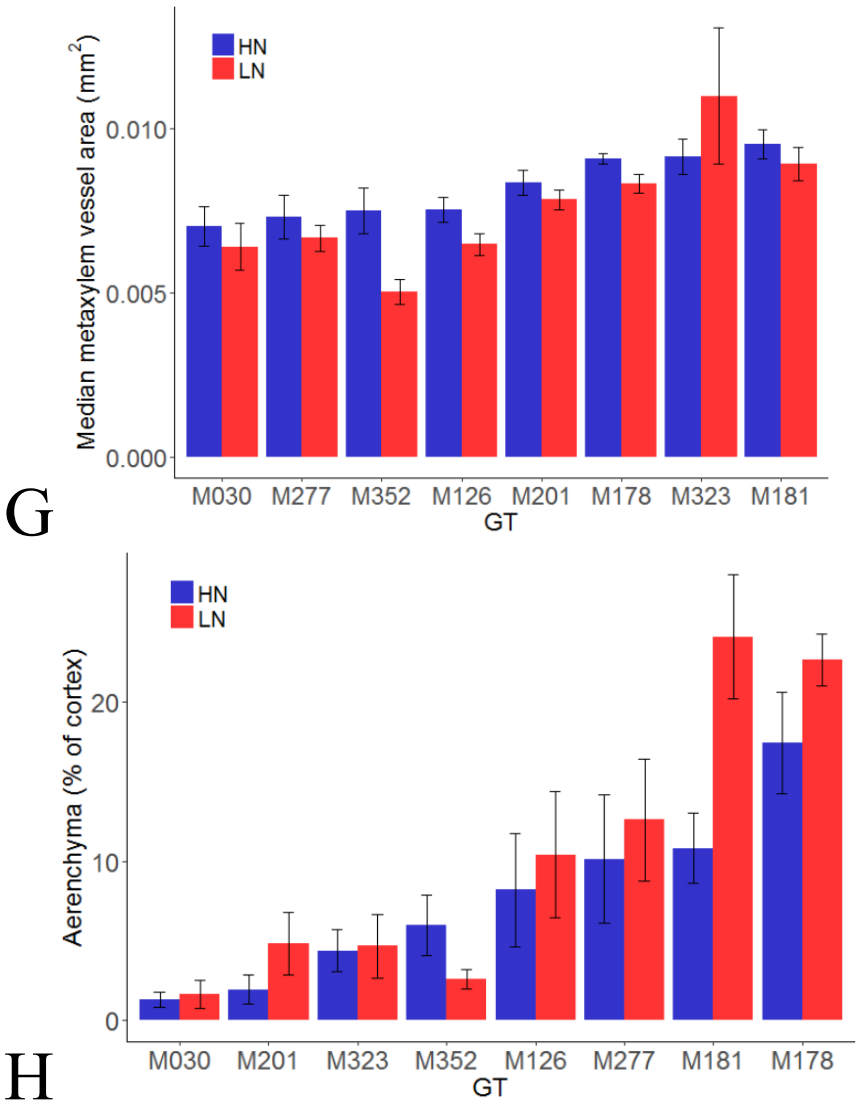

Fig S8. Genotypic contrast in nodal root anatomy among maize IBM RILs. Means ± SE of **(A)** number of cortical cell files, **(B)** mid-cortical cell diameter, **(C)** stele cross-sectional area, **(D)** cortex to stele area ratio, **(E)** total metaxylem vessel area, **(F)** number of metaxylem vessels, **(G)** median area of a single metaxylem vessel, and **(H)** percent of cortical aerenchyma, all averaged from two roots each in nodes 2 and 3, for maize RILs in GH2. Genotypes (GT) are IBM RIL numbers as indicated by M# and arranged in ascending order by high nitrogen trait values. High and low nitrogen treatments are indicated (HN, blue; LN, red).

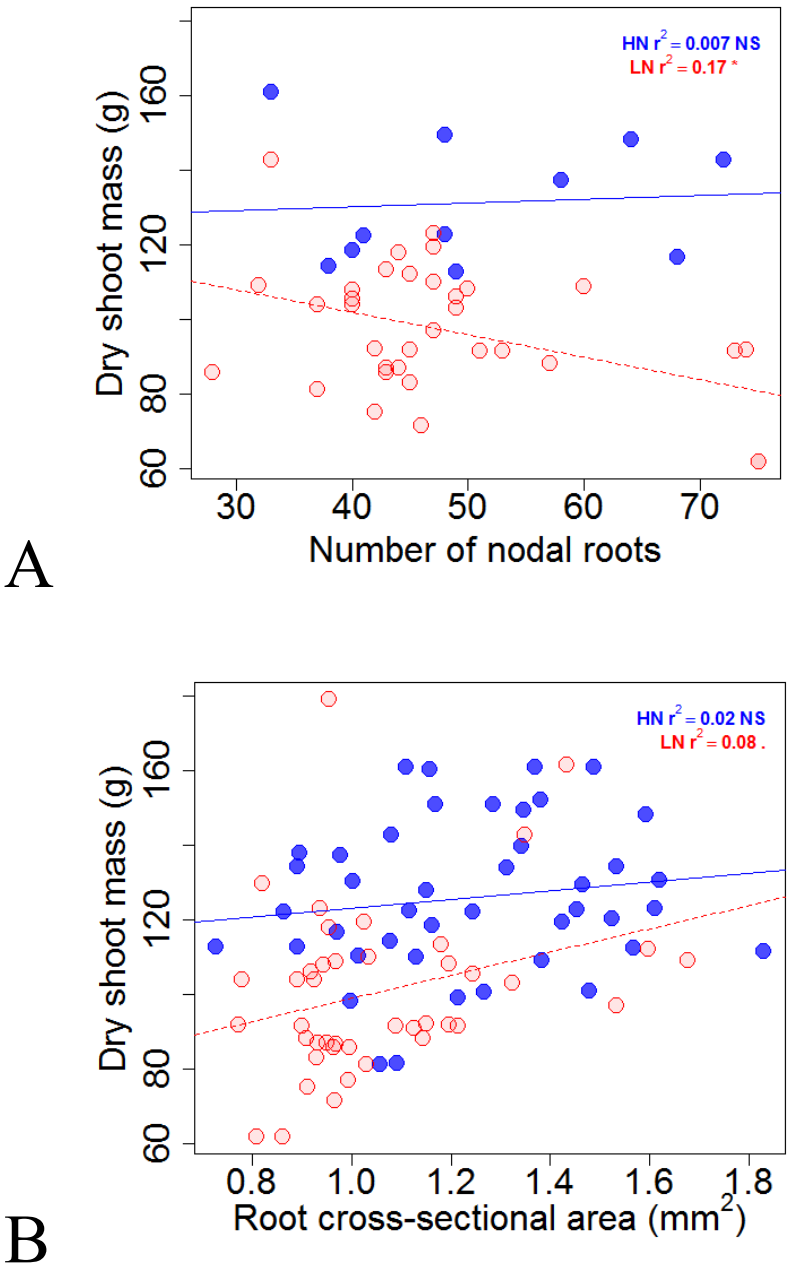

Fig S9. Relationship between shoot biomass, nodal root number and diameter among field-grown maize inbreds. Linear regression of **(A)** total number of nodal roots at harvest (NRN) and **(B)** root cross-sectional area (RXA) averaged from two roots each from the first three nodes, against total dry shoot biomass, from individual plants of 11 maize IBM RILs grown in high (HN, blue) or mild low nitrogen (LN, red) treatments in PA15. R^2 value and significance ($p< 0.1$., 0.05*, NS, not significant) are indicated. Plants with missing values were excluded. For NRN, nodal roots were evaluated in four reps in LN and one rep in HN.

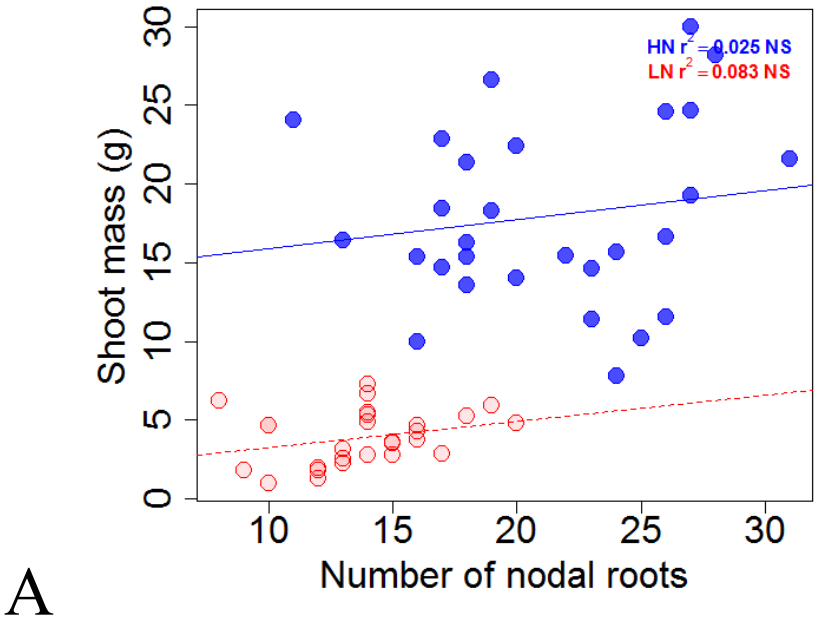

A

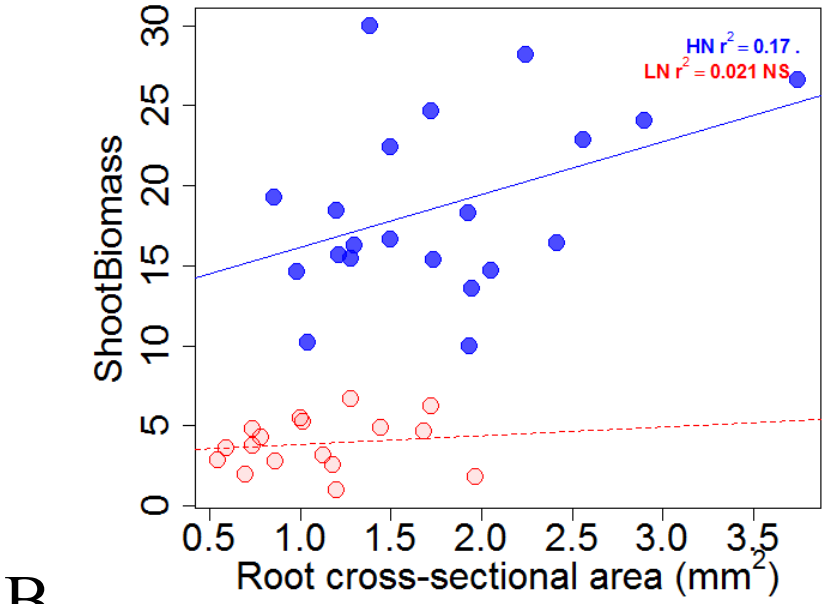

B

Fig S10. Relationship between shoot biomass, nodal root number and diameter among maize RILs under severe nitrogen stress. Linear regression of **(A)** total number of nodal roots at harvest (NRN) and **(B)** root cross-sectional area (RXA) averaged from two second and third node roots, against total dry shoot biomass, from individual plants of eight maize IBM RILs grown in high (HN, blue) or severe low nitrogen (LN, red) treatments in GH1. R^2 value and significance ($p< 0.1$., 0.05*, NS, not significant) are indicated. Plants with missing values were excluded.

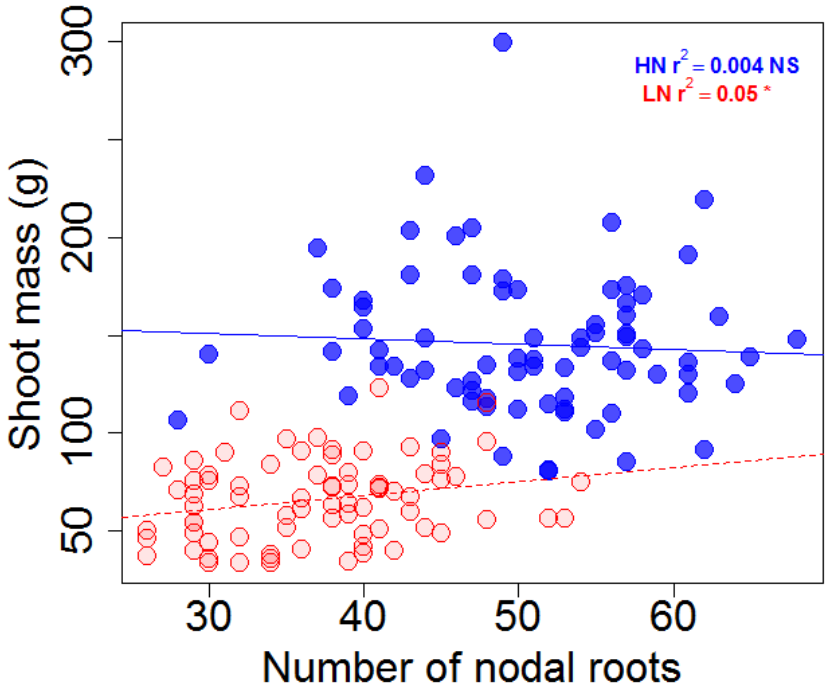
HN r2 = 0.004 NS
LN r2 = 0.05 *
Shoot mass (g)
50
100
200
300
30
40
50
60
Number of nodal roots

A

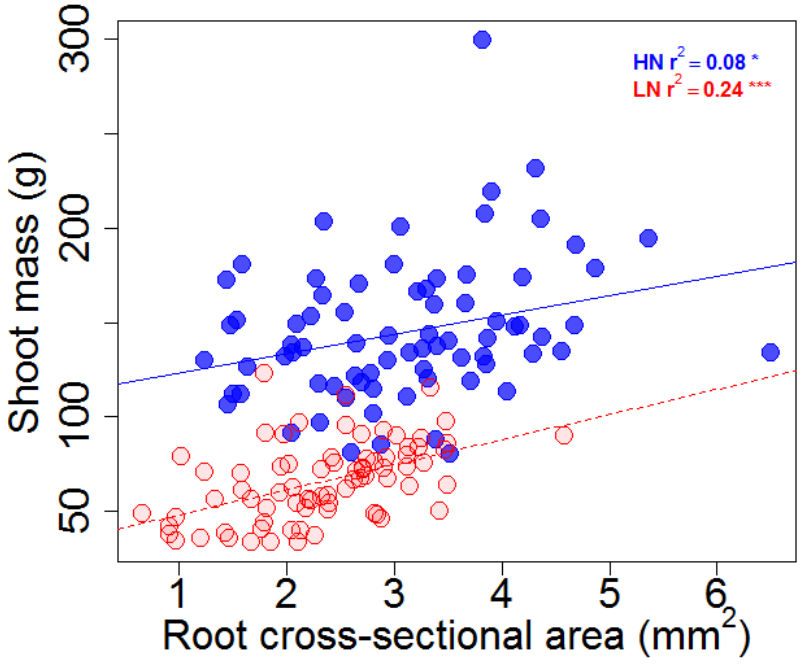
HN r2 = 0.08 *
LN r2 = 0.24 ***
Shoot mass (g)
50
100
200
300
1
2
3
4
5
6
Root cross-sectional area (mm2)

B

C

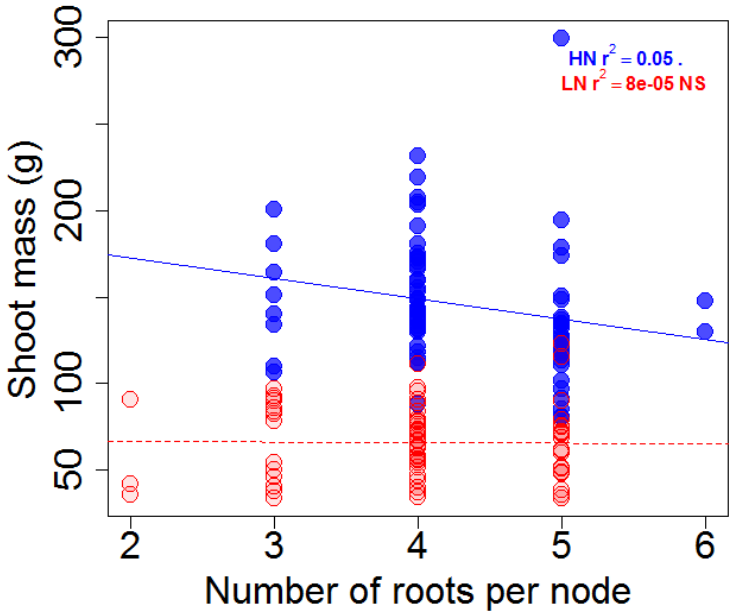

D

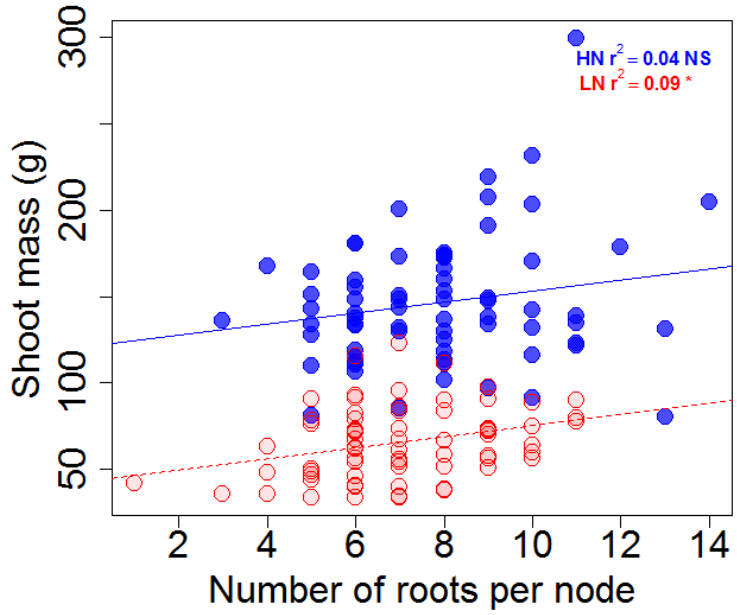

Fig S11. Relationship between shoot biomass, nodal root number and diameter among maize hybrids. Linear regression of **(A)** total number of nodal roots at harvest (NRN), **(B)** root cross-sectional area (RXA) averaged from two roots each from nodes 2, 3, and 4, **(C)** average number of roots in the first node, and **(D)** average number of nodal roots in the fifth node, against dry shoot biomass, from individual plants of 44 diverse field-grown maize hybrid genotypes grown in high (HN, blue) or moderate low nitrogen (LN, red) treatments in PA16. R^2 value and significance ($p< 0.1$., 0.05*, 0.001***, NS, not significant) are indicated. Plants with missing values were excluded.

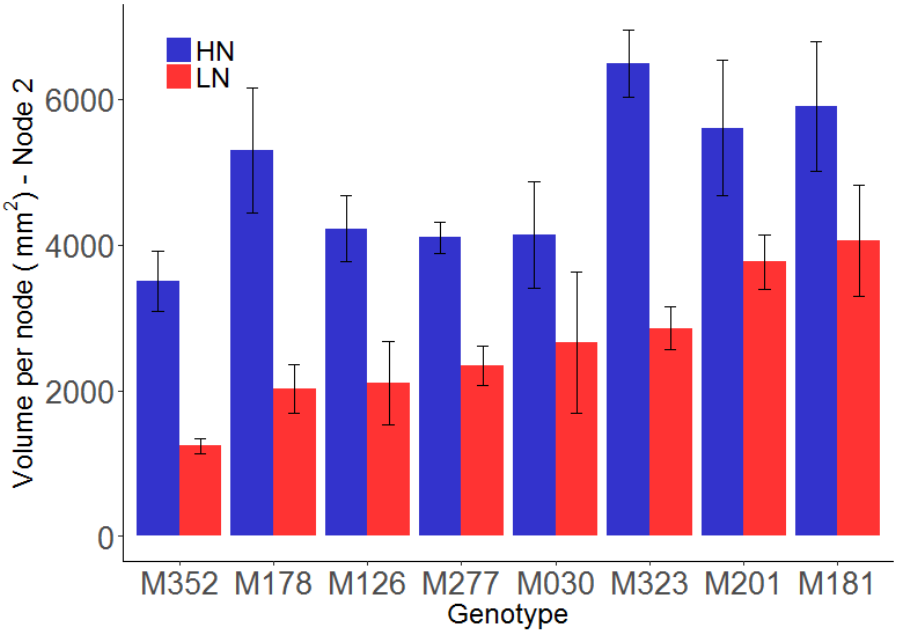
HN
LN
Volume per node (mm^2) - Node 2
6000
4000
2000
0
M352 M178 M126 M277 M030 M323 M201 M181
Genotype

A

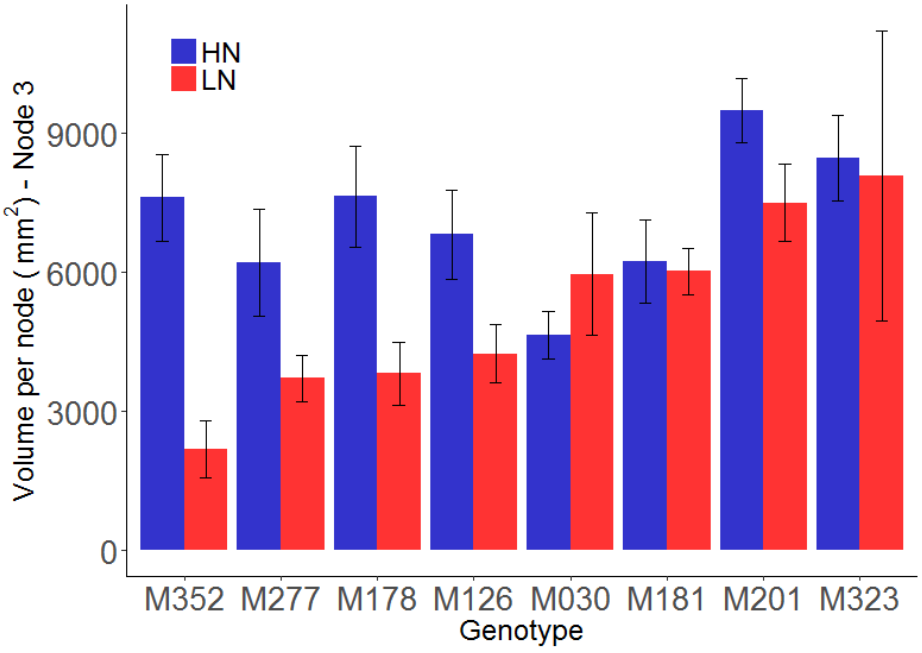
HN
LN
Volume per node (mm^2) - Node 3
9000
6000
3000
0
M352 M277 M178 M126 M030 M181 M201 M323
Genotype

B

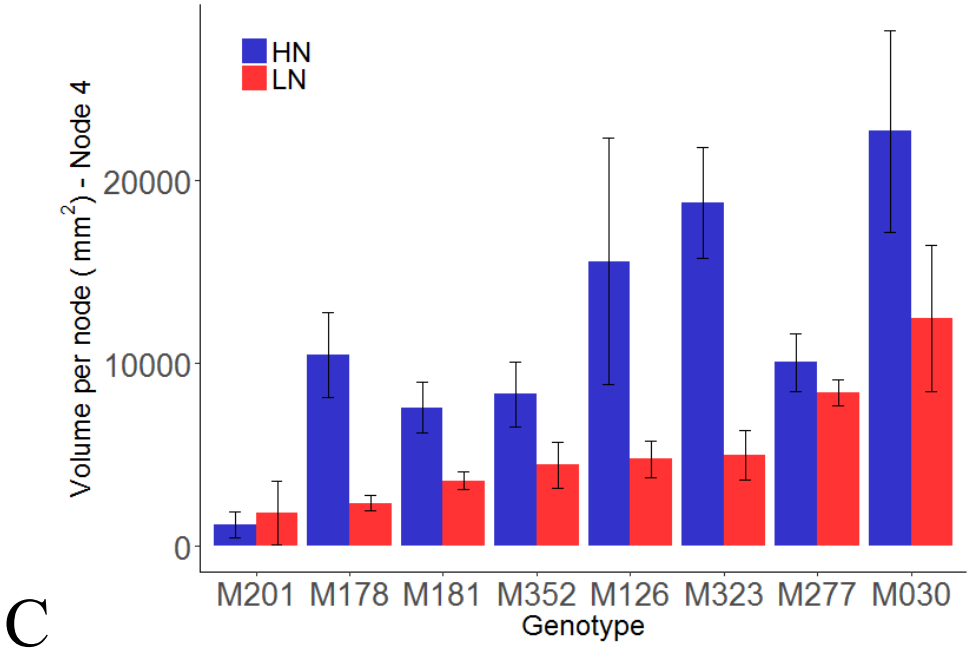

C

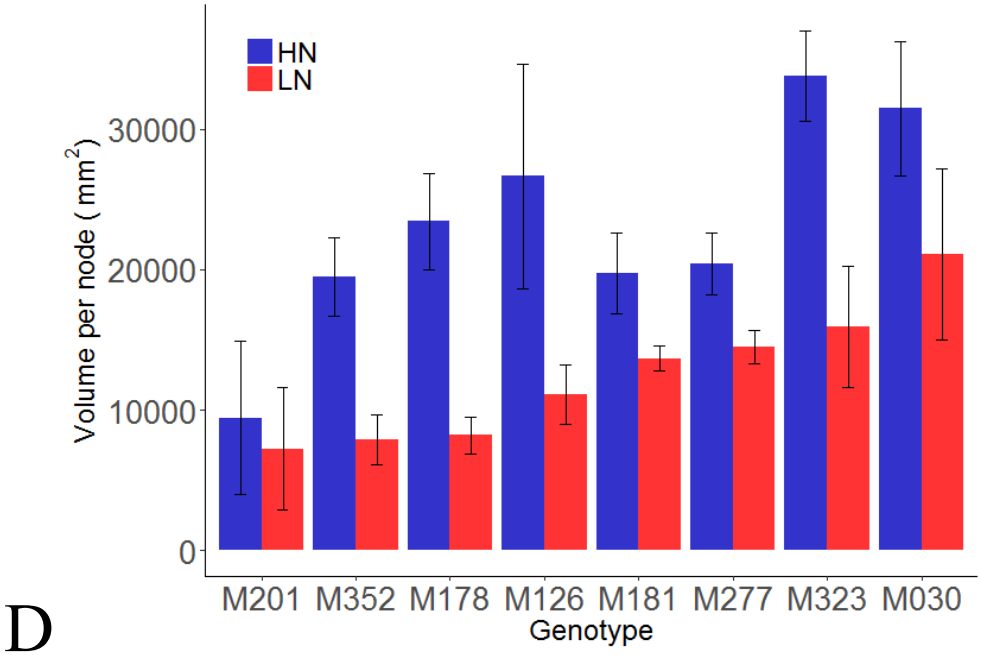

D

Fig S12. Axial root volume per node in IBM RILs. Means ± SE of total root volume (TRV) of the indicated nodes(s) at time of harvest: **(A)** node 2, **(B)** node 3, **(C)** node 4, and **(D)** the sum of all three nodes, among IBM RILs in GH2 (n=4 plants per RIL per nitrogen treatment). Genotypes are IBM RIL numbers as indicated by M# and are arranged in ascending order according to mean trait value under low nitrogen. High and low nitrogen treatments are indicated (HN, blue; LN, red). For M0 201, three plants in low nitrogen and one plant in high nitrogen did not develop fourth node roots by harvest; (C) and (D) includes these plants with fourth node values of zero.

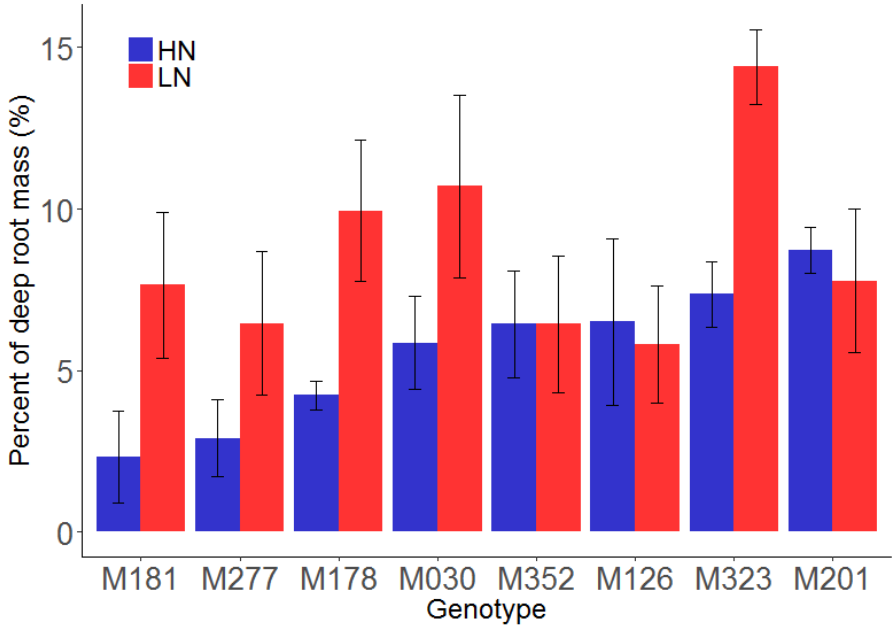
HN
LN
Percent of deep root mass (%)
0
5
10
15
M181
M277
M178
M030
M352
M126
M323
M201
Genotype

A

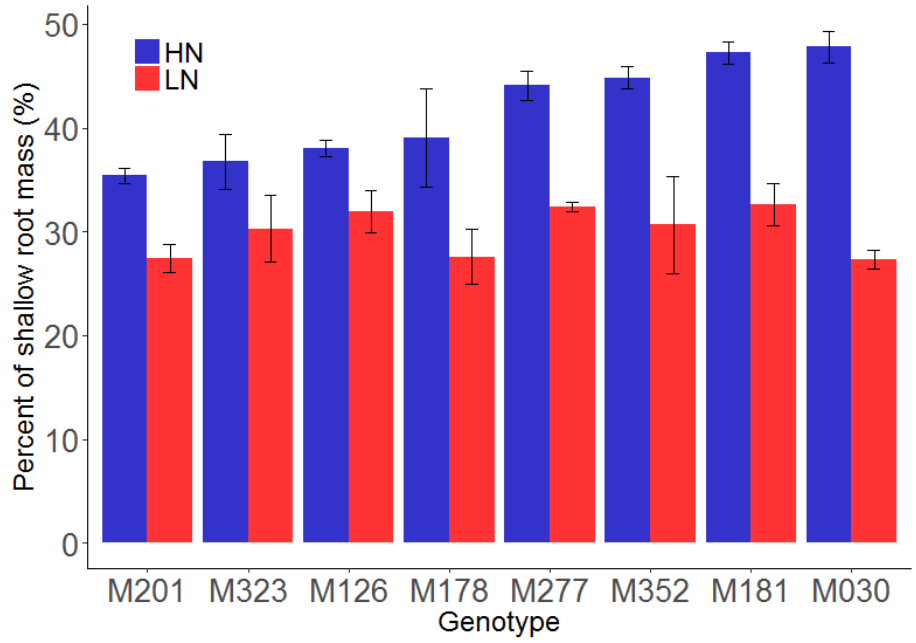
HN
LN
Percent of shallow root mass (%)
0
10
20
30
40
50
M201
M323
M126
M178
M277
M352
M181
M030
Genotype

B

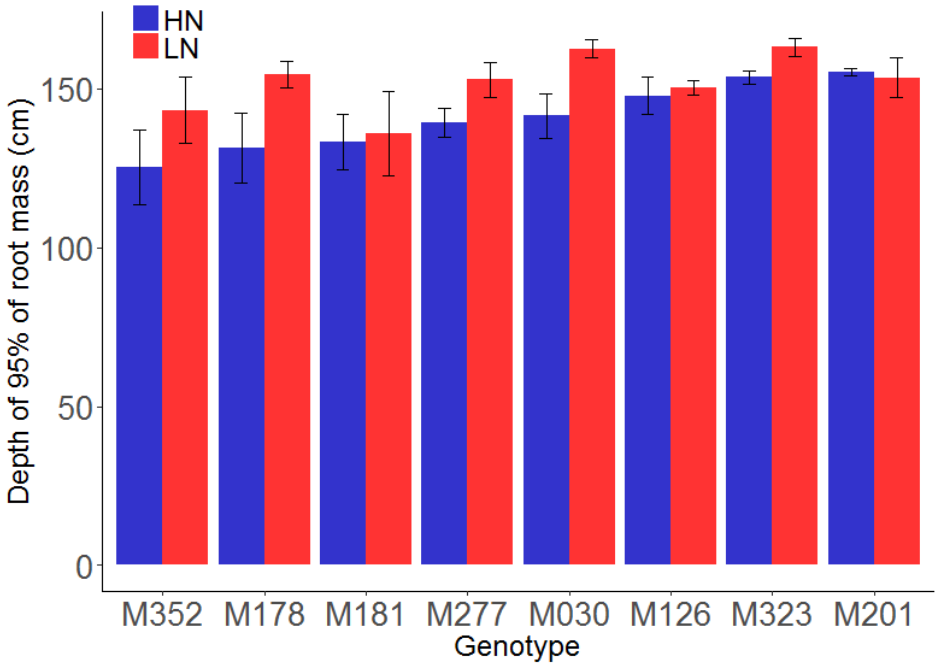
HN
LN
Depth of 95% of root mass (cm)
150
100
50
0
M352
M178
M181
M277
M030
M126
M323
M201
Genotype

C

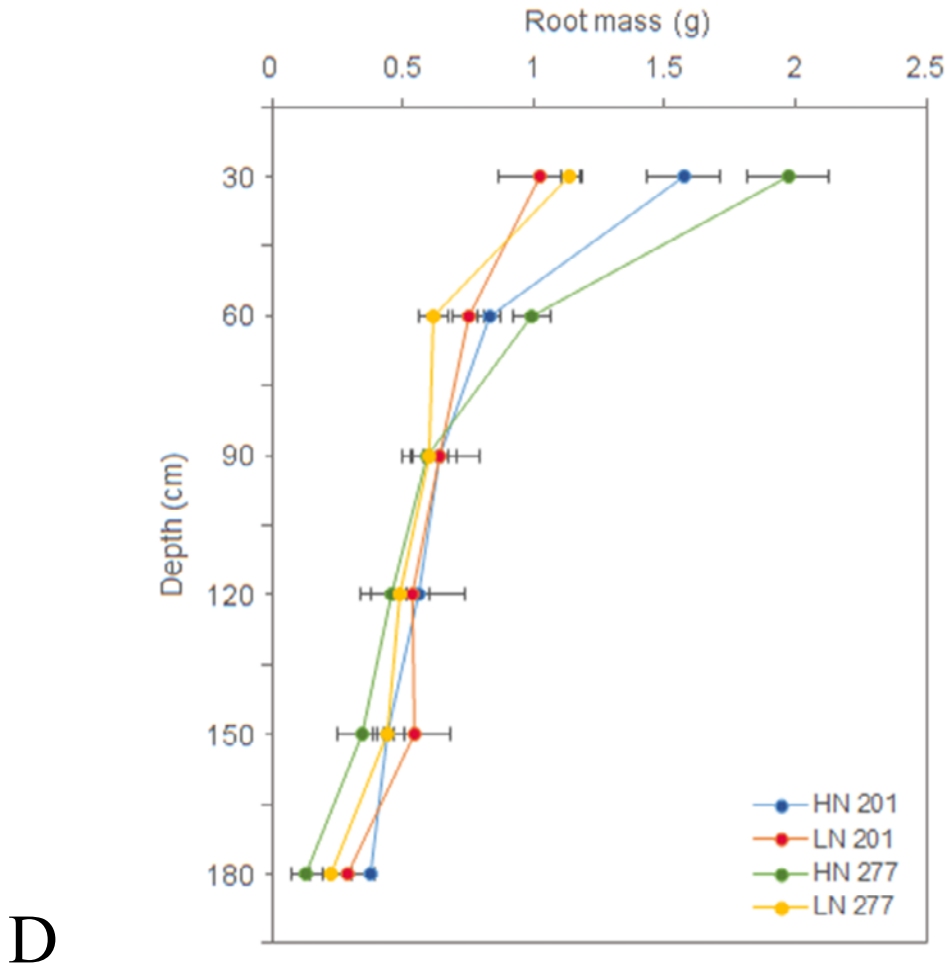

D

Fig S13. Relative root depth distributions among maize IBM RILs. Means ± SE of **(A)** the percent of total root mass at the deepest 30 cm of the root system, **(B)** percent of total root mass in the top 30 cm of media, and **(C)** depth (measured along the washed root system) above which 95% of root mass was located (D95), among IBM RILs in GH2. Genotypes are IBM RIL numbers as indicated by M# and arranged in ascending order by high nitrogen mean values. High and low nitrogen treatments are indicated (HN, blue; LN, red). **(D)** Mean ± SE root mass by depth (from excavated root systems; see Materials and Methods) for M201 and M277 under high and low nitrogen (HN, LN) in GH2 (as indicated by color legend), with D95 indicated by arrows.

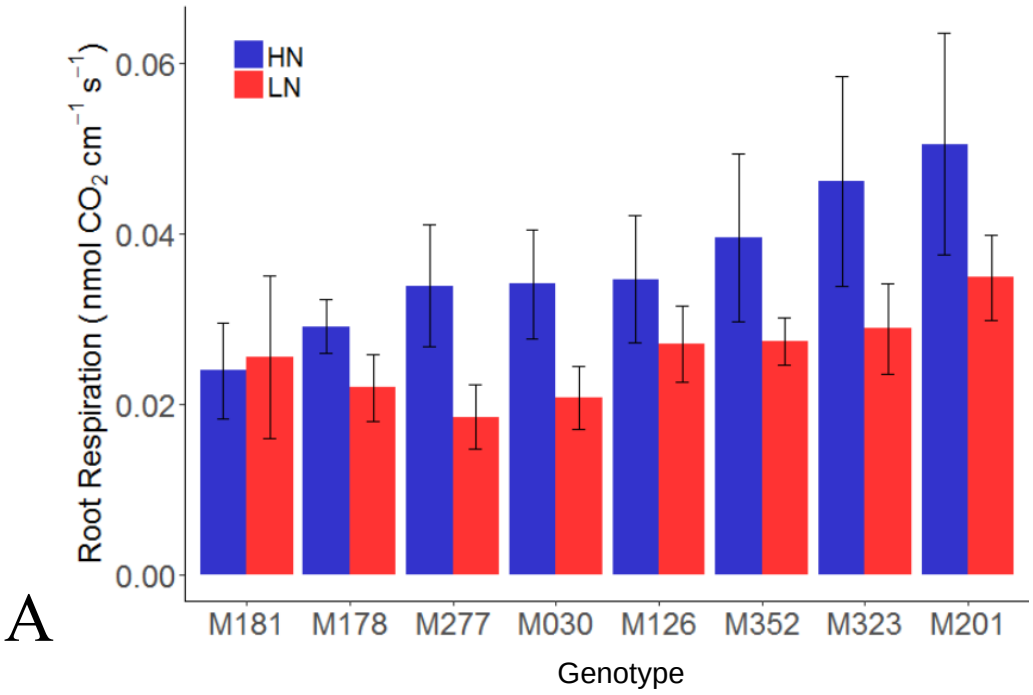
HN
LN
Root Respiration (nmol CO2 cm-1 s-1)
0.06
0.04
0.02
0.00
M181
M178
M277
M030
M126
M352
M323
M201
Genotype

A

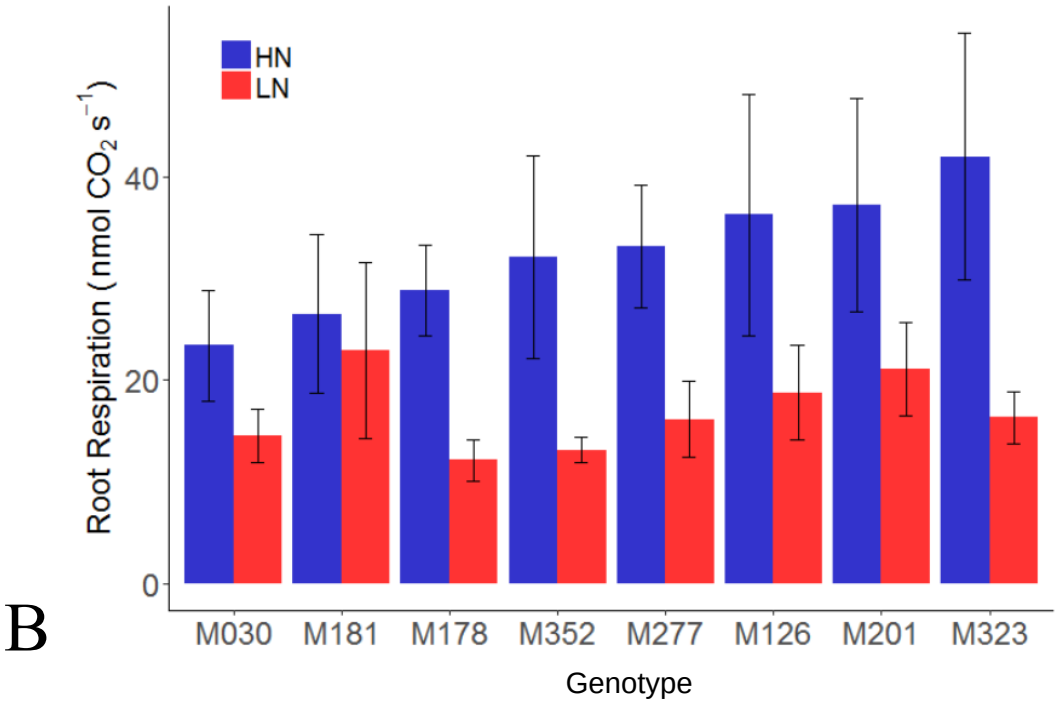
HN
LN
Root Respiration (nmol CO2 s-1)
40
20
0
M030
M181
M178
M352
M277
M126
M201
M323
Genotype

B

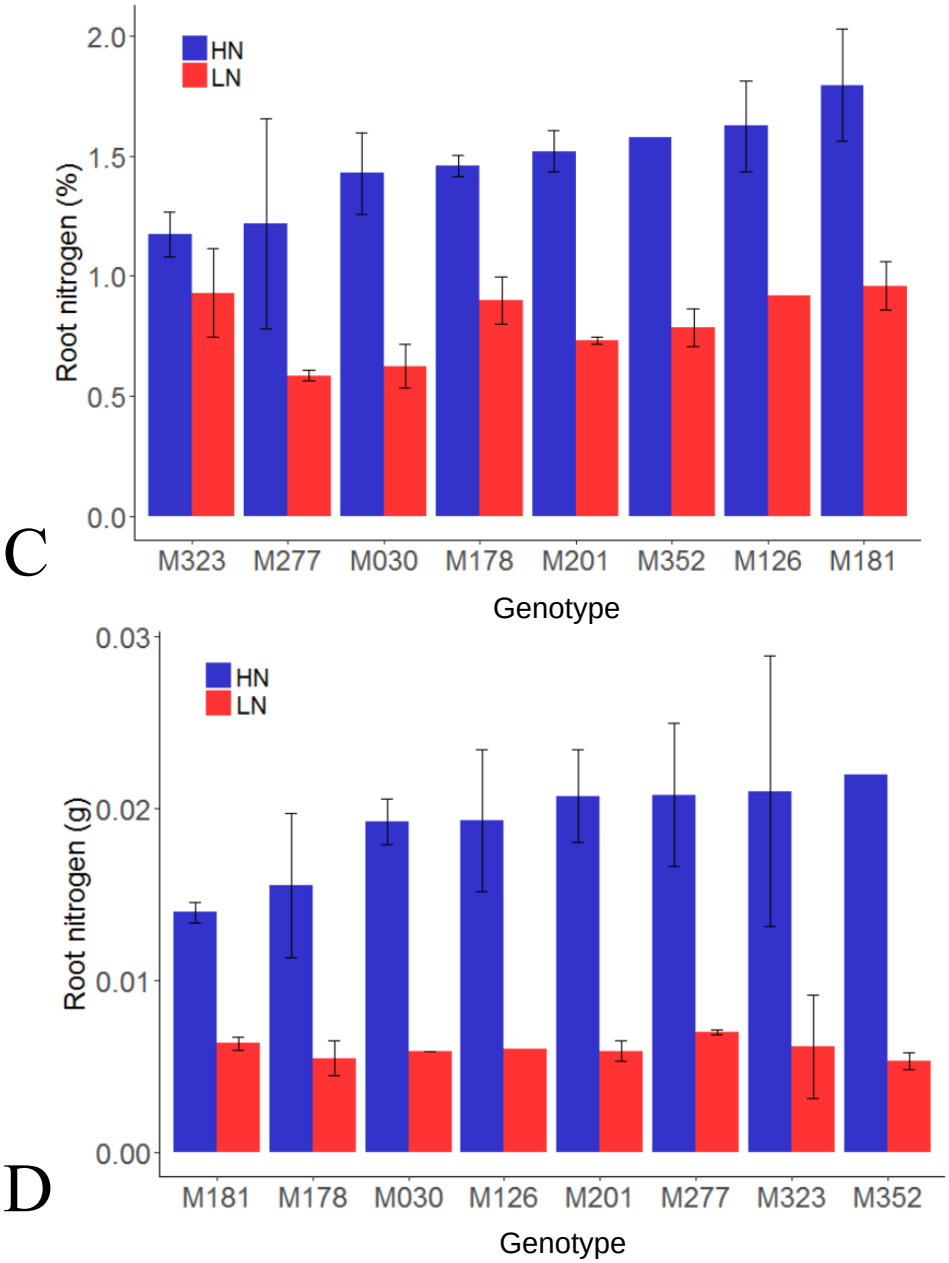

Fig S14 Root respiration and nitrogen content among IBM RILs. Means ± SE of **(A)** root respiration rates, averaged from six axial roots each, 2 to 5 cm from stem base, from nodes 2 and 3, and **(B)** total root respiration (estimated as root respiration rate multiplied by total axial root length in the given node) of nodes two and three, in GH2. Means ± SD of **(C)** root nitrogen content (percent by mass) from the top 30 cm of the root system (all root classes, homogenized), evaluated in a subset of replicates, and **(D)** total root nitrogen in the top 30 cm of the root system (percent root nitrogen multiplied by dry root mass in the top 30 cm), in GH2. Genotypes are IBM RIL numbers as indicated by M# and arranged in ascending order by high nitrogen mean values. High and low nitrogen are indicated (HN, blue; LN, red).

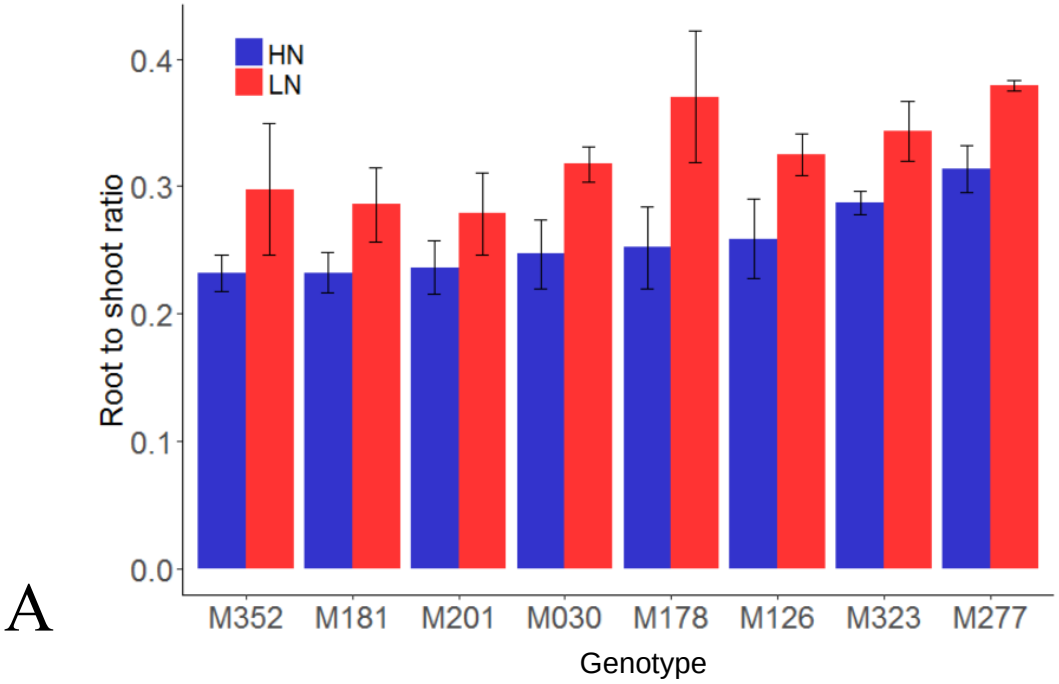

A

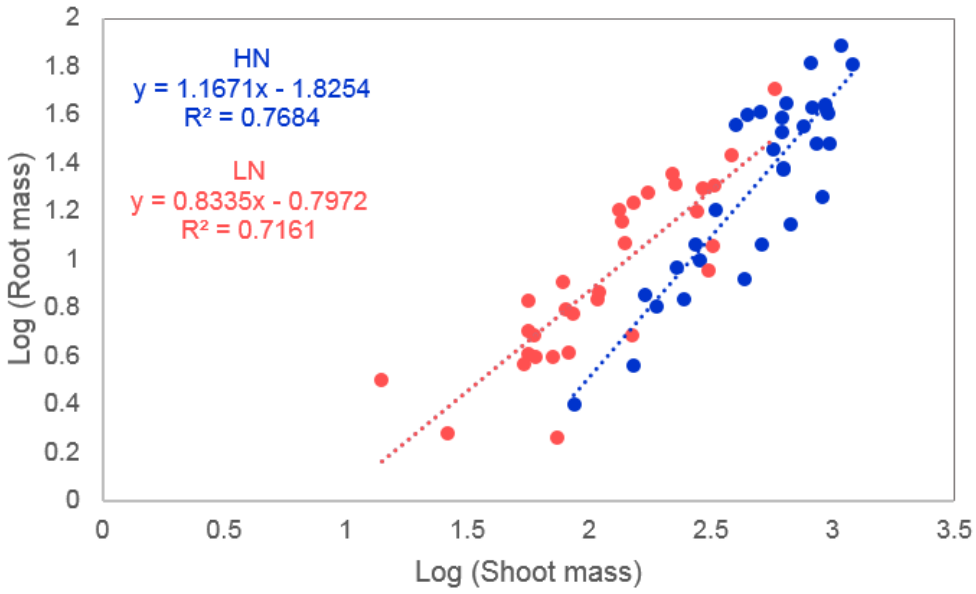

B

Fig S15. Nitrogen stress effects on root to shoot ratio among maize IBM RILs. (A) Means ± SE of root to shoot ratio (by dry mass at harvest) arranged in ascending order of high nitrogen mean values. Genotypes are IBM RIL numbers as indicated by M#. **(B)** The linear regression of the natural logarithms of total dry shoot and root mass, with regression equation and R^2 values, under high and low nitrogen conditions (HN, blue; LN, red) of all individual plants, among IBM RILs in GH2.

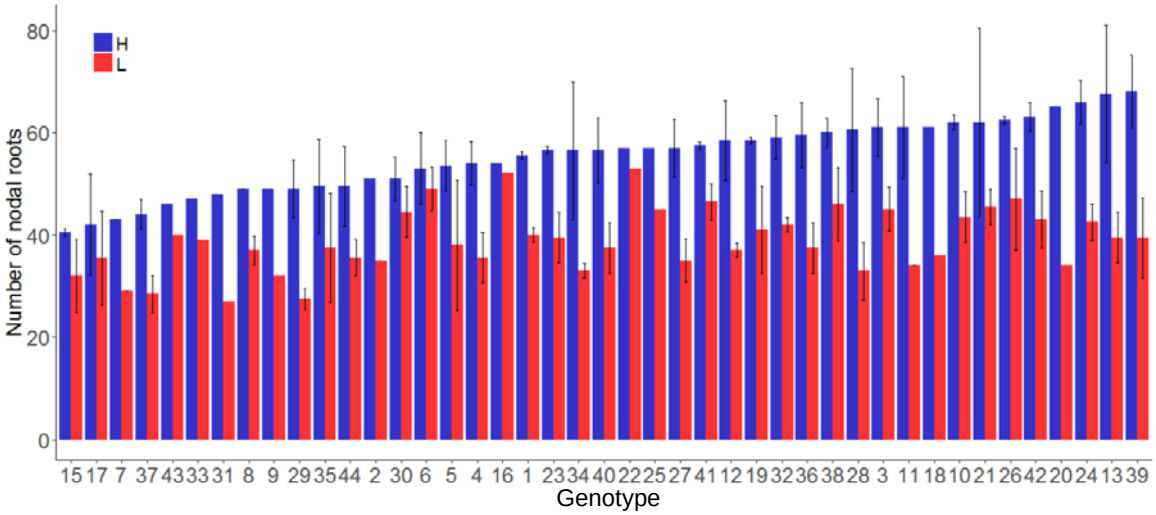
H
L
Number of nodal roots
0
20
40
60
80
15 17 7 37 43 33 31 8 9 29 35 44 2 30 6 5 4 16 1 23 34 40 22 25 27 41 12 19 32 36 38 28 3 11 18 10 21 26 42 20 24 13 39
Genotype

A

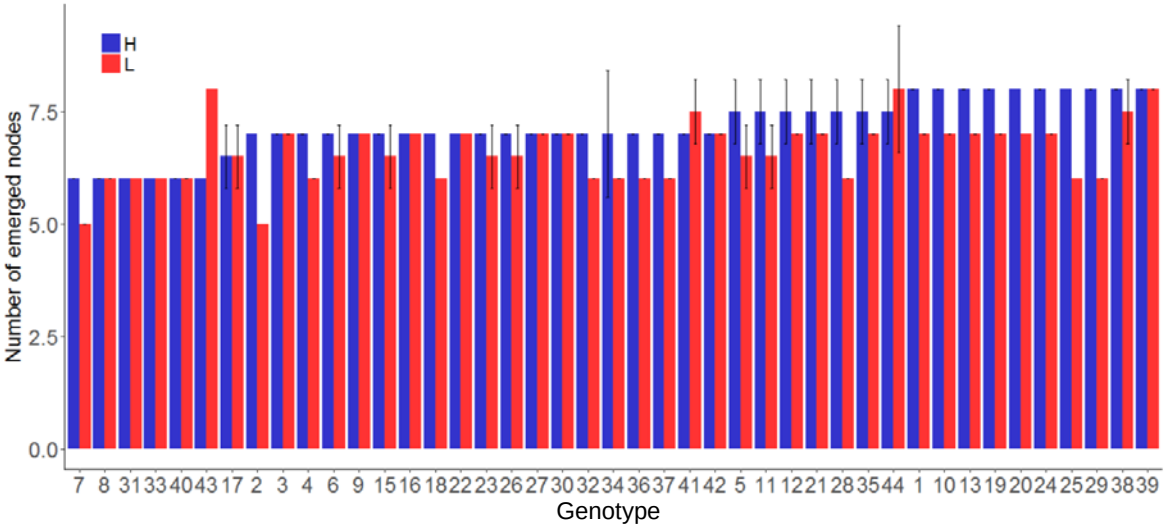
H
L
Number of emerged nodes
0.0
2.5
5.0
7.5
7 8 31 33 40 43 17 2 3 4 6 9 15 16 18 22 23 26 27 30 32 34 36 37 41 42 5 11 12 21 28 35 44 1 10 13 19 20 24 25 29 38 39
Genotype

B

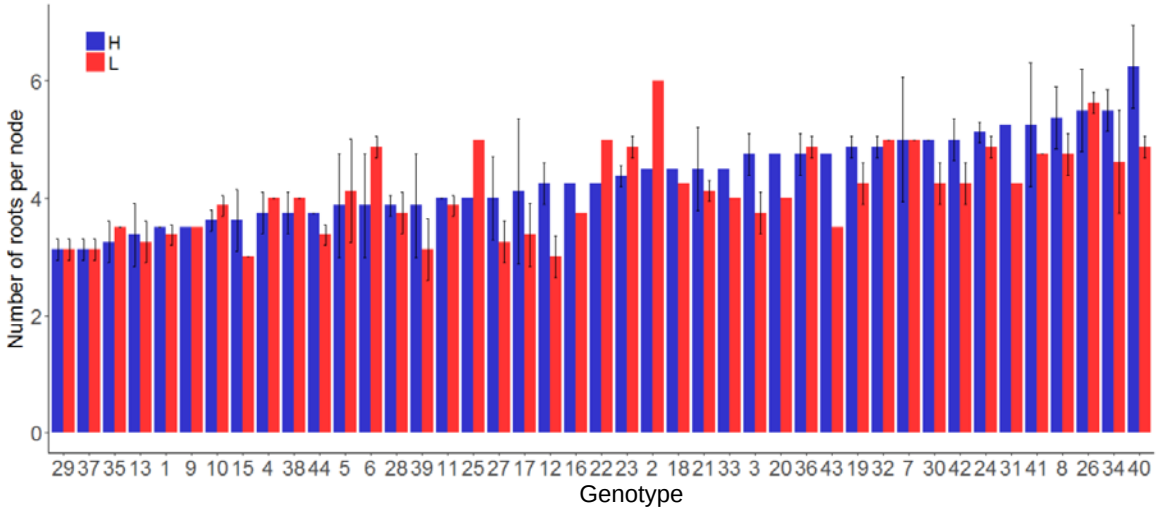

C

Fig S16. Genotypic contrast in root node number and occupancy among maize hybrids. Means ± SD of **(A)** total number of nodal roots (NRN) emerged at harvest, **(B)** the number of developed root nodes (NN), and **(C)** the number of nodal roots per node (NO), averaged from the first four nodes, for maize hybrid genotypes in PA16 (see Appendix C, Table S1 for genotype codes). Genotypes are arranged in ascending order by high nitrogen trait values. High and low nitrogen treatments are indicated (H, blue; L, red). Plants with missing values were excluded.

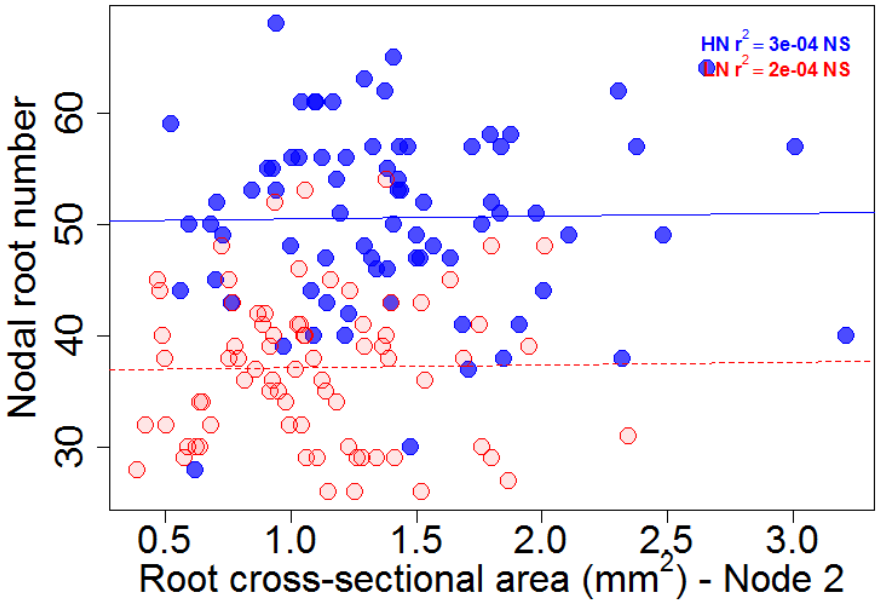
HN r2 = 3e-04 NS
LN r2 = 2e-04 NS
Nodal root number
30
40
50
60
0.5
1.0
1.5
2.0
2.5
3.0
Root cross-sectional area (mm2) - Node 2

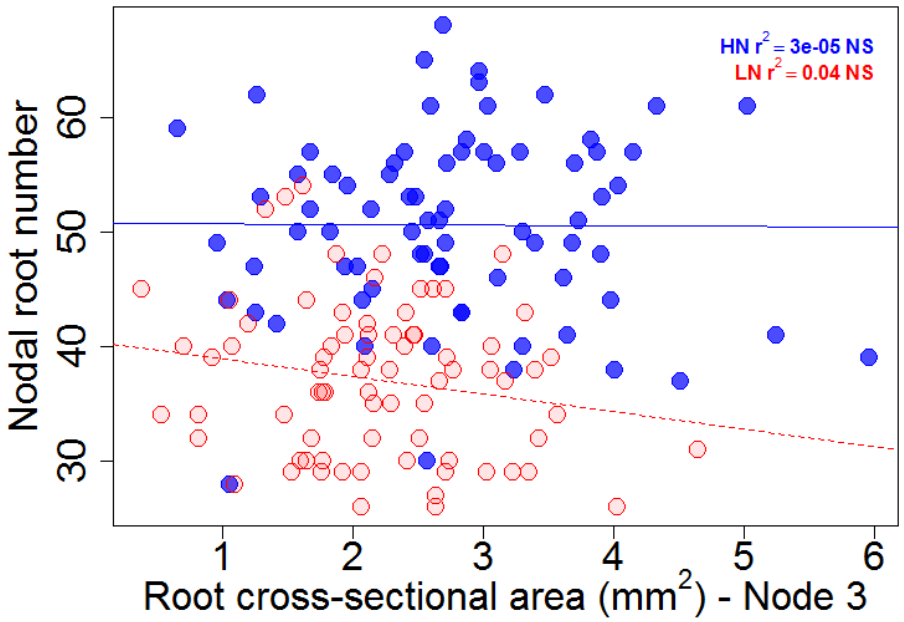
HN r2 = 3e-05 NS
LN r2 = 0.04 NS
Nodal root number
30
40
50
60
1
2
3
4
5
6
Root cross-sectional area (mm2) - Node 3

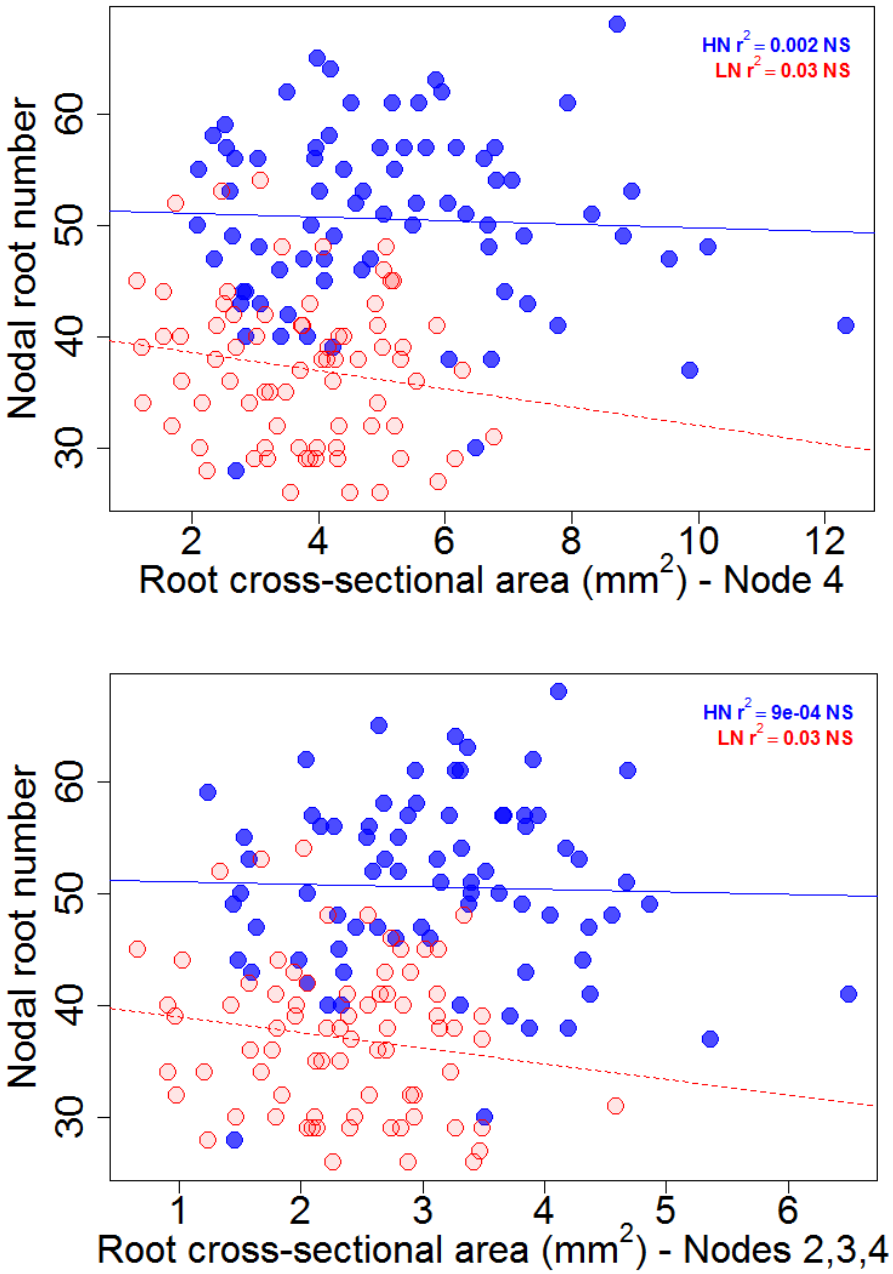

Fig S17. **Relationship between nodal root number and diameter among maize hybrids in the field**. Linear regression of total number of emerged nodal roots at harvest (NRN) and root cross-section area (RXA) averaged from two roots from each of the indicated nodes from individual plants of 44 maize hybrid genotypes grown in high (HN, blue) or low nitrogen (LN, red) treatments in PA16 (see Appendix C, Tables S1 and S2). R^2 value and significance ($p<0.001$ ***; $p> 0.1$ NS, not significant) are indicated.

Appendix D

Supplementary figures and tables for Chapter 4

Table S1. Plant materials and sampling. IBM RILs are indicated as M#. See Tables S1.1 and S1.2 below, and S1.3 for nitrogen stress levels of experiments.

Table S1.1 Plant materials

GH1	GH2	PA15
M30	M30	M30
M126	M126	M59
M178	M178	M126
M201	M181	M129
M277	M201	M178
M323	M277	M181
M352	M323	M201
M365	M352	M277
		M323
		M352
		M365

Table S1.2 Root and leaf sampling

Study	Root nodes sampled	Leaf sampled
GH1	2,3	Leaf 7, or largest expanded leaf; subset analyzed for leaf anatomy
GH2	2,3,4	Leaf 7, or largest expanded leaf
PA15	1,2,3	Ear leaf; subset analyzed for leaf anatomy

Table S1.3 Stress levels. Percent (%) reduction is the average across genotypes. Range refers to range among genotypes.

Study	No. of genotypes	Metric	% Reduction	Range
GH1	8	Dry shoot mass	80	69 – 88%
GH2	8	Dry shoot mass	46	29 – 60%
PA15	11	Yield	30	15 – 55%

A

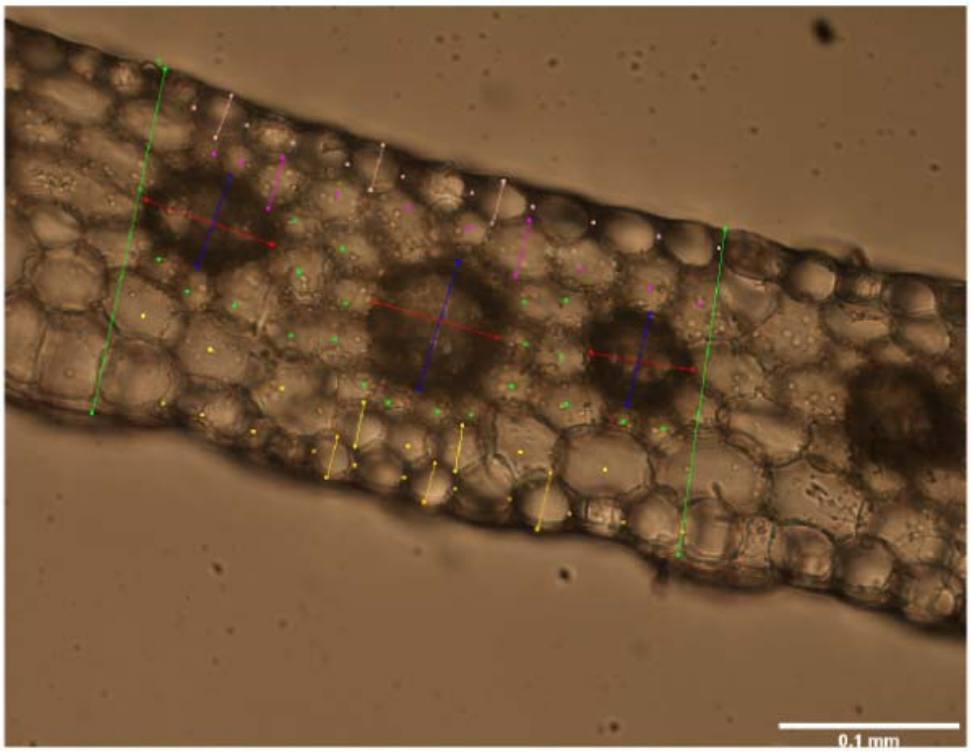

B

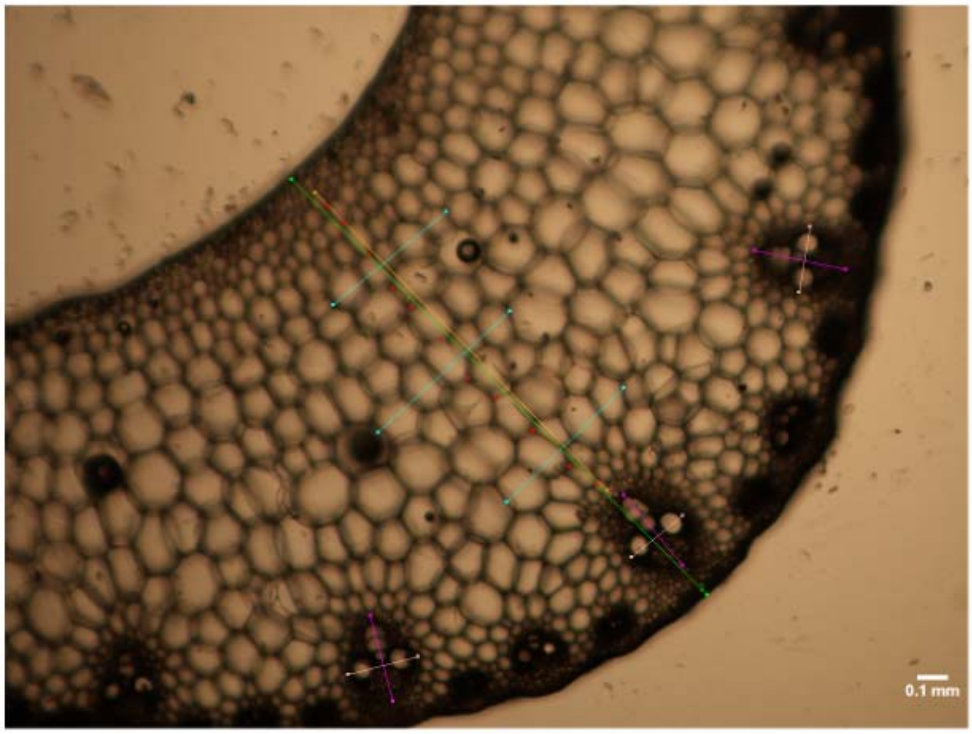

C

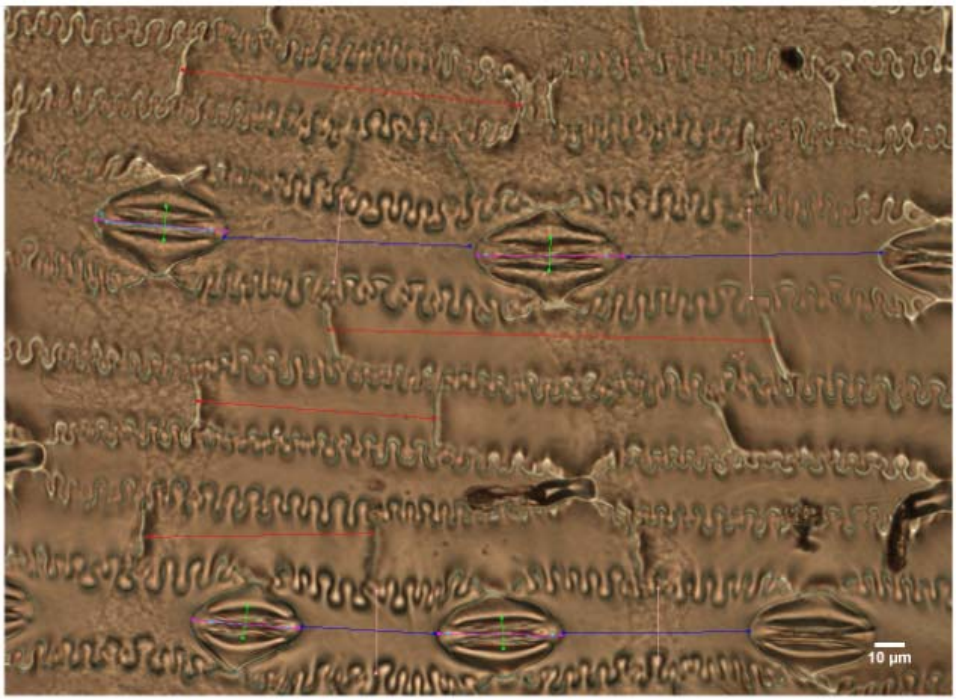

D

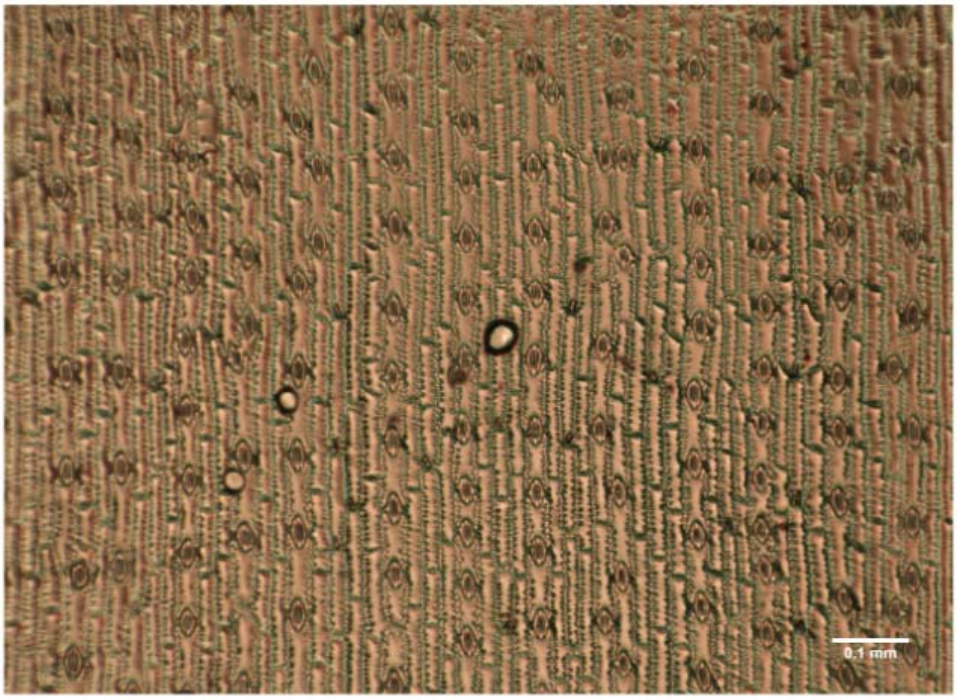

Fig S1. Leaf image analysis. Image analysis was performed using custom ObjectJ project files in ImageJ with manual sections from leaves preserved and cleared in ethanol. Leaf thickness and composition were evaluated from cross-sections of the leaf lamina with a 20X objective lens **(A)**, midrib traits were evaluated from midrib cross-sections with a 4X objective lens **(B)**, and stomatal and epidermis cell size were evaluated from an abaxial and adaxial image for each leaf (only abaxial shown here) with a 40X objective

lens **(C).** Stomatal density was manually counted from an abaxial and adaxial image for each leaf with both 10X and 20X magnification, and averaged (only 20X abaxial image shown here) **(D)**.
In **(A)**, leaf thickness was averaged from a select region of interest (green lines), epidermis and mesophyll cell diameters were averaged from adaxial and abaxial layers (pink and yellow lines), cells were counted and divided by the region of interest to estimate cell density for each tissue layer (yellow, pink, green dots), and vascular bundle size (including bundle sheath cells) and interveinal distance were calculated (red and blue lines, and the distances between their end points). In **(B)**, midrib thickness is measured across the central axis (green line) as well as "cortical thickness" (yellow line, used to calculate MidribPC). Parenchyma cell sizes were estimated from cell diameters averaged from 15 cells (blue lines) and median cell diameters across the central axis (distance between red dots). Vascular bundle size of the central bundle and two small vascular bundles were calculated (pink lines). Number of cell files across the central axis was recorded (red dots). In **(C)**, stomatal length and width were averaged from four stomates (green and dark pink lines); epidermis cell size was averaged from eight cells (red, blue lines are cell lengths; light pink lines are cell widths).

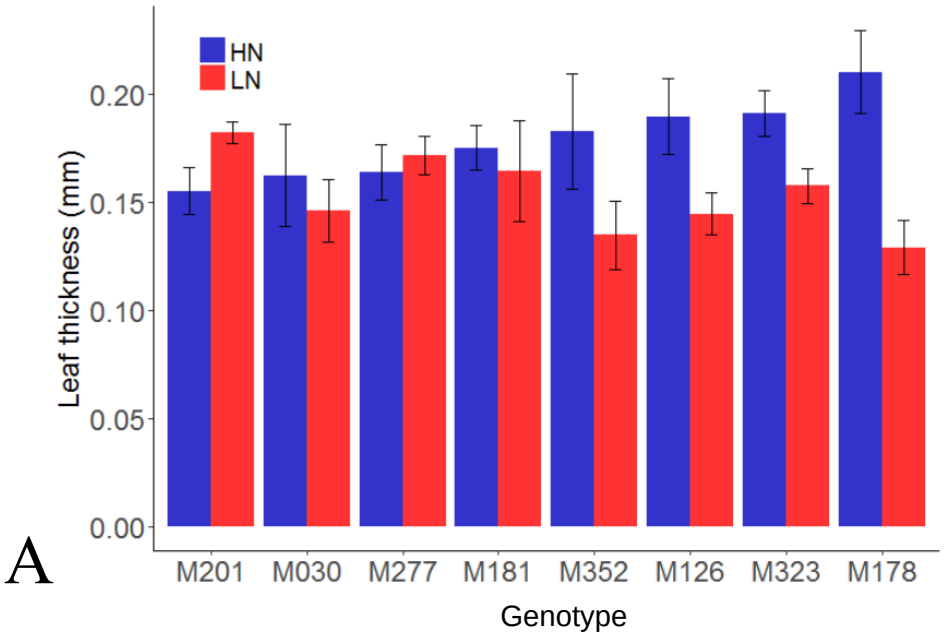
HN
LN
Leaf thickness (mm)
0.20
0.15
0.10
0.05
0.00
M201
M030
M277
M181
M352
M126
M323
M178
Genotype

A

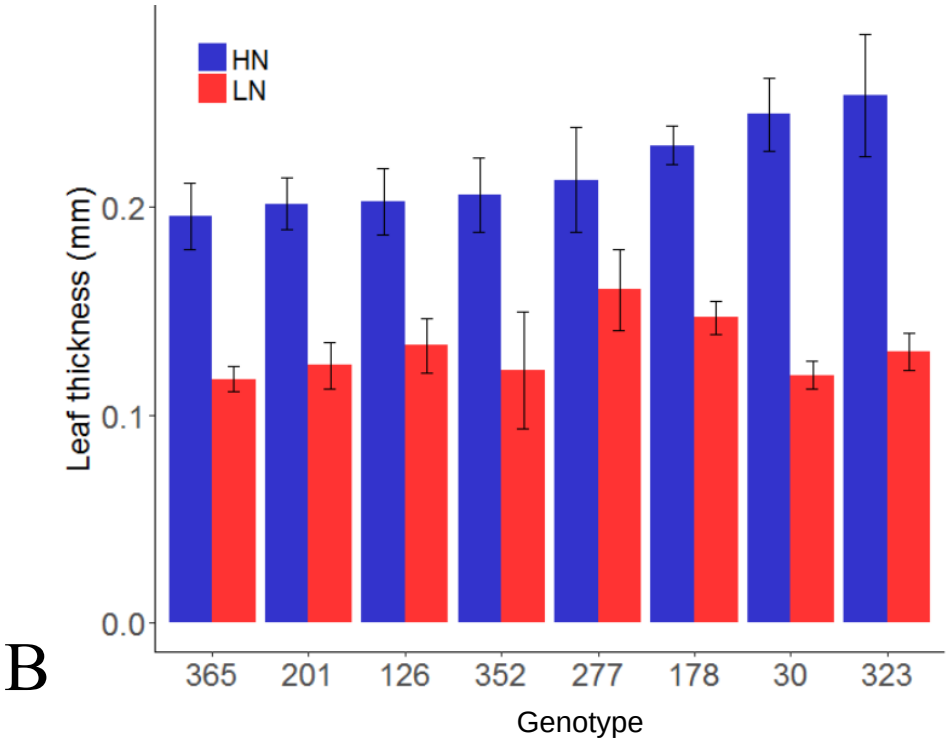
HN
LN
Leaf thickness (mm)
0.2
0.1
0.0
365
201
126
352
277
178
30
323
Genotype

B

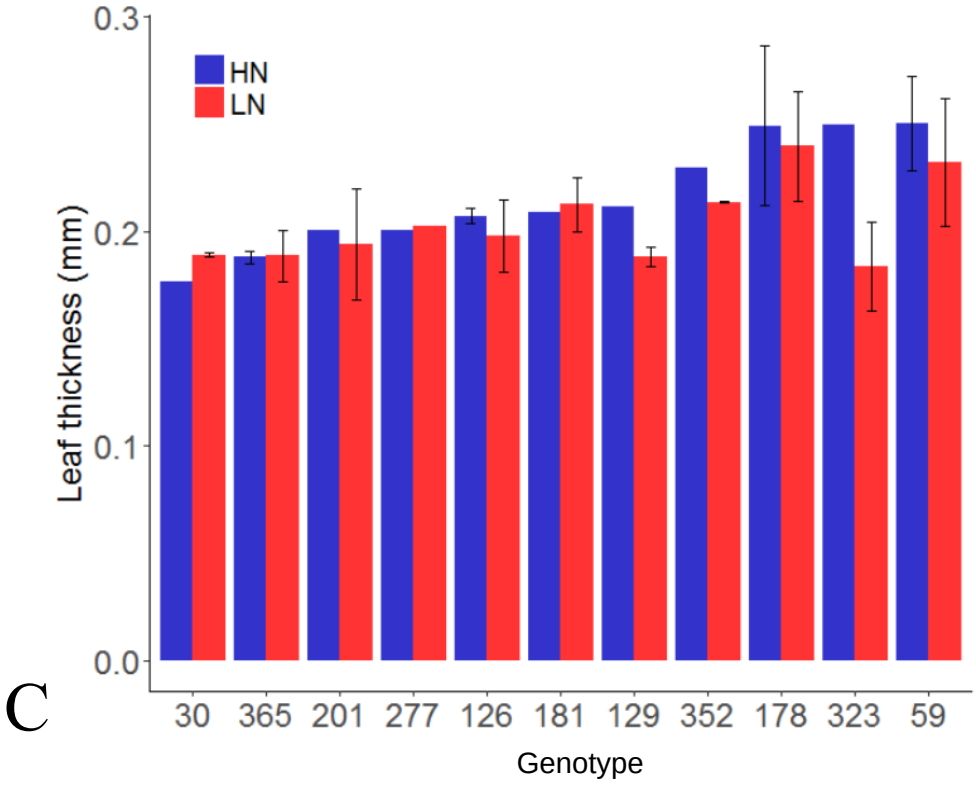

Fig S2. Leaf thickness among IBM RILs. Means ± SE of leaf thickness among IBM RILs in **(A)** GH2, **(B)** GH1, and **(C)** a subset of replicates in PA15. RILs are indicated as M#, arranged in ascending order by mean trait value under high nitrogen. High and low nitrogen are indicated (HN, blue; LN, red). See Table S1 for nitrogen stress levels of each experiment.

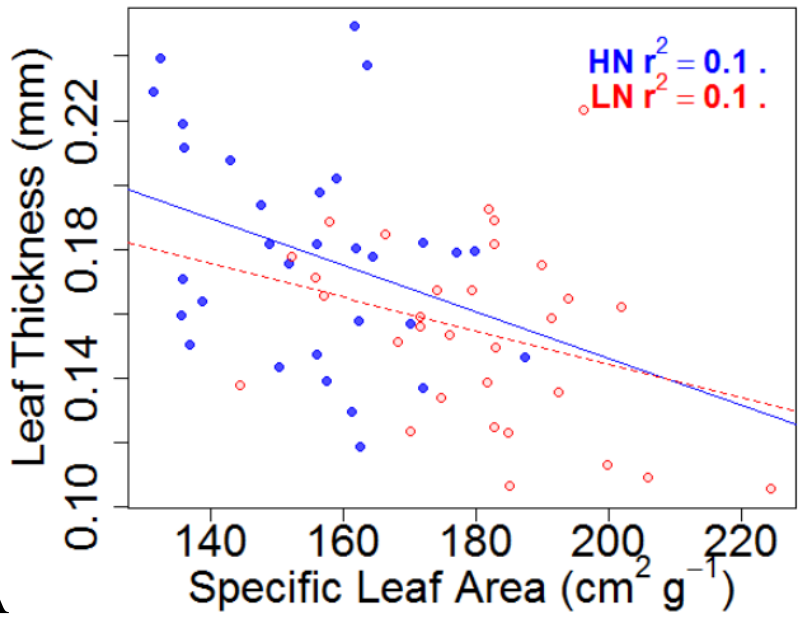
HN r2 = 0.1 .
LN r2 = 0.1 .
Leaf Thickness (mm)
0.10
0.14
0.18
0.22
140
160
180
200
220
Specific Leaf Area (cm2 g−1)

A

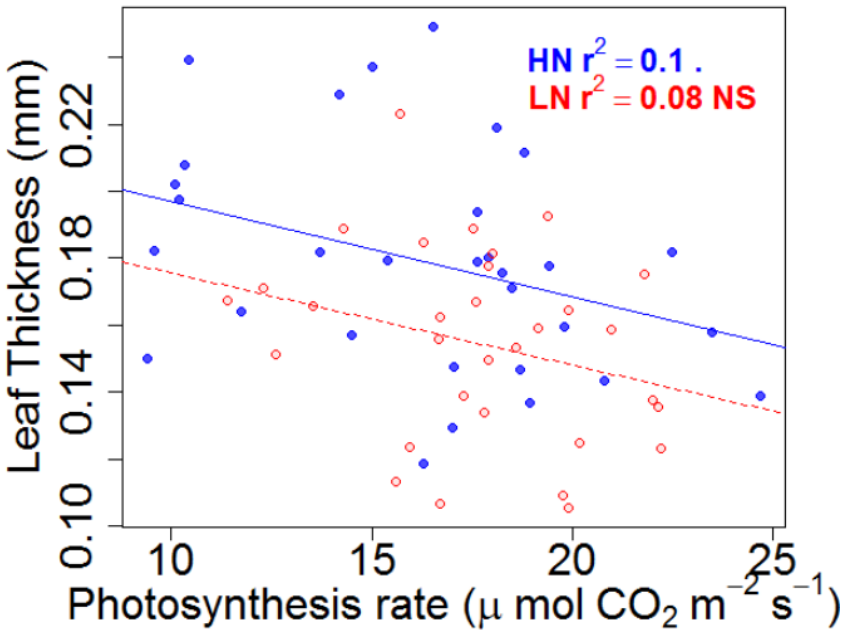
HN r2 = 0.1 .
LN r2 = 0.08 NS
Leaf Thickness (mm)
0.10
0.14
0.18
0.22
10
15
20
25
Photosynthesis rate (μ mol CO2 m−2 s−1)

B

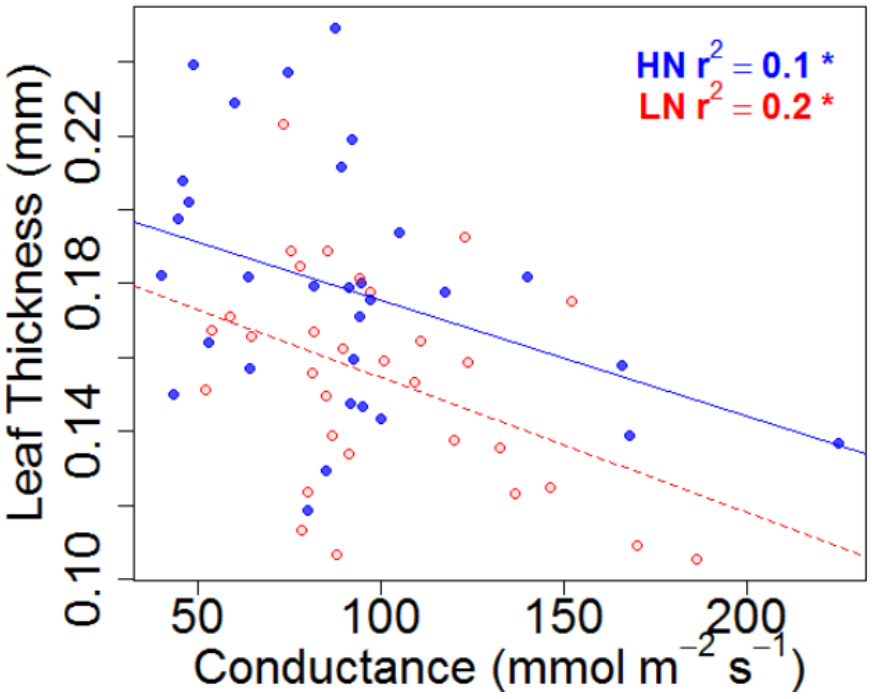
HN r2 = 0.1 *
LN r2 = 0.2 *
Leaf Thickness (mm)
0.10
0.14
0.18
0.22
50
100
150
200
Conductance (mmol m−2 s−1)

C

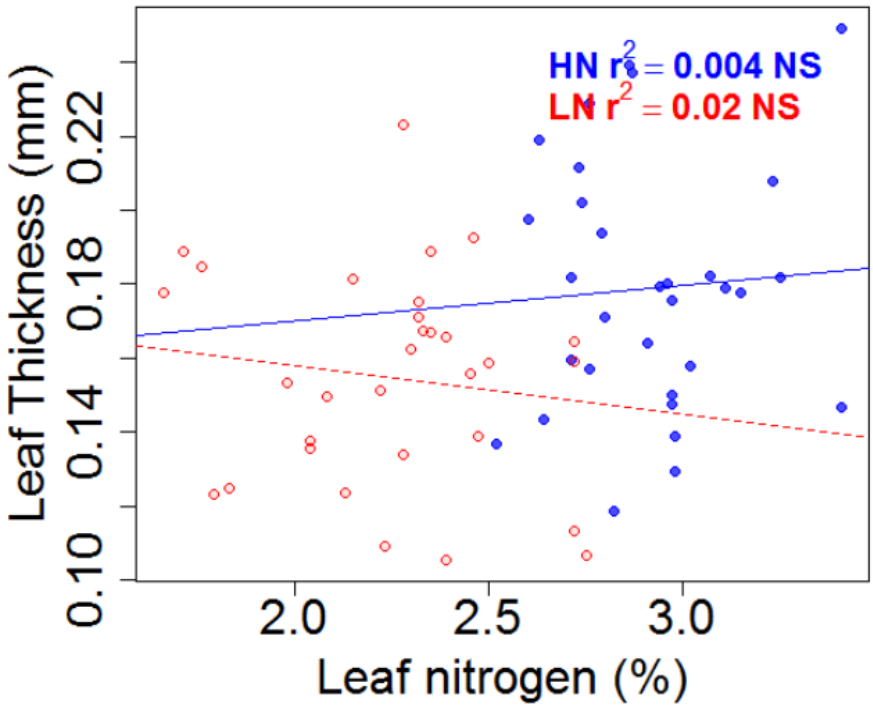
HN r2 = 0.004 NS
LN r2 = 0.02 NS
Leaf Thickness (mm)
0.10
0.14
0.18
0.22
2.0
2.5
3.0
Leaf nitrogen (%)

D

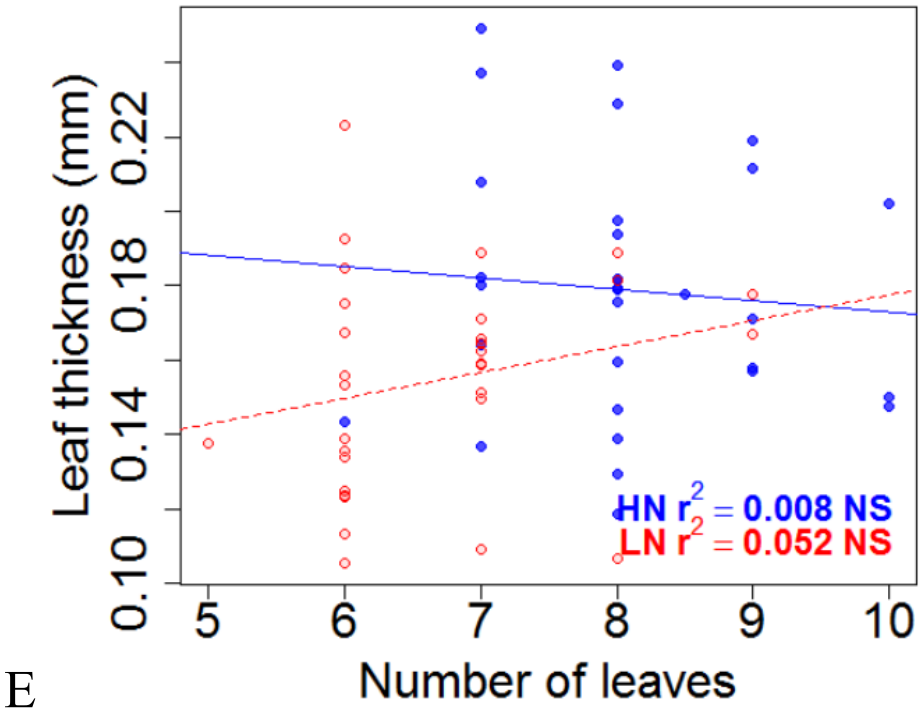

Fig S3. Relationship between leaf thickness and physiology. Linear regression of leaf thickness of a representative leaf against **(A)** specific leaf area, **(B)** carbon assimilation rate, **(C)** stomatal conductance rate, **(D)** leaf nitrogen content (from homogenized leaves), and **(E)** number of leaves, under high (HN, blue) and low (LN, red) nitrogen in GH2. R^2 value and significance (p< 0.1.,05*, p>0.1 not significant, NS) are indicated.

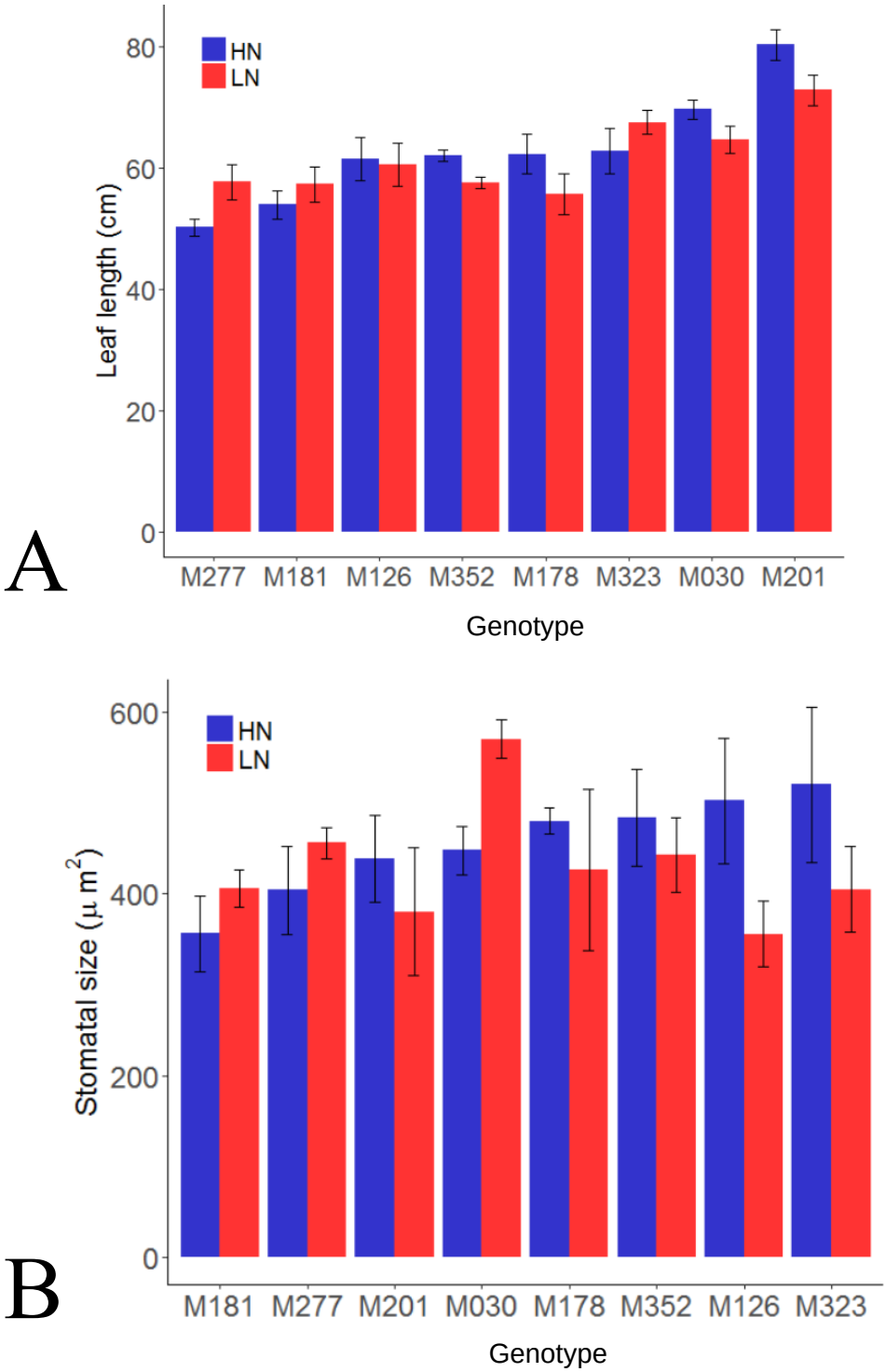

Fig S4. Leaf trait variation among IBM RILs. Means ± SE of **(A)** median leaf length and **(B)** stomatal size (average of abaxial and adaxial) among IBM RILs in GH2 (n=4 plants per RIL per nitrogen treatment). IBM RILs are indicated as M#, arranged in ascending order by mean trait value under high nitrogen. High and low nitrogen are indicated (HN, blue; LN, red).

Appendix E

Leaf and root anatomy raw data for Chapter 4

Summary data associated with **Table 3-2** and **Figure 3-3**. Minimum, maximum, mean, median, and first and third quartile values from greenhouse-grown maize inbreds. See **Table 3-1** for trait abbreviations and units.

	LeafNum	LeafArea	LAmed	LeafLenMed	LeafWidMed	LT	SLA
Min.	**5**	**554.7**	**79.95**	**46**	**2.5**	**0.1056**	**131.3**
Q1	**6**	**880.2**	**111.38**	**57**	**2.775**	**0.1442**	**155.8**
Median	**7**	**1069.3**	**123.75**	**61**	**3.05**	**0.1651**	**166.4**
Mean	**7.389**	**1133.7**	**133.5**	**62.44**	**3.106**	**0.1667**	**167.3**
Q3	**8**	**1351.1**	**150.84**	**68**	**3.325**	**0.1821**	**182.3**
Max.	**10**	**1902.8**	**219.22**	**86**	**4.1**	**0.2491**	**224.5**

	pVB	pEpi	pMeso	MesoDens	MesoCDM	VascA	IVD
Min.	**8.537**	**39.89**	**19.33**	**5.427**	**0.01812**	**0.001834**	**0.09679**
Q1	**13.525**	**51.74**	**26.24**	**8.745**	**0.02589**	**0.002441**	**0.12165**
Median	**14.602**	**57.01**	**28.42**	**10.042**	**0.02886**	**0.003037**	**0.12813**
Mean	**14.902**	**55.73**	**29.37**	**10.943**	**0.02907**	**0.003083**	**0.13358**
Q3	**16.796**	**59.75**	**32.52**	**12.427**	**0.03212**	**0.003607**	**0.14893**
Max.	**21.304**	**70.07**	**41.74**	**24.132**	**0.04528**	**0.004879**	**0.1981**

	SD.AD	SD.AB	SI.AD	SI.AB	StomA	EpiCCS	EpiCCX
Min.	**46.88**	**68.03**	**8.407**	**10.13**	**257**	**1202**	**0.000394**
Q1	**57.61**	**80.21**	**11.179**	**16.45**	**378.2**	**2127**	**0.000627**
Median	**61.38**	**86.53**	**14.027**	**19.49**	**446.2**	**2469**	**0.00074**
Mean	**61.81**	**86.93**	**13.954**	**19.46**	**441.7**	**2604**	**0.000755**
Q3	**67.11**	**92.67**	**15.997**	**22.89**	**500.5**	**3005**	**0.000854**
Max.	**75.64**	**112.48**	**21.676**	**31.66**	**685.7**	**4849**	**0.001311**

	MidribLT	MidribCF	MidribCCS	MidribPC	MidribVA
Min.	**1.606**	**9**	**0.007713**	**50.66**	**0.03165**
Q1	**1.83**	**11**	**0.010094**	**58.46**	**0.04244**
Median	**1.972**	**12**	**0.011578**	**62.29**	**0.05149**
Mean	**1.983**	**11.91**	**0.011893**	**61.98**	**0.05128**
Q3	**2.104**	**13**	**0.013469**	**64.95**	**0.05858**
Max.	**2.452**	**16**	**0.017072**	**70.66**	**0.0741**

Table continues on next page

	Total biomass	Shoot biomass	Root biomass	R:S ratio	Leaf Nitrogen %
Min.	**4.8**	**3.15**	**1.3**	**0.1784**	**1.66**
Q1	**10.02**	**7.675**	**2.265**	**0.2412**	**2.31**
Median	**14.38**	**11.53**	**3.18**	**0.2871**	**2.71**
Mean	**15.28**	**11.935**	**3.349**	**0.2909**	**2.587**
Q3	**20.38**	**16.29**	**4.39**	**0.3343**	**2.925**
Max.	**27.89**	**21.79**	**6.58**	**0.5238**	**3.41**

The following raw datasets associated with Chapters 3 and 4 are available within this open-access ScholarSphere link, which contains the files listed below: https://doi.org/10.18113/S1GG93

Greenhouse 1 (GH1) experiment:

"gh1_inbred_greenhouse_root_shoot_data.csv"

Greenhouse 2 (GH2) experiment:

"gh2_inbred_greenhouse_root_shoot_data.csv"

To cite raw data, use:
Yang, Jennifer T. (2017)."Integrating leaf and root phenotypes to enhance nitrogen use efficiency in maize (*Zea mays* L.)-Data". doi.org/10.18113/S1GG93

VITA

Jennifer T. Yang

EDUCATION

Ph.D. The Pennsylvania State University, Plant Biology, 2017
B.A. Wellesley College, Biological Sciences, 2012

RESEARCH

Graduate Fellow, Jonathan P. Lynch Lab, Penn State University, 2012–2017

- Conducted USDA-funded research on root systems and plant nutrition in maize in field, greenhouse, lab, and *in silico*, including field trials at Larson Research Station in PA; the Arizona Root Biology Center in AZ; the Ukulima Root Biology Center in South Africa.
- Supported maize inbred and hybrid phenotyping trials for Genomes to Fields Consortium
- Developed successful proposals for funding including $7500 from Edmund Optics and $5000 from NVIDIA for development of novel high throughput phenotyping platforms

Research Fellow, Thomas D. Sharkey Lab, Michigan State, June–Aug 2012

- Conducted and published NSF-funded research on photosynthesis mechanisms using *Arabidopsis thaliana* mutants, isotope labeling, gas exchange, and leaf spectroscopy, including collaboration with David Kramer's leaf phenomics lab

Research Technician, T. Kaye Peterman Lab, Wellesley College, Sept–May 2012

- Provided technical support for moss and *Arabidopsis thaliana* genetics research

Research Assistant, Emily A. Buchholtz Lab, Wellesley College, May–Aug 2010

- Conducted and published NSF-funded research on the role of the diaphragm in mammalian evolution based on 3D imaging and comparative anatomy

SELECT PUBLICATIONS AND PRESENTATIONS

- **Yang JT**, Preiser AL, Li Z, Weise SE, and Sharkey TD. 2016. Triose phosphate use limitation of photosynthesis: short-term and long-term effects. *Planta* 243 (3), 687-698.
- Buchholtz EA, Bailin HG, Laves SA, **Yang JT**, Chan M-Y, and Drozd LE. 2012. Fixed cervical count and the origin of the mammalian diaphragm. *J. Evolution & Development* 14 (5), 399-411; journal cover.
- "The Shovelomics pipeline: Large-scale phenotyping of root architecture and anatomy", Rhizosphere4, Maastricht, Netherlands, 2015. Invited speaker.
- "Differences in wheat coleoptile growth pattern impact seedling emergence", American Society of Plant Biologists, Minneapolis, MN, 2015. Poster.

SELECT AWARDS

Crop Science Society of America, Congressional Visits Day participant, Washington DC
U.S. Edmund Optics Higher Education Grant Competition, national winner
NSF Graduate Research Fellowship Program, Honorable Mention
University Graduate Fellowship and Graham Endowed Fellowship, Penn State
Dorothy Thorndike Endowed Botanic Gardens Fellowship, Wellesley College